The Dissertation Committee for Ryan Matthew Phelps Certifies that this is the approved version of the following dissertation:

MIDDLE-HAUTERIVIAN TO LOWER-CAMPANIAN SEQUENCE STRATIGRAPHY AND STABLE ISOTOPE GEOCHEMISTRY OF THE COMANCHE PLATFORM, SOUTH TEXAS

Committee:

Charles Kerans, Supervisor

Robert G. Loucks

Xavier Janson

Robert W. Scott

William L. Fisher

Terrence M. Quinn

MIDDLE-HAUTERIVIAN TO LOWER-CAMPANIAN SEQUENCE STRATIGRAPHY AND STABLE ISOTOPE GEOCHEMISTRY OF THE COMANCHE PLATFORM, SOUTH TEXAS

by

Ryan Matthew Phelps, B.S.; M.S.

Dissertation

Presented to the Faculty of the Graduate School of

The University of Texas at Austin

in Partial Fulfillment

of the Requirements

for the Degree of

Doctor of Philosophy

The University of Texas at Austin

May, 2011

Dedication

To my wife, Carla – for helping me learn things about life, love and strength that others can never teach.

To my son, Nolan Augustus – for helping me to relax through the final months of the dissertation.

To my parents – because this and many other achievements all started with you; and lately I understand you so much more.

To all the Cretaceous critters out there whose prior glory may never be fully recognized.

Acknowledgements

Many deserve my gratitude for their support over the last several years. Thanks to Charlie Kerans for mentorship, professional guidance, and always pushing me into the big picture. To Bob Loucks for daily pearls of wisdom in geology and beyond, Robert W. Scott for helpful reviews and biostratigraphic information. To David Hull, Ryan Harbor, Chris Zahm, Xavier Janson, and Steve Ruppel for productive discussions. To Carla Sanchez for listening to incoherent ramblings about the Cretaceous, while pretending to care.

Thanks to the RCRL consortium, Bureau of Economic Geology, and Jackson School of Geosciences for continual funding, to ConocoPhillips, BHP Billiton, and AAPG Grants-in-Aid for significant research scholarship money, to MJ Systems for deep discounts on raster well-logs.

Middle-Hauterivian to Lower-Campanian Sequence Stratigraphy and Stable Isotope Geochemistry of the Comanche Platform, South Texas

Ryan Matthew Phelps, Ph.D.

The University of Texas at Austin, 2011

Supervisor: Charles Kerans

Carbonate platforms contain a wealth of information regarding the changing biota, sea level, ocean-chemistry, and climate of the Cretaceous Period. The Comanche platform of the northern Gulf of Mexico represents a vast, long-lived carbonate system that extended from west Texas through the Florida panhandle. In central and south Texas, excellent outcrops and an extensive suite of subsurface data provide an opportunity to document the evolution of this system, from the shoreline to the shelf-margin and slope. This study examines the changing facies, platform morphologies, and shelf-margin architectures of the mixed carbonate-siliciclastic, middle-Hauterivian to lower-Campanian interval. Stratigraphic results are integrated with stable-isotope geochemistry to document the detrimental effects of oceanic anoxic events on the carbonate platform.

Seven second-order, transgressive-regressive supersequences of 3-14 Myr duration are defined in south Texas using sequence stratigraphic analysis of shelf-interior facies successions. Second-order supersequences are subdivided into several third-order depositional sequences of 1-3 Myr duration. In these sequences, facies proportions and stratal geometries of the shelf-interior are found to be the result of changing platform morphology and temporal evolution from distally-steepened ramp to rimmed-shelf depositional profiles. Shelf-margin trajectories, stratigraphic architectures, and facies

proportions are a function of long-term accommodation trends expressed in second-order supersequences. These characteristics are modified by lateral variability in the underlying structural/tectonic setting and localized syndepositional faulting.

The stratigraphic equivalents of oceanic anoxic events 1a, 1b, 1d, 2, and 3 are documented in the Cretaceous section of south Texas. These oceanic anoxic events coincided with maximum flooding zones of supersequences and are linked to carbonate platform drowning events on four separate occasions. The occurrence of oceanic anoxic events is found to be a fundamental driver of carbonate platform morphology, faunal composition, and facies evolution in transgressive-regressive supersequences of the northern Gulf of Mexico.

Table of Contents

List of Tables xiii

List of Figures xiv

List of Figures xiv

Chapter 1 – Introduction 1

Dissertation Scope and Relevance 1

DATA DISTRIBUTION 6

PREVIOUS WORK IN THE CRETACEOUS OF SOUTH TEXAS 8

Chapter 2 – Second-Order Supersequences, Shelf Morphology, and Sediment Distribution of the Cretaceous (Hauterivian–Campanian) Passive margin, Northern Gulf of Mexico 12

Abstract 12

Introduction 14

Regional Paleogeography of South Texas 19

Data Distribution and Methodology 23

Cretaceous Lithofacies Associations 27

Terrestrial to Shoreline Siliciclastics 28

Peritidal Mudstone to Grainstone 28

Molluscan Grainstone Shoreface / Shoal 31

Cyclic Subtidal Shelf Wackestone-Grainstone 31

Shelf-Interior Biostrome/Bioherm 33

Rhodolith/Oncoid Rudstone/Floatstone 34

Microbial-Coral-Rudist Shelf margin 34

Slope Detritus 35

Flooded Shelf Mudstone/Wackestone/Chalk 35

Flooded Shelf Shale 37

Sequence Stratigraphy 38

Hosston-Sligo Supersequence (Hauterivian – Early Aptian) 39

Lithofacies Distributions 39

Hosston-Sligo Supersequence Depositional Profile 41
Hosston-Sligo Supersequence Stratigraphy 42
James Supersequence (Early to Middle Aptian) 44
Lithofacies Distributions 44
James Supersequence Depositional Profiles 46
James Supersequence Stratigraphy 48
Bexar Supersequence (Middle Aptian – Early Albian) 49
Lithofacies Distributions 49
Bexar Supersequence Depositional Profile 50
Bexar Supersequence Stratigraphy 51
Glen Rose Supersequence (Early Albian – Middle Albian) 52
Lithofacies Distributions 52
Glen Rose Supersequence Depositional Profiles 55
Glen Rose Supersequence Stratigraphy 56
Fredericksburg Supersequence (Middle to Late Albian) 59
Lithofacies Distributions 59
Fredericksburg Supersequence Depositional Profile 62
Fredericksburg Supersequence Stratigraphy 63
Washita Supersequence (Late Albian – Middle Cenomanian) 65
Lithofacies Distributions 65
Washita Supersequence Depositional Profiles 67
Washita Supersequence Stratigraphy 68
Eagle Ford–Austin Chalk Supersequence (Late Cenomanian – Early Campanian) 70
Lithofacies Distributions 70
Eagle Ford–Austin Chalk Supersequence Depositional Profile .71
Eagle Ford–Austin Chalk Supersequence Stratigraphy 72
Sediment Distribution, Shelf Morphology and the Influence of Relative Sea level 74
Cretaceous Supersequences and the Eustatic Signal 79
Northern Mexico 81

Arabian Plate....82
Eustatic Sea-Level Curves....83
Conclusions....86

Chapter 3 – A Middle Hauterivian to Early Campanian Secular Carbon Isotope Profile from Shallow-Marine Carbonates Linked to Cretaceous Oceanic Anoxia, Northern Gulf of Mexico....89
Abstract....89
Introduction....91
Geologic Setting....94
Stratigraphic Data....94
Isotope Data and Methods....96
Stable Isotope Results....99
Diagenesis of Primary $\delta^{13}C$ Values....99
Vertical Isotope Profiles....102
Humble Oil - Pruitt #46 and Sun Oil - Handy #1....103
Magnolia Petroleum - Mercer #1 and Gulf Oil - Dix #20....103
Shell Oil - Tomasek #1....108
Shell Oil - W. Roehl #1....110
Dixel Resources - Jablonski #1....110
Prairie Producing - Brechtel #1 and Shell Oil - Leppard #1....113
Correlation to Reference Profiles....115
Hauterivian – Barremian Isotope Profiles....116
Aptian Isotope Profiles....119
Albian Isotope Profiles....122
Cenomanian Isoptope Profiles....124
Turonian – Campanian Isotope Profiles....127
OAE Control of Comanche Shelf Drowning Events....129
Early Aptian Drowning Event....130
Late Aptian Drowning Event....133
Late Albian Drowning Event....134

Cenomanian-Turonian Drowning Event....135
Environmental Control of Cretaceous Transgressive-Regressive Supersequences 137
Conclusions....141
Chapter 4 – Temporal and Spatial Variability of a Cretaceous (Albian) Shelf-margin Reef Complex, Stuart City Formation, Northern Gulf of Mexico....145
Abstract....145
Introduction....146
Geologic Background and Data Distribution....149
Facies Assemblage Description and Interpretation....152
Flooded Shelf Facies Assemblage....153
Fore-reef / Slope Facies Assemblage....155
Reef-wall Facies Assemblage....156
Reef-flat Facies Assemblage....160
Back-Reef Facies Assemblage....162
Shelf-Interior Facies Assemblage....163
Core-Based Facies Profiles....165
Stuart City Vertical Profile....165
Stuart City Depositional Profile Variability....167
Supersequence Shelf-margin Models....173
Glen Rose Supersequence Equivalent Reef....174
Fredericksburg Supersequence Equivalent Reef....176
Washita Supersequence Equivalent Reef....178
D eWitt County Cross-Section....178
Bee County Cross-Section....182
Stuart City margin Drowning....185
External Controls on Stuart City margin Deposition....187
Conclusions....192

General Conclusions 195

Supplemental Data 197

References 198

List of Tables

Table 2.1: Core names and outcrops shown in Figure 2.4.…..24

List of Figures

Figure 1.1: Regional paleogeographic map of the Comanche Shelf. 2

Figure 1.2: Stratigraphic column and carbon isotopes of the Comanche Shelf. 3

Figure 1.3: Map of wireline logs available for study. 7

Figure 2.1: Comparison of global Cretaceous carbonate reference sections. 17

Figure 2.2: Stratigraphic column of the Cretaceous in south Texas. 18

Figure 2.3: Map of the Gulf of Mexico.....20

Figure 2.4: Map of south Texas study area and data. 22

Figure 2.5: Regional cross-section along the San Marcos Arch. 26

Figure 2.6: Lithofacies assemblages of the Hosston-Sligo supersequence.....29

Figure 2.7: Lithofacies associations in the James, Bexar and Glen Rose supersequences. 32

Figure 2.8: Lithofacies associations at the Albian shelf margin. 36

Figure 2.9: Regional cross-section of the Hosston-Sligo supersequence. 40

Figure 2.10: Regional cross-section of the James, Bexar, and partial Glen Rose supersequences. 45

Figure 2.11: Regional cross-section of the upper half of the Glen Rose supersequence.. 53

Figure 2.12: Regional cross-section of the Fredericksburg supersequence. 60

Figure 2.13: Regional cross-sections of the Washita and Eagle Ford-Austin Chalk supersequences. 66

Figure 2.14: A separated view of the seven supersequences. 75

Figure 2.15: Chronostratigraphic chart. 80

Figure 3.1: Location of cores used for the stable isotope study.....95

Figure 3.2: The nine $\delta^{13}C$ profiles in a cross-section of the Comanche shelf. 97
Figure 3.3: Plot of carbon- versus oxygen-isotope sample data.. 101
Figure 3.4: Core and stable isotope data for the Handy #1 and Pruitt #46 wells.104
Figure 3.5: Core and stable isotope data for the Mercer #1 well. 106
Figure 3.6: Core and stable isotope data for the Dix #20 well. 107
Figure 3.7: Core and stable isotope data for the Tomasek #1 well. 109
Figure 3.8: Core and stable isotope data for the Leppard #1 and Roehl #1 wells.111
Figure 3.9: Core and stable isotope data for the Jablonski #1 well. 112
Figure 3.10: Core and stable isotope data for the Brechtel #1 well. 114
Figure 3.11: Hauterivian and Barremian $\delta^{13}C$ correlations. 117
Figure 3.12: Aptian $\delta^{13}C$ correlations. 120
Figure 3.13: Albian $\delta^{13}C$ correlations. 123
Figure 3.14: Cenomanian $\delta^{13}C$ correlations.....126
Figure 3.15: Turonian through early Campanian $\delta^{13}C$ correlations. 128
Figure 3.16: Response of the platform to OAEs. 131
Figure 3.17: Correlation of Eagle Ford and Austin Chalk data. 136
Figure 3.18: Phases of environmentally controlled T-R supersequences. 139
Figure 3.19: Composite $\delta^{13}C$ curves for the Comanche Shelf. 142
Figure 4.1: Simplified regional cross-section with the Stuart City margin. 148
Figure 4.2: Shelf margin study area. 151
Figure 4.3: Flooded-shelf and fore-reef/slope facies plates. 154
Figure 4.4: Reef-wall facies plates.....158
Figure 4.5: Reef-flat and back-reef facies plates. 161
Figure 4.6: Back-reef and shelf-interior facies plates. 164
Figure 4.7: Vertical profile of the Stuart City margin. 166

Figure 4.8: Shelf margin symbol key.....168
Figure 4.9: Idealized shelf margin depositional profiles 170
Figure 4.10: Seismic line-tracings across the Stuart City margin.....171
Figure 4.11: Glen Rose supersequence HST depositional model.....175
Figure 4.12: Fredericksburg supersequence depositional model.....177
Figure 4.13: Washita supersequence TST depositional model.....179
Figure 4.14: DeWitt County shelf margin cross-section. 181
Figure 4.15: Bee County shelf margin cross-section. 183
Figure 4.16: Stuart City regime variables ternary diagram.....189

Chapter 1 – Introduction

DISSERTATION SCOPE AND RELEVANCE

Mixed carbonate-siliciclastic strata from the Cretaceous section in south Texas contain world-class examples of broad carbonate shelf and ramp systems developed during first-order transgression and maximum flooding of the Zuni sequence (Sloss, 1963). Most impressive are the extensive Sligo (Hauterivian-Barremian) and Comanche (Albian) shelf systems, however ramp clinoforms in the intervening Pearsall Fm (Aptian) and several overlying Upper Cretaceous formations contain a wealth of information about processes related to shelf drowning and recovery. These units are of great interest for scientific research because the succession south of the Llano uplift (Figure 1.1) is essentially complete with few unconformities, facies assemblages are diverse, and the shoreline to shelf-margin profile is structurally simple. Diverse data types from outcrops and the subsurface are widely available, therefore the opportunity exists to reconstruct temporal changes in the carbonate depositional system and provide links to external forcing mechanisms.

Specific emphasis is placed on establishment of a regional sequence stratigraphic framework, characterization of shelf-margin heterogeneity, and integration of regional results with globally-recognized environmental perturbations (Figure 1.2). Using seismic, well-log, core, outcrop, and stable-isotope data, I address the guiding question:

> *In Hauterivian to Campanian strata of the Sligo and Comanche platforms, how does temporal facies partitioning across the platform interior relate to reef-margin architectural complexity, and to what extent were these relationships influenced by relative sea level fluctuations, antecedent structural-depositional topography, and environmental parameters such as oceanic anoxic events?*

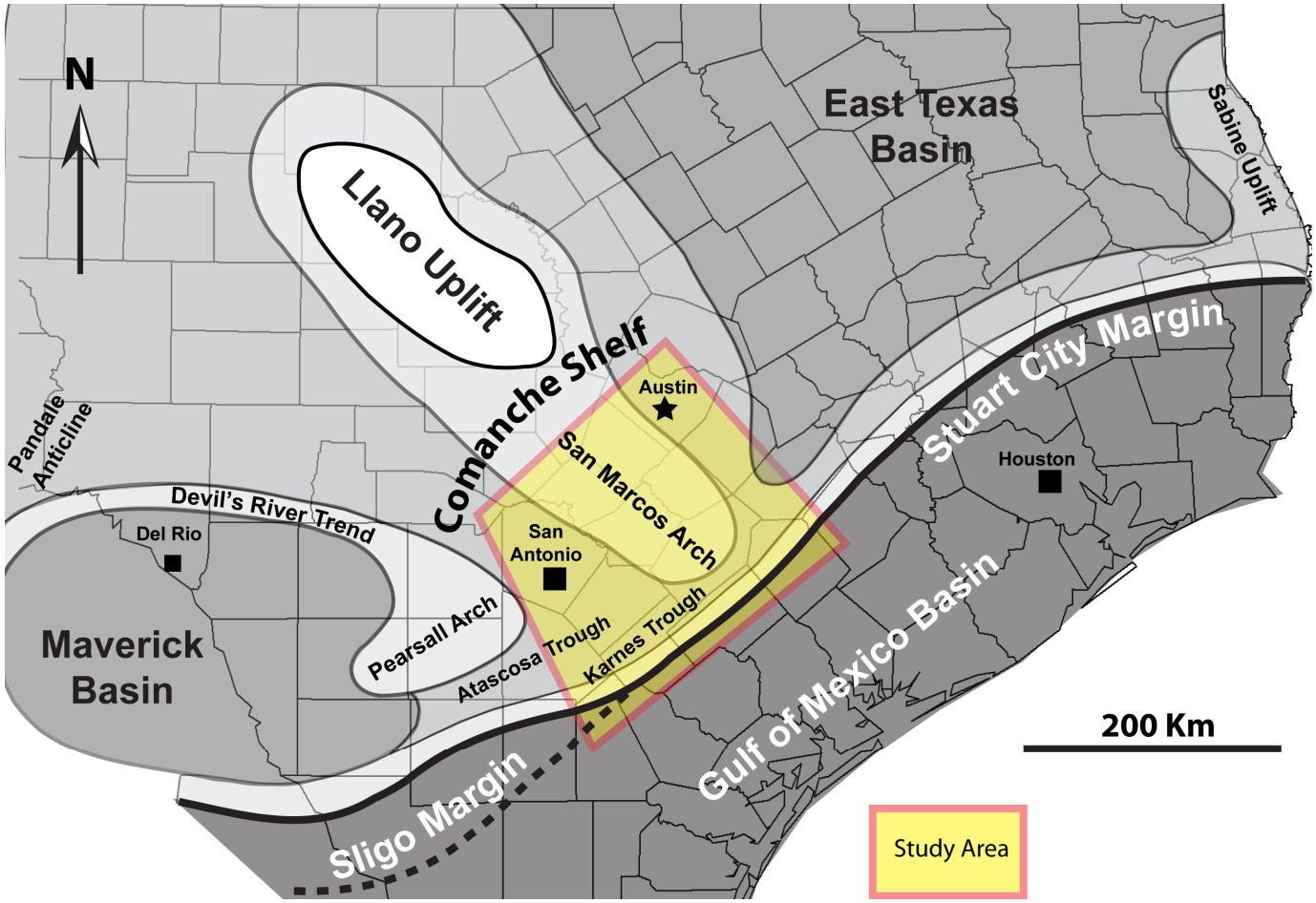

Figure 1.1: Regional paleogeographic map of the Comanche Shelf in south Texas with the area of study highlighted in yellow.

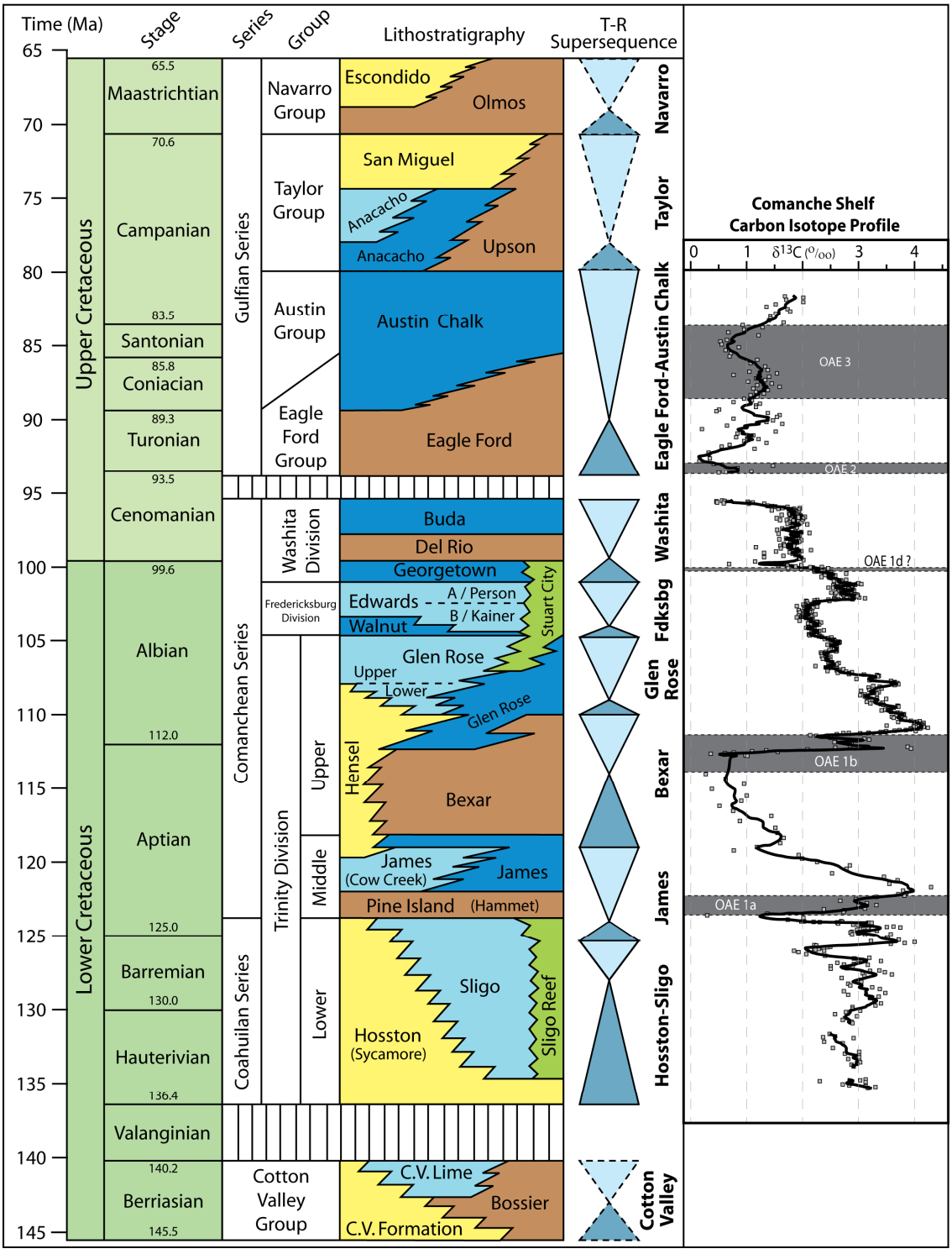

Figure 1.2: Stratigraphic column and carbon isotopes of the Comanche Shelf, with time-scale, lithostratigraphic units, and second-order supersequences.

A central assumption to this broad research question is that shelf-interior facies patterns can indeed be linked to evolution of the shelf-margins. A corollary assumption is that this link is the result of at least one common external factor. Addressing this wide-ranging topic and identification of commonalities requires subdivision of the research effort into three components that are presented in Chapters 2-4. Each of the three main chapters was designed as a stand-alone manuscript destined for submission to external journals for publication.

First, Chapter 2 examines platform interior facies successions and establishes a regional sequences stratigraphic framework at the scale of high-frequency cycle sets, depositional sequences, and supersequences. A set of shoreline to shelf-margin facies cross-sections illustrates the response of platform environments to changing accommodation settings. Delineation of rock-based sequence stratigraphic packages establishes the context necessary to compare the south Texas section to other Cretaceous carbonate provinces. From this point, a relationship is established between supersequences in the present study and those of other platforms, suggesting that eustatic cycles of 3-14 Myr duration were an influential variable affecting platform-scale architecture and facies trends.

Next, Chapter 3 employs vertical carbon isotope profiles reflective of changing global ocean-water chemistry. Prominent excursions and trends of the carbon-isotope profiles allow refined correlation of platform-interior packages to shelf-margin or flooded-shelf intervals that display ambiguous wireline log character. From this perspective, the isotope data are invaluable to the stratigraphic component of the dissertation. Furthermore, I use these profiles to circumscribe precise dates for shelf-interior sequences and their component lithologic units through correlation to European reference sections. Most importantly, these profiles allow demarcation of stratigraphic

intervals which were temporally coincident with global oceanic anoxic events. These global perturbations to the carbon cycle resulted in severe environmental stress, thereby reducing carbonate sedimentation rates. Decreased sediment accumulation rates during OAEs 1a, 1b, 1d, and 2 were combined with periods of eustatic sea level rise outlined in chapter 2 and resulted in drowning of the carbonate platform on four separate occasions. Hence a strong connection is made between eustacy, environmental stress, platform morphologies, and shelf-interior facies trends.

Last, Chapter 4 presents three distinct depositional models for facies and architectural evolution of the Albian Stuart City reef-margin. The depositional models illustrate shelf-margin facies distributions within low-angle shelf, high-angle rimmed shelf, and empty-bucket shelf morphologies of the Glen Rose, Fredericksburg and Washita supersequences. Spatial facies and architectural variability shown in the margin models resulted from antecedent structural/depositional topography of the Sligo Fm and pre-existing tectonic elements of the San Marcos Arch, East Texas Basin, and Maverick Basin. These models are paired with shelf-margin cross-sections to further illustrate the impact of eustatic and structural/tectonic variables on late Albian reef-margin patterns. Drowning of the Stuart City margin at the Albian-Cenomanian boundary is suggested to be the result of eustatic transgression and environmental stress related to OAE 1d. This chapter closes the link between shelf-interior facies patterns, shelf-margin evolution, and the external forcing mechanisms of eustacy, oceanic anoxic events, and regional structural/tectonic heterogeneity.

Results of this study will impact multiple geologic communities, including: (1) carbonate stratigraphers who possess few rock-based examples in which the full spectrum of depositional environments is examined across such a broad carbonate system, (2) those who seek stratigraphic models to expand exploration and production of hydrocarbons in

south Texas, whose past efforts and data enabled this dissertation, (3) geologists seeking additional data to refine the eustatic sea level curve for the Hauterivian-Albian, and (4) chemostratigraphers who have no high-resolution reference section for carbon isotope stratigraphy covering the Hauterivian-Campanian in the Gulf of Mexico, and who generally lack a high-resolution Albian isotope profile as a whole.

DATA DISTRIBUTION

Given the regional scope of this dissertation, the distribution of well-log, core, and outcrop data is of paramount importance. Approximately 4,500 depth-registered raster and digital wireline logs penetrating the top of the Fredericksburg supersequence were available in an area extending from the Maverick Basin to the East Texas Basin (Figure 1.3). For the geographic extent of this project roughly 1,000 of these have been used for regional stratigraphic correlation. Twenty-nine cores from the platform-interior and both shelf-margins were described in feet to facilitate integration with subsurface wireline logs. Most cores are located along the San Marcos Arch, although some are displaced laterally along the Stuart City shelf-margin. Most cores are available for public viewing in BEG core facilities. Additional cores from the Stuart City margin acquired by Pioneer Natural Resources were available for viewing and sampling. Outcrop measured sections within the Glen Rose Formation and Edwards Group are located along Hwy 360 west of Austin and are integrated with core data for regional cross-sections. Visits to Cretaceous outcrop localities in the Texas Hill Country during the course of dissertation research have bolstered the authors understanding of stratal geometries and facies distributions; particularly with respect to the Cow Creek member of the Pearsall Formation and the Fort Terret Formation. Approximately 265 petrographic thin-sections

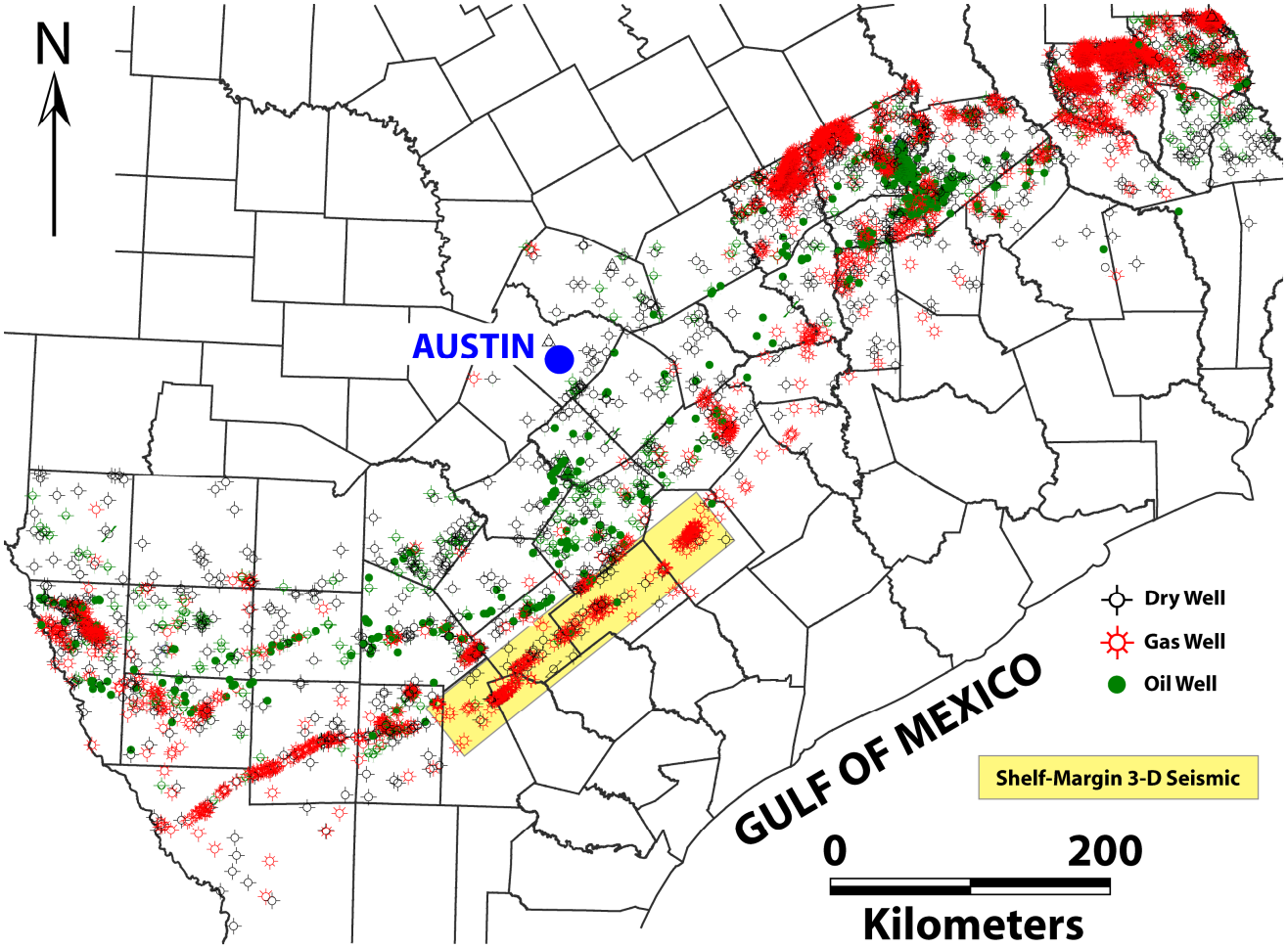

Figure 1.3: Map of south Texas counties and the location of wireline logs available for study. The area highlighted in yellow contains 3-D seismic volumes that were consulted for shelf-margin analysis.

were acquired from core and outcrop intervals to assess allochem composition, confirm hand-sample rock fabric description, and determine the extent of microbial binding in reefal fabrics.

Modern 3-D seismic data volumes (30 Hz dominant frequency) covering approximately one-third of the lower Cretaceous shelf margin and limited 2-D regional seismic lines were available for viewing. The shelf margin 3-D volumes are sufficient to recognize large-scale relationships between the Sligo and Stuart City Margins, as well as to generally document shelf margin progradation patterns, strike variability in the margin, and distal platform-interior stratal geometries.

Eight-hundred and eighty-seven powdered core samples were sent to stable isotope laboratories at the University of Texas at Austin and the University of Miami for carbon and oxygen isotope analysis. The results were assembled into vertical $\delta^{13}C$ and $\delta^{18}O$ isotope profiles for nine cores representing numerous depositional environments and spanning the full study interval. The profiles are fitted with three- or five-point moving averages to smooth curve volatility related to diagenesis of the original isotope ratios.

PREVIOUS WORK IN THE CRETACEOUS OF SOUTH TEXAS

The current level of understanding regarding the regional stratigraphy and character of Cretaceous shelf margins in the south Texas platform is an artifact of the intensive early focus on lithostratigraphy, sedimentology, and diagenesis. A further detriment to coherency in terminology and establishment of high-resolution stratigraphy stems from a general segregation of outcrop and subsurface studies.

In the 1950's and early 1960's, following initial studies focused on applying formation names to lithostratigraphic units, researchers associated with Shell Oil Co. and

the Bureau of Economic Geology began extensive research into the stratigraphic relationships of outcropping units in Central and North Texas. While some authors elaborated on formation nomenclature and description of additional outcrop locales (Lozo and Stricklin, 1956; Lozo et al., 1959; Lozo and Smith, 1964) others linked laterally equivalent formations or mapped porosity and lithofacies relationships in grainstone belts (Moore, 1964; Amsbury, 1965). Fisher and Rodda (1969) began applying depositional systems analysis to Edwards Group carbonates, spurring future workers to interpret formation- and member-level units with respect to the dominant physical or biologic processes, often placing the local interpretation within a larger depositional model and paleogeographic context (Stricklin et al., 1971; Rose, 1972; Perkins, 1974; Scott et al., 1975; Loucks, 1977; Scott et al., 1978; Inden and Moore, 1983).

Formal sequence stratigraphic terminology wasn't used to organize outcrop stratigraphy until the mid 1990's, however previous workers had recognized large-scale transgressive-regressive cycles of the Coahuilan, Comanchean, and Gulfian Series and split these into finer transgressive-regressive divisions, such as the Trinity, Fredericksburg and Washita Divisions (Hill, 1887a; Hill, 1887b; Lozo and Stricklin, 1956). Subsequent re-examination of the outcropping Comanche Shelf resulted in published sequence stratigraphic interpretations ranging in focus from high-frequency cycles to packages on the scale of second-order sequences (Amsbury, 1996; Hovorka, 1996; Moore, 1996; Talbert and Atchley, 2000; Scott et al., 2002; Mancini and Scott, 2006; Ward and Ward, 2007). Many of these interpretations were based on limited study areas or used isolated outcrop successions in the North Texas. The most recent outcrop work has combined detailed sequence stratigraphic mapping with interpretations of depositional environments to establish predictive models of reservoir scale facies distributions (Kerans, 2002; Kerans and Loucks, 2002).

Although subsurface studies Hauterivian-Campanian carbonates in south-central Texas benefited from comparatively widespread amounts of rock, well-log, and seismic data, the study objectives and conclusions have followed a similar path as the outcrop work. Early publications focused on lithostratigraphic formation designation and regional cross-sections intended to demonstrate stratigraphic relationships among equivalent units (Imlay, 1945; Forgotson, 1957; Winter, 1961). Additional work then focused on the depositional environments of ecologic and stratigraphic reef facies in the James, Glen Rose, and Stuart City formations (Achauer and Johnson, 1969; McNamee, 1969; Bebout, 1974; Tartamella, 1982), as well as stratigraphic trends and diagenetic relationships in the Glen Rose Formation and Edwards Group (Rose, 1972; Burkholder and Lumsden, 1973). This line of work climaxed in several publications summarizing the depositional environments, porosity development, paleontology, and geochemistry of subsurface Cretaceous units of the Sligo shelf, Comanche shelf and Stuart City margin (Bebout, 1977; Bebout and Loucks, 1977; Loucks, 1977; Bebout and Schatzinger, 1978; Bay, 1982; Pittman, 1989). Since the broad implementation of sequence stratigraphy, most core-based subsurface studies have primarily been accomplished on a local scale (Zahm et al., 1995; Fitchen et al., 1997; Fritz et al., 2000; Loucks and Kerans, 2003; Waite et al., 2007). On the other hand, regional publications covering the subsurface of south Texas have focused on seismic stratigraphy and well-log interpretation in order to define third-order depositional sequences or paleogeography, generally without incorporating significant core data or drawing conclusions about the finer scale stratigraphy (Winker and Buffler, 1988; Scott, 1993; Yurewicz et al., 1993; Mancini et al., 2008).

Regardless of any potential shortcomings of these previous works, they serve as a foundation for the research discussed in subsequent chapters, particularly with regard to basic sedimentologic description and interpretation of depositional environments. In

addition, excellent case studies have established key stratigraphic relationships and paleontologic databases (Coogan, 1977; Young, 1986; Jiang, 1989; Scott et al., 2002; Waite et al., 2007) have been developed, which are of chief importance for translation of lithostratigraphic units into the sequence stratigraphic realm.

Chapter 2 – Second-Order Supersequences, Shelf Morphology, and Sediment Distribution of the Cretaceous (Hauterivian–Campanian) Passive margin, Northern Gulf of Mexico[1]

ABSTRACT

An integrated sequence stratigraphic study based on outcrop, core, and geophysical data documents the combined impact of Cretaceous eustacy and global environmental perturbations on carbonate shelf morphology, stratal architecture, and shelf-interior to shelf-margin lithofacies distribution in the northern Gulf of Mexico. Regional cross-sections extending across the 200 km-wide, shoreline to shelf-margin profile provide a cycle-scale, continuous record of mixed carbonate-siliciclastic strata for the Hauterivian through lower Campanian stages (~136-80 Ma) of the Sligo and Comanche shelves. The location of the study window on the slowly-subsiding San Marcos Arch in the Gulf of Mexico passive margin allows the stratigraphic response to external forcing mechanisms to be isolated from local/regional tectonic and structural processes.

Significant shifts in shelf-interior depositional environments and changes in platform morphology are associated with second-order supersequence boundaries. Second-order global transgressions that were coupled with the onset of oceanic anoxic events caused termination of the carbonate shelf system and led to deposition of condensed shale units with distally-steepened ramp profiles. Lower Cretaceous supersequence highstands contain a greater abundance of grain-dominated lithofacies and intertidal environments. These include grainstone or siliciclastic sandstone shoreface

[1] Written for submission to *Sedimentology*.

systems within ramp profiles, and intertidal grainstone sand flats or mudstone tidal flats within shelf profiles. Siliciclastic sandstones and conglomerates were generally sequestered along inner-shelf and inner-ramp shorelines but siliciclastic pulses deposited across the platform (Hosston, Hensel, Paluxy, Woodbine formations) are associated with maximum regressions or lowstands of some supersequences. Transgressive-regressive, third-order depositional sequences typical of Cretaceous greenhouse carbonate systems are delineated based on lithofacies proportions and cycle stacking patterns in shelf-interior strata. These depositional sequences are poorly expressed within the shelf-margin and the driving mechanisms were insufficient to cause long-term modifications in shelf-margin trajectory. Permanent shifts in shelf-margin trajectory required greater amplitude, externally forced changes in accommodation at the scale of supersequences.

Correlation of the supersequences observed in south Texas to other basins and previously published global sea level curves demonstrates that these 3-14 Myr events are a result of eustatic sea level changes with amplitudes of 20-60 meters. These second-order eustatic cycles are interpreted as the result of changing volcanism rates along mid-ocean ridges and in large igneous provinces. Depositional sequences are less frequently correlatable among basins but show the highest degree of similarity with eustatic records created from Pacific Guyot sedimentary successions. The diverse lithofacies and abundant data of the Hauterivian to Campanian section in the Sligo and Comanche shelves provide a sensitive record of the external processes affecting carbonate platform development and serve as a nearly complete global reference section for Cretaceous carbonate platforms worldwide.

INTRODUCTION

A unique set of tectonic, climatic and oceanographic conditions persisting during the Cretaceous period (~65-145 Ma) promoted the development of ubiquitous carbonate platforms and profoundly affected their faunal composition, facies assemblages, and stratal architecture. Because carbonate systems are sensitive indicators of changing climate, sea level, and oceanography, Cretaceous platforms are valuable records of this distinctive period in Earth history.

The main catalyst for dramatic changes observed in terrestrial and marine environments during the Cretaceous was intense submarine volcanism along rapidly spreading mid-ocean ridges (Larson, 1991) and in large igneous provinces (Frey et al., 2000). Volcanism increased carbon dioxide concentrations in the atmosphere to values at least four times the modern level and shifted the global climate to that of a greenhouse system with minimal latitudinal thermal gradients (Barron et al., 1993; Huber et al., 2002). Mid-ocean ridge volcanism created a first-order trend of eustatic sea level rise peaking in the Late Cretaceous and changing rates of submarine volcanism are shown to have been the primary driver of the second-order Cretaceous eustatic signal (Hallam, 1971; Hays and Pitman, 1973; Kominz, 1984; Haq et al., 1987; Sahagian et al., 1996; Miller et al., 2004). Lacking a third-order eustatic signal driven entirely by the waxing and waning of polar icecaps (Huber et al., 2002; Miller et al., 2005; Forster et al., 2007), high-frequency lithofacies repetitions in greenhouse Cretaceous platforms predominately consist of meter-scale cycles that commonly aggraded to sea level and were capped by intertidal strata (Goldhammer et al., 1991; Read, 1998). In addition, occurrences of oceanic anoxic events (OAEs) throughout the Cretaceous generally coincide with the emplacement of large igneous provinces (Sinton and Duncan, 1997; Weissert and Erba, 2004). OAEs are shown to have a detrimental effect on carbonate sediment production

and caused deposition of shale condensed sections on carbonate platforms (Follmi et al, 1994; Weissert et al., 1998).

Documenting the combined expression of eustacy and environmental changes in carbonate depositional systems requires a detailed sequence-stratigraphic framework based on integration of multiple data types and a continuous sedimentary record spanning several stages (>10 Myr). Noteworthy sequence stratigraphic studies of Cretaceous carbonate provinces include successions in the Coahuilan, Valles, and Tuxpan platforms of Mexico (Enos, 1988; Lehmann et al., 1999; Janson et al., 2011), the Arabian plate of Oman (Scott, 1990; Immenhauser et al., 2001; Pittet et al., 2002; van Buchem et al., 2002; Hillgartner et al., 2003; Van Buchem et al., 2010), the Maiella, Vercors, and Urgonian platforms of the northern paleo-Tethys (Eberli et al., 1993; Everts et al., 1995; Fouke et al., 1996; Godet et al., 2010), the Egyptian Sinai basin of the southern paleo-Tethys (Bachmann and Kuss, 1998; Bachmann et al., 2003; Bauer et al., 2003), the Sergipe and Campos basins of Brazil (Bertani and Carozzi, 1985; Koutsoukos et al., 1993), and the Maracaibo Basin of Venezuela (Vahrenkamp et al., 1993; De Romero et al., 2003). Here I add to this rich global stratigraphic database by examining the long-term evolution of the passive margin in the northern Gulf of Mexico. The primary goal of the study is to establish a modern sequence-stratigraphic framework for the Hauterivian to early Campanian section in south Texas based on rock, geochemical, geophysical, and paleontologic data while providing a link between lithofacies distribution, shelf morphology, eustacy, and environmental forcing mechanisms. The stratigraphy presented here isolates the response of a carbonate passive margin (McFarlan and Menes, 1991) to the global conditions present during the Cretaceous.

Several characteristics lend the south Texas margin to development as a reference section for Cretaceous carbonate systems. The interval of study exceeds 1,300 meters in

thickness and the time duration covered is on par (~55 Myr) with that of other prominent Cretaceous carbonate reference sections (Figures 2.1 and 2.2). Because the supersequences were deposited on a passive margin, there was minimal influence of regional tectonics on sediment supply or shelf accommodation and no tectonic unconformities are present along the main line of section (McFarlan and Menes, 1991). Post-depositional structural deformation is limited to normal faults within the Balcones, Luling, and Karnes Fault Zones; thus reconstructing the stratigraphic succession from the outcrop belt through the subsurface is a relatively simple task (Ewing, 1991). In addition to numerous exposures in the outcrop belt, subsurface core and wireline log data are available across the shelf profile, creating a well-constrained data set that extends from the shoreline to the shelf-margin.

Several sequence stratigraphic interpretations of the northern Gulf of Mexico have been published, however many of those previous studies are either (1) based on wireline log and seismic data with little or no lithologic information provided (Scott, 1993; Yurewicz et al., 1993; Goldhammer and Johnson, 2001; Mancini et al., 2001; Mancini et al., 2008), or (2) focused on a limited vertical section or confined area of study that does not include the subsurface portion of the platform (Amsbury, 1996; Hovorka, 1996; Moore, 1996; Fitchen et al., 1997; Fritz et al., 2000; Talbert and Atchley, 2000; Kerans, 2002; Kerans and Loucks, 2002; Mancini and Scott, 2006; Ward and Ward, 2007). This sequence-stratigraphic study steps beyond the scope of previous work by (1) using detailed lithofacies information, as opposed to wireline logs or seismic, as a basis for the interpretations, (2) assessing the evolution of the platform throughout the full Cretaceous section, and (3) including data for both the outcrop and subsurface portion of the shelf while integrating changes in the shelf-interior with those of the shelf-margin.

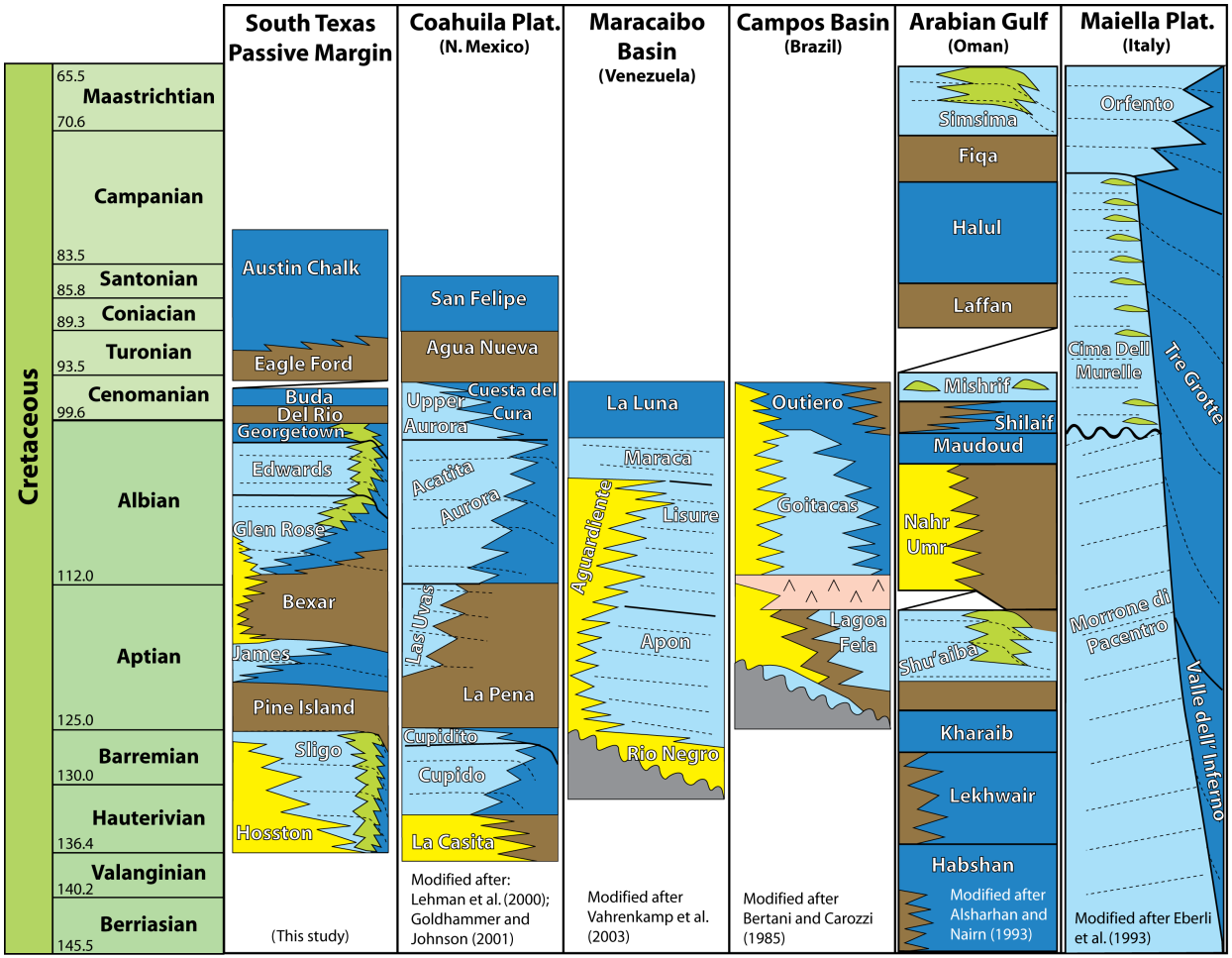

Figure 2.1: Comparison of global Cretaceous carbonate reference sections, including generalized depositional profiles, formations, lithologic distributions, and temporal durations. Note the long-term duration of the south Texas carbonate section relative to many other global platforms.

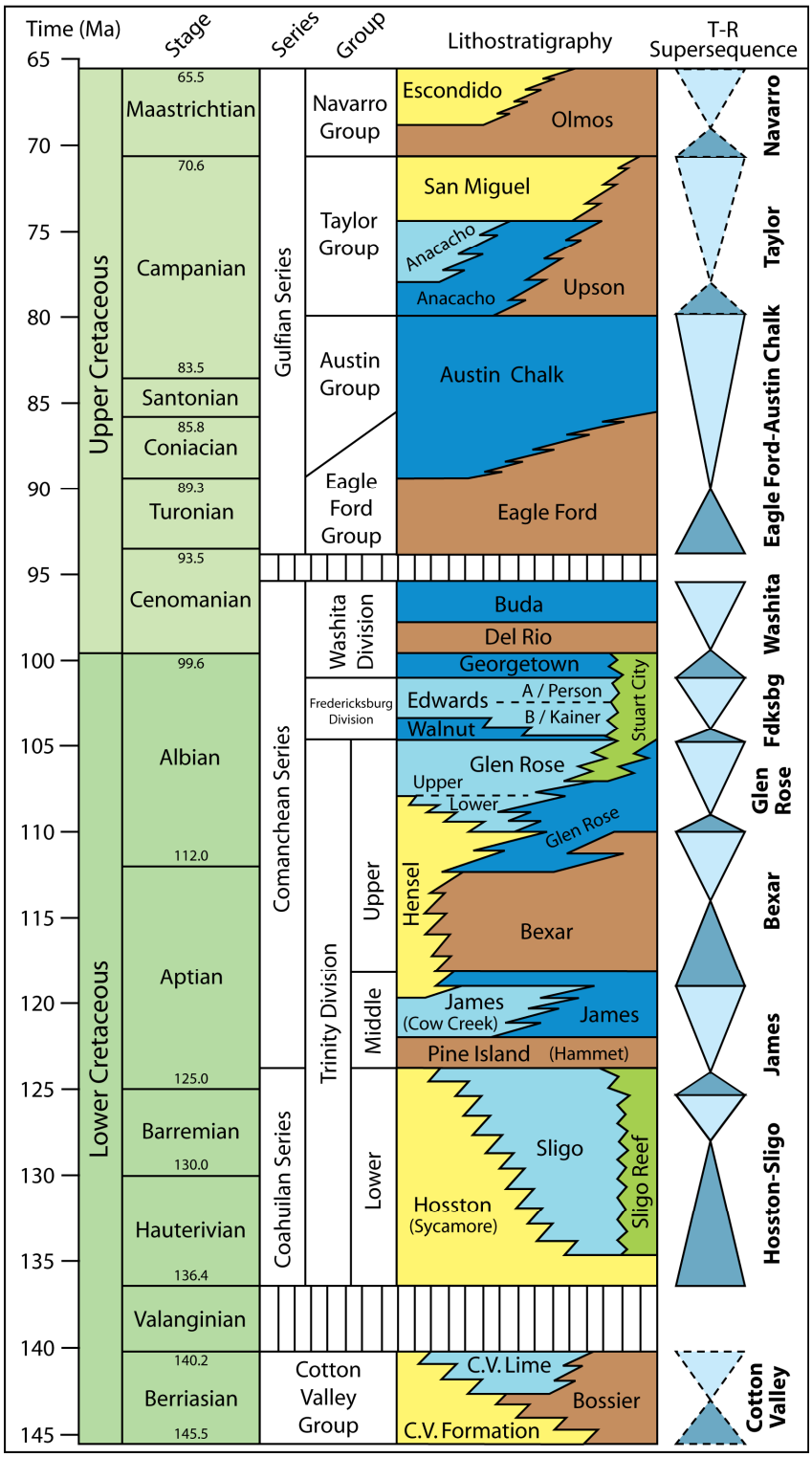

Figure 2.2: Stratigraphic column of the Cretaceous in south Texas, showing

lithostratigraphic units, their lateral relationships, and ages. Ages of stratigraphic units are determined based on correlations of stable isotope data to other global sections (Chapter 3) and previously published data.

Here I present a sequence-stratigraphic framework at multiple scales that is focused on interpretations of shelf-interior facies successions. This framework is related to concomitant changes in shelf morphology and facies patterns across the profile. Parallel trends with other carbonate platforms are noted and universal principles that can be applied to global Cretaceous systems are discussed.

REGIONAL PALEOGEOGRAPHY OF SOUTH TEXAS

Following breakup and rifting of the Pangean supercontinent in late Triassic through early Jurassic time, accumulations of middle to late Jurassic salt exceeding 1,000 meters in thickness were deposited in numerous salt basins throughout the U.S. Gulf of Coast (Salvador, 1991). Many of these salt basins, including the Rio Grande Embayment (Maverick Basin) and East Texas Basins (Figure 2.3), initiated within rift grabens and later acted as zones of increased subsidence and sedimentation throughout the Cretaceous and early Cenozioc (Salvador, 1991). Attenuation of transitional continental crust occurred during the middle and late Jurassic as oceanic crust formed in the center of the Gulf of Mexico Basin (Salvador, 1991; Sawyer et al., 1991). Transitional crust is divided into "thick transitional" crust, which contains blocks of continental crust enveloped by more attenuated regions, and "thin transitional" crust, which is strongly attenuated throughout (Buffler and Sawyer, 1985). Formation of the Lower Cretaceous Sligo and Comanche shelves occurred atop Jurassic ramp sediments lacking a distinct shelf-margin. The terminal locations of both progradational Cretaceous shelf-margins appear to be

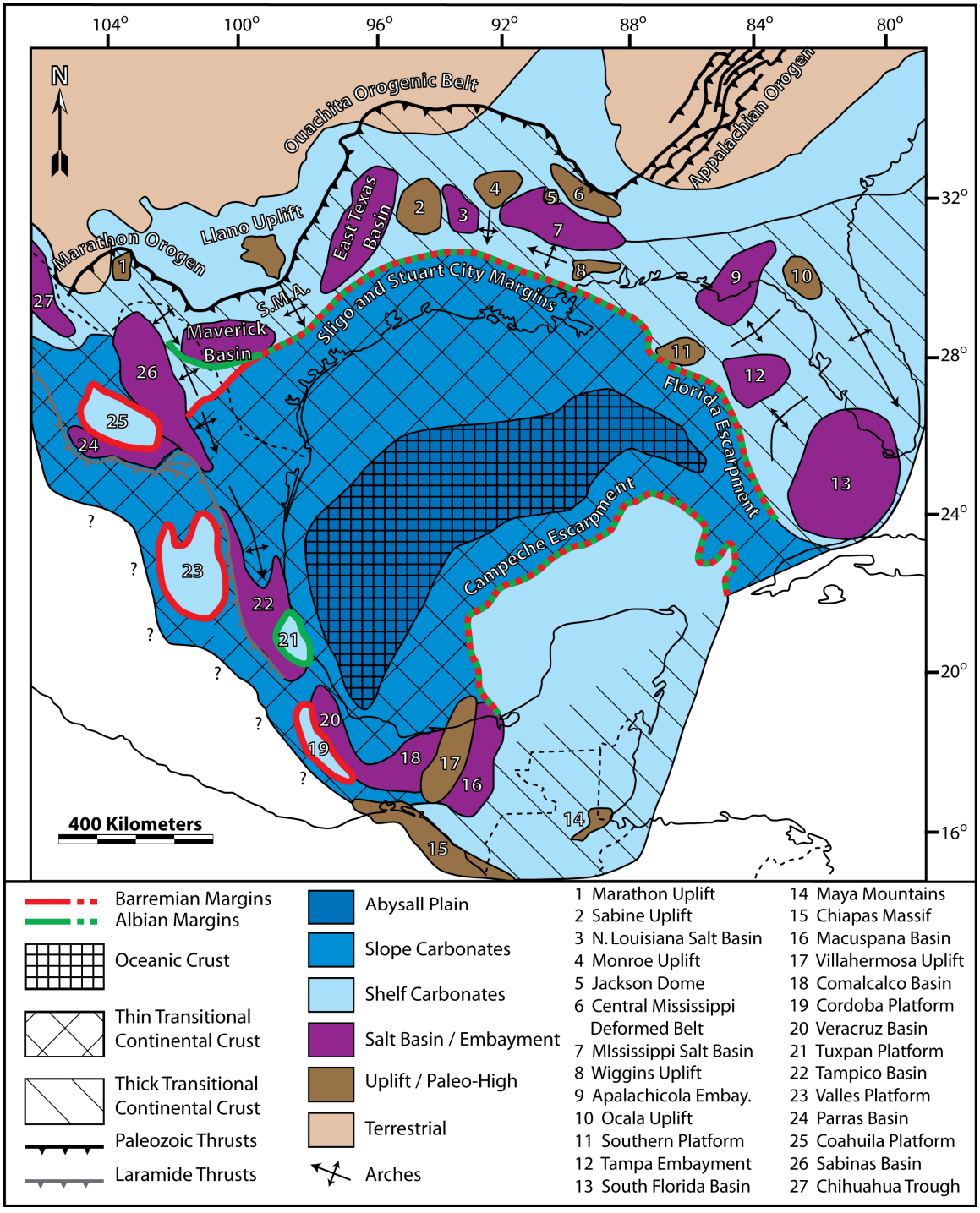

Figure 2.3: Map of the Gulf of Mexico, including modern geography, paleogeography, prominent structural features, salt basins, embayments, and platforms of the Cretaceous. The study area is centered over the San Marcos Arch (S.M.A.)

south of the Llano Uplift and extends to the Sligo and Stuart City shelf margins. The terminal shelf-margin locations are controlled by the tectonic hinge between more rapidly subsiding thin transitional continental crust and more slowly subsiding thick transitional continental crust. Map modified after: Winker and Buffler (1988), Ewing (1991), McFarlan and Menes (1991), Goldhammer and Johnson (2001).

limited by a hinge zone between more slowly subsiding, thick transitional crust and thin transitional crust that displays faster subsidence rates (Winker and Buffler, 1988).

The study area begins approximately 50 km south of the Llano Uplift, trending 150 km along the San Marcos Arch, and across the Sligo and Stuart City (Comanche) shelf-margins (Figure 2.4). The San Marcos Arch is a subsurface extension of granitic and metamorphic rocks of the Llano uplift, serving as an area of decreased subsidence surrounded by zones of greater subsidence in the East Texas and Maverick Basins (Rose, 1972; Ewing, 1991). Because of the lower subsidence rate, systematic shoaling of carbonate lithofacies and more frequent subaerial exposure atop the San Marcos Arch are documented throughout the Cretaceous (Rose, 1972; Dravis, 1980; Young, 1986; Hovorka, 1996).

Faulting contemporaneous with carbonate sedimentation in the Comanche shelf occurred along the Karnes Fault Zone during the late Albian (Rose, 1972). These normal faults caused thickening of Georgetown-age and younger sediments but do not appear to have affected broader sedimentation patterns of the shelf-interior. Post-Cretaceous structural deformation occurred during uplift of the Edwards Plateau and Llano regions through the Oligocene and Miocene (Fullmer and Lucia, 2005). At this time, a series of normal faults with cumulative displacements of 300 to 600 meters formed in the Balcones and Luling Fault zones that overlay the Paleozoic Ouachita orogenic belt (Flawn et al., 1961; Ewing, 1991). Preservation of Cretaceous strata is variable north of the Balcones fault zone, but well-cemented Aptian to Albian carbonates are generally

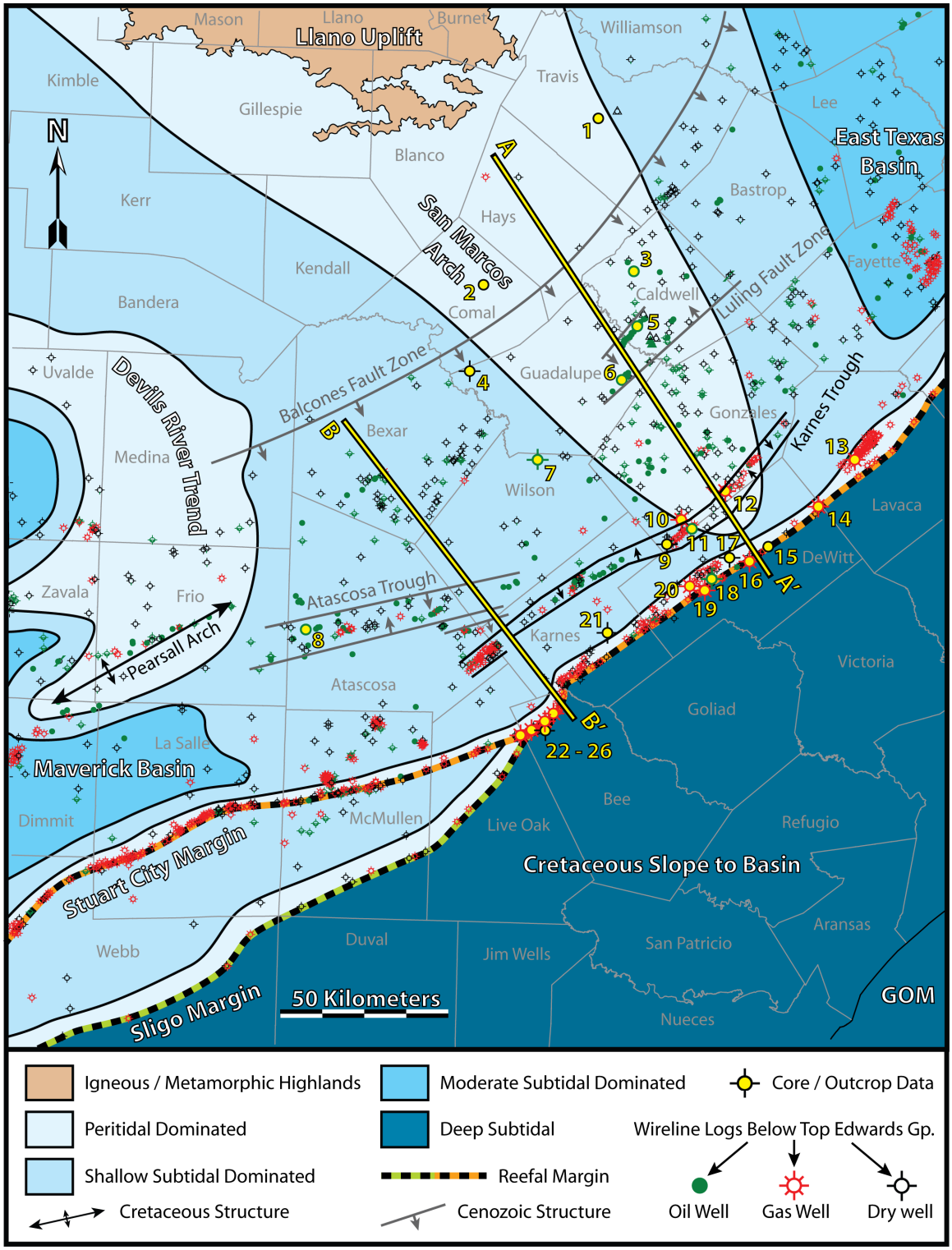

Figure 2.4: Map of south Texas counties, Cretaceous paleogeography, Cretaceous and

Cenozoic structural features, modern extent of the Llano Uplift outcrop and lines of section for the regional cross-sections presented in this manuscript. Information for numbered cores and outcrops is listed in Table 1.1. Well symbols denote the locations of wireline logs penetrating the top of the Edwards Group. Bathymetric zones are generalized and incorporate depositional features found throughout the Cretaceous of south Texas.

preserved, whereas Miocene to Recent erosion has removed most Upper Cretaceous strata (Galloway et al., 1982; Fullmer and Lucia, 2005).

During the Cretaceous, the North American plate drifted northward through paleolatitudes approximately 20 to 30 degrees north of the equator (Scotese et al., 1988). Based on the presence, but not abundance, of evaporites observed throughout the section (i.e., Hosston, Sligo, Glen Rose, Person, and Kainer formations) and the occurrence of caliche profiles along some exposure surfaces (i.e., Hosston, James, Hensel formations), the climate is interpreted to have been semi-arid. Fine- and coarse-grained siliciclastics were sourced from Precambrian to upper Paleozoic granitic, metamorphic, and sedimentary units of the Llano Uplift, Ouachita Mountains, and Marathon Uplift (Figure 2.3) (Flawn et al., 1961; Stricklin et al., 1971; Scott et al., 1975; Talbert and Atchley, 2000).

DATA DISTRIBUTION AND METHODOLOGY

Approximately 1,000 spontaneous potential, resistivity and gamma-ray wireline logs penetrating the top of the Edwards Group, and 100 logs penetrating the top of the Sligo Fm are available for correlation in the study area. Confidential industry seismic data are available across the shelf margin. Log data are integrated with lithofacies information from 26 cores and 15 road-cuts totaling approximately 5,200 meters of section (Figure 2.4; Table 2.1). Because the cores used are commonly 100 meters or

Number	Operator	Lease	County
1	Highway 360 Roadcuts		Travis
2	Canyon Lake Cores	U.S. Corps Eng.	Comal
3	Southern Prod. Co.	Jolly #1	Caldwell
4	Stanolind Oil	Schmidt #1	Guadalupe
5	Magnolia (Mobil)	Mercer #1	Caldwell
6	Gulf Oil Co.	Dix #20	Guadalupe
7	Prairie Producing Co.	Brechtel #1	Wilson
8	Humble Oil & Rfng.	Pruitt #46	Atascosa
9	Gulf Coast et al. (Shell)	Jacobs #1-A	Gonzales
10	Tenneco Oil Co.	Ullman #1	Gonzales
11	Mosbacher	Frisbie #1	Gonzales
12	Superior	Dubose #1	Gonzales
13	Mobil	Kahanek #1	Lavaca
14	Mobil	Boyd #1	DeWitt
15	Pioneer Nat. Res.	Kelley #3-4	DeWitt
16	Pioneer Nat. Res.	Blackwell #1-3	DeWitt
17	Gulf Oil Co.	Mueller #1	DeWitt
18	Dixel Res.	Jablonski #1	DeWitt
19	Shell Oil Co.	W. O. Roehl #1	DeWitt
20	Shell Oil Co.	Respondek #1	DeWitt
21	Sun Oil Co.	Handy #1	Karnes
22	Pioneer Nat. Res.	Schroeder #1	Bee
23	Shell Oil Co.	Leppard #1	Bee
24	Pioneer Nat. Res.	Benham #1-A	Live Oak
25	Shell Oil Co.	Tomasek #1	Bee
26	Shell Oil Co.	Alvarado #1	Bee

Table 2.1: Numbered cores and outcrops shown in Figure 2.4, indicating the well operator, well name, and county.

greater in length, with some exceeding 500 meters, the vertical profiles provide a nearly continuous record of the shelf-interior and shelf-margin response to long-term accommodation changes at a given location.

Core and outcrop data were assimilated to create a cross-section characterizing the full south Texas carbonate succession for the Cretaceous (Figure 2.5), which has been divided into 5 intervals displayed in six cross-sections. Each cross-section is datumed from a sequence boundary or a lithostratigraphic surface that is regionally extensive and presumed to approximate a nearly horizontal depositional timeline. With the exception of one upper Cretaceous cross-section along B-B', all cross-sections follow line A-A' (Figure 2.4). Wireline logs spread along the line of section were used to constrain correlations between core and outcrop intervals. Nine carbon isotope profiles (Chapter 3) that record isochronous changes in global Cretaceous ocean-water chemistry (Scholle and Arthur, 1980) were used to constrain correlations of cyclic shelf-interior successions to shelf-margin intervals that lack a detailed wireline log signature. Estimated ages of sequence stratigraphic and lithostratigraphic boundaries listed in the manuscript are derived from comparison of the south Texas carbon isotope profile with well-dated reference profiles (Chapter 3). Additional ages are incorporated from published biostratigraphic studies (Jiang, 1989; Scott et al., 2000; Scott et al., 2002).

Interpretations of high-frequency cycles (fifth-order) were recorded during description of lithologic units. The majority of high-frequency cycles (HFCs) are inferred to be asymmetric and shallow-upward as deduced from one or more of the following trends: (1) an upward decrease in mud within rock texture, (2) an upward increase in hydrodynamic sedimentary structures, (3) an upward increase in grain size and sorting, (4) shallowing of peritidal biogenic and sedimentary structures (Ginsburg et al., 1977), (5) a change from horizontal, argillaceous *Planolites*-burrowed facies to vertical,

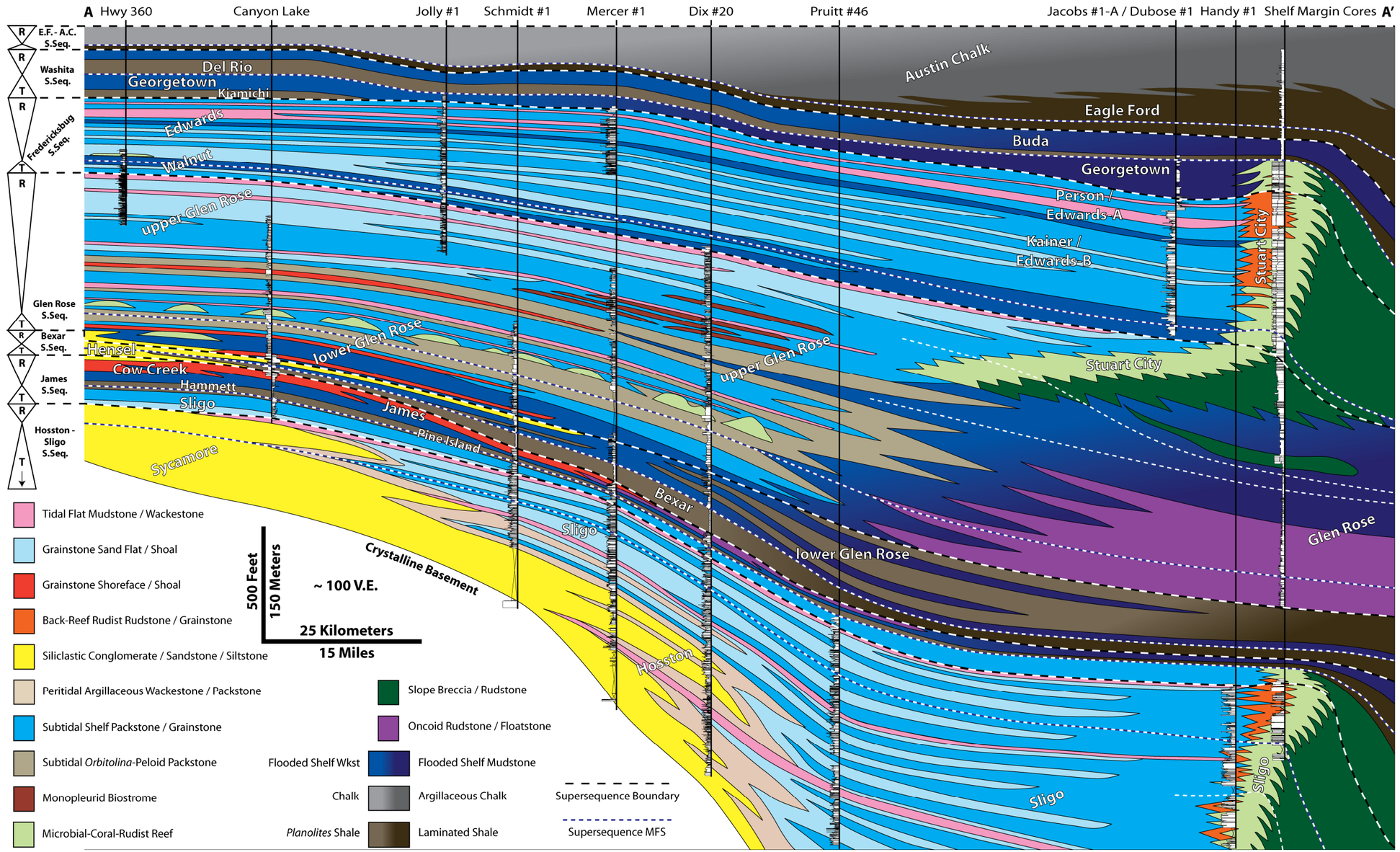

Figure 2.5: Regional cross-section along the San Marcos Arch extending from the middle Hauterivian through the lower Campanian. The top of the Austin Chalk Group is used as a datum. T-R supersequences are shown at left. The cross-section was constructed using selected outcrop and core intervals (descriptions in white), wireline logs (not shown), and stable isotope profiles (Chapter 3).

Thallasinoides-burrowed units lacking terrigenous fractions, and (6) changes in faunal assemblages. Most HFCs throughout the succession were deposited entirely in a subtidal environment with few aggrading into a peritidal setting (*sensu* Folk, 1973). HFC sets, and in some examples high-frequency sequences (fourth-order), were identified using lithofacies proportions and cycle stacking patterns within vertical outcrop and core profiles (Goldhammer et al., 1990; Mitchum and Van Wagoner, 1991; Kerans and Tinker, 1997).

At the scale of depositional sequences, rapid basinward and landward shifts in facies are a rare occurrence in greenhouse systems (Lehrmann and Goldhammer, 1999; Read, 1998). Instead, changing lithofacies proportions between successive HFC sets, their progradational to retrogradational stacking patterns across the shelf profile, and the frequency of short-term exposure surfaces were used to define transgressive-regressive depositional sequences (Embry and Johannessen, 1993) of third-order (~1-3 Myr) duration (Lehrmann and Goldhammer, 1999). Second-order supersequence boundaries (~3-14 Myr duration) are delineated based on significant facies shifts across the shelf, prominent changes in shelf-margin trajectory, and regional exposure surfaces represented by caliche profiles, soil zones, or karst horizons.

CRETACEOUS LITHOFACIES ASSOCIATIONS

Ten lithofacies associations are representative of the full Cretaceous depositional system in south Texas. Lithofacies forming each association are briefly described and interpreted. Water depths listed for each lithofacies association are estimated based on the vertical distance to overlying intertidal units.

Terrestrial to Shoreline Siliciclastics

Lithofacies in this siliciclastic assemblage are dominated by terrigenous sediment ranging in grain size from mixed clay and silt, to very-fine and fine sand, to pebble-size quartz. In areas proximal to the Llano Uplift, the Sycamore, Hosston, and Hensel formations consist of variably colored shales, fine- to coarse-grained sandstones, and conglomerates. Based on poor sediment sorting, channel-form geobodies, and the presence of large boulders, previous workers have interpreted these facies as alluvial to fluvial in origin (Stricklin et al., 1971; Amsbury, 1974; Inden and Moore, 1983).

Distally, the Hosston and Hensel formations contain mixed siliciclastic sandstones, siltstones, and claystones that are typically rippled, laminated, cross-bedded, massive, burrowed, or churned, and may exhibit bi-directional cross-stratification, flaser laminae, mud drapes, sandstone lenses, and mudcracks (Figure 2.6). Hensel Fm marine sandstones contain variable glauconite concentrations. As suggested by Bebout (1981), sedimentary structures indicative of tidal influence, combined with the lateral proximity of these facies to carbonate peritidal units and caliche profiles suggest they were deposited in shoreface, tidal flat, or nearshore environments. Water depth ranges may have been on the order of zero to five meters and were above fair-weather wave-base.

Peritidal Mudstone to Grainstone

The unifying characteristic of this carbonate lithofacies assemblage is the presence of sedimentary structures indicating tidal influence and deposition in a peritidal setting. Argillaceous-skeletal-peloidal wackestones/packstones are often burrowed and contain sporadic plant fragments (Figure 2.6). Oxidation/reduction mottling along burrow margins and planar laminae of terrigenous silt to clay may be present. This facies was

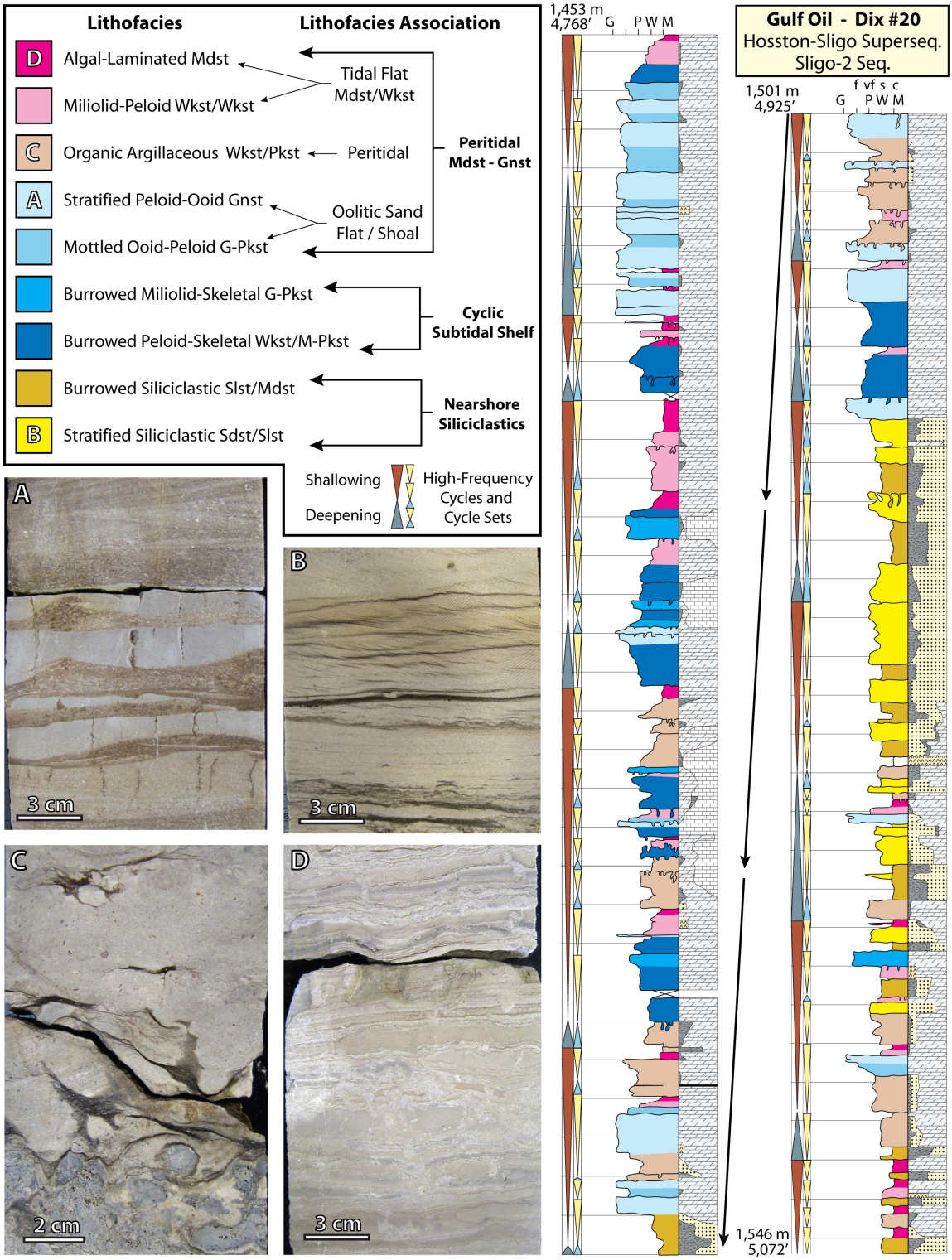

Figure 2.6: Lithofacies assemblages of the Hosston-Sligo supersequence. At right is a

partial core description of the Dix #20 core within the Sligo-2 depositional sequence. At top left is a lithofacies key with interpreted depositional environments and lithofacies associations discussed in the text. At bottom left are (A) cross-stratified grainstones with mudstone flasers representative of intertidal sand flats, (B) cross-bedded and rippled very-fine grained sandstones with clay drapes from the Hosston Fm, (C) burrowed peritidal, argillaceous mud-dominated wackestone and packstone of the Hosston Fm, and (D) mud-cracked, wavy and pustular algal-laminated mudstones of Sligo Fm tidal flats.

likely deposited in a very shallow-subtidal to lower intertidal environment (< 1 m) and is laterally transitional with more proximal nearshore siliciclastics.

Carbonate mudstones/wackestones (Figure 2.6) are massive, wavy or pustulose algal-laminated, with oxidized burrow margins, polychaete worm burrows, fenestrae, and root tubules characteristic of modern, low-energy tidal flat environments (Ginsburg et al., 1977). Bored firmgrounds are common and no visible terrigenous clay or silt is present. This facies is interpreted as lower-intertidal to supratidal and is present throughout the lower Cretaceous section.

Mixed grain-dominated packstones/grainstones are rippled, cross-bedded, and laminated with carbonate mud flasers, intraclasts, and iron-stained, bored firm-grounds (Figure 2.6). Skeletal grains and ooids are dominant in the Sligo Fm, while peloids, miliolids and gastropods are dominant in the Glen Rose Fm and Edwards Group. This facies is vertically and laterally mingled with tidal flat mudstones/wackestones and is interpreted to represent high-energy, intertidal sand flats or shoal systems.

Commonly, the preceding peritidal lithofacies are sparsely inter-bedded with thin-bedded and nodular anhydrite. Also present are 5-cm to 1-meter thick, polymictic breccias with centimeter- to decimeter-scale mudstone, grainstone, gypsum, and silicified evaporite lithoclasts. These units are laterally continuous for tens of kilometers, bundled with intertidal grainstones and mudstones, and are interpreted as solution collapse

breccias possibly representative of evaporite dissolution by meteoric water during subaerial exposure of overlying peritidal strata.

Molluscan Grainstone Shoreface / Shoal

Echinoid, gastropod, bivalve, and oyster debris, listed in increasing order of abundance, are the primary constituents in land-attached, cross-bedded grainstone and coquina lithofacies of the Cow Creek and James Members of the Pearsall Fm (Figure 2.7). Corals are rare. Previous workers have extensively documented the interpretation of these grainstone complexes as a high-energy, progradational shoreface system (Lozo et al., 1958; Inden and Moore, 1983; Kerans and Loucks, 2002). In the outcrop belt, upper-shoreface clinoforms are mixed with minor quartz sand and quartz pebbles (Inden and Moore, 1983). Similar echinoid-mollusk fauna are mixed with serpulid worm-tube clusters in biostromes and shoals of the Lower Glen Rose Member. Molluscan grainstone lithofacies spanned from supratidal to 5-10 m depths.

Cyclic Subtidal Shelf Wackestone-Grainstone

Lithofacies in this assemblage contain assorted allochems, varied fauna, and range from wackestone, to mud- and grain-dominated packstone, to grainstone (Figure 2.7). Facies include: (A) peloid, concentric coated-grain, miliolid grainstone, (B) microbial coated-grain, peloid packstone, (C) skeletal, miliolid, peloid wackestone/packstone, (D) argillaceous, skeletal wackestone/packstone, (E) *Orbitolina*, peloid packstone, and (F) echinoid-oyster wackestone/packstone. Dasycladacean green algae and mollusk fragments are present. Lithofacies B and C are usually *Thallasinoides*-burrowed, whereas facies D-F are usually *Planolites*-burrowed. Facies D-F may have up to 50% terrigenous

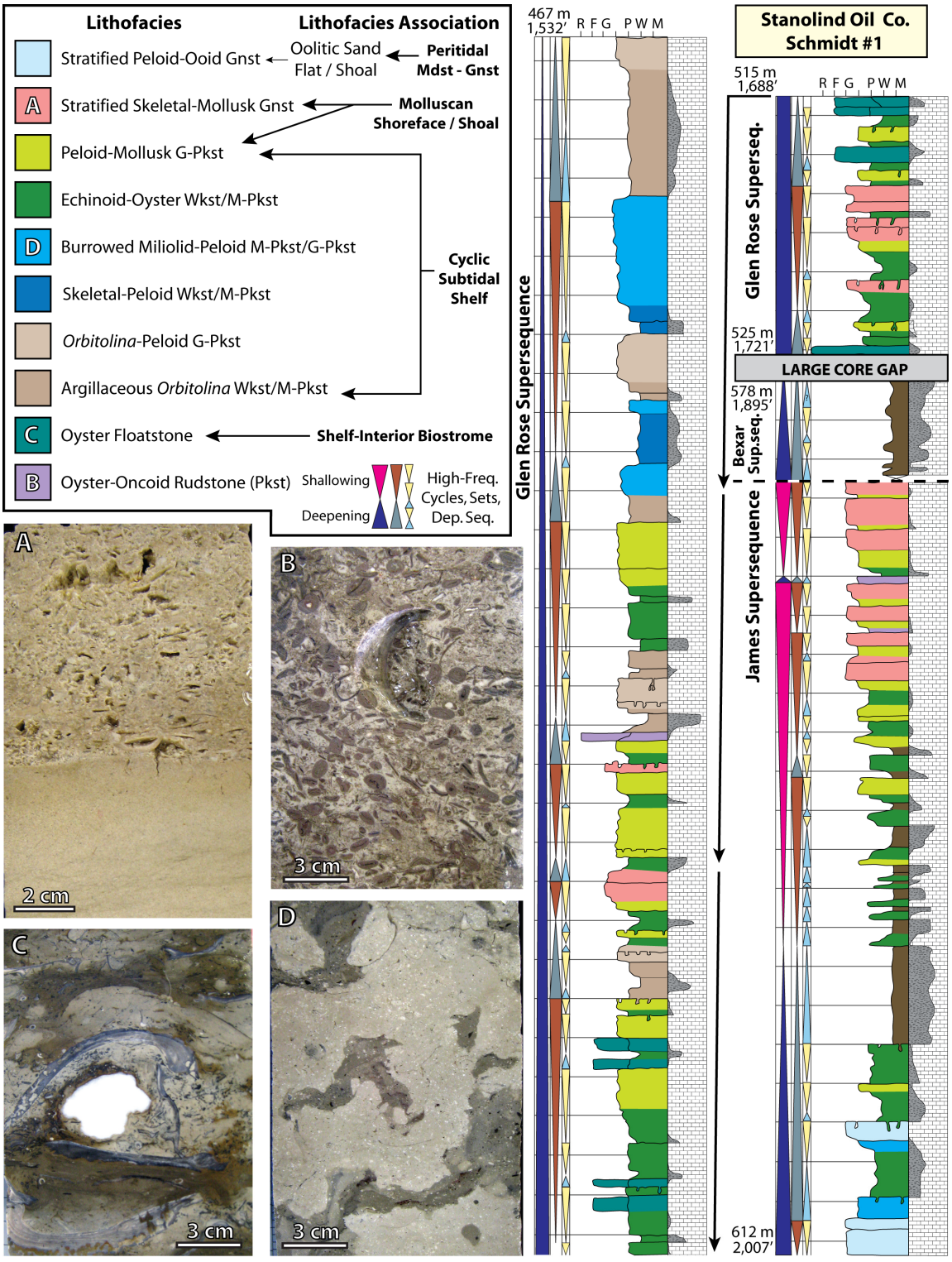

Figure 2.7: Lithofacies associations in the James, Bexar and Glen Rose supersequences

and a partial core description and lithofacies key for the Schmidt #1 core. Below the gap in the core description are strata representative of the James supersequence (Sligo Fm, Pine Island and James Members of Pearsall Fm) and lowermost shales of the Bexar supersequence. Above the core gap are strata from Lower Glen Rose Member of the Glen Rose supersequence. At bottom left are example photos from nearby cores of (A) molluscan grainstones and coquinas of the James supersequence, (B) oncoid rudstones with a packstone matrix in the James supersequence, (C) Planolites-burrowed oyster floatstones, serpulid worm tubes and nodular anhydrite within an oyster biostrome of the Glen Rose supersequence, and (D) burrowed miliolid-peloid mud-dominated packstones of the cyclic subtidal shelf in the Glen Rose supersequence.

clay matrix, contain serpulid worm-tube clusters, and are interpreted as deeper and more open-marine than lithofacies A-C. Peritidal sedimentary structures are absent, burrowing is common to pervasive, and relative sea level may have controlled vertical lithofacies cyclicity. For these reasons the facies are interpreted as shallow- to moderate-subtidal in origin, possibly ranging from 1 meter of water depth in restricted settings to approximately 20 or 30 meters (above storm wave-base) in open-marine settings.

Shelf-Interior Biostrome/Bioherm

Lithofacies in this assemblage are constrained to the shelf-interior and do not include shelf-margin strata. Examples contain a high-density of the component macrofauna, may construct strata of positive relief above the surrounding lithofacies, and exhibit bindstone, bafflestone, and floatstone fabrics. Bioherms of the lower Glen Rose consist of coral-stromatoporoid-toucasid-caprinid bafflestone/bindstone and developed 2-5 meters of synoptic relief. Biostromes of monopleurid bafflestone and caprinid-toucasid bafflestone were laterally continuous for 10's of kilometers, but the shallow-subtidal setting limited their vertical relief. Toucasid-oyster-chondrodont bafflestones/floatstones (Figure 2.7) generally contain mud-dominated matrix sediment and were deposited in

low-energy settings. Water depths for biostromal/biohermal facies likely ranged from 1-20 m (Perkins, 1974).

Rhodolith/Oncoid Rudstone/Floatstone

Oncoid rudstones with 2-10 mm diameter oncoids in an argillaceous, molluscan packstone matrix are offshore equivalents of the James (Cow Creek) shoreface grainstone clinoforms (Figure 2.7). Oncoid rudstones of the Sligo and Georgetown Formations are up to 5 cm in diameter, contain variable rudist fragments, and are located directly landward of the Sligo and Stuart City margins. Rhodolith rudstones, with 1-4 cm diameter rhodolites, are only encountered in the lower Glen Rose member and are associated with *Orbitolina*-peloid packstones. Rhodoloith/oncoid rudstones were deposited above storm wave-base, likely in 5-20 meters (16-66 ft) of water depth. Oncoid floatstones with a mudstone/wackestone matrix and accessory globigerinids are found in distal, deep-subtidal (50-100 m-deep) portions of Glen Rose Fm clinoforms.

Microbial-Coral-Rudist Shelf margin

Sligo and Stuart City shelf margin lithofacies include microbial-coral-rudist reef bafflestones, bindstones and framestones (Winter, 1961; Bebout, 1974; Bebout 1977; Scott, 1990; Waite et al. 2007; Chapter 4). Fauna consist of abundant caprinid, requienid, and radiolitid rudists accompanied by common coral, Solenapora red algae, stromatoporoids, calcitic sponges, mollusks, dictyoconid foraminifera, and the microbial binder *Lithocodium-Bacinella*. Vertical reef fabrics and bored hard-grounds are common. Early marine cements are abundant and syndepositional fractures are common, indicating rapid cementation of reefal sediments and over-steepening of the reef-wall.

Rudist-dominated lithofacies of the reef-flat were the source of back-reef, rudist grainstone/rudstone with fining-upward grain size profiles and abundant early marine cements (Figure 2.8). Interpreted as semi-continuous storm berms and shoal complexes, rudist grainstone/rudstone lithofacies accumulated above the surrounding environments and contain pendant cement zones indicative of brief subaerial exposure.

Slope Detritus

Each of the following lithofacies was deposited seaward of the Sligo and Stuart City shelf margins on the middle to upper slope. Polymictic breccias with angular 1-15 cm-scale clasts of skeletal grainstone and microbial-coral-rudist reef lithofacies contain a mud-dominated matrix and generally lack sedimentary structures or grading. They are interpreted as upper slope debrites and talus aprons sourced from collapse of the Sligo and Stuart City reef-margins.

The rudist-skeletal grainstone/rudstone lithofacies contains robust caprinid rudists and accessory coral cobbles that are overturned and battered. Matrix grainstones are cross-stratified and medium- to coarse-grained. This facies is overlain by microbial-coral-rudist reef lithofacies and is interpreted as detrital sediment on a high-energy, low-angle fore-reef or upper slope. *Planolites*-burrowed, very fine-grained, skeletal and peloidal wackestones/packstones are distal of the fore-reef and represent a middle-slope setting.

Flooded Shelf Mudstone/Wackestone/Chalk

Lithofacies in this assemblage contain fauna indicative of deep-subtidal depositional environments, such as calcispheres and globigerinid foraminifera. Rock fabrics include lime mudstone and skeletal-peloidal wackestone, both of which may be

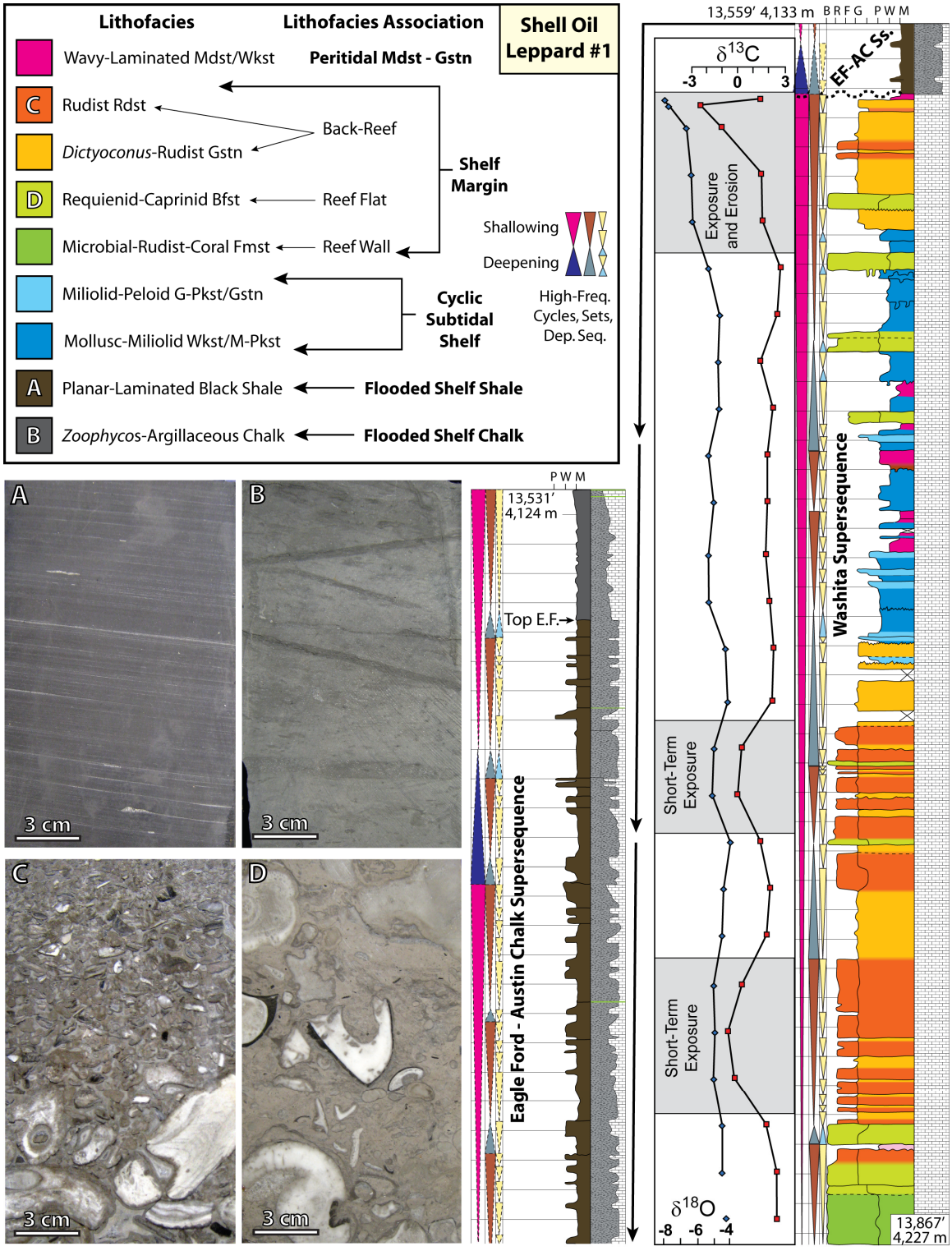

Figure 2.8: Lithofacies associations at the Albian shelf margin and a partial core

description of the Leppard #1 core. Shown are shelf-margin and flooded shelf shale to chalk lithofacies of the Stuart City Fm, Eagle Ford Group and Austin Chalk Group. Stable isotope data (scales in per-mil notation relative to VPDB standard) within Geogetown-equivalent strata of the Stuart City margin are shown for the Washita supersequence. Negative excursions greater than 1 ‰ in both $\delta^{18}O$ and $\delta^{13}C$ are shaded with grey boxes and indicate zones of likely subaerial exposure and meteoric diagenesis. Short-term exposure (<20 ka) occurred in back-reef rudstone/grainstone complexes, while long-term exposure (>40 ka) on top of the Washita supersequence at the Mid-Cretaceous unconformity eroded the flooded shelf shales and mudstones of the Del Rio and Buda Fms prior to deposition of the Eagle Ford – Austin Chalk supersequence. At bottom left are (A) planar laminated black shales of the Eagle Ford Group, (B) *Zoophycos*-argillaceous chalk of the Austin Chalk Group, (C) rudist rudstones with a fining-upward grain size profile and thin, black rinds of pendant cement (black) at the base of some grains, and (D) requienid-caprinid bafflestone of the reef-flat in the Stuart City margin.

argillaceous, pyritic, and *Thallasinoides*- or *Planolites*-burrowed. Deposition was below storm wave-base on a flooded shelf under water-depths likely exceeding 50 meters. Austin chalk lithofacies include glauconitic, *Planolites*-burrowed chalk consisting of abundant coccolithophorids, accessory globigerinids, and Inoceramus bivalve fragments, as well as a more distal *Zoophycos*-burrowed, argillaceous chalk with similar faunal assemblages (Figure 2.8). Outcrop-belts and tunnels within the Austin Group locally display meter-scale erosive channels, debris flows, and turbidites containing bored intraclasts, all of which indicate down-dip sediment transport (Dravis, 1980; Hovorka and Nance, 1994).

Flooded Shelf Shale

Four lithofacies in this assemblage contain less than 50% carbonate mud and are dominated by terrigenous clay and organic-rich sediment. Proximal oyster-shale of the Del Rio Fm contains reworked lags of *llymatogyra arietina* and *Exogyra cartledgei*

oysters and the agglutinated foraminifera *Cribratina texana* (Lock et al., 2007). The Pine Island and Bexar Members of the Pearsall Fm, as well as distal portions of the Del Rio Fm, consist of *Planolites*-burrowed shale with rare oyster fragments, plant fragments, pyrite, and serpulid worm tubes. Landward, carbonate-rich lenses of gastropod and skeletal debris are interpreted as runnels of dilute turbidites. Rare ammonites increase in abundance down depositional dip and burrowing decreases (Loucks, 1976). This facies contains globigerinid foraminifera in the lowermost Bexar Member (Loucks, 1976; Amsbury, 1996) and the Del Rio Fm.

Eagle Ford shale lithofacies include planar-laminated black shale (Figure 8) found in more basal and distal portions of the succession, and a more proximal lithofacies consisting of intercalated, planar-laminated, calcareous silt and shale. Centimeter-scale bentonite horizons are scattered throughout the Eagle Ford cores. Planktonic globigerinid foraminifera are commonly present in the Eagle Ford and are accompanied by bivalve and echinoderm fragments (Dawson, 1997). Planar laminations of the Eagle Ford are interpreted to be the result of hemi-pelagic deposition and sediment transport by dilute turbidites.

SEQUENCE STRATIGRAPHY

Seven transgressive-regressive (T-R) supersequences recognized in the Hauterivian to lower Campanian portion of the south Texas passive margin are termed the Hosston-Sligo, James, Bexar, Glen Rose, Fredericksburg, Washita, and Eagle Ford-Austin Chalk supersequences (Figures 2.2 and 2.5). The following sections of this investigation detail the internal characteristics of each supersequence, including the component lithostratigraphic units, lithofacies association distributions, depositional

environments, stratal geometries, platform-scale morphologies, and the character of higher-order depositional sequences.

Hosston-Sligo Supersequence (Hauterivian – Early Aptian)

Lithostratigraphic units found in the Hosston-Sligo supersequence include the siliciclastic-dominated Hosston (subsurface) and Sycamore (outcrop) formations, combined with the mixed dolostone/limestone Sligo Fm (Lozo and Smith, 1964). The supersequence overlies several Precambrian to Paleozoic granitic, metamorphic and sedimentary units taken here as the "basement" of the Cretaceous system (Flawn et al., 1961). The contact between the Hosston and Sligo formations (Figure 2.9) is diachronous and the two units interfinger along the depositional dip profile (Stricklin et al., 1971; Bebout et al., 1981). Ewing (2010) interpreted deltaic and shoreline sands in a basal Hosston sandstone package that extended across the previously exposed shelf of the underlying Cotton Valley Group (Tithonian-Berriasian). This Valanginian/Hauterivian unconformity is used as the lower boundary of the Hosston-Sligo supersequence.

Lithofacies Distributions

Hosston Fm nearshore siliciclastics directly overlay basement metamorphic rocks and extend from the outcrop belt into undescribed portions of the Schmidt #1 core. Approximately 2 to 3 meters of conglomeratic sandstone present at the base of the Mercer #1 and Dix #20 cores are likely the result of basement exposure and transgressive ravinement. Tidally-influenced nearshore siliciclastics are interbedded with argillaceous, peritidal wackestone/packstone and carbonate tidal flat mudstone/wackestone. The

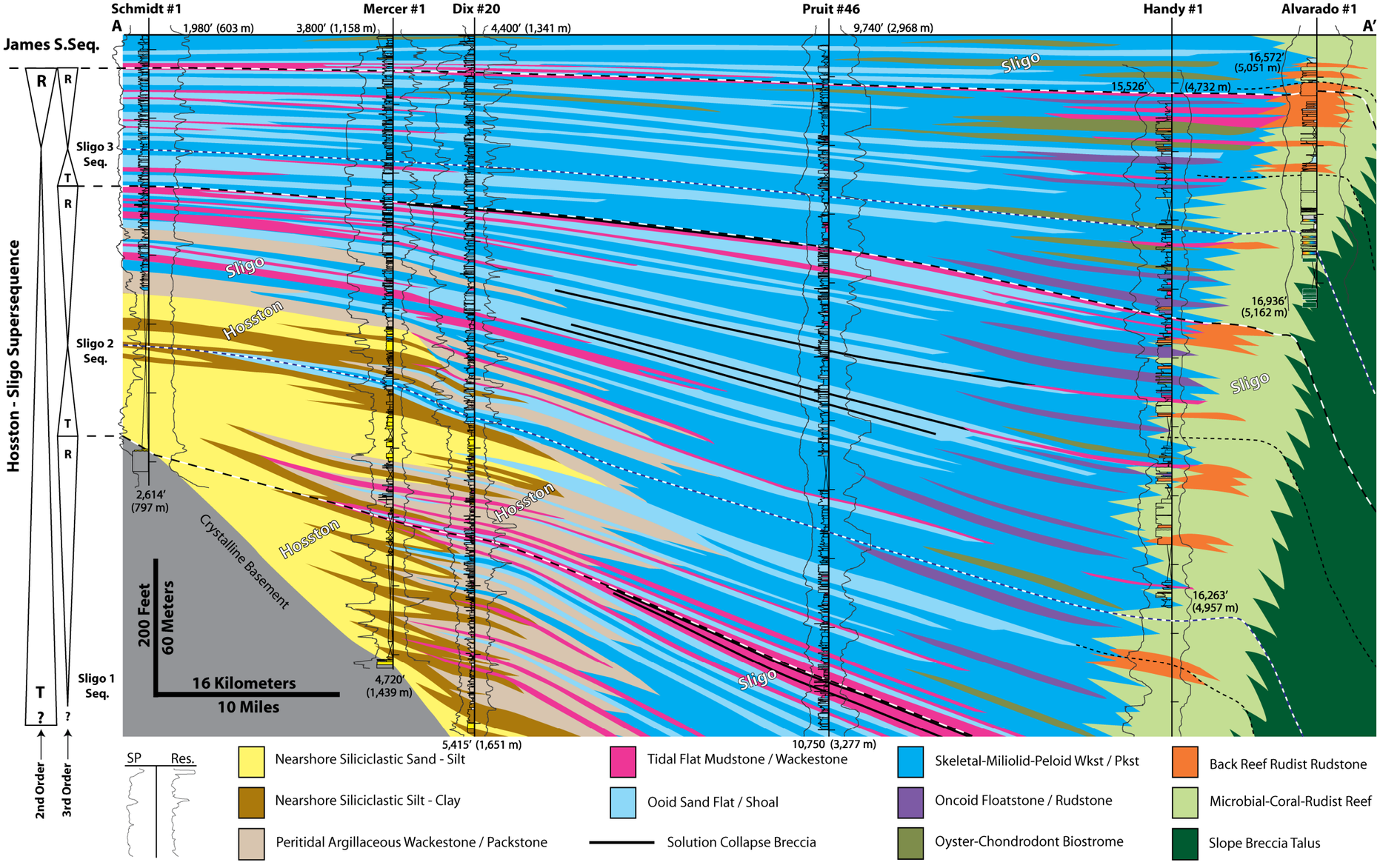

Figure 2.9: Regional sequence stratigraphic cross-section of the Hosston-Sligo supersequence. The cross-section is datumed to the base of the Pine Island Shale. Three depositional sequences are identified, termed the Sligo-1, Sligo-2, and Sligo-3. The base of the cross-section does not extend to the bottom of the supersquence due to a lack of rock data.

presence of nodular to bedded anhydrite suggests development of elevated salinities and evaporative salinas in the tidal flat setting.

Farther basinward along the depositional profile, Hosston Fm peritidal lithofacies transition into peloid-miliolid-skeletal packstones in the cyclic subtidal shelf of the Sligo Fm (Figure 2.9). HFCs in this setting are usually asymmetric, grading upward from a mud-dominated to a grain-dominated packstone fabric. Skeletal-ooid sand flats and shoals are found at or near the top of HFC sets, some of which shallow upward into tidal flat mudstones/wackestones with solution collapse breccias. More distal Sligo Fm facies include oyster-chondrodont and toucasid biostromes, as well as oncoid floatstones/rudstones. Shelf-margin reef and back-reef lithofacies laterally transition into upper-slope polymictic breccia talus within a 2-3 kilometer distance.

Hosston-Sligo Supersequence Depositional Profile

Six depositional environments, similar to those of Bebout et al. (1981), are distinguished in cores of the Hosston-Sligo supersequence: (1) terrestrial, (2) inner-shelf, (3) middle-shelf, (4) outer-shelf, (5) reef-margin, and (6) upper slope. Terrestrial environments consisted of subaerially exposed basement rocks, as well as alluvial and fluvial mixed siliciclastics with scattered caliche profiles (Stricklin et al., 1971; Amsbury, 1974). Inner-shelf lithofacies transitions are suggestive of a semi-arid sabkha (Bebout et al., 1981) that consisted of tide-influenced siliciclastics, peritidal carbonates, and evaporites of the Hosston Fm. Alternations between siliciclastic- and carbonate-dominated portions of the inner-shelf generally occur at the scale of HFC sets, with some progradational pulses of nearshore siliciclastics equivalent to peritidal carbonates of the middle-shelf. Middle-shelf lithofacies include all Sligo Fm subtidal packstones, oolitic

sand flats/shoals, and mudstone/wackestone tidal flats. Peritidal carbonates commonly prograded across much of the low-angle shelf-interior, leaving a significant portion of the shelf profile within an intertidal setting (Figure 2.9). Mixed subtidal packstones, oncoid rudstones/floatstones, and oyster-chondrodont biostromes are characteristic of the outer-shelf. Low-energy peritidal and subtidal outer-shelf facies were protected from open-ocean waves by the reef-margin and back-reef grainstone/rudstone complexes. Based on frequent observations of common syndepositional fractures, pervasive microbial cementation, and the presence of upper-slope talus breccias in the Alvarado #1 core, the shelf margin is interpreted to possess a high-angle profile with 30 to 60 degree depositional dips. In summary, the generalized Hosston-Sligo supersequence depositional profile is that of a rimmed shelf which intermittently shallowed to an intertidal setting along much of its dip extent.

Hosston-Sligo Supersequence Stratigraphy

I suggest restricting use of the terms Lower Sligo Fm and Upper Sligo Fm (Bebout, 1977), as these are based on the interfingering and diachronous boundary between dolostone and limestone Sligo carbonates. Rather, sequence stratigraphic boundaries within the Hosston-Sligo supersequence (~136–124 Ma) provide a more effective means of packaging the strata into regionally correlatable packages such as depositional sequences and HFC sets.

High-frequency cycles defined during core description cannot be confidently correlated between core locations over distances exceeding 5 km. However, HFC sets defined by facies trends among HFCs do appear to be regionally correlative for 10's of km along the shelf-interior profile in strike- and dip-orientations. Analysis of HFC set

stacking patterns and facies proportions allows recognition of three T-R depositional sequences within the Hosston-Sligo supersequence, each of which appears to be 2-4 Ma in duration. Additional sequences may be present beneath the studied interval. Each sequence boundary is defined based on the greatest thickness and basinward extent of mudstone tidal flats. The lower two sequences also contain solution collapse breccias beneath their upper sequence boundaries (Figure 2.9). Note that each successive sequence contains lesser proportions of mudstone tidal flats and transgressed farther landward over Hosston Fm siliciclastics. Despite persistent transgression of the shoreline during each subsequent sequence, the reef-margin continued to prograde, possibly because of greater sediment accumulation rates of shelf margin lithofacies.

Farther landward, long-term exposure on top of the Sligo-3 sequence boundary is interpreted from the presence of a pisolitic caliche profile atop the Sycamore Fm in Blanco County (Stricklin et al., 1971) and a soil horizon in the Canyon Lake core set of Comal County (Figure 2.4). This major exposure surface on top of the Sligo-3 depositional sequence is the basis for placing a supersequence boundary at this location. Facies proportions and stacking patterns above this second-order boundary are transgressive and retrogradational, thus the supersequence boundary is below the lithostratigraphic top of the Sligo Fm, as it is in the eastern Gulf of Mexico (Yurewicz et al., 1993). The uppermost 12-15 meters of the Sligo Fm partially forms the transgressive portion of the James supersequence.

Many previous studies characterize the Hosston-Sligo section as a third-order sequence (Tyrrell and Scott, 1989; Scott, 1993; Yurewicz et al., 1993), or as a long-term transgression within a larger T-R cycle (Mancini and Puckett, 2002; Mancini et al., 2008). However, their studies used mainly wireline-log or seismic data, and therefore did not resolve the Sligo 1-3 depositional sequences recognized here using multiple cores.

The internal stacking patterns and facies distributions of the Hosston-Sligo section, the 12 Myr duration of the interval (Chapter 3), the unconformity and soil zones in the upper Sligo, and the dramatic rise in relative sea level in the overlying Pine Island Member together argue for a second-order signal with nested third-order subsets.

James Supersequence (Early to Middle Aptian)

The James supersequence is comprised of three diverse lithostratigraphic units, including the uppermost Sligo Fm, as well as the Pine Island Shale and James Limestone Members of the Pearsall Fm (Figure 2.10). Relatively few descriptions of the Pine Island Shale and its outcropping equivalent Hammettt Shale have been published (Loucks, 1976); however the unit has long been regarded as the product of a major transgressive event (Lozo and Stricklin, 1956; Stricklin et al., 1971; Loucks, 1976). Seminal studies of the Pearsall Fm highlighted three prograding grainstone complexes, the oldest of which is the James Limestone and its outcrop equivalent, the Cow Creek Member (Lozo and Stricklin, 1956; Lozo et al., 1958; Stricklin et al., 1971; Loucks, 1976; Loucks, 1977).

Lithofacies Distributions

Beneath the Hosston-Sligo supersequence boundary, successive HFC sets shallowed upward from subtidal cyclic shelf packstones into oolitic grainstone sand flats and amalgamated mudstone tidal flats (Figure 2.9). In contrast, lithofacies above the supersequence boundary primarily consist of subtidal cyclic shelf packstones and few oolitic shoals (Figure 2.10). In the transition from the Sligo to the Pearsall formations, subtidal lithofacies contain an increasing proportion of terrigenous and carbonate mud,

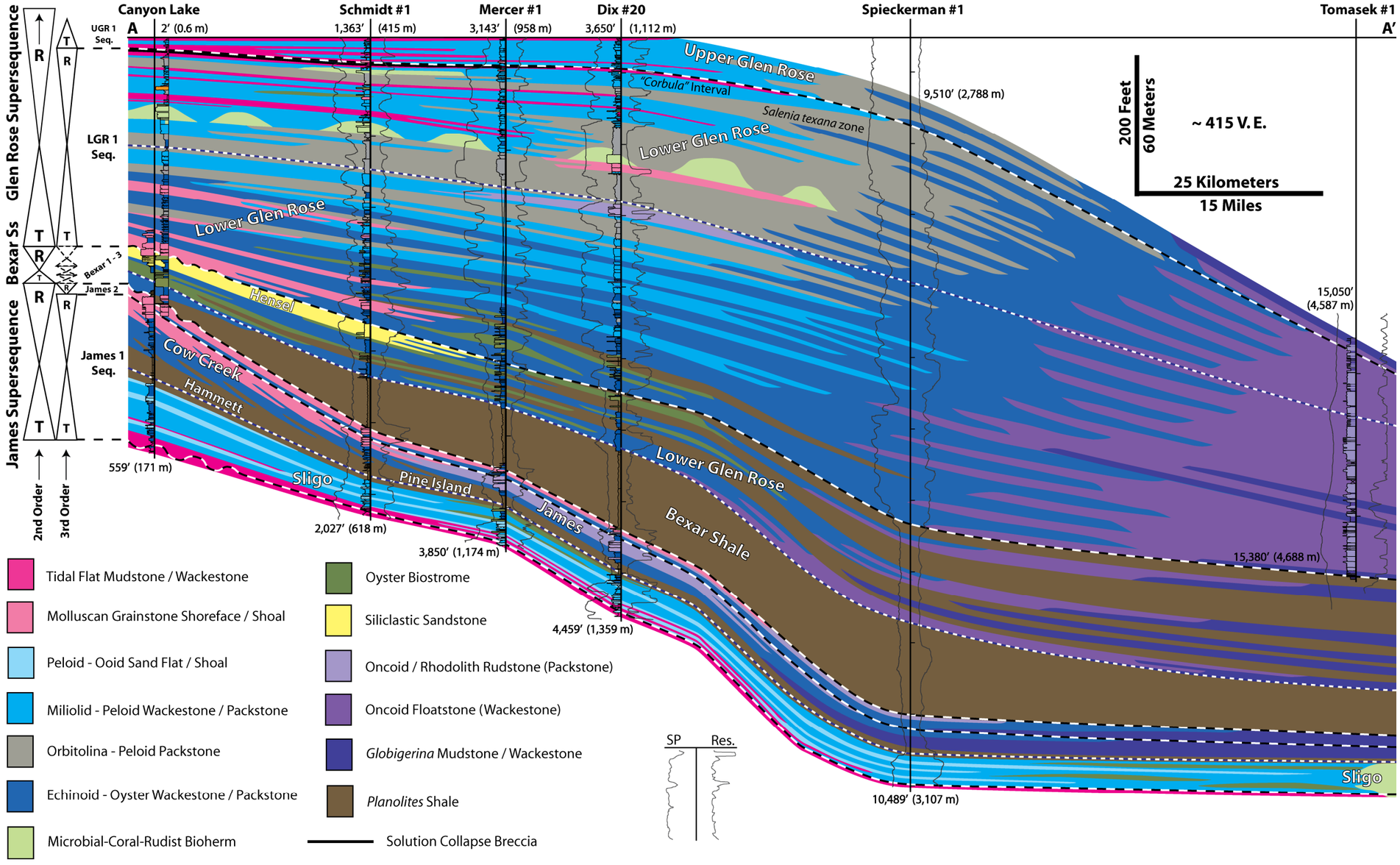

Figure 2.10: Regional sequence stratigraphic cross-section of the James, Bexar, and lower half of the Glen Rose supersequences. The cross-section is datumed to tidal flats in the upper Glen Rose Member. Transgressive systems tracts of depositional sequences in the James and Bexar supersequences represent condensed sections. The upper half of the Glen Rose supersequence is shown in Figure 2.11.

with many iron-stained, pyritic, bored hardgrounds present. Lenticular chondrodont-oyster biostromes with argillaceous matrix sediment became widespread as outer-shelf lithofacies extended landward and immediately preceded the first shale of the Pine Island Member.

Pine Island (Hammett) *Planolites*-burrowed shale contains rare ammonites that increase in abundance down depositional dip. The upward transition from shale to lowermost James echinoid-oyster wackestone/packstone is gradational and interfingering, reflecting the sporadic resumption of carbonate sedimentation and progradation of James clinoforms (Figure 2.10). Upward coarsening to molluscan grainstone shoreface lithofacies is observed in the Canyon Lake and Schmidt #1 cores, which pass down depositional dip into offshore oncoid rudstones. Each core exhibits a flooding event within the shoreface grainstones and correlative oncoid rudstones. In the subsurface, this is represented by a 1-meter package of clay-rich, echinoid-oyster packstone that it is equivalent to a coralline boundstone at Canyon Lake. Younger outcropping upper-shoreface clinoforms are capped by a well-developed caliche profile indicative of significant subaerial exposure (Lozo et al., 1958; Inden and Moore, 1983).

James Supersequence Depositional Profiles

During the Hosston-Sligo supersequence, long-term shoreline transgression and aggradational to progradational shelf-margin trajectories led to development of a high-angle, rimmed shelf depositional profile. At the base of the James supersequence, further transgression within the uppermost Sligo Fm accentuated this morphology. Unpublished seismic lines across the Sligo shelf-margin in Lavaca County display aggradational reef geometries during this period of sedimentation with younger Pine Island reflections

onlapping and draping the reef-margin. This empty-bucket morphology reflects an effort by the reef-margin to keep pace with the incipient rise in relative sea level prior to drowning.

No shelf-margin reefs are recognized in the Pearsall Fm. Rather, laminated, ammonite-rich shale of the Pine Island and lime mudstone of the James occupy the position of the underlying Sligo reef system. Thus the James supersequence developed a distally-steepened ramp profile which increased declination at the palimpsest Sligo shelf-margin (Figure 2.10). Shelf environments used for the Sligo supersequence no longer apply to the ramp profile, but are replaced with the terms inner-ramp, middle-ramp, outer-ramp, and distal-outer-ramp. The inner-ramp corresponds to areas in which grainstone shoreface strata were deposited, while middle-ramp refers to offshore sediment, including subtidal shelf and oncoid rudstone lithofacies. The outer-ramp includes flooded shelf mudstone/wackestone lithofacies deposited landward of the former Sligo shelf break, while the distal-outer-ramp encompasses environments beyond the Sligo margin.

The early to middle Aptian age (124-119 Ma) of the James supersequence generally coincides with the extent of OAE 1-A from approximately 123-122 Ma (Foellmi et al., 2006; Vahrenkamp, 2010). Environmental stress may have contributed to the demise of the Sligo carbonate factory and the shift to shale deposition. Sediment of the James (Cow Creek) Member was primarily limited to depauperate fauna consisting of echinoids, oysters, and other mollusks. This limited faunal assemblage and the minor volumes of carbonate sediment (18 - 20 meters in Canyon Lake cores, 14 meters in Dix #20 core) generated during this 3 Myr interval suggest that the carbonate factory resumed sedimentation under stressed conditions. Because the locus of sedimentation was located along the land-attached shoreline, the profile of the James supersequence evolved into a

distally-steepened ramp with grain size distributions, sedimentary structures, and energy regimes similar to those of siliciclastic shoreface systems (Lozo et al., 1958; Kerans and Loucks, 2002).

James Supersequence Stratigraphy

Because of the large-scale T-R pattern of the uppermost Sligo and Pine Island to James stratigraphy, as well as its duration (~124-119 Ma), the interval is regarded as a second-order supersequence. The uppermost 12-15 meters of Sligo carbonates are retrogradational with increasingly subtidal lithofacies proportions; therefore I place this portion of the Sligo section and its reefal equivalent in the transgressive systems tract of the James supersequence. This interpretation is in agreement with studies from the eastern Gulf of Mexico (Yurewicz et al., 1993; Mancini and Puckett, 2002), but was not included in the sequence stratigraphic interpretation of Amsbury (1996).

Based on the core data, two depositional sequences, the older James-1 and younger James-2, are tentatively recognized (Figure 2.10). The James-1 sequence includes the transgressive uppermost Sligo section, the Pine Island Member, and most of the James limestone. Maximum flooding of the James-1 sequence, coincident with maximum flooding of the full James supersequence, is placed in the lower third of the Pine Island shale. The base of the flooding event that interrupted molluscan shoreface deposition separates the James-1 and James-2 sequences. Shoreface progradation resumed in the highstand of the James-2 sequence and was later overprinted by regional exposure.

Although the James-2 depositional sequence is quite thin at ~ 5.5 meters in thickness, the time-duration encompassed by the supersequence and the minimal

sediment accumulation rates for the James Member (0.5 cm/ky in Dix #20, 0.6 cm/ky in Canyon Lake) allow this sequence to span approximately 1 Myr. This duration is within the 1-3 Myr time range of third-order depositional sequences (Mitchum and Van Wagoner, 1991; Lehrmann and Goldhammer, 1999). Additional sequences may be present within the Pine Island interval and lower portions of the James Member, but they cannot be subdivided because of the deep-subtidal bathymetry of the depositional environments. Recognition of higher-order HFC sets and HFCs within the Pine Island and James is difficult in the deep-subtidal setting, whereas many HFCs appear to be amalgamated within the James shoreface system. Although not explicitly recognized by Loucks (1977), visual inspection of his cross-sections through the James limestone also suggests the presence of two third-order depositional sequences above the Pearsall Arch (James-1 and James-2).

Bexar Supersequence (Middle Aptian – Early Albian)

Lithostratigraphic units within the Bexar supersequence include the Bexar Member of the Pearsall Fm, carbonates of the Lower Glen Rose Member and sandstones of the Hensel Fm (Figure 2.10). Discussions of the Bexar Member, Hensel Fm, and Glen Rose Fm by Loucks (1976) and Amsbury (1996) offer conflicting perspectives of the shale-dominated succession. Ammonite zonations are detailed by Young (1976).

Lithofacies Distributions

In cores from the Mercer #1 and Dix #20 wells, the top James supersequence boundary is succeeded by 1 meter of subtidal shelf wackestone and followed by up to 30 meters of *Planolites*-burrowed shale. Bexar shale directly rests upon James grainstones in

the Schmidt #1 core as well as the top-Cow Creek caliche profile in the Canyon Lake cores (Figure 2.10). At Canyon Lake, the Bexar shale unit increases in carbonate content, thins to approximately 6 meters, and is overlain by oyster biostromes. These units are encased by subtidal echinoid-oyster wackestone in the middle-ramp of the Glen Rose Fm. Distal tongues of outer-ramp brown shale interfinger with these Glen Rose Fm carbonates. The top of the supersequence contains a 1-6 meter wedge of Hensel Fm sandstone that is capped by an iron-stained, caliche zone in Canyon Lake.

Because Hensel Fm siliciclastics and caliches lay directly above the top James (Cow Creek) unconformity in landward areas toward the Llano Uplift, both Young (1986) and Amsbury (1996) argued that the Bexar shale is stratigraphically older than all Hensel Fm siliciclastics. However, coarse-siliciclastics sourced from the Llano Uplift are found in surrounding shorelines of the Hosston-Sligo, James, and Glen Rose supersequences (Lozo and Stricklin, 1956; Stricklin et al., 1971; Inden and Moore, 1983); thus I argue that shoreline siliciclastic sedimentation also occurred throughout the time required to deposit terrigenous clay in the Bexar supersequence. I reason that lower Hensel Fm terrestrial siliciclastics are an up-dip facies equivalent of regressive shoreface strata in the James supersequence and are also equivalent to deep-subtidal shales/carbonates of the Bexar supersequence.

Bexar Supersequence Depositional Profile

The distally-steepened ramp profile inherited from the James supersequence was reinforced as Bexar shales were deposited across the platform. The timing of OAE 1-B (~113-110 Ma) in the middle Aptian to Earliest Albian (Bralower et al., 1999; Foellmi et al., 2006) is generally coincident with age of shale wedges in the Bexar supersequence

(~119-110 Ma). Environmental stress, combined with transgression at the onset of shale deposition, likely caused reversion back to shale deposition and the demise of the carbonate factory (Chapter 3). Distally-steepened ramp environments of the James supersequence are used to describe the Bexar supersequence. *Planolites*-burrowed shales are representative of the outer-ramp, oyster-echinoid wackestones and oyster biostromes of the Glen Rose Fm are characteristic of the middle-ramp, and Hensel Fm shoreline siliciclastics are found in the inner-ramp.

Bexar Supersequence Stratigraphy

The temporal duration of the Bexar supersequence is estimated to be approximately 9 Myr (119-110 Ma). Approximately 7 Myr of this time span (Chapter 3) are represented by ~25 meters of *Planolites*-burrowed shale, which contributes roughly one-half of the sediment volume in the sequence (Figure 2.10). Maximum flooding of the Bexar supersequence is placed at the top of the globigerinid-bearing shale package. Two shoal-water complexes recognized by Loucks (1976) over the Pearsall Arch are not developed along the San Marcos Arch, but are equivalent to the thick wedge of *Planolites*-burrowed shales in the Bexar Member. These likely represent third-order depositional sequences that are not easily identified with this data set because of the deep-subtidal environment. I propose that three nested depositional sequences are present in the Bexar supersequence but are best resolved over the Pearsall Arch. The top supersequence boundary is located above the regressive Hensel Fm sand wedge with its landward caliche profile. The Bexar supersequence and higher-order depositional sequences outlined in this study are not recognized by previous authors, who include the

Bexar member as a transgressive facies of lower Glen Rose sequences (Scott, 1993; Mancini and Puckett, 2002; Mancini and Scott, 2006).

Glen Rose Supersequence (Early Albian – Middle Albian)

Lithostratigraphic units encompassed by the Glen Rose supersequence include Hensel Fm siliciclastics and diverse carbonates of the Glen Rose Fm. Components of this 5 Myr supersequence (110-104 Ma) have been studied in great detail, owing to the widespread outcrops and dam-site engineering cores north of the Balcones Fault zone, as well as the abundance of hydrocarbon producing wells within the Maverick and East Texas Basins (Lozo et al., 1958; McNamee, 1969; Stricklin et al., 1971; Perkins, 1974; Loucks, 1976; Bay, 1982; Tartamella, 1982; Pittman, 1989; Fitchen et al., 1997; Amsbury, 1996; Scott, 2003; Scott et al., 2007; Ward and Ward, 2007; Aconcha et al., 2008). Due to the thickness (>380 m) and facies variety of the supersequence, lithofacies distributions and stratigraphic details are split among two overlapping cross-sections (Figures 2.10 and 2.11). The cross-sections are arbitrarily divided by a lithostratigraphic boundary between the Lower and Upper Glen Rose Members, defined by the "Corbula" zone containing abundant *Eoursivivas harveyi* bivalves (Scott et al., 2007; Ward and Ward, 2007).

Lithofacies Distributions

At Canyon Lake, the top Bexar supersequence boundary is overlain by a molluscan biostrome that is taken by previous workers to locally define the base of the Glen Rose Fm (Abbott, 1966). Nearshore siliciclastics and sporadic caliches of the upper

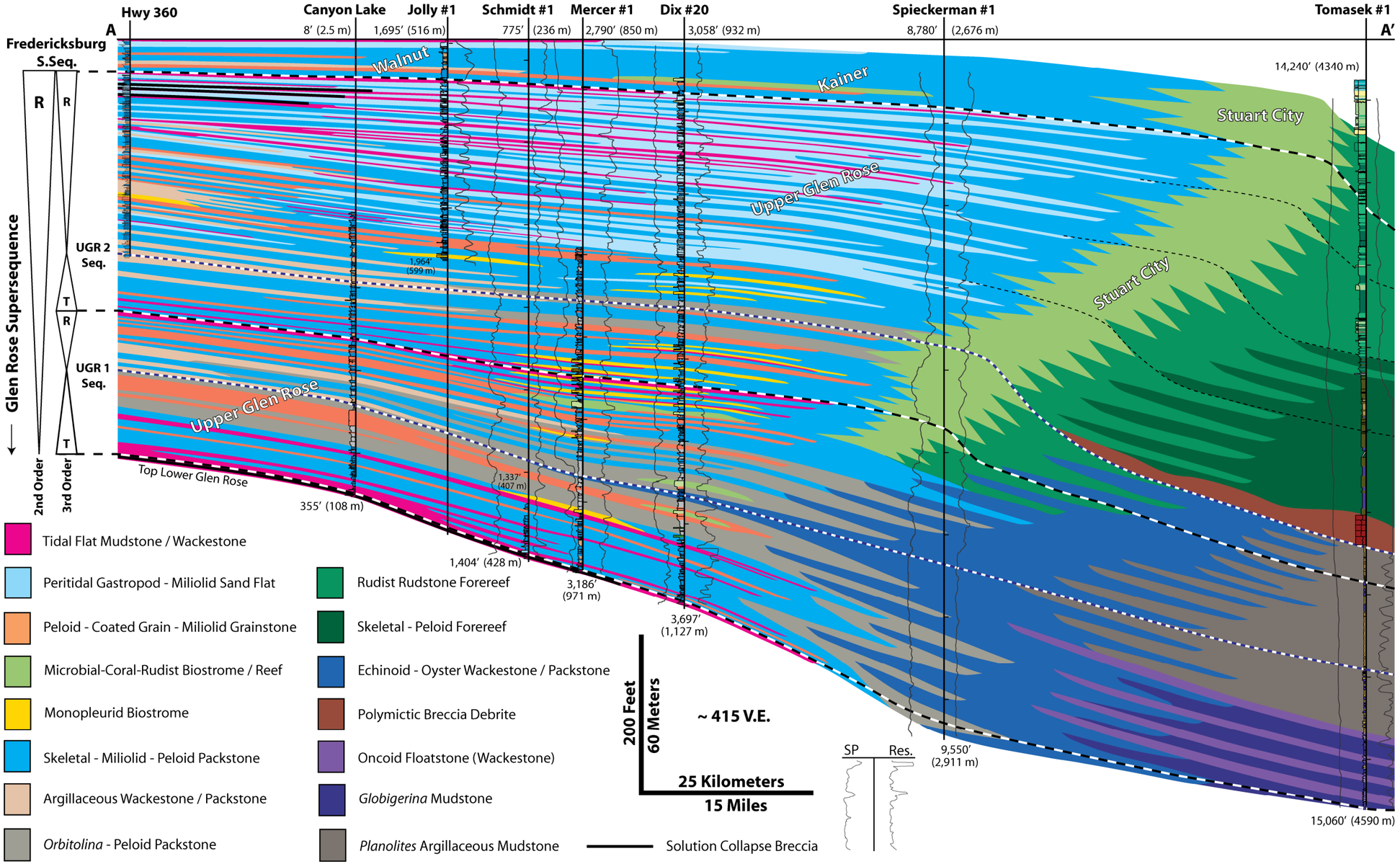

Figure 2.11: Regional sequence stratigraphic cross-section of the upper half of the Glen Rose supersequence. The cross-section is datumed to the top of the Bull Creek Member in the Fredericksburg Group.

Hensel Fm form the lower Glen Rose shoreline and were locally present through much of the Glen Rose supersequence (Figures 2.2 and 2.5) (Amsbury, 1996).

A series of retrograding, cyclic subtidal shelf wackestones to grainstones aggraded the middle-ramp for an additional 60 meters through most of the lower Glen Rose (Figure 2.10). This interval is approximately equivalent to 30 m of stacked coralrudist biostromes in Blanco County (Figure 2.4), which are thought to represent open marine conditions (Scott et al., 2007). *Orbitolina*-peloid packstones form an additional 5-20 meters of strata and encase an interval of toucasid-caprinid bioherms of the Pipe Creek patch-reef complex (Perkins, 1974; Scott, 2003). Landward in the line of section, the bioherms are capped by tidal flats and local subaerial exposure surfaces with isolated karst breccias (Schmidt #1 core). Miliolid-bearing, cyclic subtidal shelf packages suggestive of slightly restricted conditions are succeeded by *Orbitolina*- and echinoid-rich facies within the *Salenia texana* zone. One-meter above the "Corbula" interval, a series of algal-laminated tidal flat mudstones prograded across the ramp and contain a regionally continuous solution collapse breccia. All of the preceding Glen Rose lithofacies are equivalent to oncoid floatstones within the Tomasek #1 core.

In the basal Upper Glen Rose (Figure 2.11), retrograding tidal flat mudstones and miliolid-skeletal packstones are overlain by a succession cyclic shelf packstones to grainstones and caprinid-toucasid biostromes. Progradation again brought miliolid-skeletal packstones, monopleurid biostromes, and tidal flats across the shallow marine profile. The presence of monopleurid and caprinid biostromes in the Upper Glen Rose, in addition to well-documented bioherms from the Lower Glen Rose outcrop belt (Perkins, 1974), suggests that these fauna consistently occupied similar environmental positions in the ramp profile. Shallow-subtidal shelf cycles, grainstone sand flats, and mudstone tidal flats typify the youngest 80-100 meters of the Upper Glen Rose Member. Frequent

solution collapse breccias are found in the Hwy 360 sections just below the Glen Rose supersequence boundary and indicate deposition of supratidal sabkha evaporite beds.

The Tomasek #1 core, which recorded sedimentation in distal portions of the Glen Rose profile, exhibits a long-term coarsening upward profile above the outer-ramp oncoid floatstones and flooded shelf mudstones in the base and middle of the supersequence (Figures 2.10 and 2.11) (Scott, 1990). Eleven meters of polymictic breccia slope debrites were likely sourced from a rapidly prograding Stuart City reef located farther landward within the Upper Glen Rose depositional system. Detrital middle-slope wackestones/packstones overlain by grainstone/rudstone forereef lithofacies are distal equivalents of a mature Stuart City margin.

Glen Rose Supersequence Depositional Profiles

The distally-steepened ramp profile of the James and Bexar supersequences was maintained throughout much of the Lower and Upper Glen Rose Members. Hence the terminology describing inner-, middle-, outer-, and distal outer-ramp environments is retained until evidence of a reefal shelf-margin is observed in the Upper Glen Rose.

The distally-steepened ramp bathymetric profile found throughout much of the Bexar Member and Glen Rose Fm caused progressive coarsening of lithofacies from outer-ramp floatstones and mudstones to cyclic subtidal shelf lithofacies of the middle-ramp, and lastly to peritidal grainstones and mudstones of the inner-ramp (Figures 2.10 and 2.11). *Orbitolina* foraminifera facies transgressed across the ramp during flooding events, whereas miliolid foraminifera were most abundant in the more restricted inner-ramp peritidal complexes. The absence of a shelf-margin reef in the Lower and Upper

Glen Rose ramp profiles allowed circulation of normal-marine water into the platform interior and promoted growth of coral-rudist patch reefs and biostromes

After initiation of shelf-margin reefs in the Upper Glen Rose section, the distally-steepened ramp profile transitioned to a low-angle shelf system with a strongly progradational shelf-margin trajectory (70 km of progradation / 140 m of aggradation). Limited accommodation and shelf-margin progradation promoted expansion of mudstone tidal flats and grainstone sand flats across the 170 km-wide shelf. The true basinward extent of these intertidal complexes is unknown and interpreted in from wireline log motifs (Figure 2.11). Based on this interpretation, only inner-shelf and middle-shelf environments were present during Upper Glen Rose deposition. In the upper 65 meters of the Glen Rose supersequence, the mollusk-miliolid faunal assemblage and observations of thin solution collapse breccias indicate restricted conditions and elevated salinities were present across the broad shelf. With the exception of two transgressive pulses of Oribitolina-rich packstone, these foraminifera are absent from Upper Glen Rose shelf sediments, as are the coral-rudist biostromal facies.

The highest energy portions of the Upper Glen Rose shelf profile appear to have been located in the low-angle forereef, as opposed to back-reef locations in the Sligo margin (Figures 2.9 and 2.11). The absence of back-reef grainstone/rudstone complexes in the Upper Glen Rose margin likely prevented development of a low-energy shadow zone characteristic of the Sligo Fm outer-shelf.

Glen Rose Supersequence Stratigraphy

Three depositional sequences of third-order duration are recognized and termed the Lower Glen Rose-1 (LGR-1), Upper Glen Rose-1 (UGR-1), and Upper Glen Rose-2

(UGR-2) sequences (Figures 2.10 and 2.11). The LGR-1 sequence extends upward to the solution collapse breccia one meter above the lithostratigraphic top of the Lower Glen Rose Member. Maximum flooding of the LGR-1 sequence and the Glen Rose supersequence are placed above retrograding HFC sets of subtidal shelf wackestone-grainstone and within *Orbitolina*-peloid packstones with accessory oncoids and whole echinoids. This interpretation places the widespread toucasid-caprinid bioherms immediately after the maximum flooding interval and in the early highstand of the sequence (Figure 2.10). Subaerial exposure surfaces capping these bioherms are not observed in inter-mound cores and are local in extent. These exposure events are representative of a fourth-order high-frequency sequence boundary, with the overlying *Salenia texana* zone indicative of a fourth-order maximum flood. My LGR-1 sequence boundary is slightly higher than the location proposed by Ward and Ward (2007), but is interpreted to approximate a surface of regional subaerial exposure.

Tidal flat-capped HFC sets within the UGR-1 sequence show an aggradational to retrogradational stacking pattern prior to maximum flooding during deposition of *Orbitolina* wackestones/packstones (Figure 2.11). Progradational, cyclic subtidal packstones to grainstones are characteristic of the middle-ramp during the early highstand. Inner-ramp peritidal cycles with abundant monopleurid biostromes form the late highstand of the sequence, with the top UGR-1 sequence boundary placed in the thickest mudstone tidal flats.

The transgressive systems tract of the UGR-2 sequence exhibits landward migration of tidal flat mudstones at the top of HFC sets. In similar style to the UGR-1 sequence, maximum flooding is placed in argillaceous, Oribitolina-dominated lithofacies. The UGR-2 sequence is the most progradational third-order package within the Glen Rose supersequence and its highstand systems tract contains ubiquitous shallow-subtidal

to supratidal cycles throughout the study area. Strongly progradational geometries are not only observed in the shelf-interior, but are also observed in industry seismic over the Stuart City reef-margin (Chapter 4). Limited platform-top accommodation likely contributed to the morphologic transition from distally-steepened ramp to low-angle shelf observed in this sequence. The UGR-2 sequence and Glen Rose supersequence extend upward to the last tidal flats of the Glen Rose Fm and are overlain by subtidal cycles of the Fredericksburg supersequence.

Third-order sequence boundaries in the Glen Rose supersequence are placed in stacked peritidal cycles based on the greatest thickness and basinward extent of tidal flat mudstones. Maximum flooding surfaces are located in argillaceous, echinoid-bearing, *Orbitolina*-peloid wackestones/packstones. This interpretation is consistent with sequence stratigraphic studies from the Lower Cretaceous of Oman, the southern Tethyan realm, and the French Jura (Arnaud-Vanneau and Arnaud, 1990; Pittet et al., 2002; Bachmann and Hirsch, 2006). HFC sets and high-frequency sequences (fourth-order) are easily defined and correlated with confidence for 10's of kilometers along depositional dip. Fifth-order HFCs can also be tracked regionally in subtidal portions of the ramp/shelf, but cannot be easily correlated in peritidal settings due to autocyclicity in the depositional system and amalgamation of cycles.

The interpretation of the Glen Rose Fm as a second-order T-R supersequence is supported by interpretations published by Mancini and Puckett (2002), and Mancini and Scott (2006). Several previous studies split the lower Glen Rose and upper Glen Rose, as well as their East Texas Basin equivalents, into two depositional sequences (Scott, 1993; Yurewicz et al., 1993; Mancini and Puckett, 2002; Mancini and Scott, 2006; Scott et al., 2007; Mancini et al., 2008). I am in general agreement with these authors; however

delineation of an additional depositional sequence is merited based on lithofacies proportions and cycle stacking patterns.

Fredericksburg Supersequence (Middle to Late Albian)

The Fredericksburg supersequence consists of all lithostratigraphic units composing the Fredericksburg Division, including the Palxuy, Walnut, Goodland and Comanche Peak formations of central and north Texas, as well as the Person, Kainer, and Fort Terrett formations of the Edwards Group in south Texas (Moore, 1964). Contacts at the top and base of the Fredericksburg are demonstrated to be unconformities in central and north Texas (Nelson, 1959; Moore, 1964; Amsbury, 1965; Moore, 1996; Talbert and Atchley, 2000; Scott et al., 2003), though supersequence boundaries in the subsurface study appear conformable. Despite recent modifications (Waite et al., 2007), lithostratigraphic terminology from Rose (1972) is the standard reference for the outcropping and subsurface Edwards Group. However, my regional correlations follow those of Waite et al. (2007) who demonstrated that the Regional Dense Marker (RDM) is not the temporal equivalent of the Kiamichi Fm in the East Texas Basin, and the Person Fm, or the "Edwards-A" of the oil industry (Fisher and Rodda, 1969), is not the temporal equivalent of the Georgetown Fm. Rather, the RDM and the Person Fm are internal to the Fredericksburg Division, with the Person Fm equivalent to the Goodland Fm of east Texas (Scott et al., 2002; Waite et al., 2007).

Lithofacies Distributions

The cross-section of the Fredericksburg supersequence (Figure 2.12) is datumed to the RDM. The lower portion of the supersequence displays open-marine subtidal shelf

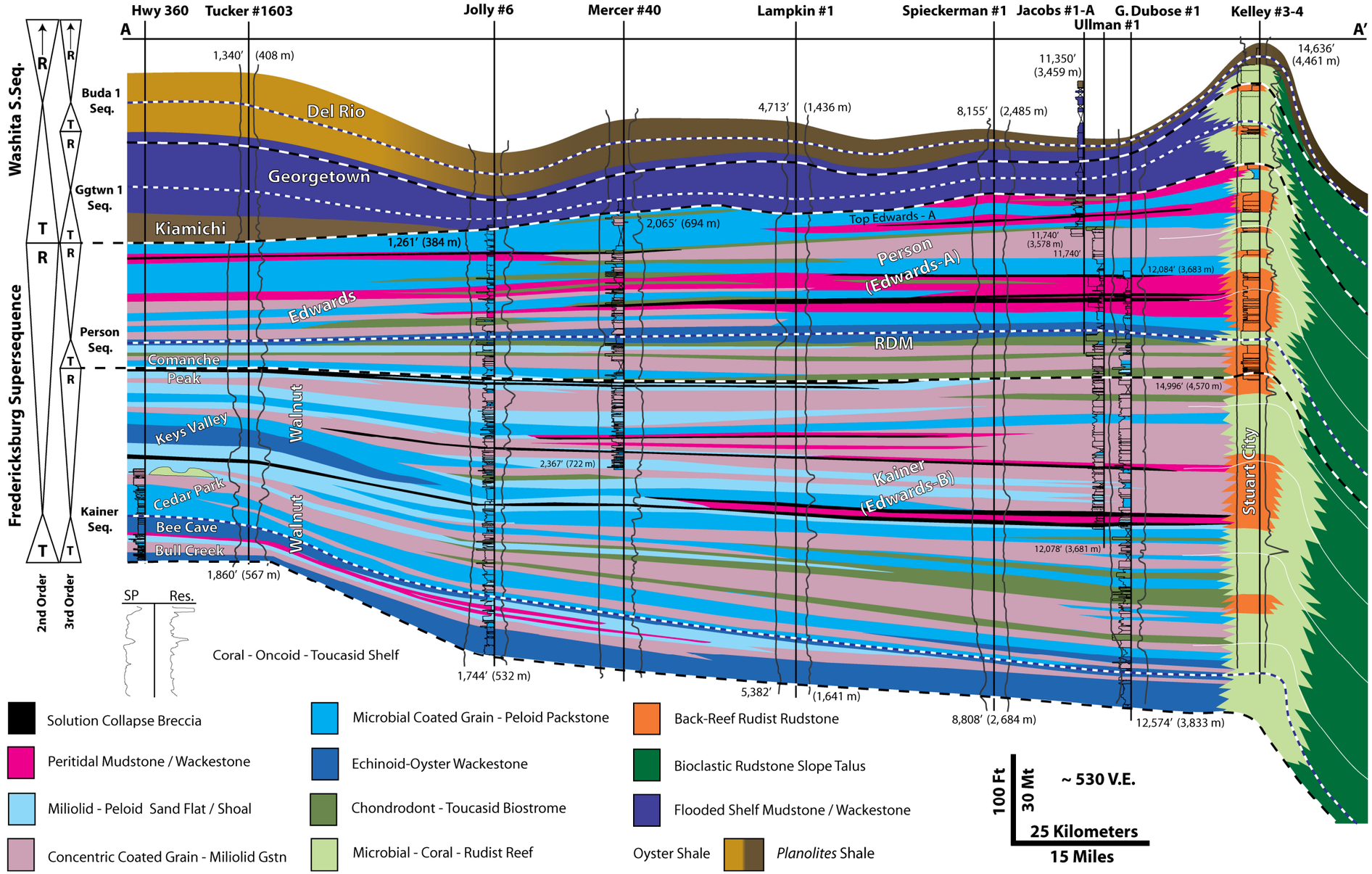

Figure 2.12: Regional sequence stratigraphic cross-section of the Fredericksburg supersequence and its component Person-1 and Kainer-1 depositional sequences.

to tidal flat mudstone lithofacies in the Bull Creek and Bee Cave Members of the Walnut Fm. These units are overlain by restricted shallow-subtidal lithofacies of the Kainer Fm, including coated grain-peloid packstones and abundant skeletal-miliolid grainstones. Interpreted as wave- and current swept areas of the subtidal shelf, the skeletal-miliolid grainstones thicken toward the shelf-margin and are often the distal equivalent of miliolid-peloid sand flats.

At the base of the RDM are laterally persistent chondrodont-toucasid biostromes that commonly thin in the landward direction. The biostromes are overlain by subtidal, argillaceous, gastropod-oyster wackestone/mudstone. At the shelf margin in the Schroeder #1 core (Figure 2.4), the RDM is a transgressive interval consisting of mud-dominated, *Lithocodium-Bacinella* bindstones (Waite et al., 2007). In the southern Tethys, *Lithocodium-Bacinella* are ubiquitous in carbonate strata deposited under environmentally stressed conditions of OAE 1a (Huck et al., 2010). The limited shelf-interior fauna, close vertical association with shallow-subtidal lithofacies, and abundance of *Lithocodium-Bacinella* at the shelf-margin, suggest the RDM represents an intermediate-frequency transgression within the Edwards Group during a period of local environmental stress.

Additional lithofacies common to the Edwards shelf-interior include solution collapse breccias up to 2 meters thick (Fisher and Rodda, 1969) and very shallow subtidal to intertidal mudstones/wackestones (Rose, 1972). The tabular nature of the solution collapse breccias and their association with peritidal units imply that the precursor evaporites were precipitated in a hypersaline, shallow-subtidal shelf-interior.

Boundstone lithofacies of the Stuart City margin contained well-zoned, diverse fauna throughout the reef-wall and reef-flat (Chapter 4). Stuart City back-reef storm berms display well-developed pendant cement zones revealing surfaces of subaerial

exposure (Figure 2.8). These grainstone/rudstone belts transitioned landward into low-energy, cyclic shallow-subtidal wackestones and tidal flat mudstones in a protected shelf-interior setting. Distal of the reef are seismic-scale wedges of onlapping sediments presumed to consist of detrital slope lithofacies (Chapter 4), although no cores in the study area have directly sampled slope sediments of the Fredericksburg supersequence.

Fredericksburg Supersequence Depositional Profile

Transgression at the base of the Fredericksburg supersequence not only caused a shift from intertidal to subtidal shelf-interior sedimentation, but also caused a shift from strongly-progradational to aggradational shelf-margin trajectories (Figure 2.5). Aggradational shelf-margin geometries throughout the Fredericksburg supersequence were partially a result of rising relative sea level, but were later reinforced because of the position of the Stuart City margin above the terminal Sligo shelf-margin. Dramatically increased accommodation beyond the palimpsest Sligo margin prevented the Stuart City reef from prograding into the former slope and basin. The presence of vertical reef-wall fabrics and abundant, large syndepositional fractures suggest transformation from a low-angle reef-margin in the UGR-2 sequence to a high-angle reef-margin in the Fredericksburg supersequence. This margin likely contained 30-80 degree depositional dips and a near vertical escarpment created by periodic collapse of the reef-wall.

Grain-dominated sand flats and mud-dominated peritidal strata are both interpreted to extend across the full extent of the shelf profile (Figure 2.12). Intertidal sand flats predominate below the RDM and few mudstone tidal flats are well-developed. The grainstone sand flats were primarily located in a high-energy belt closer to the shoreline, whereas low-energy peritidal strata above the RDM were deposited closer to

the reef-margin. Peritidal wackestones/mudstones and former evaporites (now solution collapse breccias) indicate restricted conditions across the shelf. The increased occurrence of former evaporite zones upward through the Fredericksburg supersequence is synchronous with the expansion of backreef grainstone/rudstone belts in the Stuart City margin. As the shelf-margin aggraded, the semicontinous detrital barrier was intermittently exposed and perhaps served as an energy and fluid-flow barrier. Similar contemporaneous grainstone complexes, for example Moffat Mound (Amsbury, 1965) and the Whitestone Member (Moore, 1964), developed on the eastern margins of the San Marcos Arch in the Central Texas reef trend (Fisher and Rodda, 1969). These grainstone barriers prevented the effective exchange of shelf-interior fluids with normal marine waters of the Gulf of Mexico and East Texas Basin. The sediment barriers promoted low-energy sedimentation in the shelf-interior and contributed to hypersaline conditions with deposition of evaporites (Fisher and Rodda, 1969). In this manner, the facies distributions and architecture of the Stuart City margin, combined with grainstone complexes bordering the San Marcos Arch, served to influence the energy-regime and shelf-interior sedimentary patterns within the Fredericksburg supersequence.

Fredericksburg Supersequence Stratigraphy

I take the Edwards Group and all equivalent strata of the Fredericksburg Division as a second-order supersequence (104-101 Ma) that contains two subordinate depositional sequences, the Person-1 and Kainer-1 sequences (Figure 2.12). Maximum flooding of the Kainer-1 sequence is above the transgressive high-frequency sequence formed by the Bull Creek Member of the Walnut Fm and placed within the open-marine Bee Cave Marl. This location also coincides with maximum flooding of the

Fredericksburg supersequence. The top Kainer-1 sequence boundary is placed on top of intertidal sand flats containing thin solution collapse breccias. Maximum flooding of the Person-1 sequence is located above a transgressive, subtidal to intertidal cycle set and within argillaceous mudstones of the RDM. The top Fredericksburg supersequence boundary is located on top of the regional exposure surface in north-central Texas (Nelson, 1959; Amsbury, 1965; Hovorka, 1996), and beneath the Kiamichi and Georgetown formations. Solution collapse breccias common in the Fredericksburg supersequence are limited to third-order highstands and are not found in the transgressive systems tracts.

Interpretation of the Fredericksburg Division as a supersequence with two nested depositional sequences is largely based on internal cycle stacking patterns and regional unconformities in the outcrop belt. The 3 Myr duration of the package is shorter than typical second-order durations, although Scott et al. (2002) also considers the Fredericksburg Division a second-order package. Hovorka (1996) compiled additional measured sections from the Balcones Fault Zone on the San Marcos Arch and split the Edwards Group into two intermediate-scale cycles similar to the Person-1 and Kainer-1 sequences

The influx of paralic sands, silts and shales of the Paluxy Fm at the base of the supersequence in North Texas and the eastern Gulf of Mexico complicate the stratigraphic interpretation. Regardless, most authors consider the Paluxy and overlying Fredericksburg intervals to be one long-term T-R sequence of varying hierarchy and may or may not recognize internal higher-order cycles (Scott, 1993; Yurewicz et al., 1993; Moore, 1996; Talbert and Atchley, 2000; Mancini and Puckett, 2002; Mancini et al., 2008).

Washita Supersequence (Late Albian – Middle Cenomanian)

Lithostratigraphic units within the Washita supersequence (Figures 2.12 and 2.13) include carbonates and shales of the Stuart City, Kiamichi, Georgetown, Del Rio, and Buda formations, as well as time-equivalent components of the Washita Group not found in the study area. The Georgetown Fm is equivalent to the Segovia Fm in the Edwards Plateau, the Devils River and Salmon Peak formations of the Maverick Basin, and lower formations in the Washita Group of north Texas (Rose, 1972; Scott et al., 1978; Kerans, 2002; Scott et al., 2002). In the East Texas Basin, the Del Rio Fm is referred to as the Grayson Fm (Scott et al., 1978).

Lithofacies Distributions

Apart from the Stuart City equivalent of the Georgetown Fm, little core data is available for this supersequence and outcrop exposures are generally poor in the study area. Two upper Cretaceous cross-sections along the San Marcos Arch and east of the Maverick Basin (Figure 2.13) depict divergent regional stratigraphic relationships at the Stuart City margin. Both cross-sections illustrate the time equivalence of flooded shelf mudstones/wackestones to reefal and back-reef Stuart City margin facies.

In the Hays to Dewitt County section (A-A'; Figures 2.4 and 2.13), Georgetown equivalent strata of the Stuart City margin are in a down-thrown fault block and contain an upward-deepening succession of reefal boundstones and back-reef grainstones. These pass laterally landward (northwest) into coral-oncoid rudstones and flooded-shelf mudstones. Interpreted deepening of lithofacies above the Fredericksburg supersequence boundary and the presence of Georgetown-age rudists in multiple reef cores (Coogan, 1977; Chapter 4) provide confidence in the time-equivalent relationship between flooded

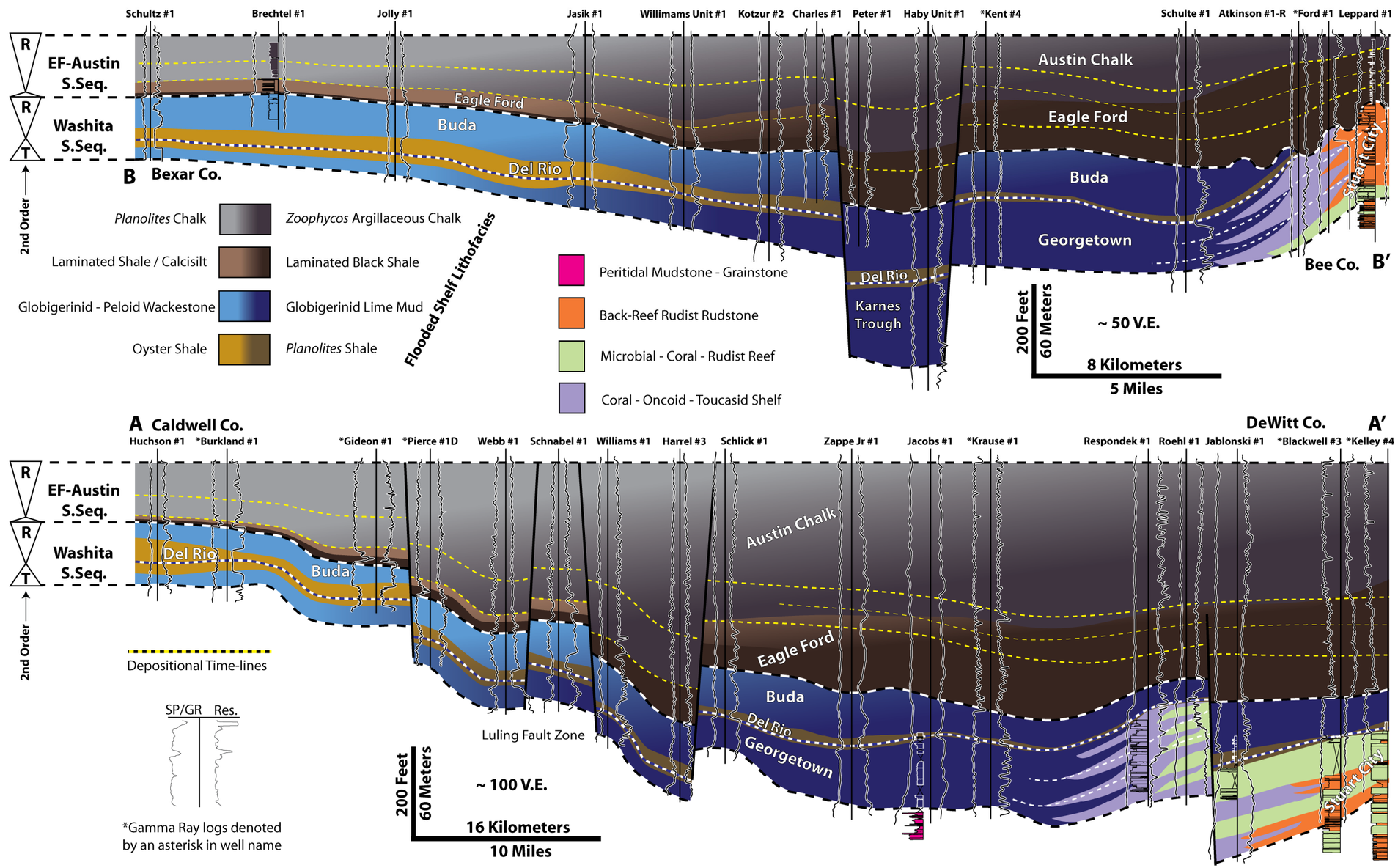

Figure 2.13: Cross-sections of the Washita and Eagle Ford-Austin Chalk (EF-AC) supersequences. Both are datumed to the top Austin Chalk. Third-order sequences are not shown due to space constraints. Depositional time-lines (dashed-yellow) show gradational facies changes in ramp clinoforms and pass through lithostratigraphic boundaries between the Eagle Ford and Austin Chalk Groups.

shelf and reef-margin strata. In the Bexar to Bee County section (B-B'; Figures 2.4 and 2.13), a similar time-equivalent relationship is inferred between the Georgetown and the Stuart City. However, the shelf-margin in Bee County was not down-faulted at the time of deposition as it was in DeWitt County, thus the contact between the Fredericksburg and Washita Supersequences is not readily discernible amongst the shallow reef and back-reef facies.

In both cross-sections, oyster-shale lithofacies of the Del Rio Formation thin down depositional dip to ~3 m at the shelf-margin where preservation of the corresponding deep-subtidal, *Planolites*-burrowed shale is variable (Figure 2.13). The Buda Fm consists of deep-subtidal, flooded-shelf mudstone/wackestone and maintains near constant thickness of 20-30 meters along the shelf profile. Divergence in the two regional cross-sections occurs over the shelf-margin, where the Del Rio and Buda Fm are not present in Bee County, but are present in DeWitt County.

Washita Supersequence Depositional Profiles

Flooding at the base of the Georgetown Fm above cyclic subtidal shelf and peritidal lithofacies of the Fredericksburg supersequence caused drowning in the shelf-interior along the San Marcos Arch and much of the East Texas Basin (Figures 2.12 and 2.13). Greater sediment production rates within the Stuart City margin allowed it to aggrade vertically during initial transgression of the Washita supersequence. Simultaneously, high-energy shoal complexes and caprinid build-ups of the Devils River Fm bordering the Maverick Basin were able to prograde over oyster-rich marls of the basinal Salmon Peak Fm (Kerans, 2002). During deposition of the Georgetown Fm and equivalent strata, combination of aggraded shelf-margins with drowned shelf-interiors

and salt-withdrawal basins accentuated the rimmed-shelf depositional profile and created an empty-bucket morphology (Figures 2.5, 2.12, 2.13).

Complete drowning of the Stuart City margin occurred during deposition of Del Rio shales. Blanketing of the platform during this phase of deposition began filling the differential shelf-to-margin topography and continued through deposition of the Buda Fm. This period of sedimentation resulted in a distally-steepened ramp morphology with inflection of the profile over the drowned Albian shelf-margin.

Washita Supersequence Stratigraphy

The Washita succession encompassing the Georgetown, Del Rio and Buda formations is interpreted as a second-order supersequence (~101-96 Ma). In DeWitt County, Georgetown equivalent strata of the Stuart City margin display aggradational HFC sets that are later followed by a transgressive HFC set representative of reef drowning. Kerans (2002) noted similar trends in the Devils River Fm bordering the Maverick Basin and defined an upper Albian depositional sequence that is time-equivalent to aggradational HFC sets of the uppermost Stuart City margin. Scott et al. (2002) also described several high-frequency sequences internal to the Washita Group of the East Texas Basin. Taking their data into account, I tentatively define a Georgetown-1 depositional sequence that encompasses all Georgetown-equivalent strata of the Stuart City margin, with the exception of the last HFC set (Figure 12).

Because of the middle- to outer-ramp setting during deposition of the Del Rio and Buda formations, I am unable to further subdivide these portions of the Washita supersequence into depositional sequences. However, due to the conformable relationship among the two units in the study area and incorporating studies by Scott et al. (1978),

Scott et al. (2002), and Mancini et al. (2008) I tentatively group the uppermost Georgetown, Del Rio, and Buda formations into a single third-order package termed the Buda-1 sequence (Figure 2.12). Nonetheless, I acknowledge the work on roadcuts northwest of the Maverick Basin by Lock et al. (2007) who interpreted the Del Rio and Buda formations as separate depositional sequences. Maximum flooding surfaces of the Buda-1 sequence and the Washita supersequence are placed in the lower portion of the Del Rio Fm (Figure 2.13).

This supersequence is capped by an unconformity above the Buda Fm, known as the Mid-Cretaceous unconformity, which is recognizable in seismic data throughout the Gulf of Mexico (Buffler et al., 1980; Faust, 1990) and contains an incised valley system through which Woodbine Group sands and conglomerates passed into the East Texas Basin (Ambrose et al., 2009). The dip-extent of this unconformity is unknown in south Texas, however biostratigraphic data suggest it is present in the Brechtel #1 core and confirms a lower Cenomanian age of the Buda Fm (R.W. Scott, personal communication). Stratigraphic evidence indiates the unconformity may be present in some bathymetrically shallow areas above the drowned shelf-margin. In Bee County, the Del Rio and Buda formations are not present, while Georgetown-age Stuart City lithofacies are unconformably overlain by black shales of the Eagle Ford Fm in the Leppard #1 core. Stable-isotope data through the Leppard #1 core display a prominent negative excursion beneath this contact (Figure 2.8); a trend that is often the result of subaerial exposure (Allan and Matthews, 1982). The geochemical data and absence of the Del Rio and Buda formations in bathymetrically shallow areas over the former shelf-margin are taken as evidence for subaerial exposure and erosion of these units at the Washita supersequence boundary. In contrast, bathymetrically deeper areas of the

palimpsest margin, such as down-dropped fault blocks in DeWitt County, contain preserved accumulations of the Del Rio and Buda formations (Figure 2.13).

Eagle Ford–Austin Chalk Supersequence (Late Cenomanian – Early Campanian)

Lithologic units of the Eagle Ford–Austin Chalk Supersequence (EF-AC) include shales of the Eagle Ford Group and the equivalent Boquillas Fm of West Texas (Dawson, 1997; Dawson, 2000; Lock and Peschier, 2006), as well as numerous formations of the Austin Chalk Group (Young, 1986). Fluvial-deltaic siliciclastics of the Woodbine Group and Maness Shale in the East Texas Basin are not present in the study area but are demonstrated to be younger than the top of the Washita supersequence (Ambrose et al., 2009).

Lithofacies Distributions

Eagle Ford Group lithofacies consist of planar-laminated black shale and laminated shale/calcisilt. The age of the Eagle Ford Group is latest Cenomanian through Turonian (Jiang, 1989), which spans the global records of OAE 2 (Jenkyns, 1980). Planar laminations and the absence of biogenic sedimentary structures are the physical manifestation of anoxia in Eagle Ford shales. Proximal Austin Chalk lithofacies include *Planolites*-burrowed chalk and a more distal, argillaceous, *Zoophycos*-burrowed chalk (Figure 2.8).

My lithostratigraphic boundary between the Eagle Ford and Austin Chalk Groups in the Brechtel #1 and Leppard #1 cores (Figures 2.4 and 2.8) is placed at the contact between planar-laminated calcareous shale and burrowed argillaceous chalk, respectively. This change is thought to reflect the shift from anoxic conditions at the sediment-water

interface during Eagle Ford deposition to dysoxic and oxygenated conditions during Austin Chalk deposition (Schlanger and Jenkyns, 1976; Arthur and Sageman, 1994). The contact between the two groups appears conformable in my cores but in some north Texas outcrops the contact is disconformable and locally erosive (Grabowski Jr., 1995; Hovorka and Nance, 1994; Lock and Peschier, 2006; Stapp, 1977; Hancock and Walaszczyk, 2004). South Texas subsurface data (Figure 2.13) show Eagle Ford shale thickening substantially from a landward to basinward direction, which occurs as overlying Austin Chalk facies thin toward the shelf-margin. As the Eagle Ford Group thickens down depositional-dip, the planar-laminated shale/calcisilt facies is no longer present.

Eagle Ford–Austin Chalk Supersequence Depositional Profile

Stapp (1977) discussed the "shaling-out" of the Austin Chalk in a line of section from Bexar to Bee Counties (see B-B' in Figure 2.13) as the proportion of terrigenous clay within the Austin Chalk increased down depositional-dip. Dravis (1980), Hovorka and Nance (1994), and Grabowski Jr. (1995), each recognized the presence of a "lower" Austin Chalk lithofacies with laminated chalks to marls. These lithofacies contain organic contents reaching up to 3.7% TOC, which is slightly less than the average 5.2% TOC in the basal Eagle Ford (Grabowski Jr., 1995; Dawson, 2000). They interpreted the sparsely-burrowed lower Austin Chalk as a relatively deep-water unit deposited under suboxic to dysoxic bottom conditions (Hovorka and Nance, 1994; Grabowski Jr., 1995).

Incorporating the data and observations of previous workers with the lithofacies distributions in south Texas, I argue that the "lower" Austin Chalk is a landward, time-equivalent facies of basinward, upper Eagle Ford shale. At the regional scale, the Eagle

Ford/Austin Chalk contact is interpreted as diachronous and becomes younger down depositional dip. Therefore the depositional profile is that of a distally-steepened ramp with aggradational "lower" Eagle Ford laminated black shale, followed by progradational Austin Chalk to Eagle Ford clinothems with chalk foresets and shale bottomsets. The progradational clinothems contain *Planolites*-burrowed chalk grading down-dip into argillaceous, *Zoophycos*-burrowed chalk, which then interfinger with the planar-laminated shale/calcisilt, before finally passing into the deepest-water, planar-laminated black shale lithofacies.

This model is a departure from those of previous authors who correctly separate the Eagle Ford and Austin Chalk as distinct lithologic units in central and north Texas (Surles, 1987; Sohl, et al. 1991; Grabowski, 1995; Dawson, 1997). In support of the correlation model presented here, west Texas outcrops exhibit locally conformable and gradational contacts separating the Boquillas Fm (upper Eagle Ford equivalent) and the Austin Group (Pessagno, 1969; Surles, 1987; Locke and Peschier, 2006). In south Texas, interpretation of similar gradational lithofacies relationships along isochronous depositional profiles explains the dip-oriented thickness changes of the Eagle Ford and Austin Groups. Sufficient subsurface paleontologic data are currently lacking to confirm or reject this correlation scheme and it is presented as a working hypothesis.

Eagle Ford–Austin Chalk Supersequence Stratigraphy

Where the contact with the underlying Washita supersequence is conformable in south Texas, the EF-AC supersequence spans an interval of 14 Ma (94-80 Ma) (Jiang, 1989). Maximum flooding is interpreted to be within the Eagle Ford Group above the most landward extent of planar laminated black shale (Dawson, 1997) (Figure 2.13). The

Eagle Ford/Austin Chalk lithostratigraphic contact in outcrops of north and central Texas is located in the upper Turonian and approximates the Turonian/Coniacian boundary (Jiang, 1989; Dawson, 1997; Hancock and Walaszczyk, 2004). A hiatus at this disconformable contact may be the result of storm ravinement during progradation of younger clinoforms or scouring during down-dip transport of sediment-gravity flows. The disconformity likely represents a third-order sequence boundary and is approximately the same age as depositional sequence boundaries recognized in other global successions (Hancock, 1990; Liro et al., 1994; Dawson, 1997; Hardenbol and Robaszynski, 1998; Hancock and Walaszczyk, 2004; Gil et al., 2006). The correlative conformity of this sequence boundary may be present in Eagle Ford black shale above the Albian shelf-margin. The supersequence designation is based on the underlying Mid-Cretaceous unconformity, deepening in the basal Eagle Ford Group, and the shallowing-upward trend in the Austin Chalk documented by previous authors (Liro et al., 1994; Dawson, 1997; Dravis, 1980; Hovorka and Nance, 1994; Grabowski Jr., 1995). The top of the supersequence is placed beneath Taylor Group shales along a local submarine hardground and surface of nondeposition observed by Hovorka and Nance (1994). On the San Marcos Arch, the EF-AC supersequence may be treated as a long-term T-R package, however in the East Texas Basin, Woodbine Group siliciclastics may be incorporated as a third-order lowstand systems tract. Additional relative sea level cycles on the scale of third-order depositional sequences likely occurred (Liro et al., 1994; Dawson, 1997; Hancock and Walaszczyk, 2004) but are not recognizable in this data set.

SEDIMENT DISTRIBUTION, SHELF MORPHOLOGY AND THE INFLUENCE OF RELATIVE SEA LEVEL

With the exception of the upper boundary of the EF-AC supersequence, all T-R supersequences outlined in this study are bound by erosive unconformities with iron-stained hard-grounds or caliche soil zones. Taken as a whole, the long-term trend of the seven supersequences is that of a first-order eustatic sea level rise during transgression in the Zuni sequence (Sloss, 1963), which peaked with maximum flooding of the EF-AC supersequence. Continual retrogradation of Hosston Fm and Hensel Fm shoreline siliciclastics sourced from the Llano uplift reflects this eustatic rise (Figure 2.5).

Supersequence-scale changes in the rate of accommodation creation promoted dramatic changes in shelf morphology, shelf-margin trajectory, shelf-interior sediment distributions, and faunal assemblages. Sligo and Stuart City shelf-margin trajectories appear to have evolved in cyclic fashion from (1) no active margin to (2) strongly-progradational to (3) aggradational to (4) retrogradational to (5) no active margin. As a result, corresponding morphologies of the platform reorganized sequentially from (1) distally-steepened ramp to (2) low-angle shelf to (3) high-angle rimmed-shelf to (4) empty-bucket rimmed-shelf to (5) distally-steepened ramp (Figure 2.14). With the exception of the Sligo supersequence, marine shales are associated with supersequence maximum flooding surfaces. Maximum flooding surfaces encompassed by shales of the James, Bexar, Washita, and EF-AC supersequences represent classic condensed sections that thinned down depositional dip. In contrast, argillaceous carbonate zones (marls) containing Glen Rose and Fredericksburg supersequence maximum flooding surfaces appear to have maintained sedimentat accumulation rates similar to those of the surrounding carbonate strata (Figure 2.14). Supersequences with shelf morphologies and vigorous carbonate factories produced sediment at an average rate of 2.6 – 5.5 cm/ky in

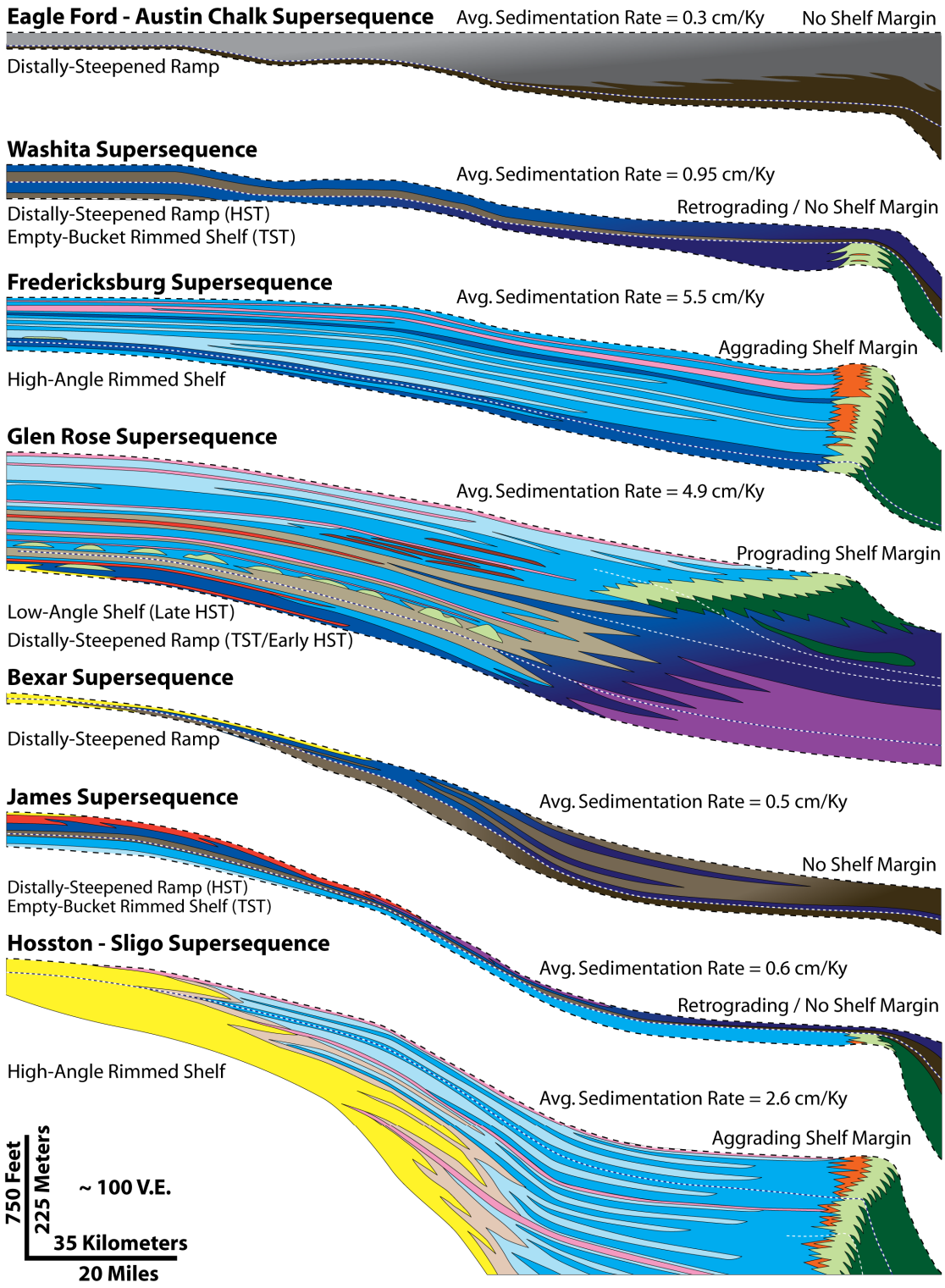

Figure 2.14: A separated view of the seven supersequences. Changes in platform

morphology as related to supersequence development are discussed in the text. Average sediment accumulation rates for each supersequence do not account for compaction. They are calculated in the middle platform using thicknesses measured from the Pruit #46 core for the Hosston-Sligo supersequence and the Mercer #1 core or wireline-logs for the remaining six supersequences. Durations of the supersequences are listed in the text. A facies key is provided in Figure 2.5.

the middle-shelf. This is roughly three to eighteen times greater than the supersequences with distally-steepened ramp morphologies and condensed shale maximum floods (0.3 – 0.9 cm/ky) that were coincident with globally recognized OAEs 1a, 1b, and 2.

Marked changes in shelf-margin trajectory and platform morphology only occurred at the supersequence-scale as a result of long-term transgressive or regressive trends. From the regional perspective of the study, relative sea level fluctuations on the order of depositional sequences appear to have had no discernable impact on shelf-margin trajectory or platform morphologic evolution. This is largely a result of the low-amplitude (10-15 m) third-order eustatic signal characteristic of greenhouse systems (Grotzinger, 1986; Goldhammer et al., 1987; Strasser, 1988; Montanez and Read, 1992; Read, 1998). Changes in third-order sea level trends, which are clearly manifest in shelf-interior lithofacies migration patterns, may have caused changes in facies distributions within the reefal margin, but were insufficient to significantly affect the long-term shelf-margin trajectory of the highly productive reef system or to cause reef drowning. Rather, major modifications to the shelf-margin trajectory or shifts in the morphology of the platform required greater magnitude changes in platform accommodation that were externally forced and of longer duration (~3-10 Ma) than typical greenhouse third-order sequences. Plausible mechanisms include eustatic sea level changes induced by variable volcanism along mid-ocean ridges (Hays and Pitman, 1973; Bay, 1977; Larson, 1991) and reduction in carbonate sediment production as a result of environmental deterioration

surrounding OAEs (Bachmann and Hirsch, 2006; Follmi et al., 1994; Weissert et al., 1998; Wissler et al., 2003; Chapter 3). These processes, though not limited to the Cretaceous Period, are two prominent aspects of the Cretaceous world which not only affected climate, but also controlled long-term sedimentation patterns of carbonate platforms.

During supersequences in which shelf-margins were absent, sediment grain size and sorting patterns increased toward the landward direction in tandem with the decrease in bathymetry along the ramp profile (Figures 2.5, 2.10, 2.13, 2.14). In these units, hydrodynamic processes, rather than biological processes, controlled the sediment patterns, facies distributions, and morphologic profile of the platform. In third-order transgressive systems tracts, shales and mud-dominated carbonates were the chief sedimentary components of the middle- to outer-ramp, with few grainstone units capping increasingly subtidal HFC sets. Open-marine conditions across the ramp profile allowed stromatoporoid-coral-rudist assemblages typically found at the shelf-margin to build middle-ramp biohermal and biostromal communities during early highstands of depositional sequences. Highstand systems tracts within these settings contain strongly progradational, land-attached grainstone and siliciclastic sandstone shoreface systems that were isolated to the inner-ramp. If no high-energy shoreface system was present, highstand HFC sets capped by low-energy tidal flat systems became increasingly common upward in the supersequence. As noted by Read (1998), this observed distribution of subtidal and peritidal cycles as related to transgressive and highstand systems tracts appears to be a universal principle among greenhouse ramp systems through geologic time (Montanez and Read, 1992; Elrick, 1995).

In supersequences with well-developed shelf-margins, the predominance of miliolid-rich faunal assemblages and periods of laterally extensive evaporite deposition

indicate generally restricted conditions in the shelf-interior. Peritidal grainstone sand flats and mudstone tidal flats that surround depositional sequence boundaries commonly extended across much of the middle- and outer-shelf, as opposed to their ramp counterparts which were more closely anchored to the inner-ramp shoreline. The presence of a rimmed-shelf-margin with high-energy, back-reef grainstone/rudstone belts in the Sligo and Fredericksburg supersequences created energy-shadows behind the shelf-margin and allowed mud-dominated strata with oyster, chrondrodont and toucasid biostromes to flourish. Low-angle shelves of the Glen Rose supersequence do not exhibit similar back-reef grainstone belts and thus do not have appreciable energy shadows.

As is typical of greenhouse carbonate systems (Montanez and Read, 1992; Read, 1998; Lehrmann and Goldhammer, 1999), the third-order sequence boundaries not associated with second-order supersequence boundaries are largely defined by cycle stacking patterns and lithofacies proportions within zones of minimal accommodation. Unlike supersequence boundaries, depositional sequence boundaries do not display thick soil horizons or significant unconformities indicative of long-term subaerial exposure. For these reasons, the sequences are interpreted as T-R sequences and have no lowstand systems tract. Third-order maximum flooding surfaces, in ramp and shelf settings, are mud-dominated and typically contain more open-marine fauna such as echinoderms, rudists, coral, and *Orbitolina*.

The above generalizations are not the case for the Washita and EF-AC supersequences, which contained mud-dominated, flooded-shelf/ramp strata throughout their development and closely correspond with maximum flooding of the first-order eustatic trend. Proper characterization of lithofacies distributions and sequence stratigraphic interpretation in these broad, deep-subtidal shelf and ramp settings is problematic due to (1) gradational stratigraphic contacts, (2) minimal conformance of

lithofacies patterns and grain size trends to higher-order relative sea level cycles, and (3) the lack of isochronous stratigraphic datums on which to base regional correlations. As shown, gradational facies changes along subtle depositional dips (EF-AC supersequence) or across diverse paleoenvironmental settings (Washita supersequence) are likely the rule and not the exception in moderate- to deep-subtidal settings. Furthermore, as is the case at the shelf-margin of the lower Washita supersequence, localized syndepositional faulting or structural modification of bathymetric trends can affect stratigraphic interpretations if confined to narrow study windows.

CRETACEOUS SUPERSEQUENCES AND THE EUSTATIC SIGNAL

Direct comparison of the Cretaceous carbonate succession in south Texas with other worldwide carbonate provinces and published "global" sea level curves highlights numerous common trends illustrative of the Cretaceous eustatic signal. Figure 2.15 displays a schematic chronostratigraphic chart of the south Texas section, as well as sequence stratigraphic interpretations from this study, northern Mexico (Lehmann et al., 2000; Goldhammer and Johnson, 2001), and the Arabian plate (Haq et al., 2005; Sharland et al., 2001; Van Buchem et al., 2010). These sequence stratigraphic data are then integrated with eustatic sea level curves from the New Jersey passive margin (Miller et al., 2004), Pacific Ocean Guyots (Roehl and Ogg, 1996), the Russian Platform (Sahagian et al., 1996), and the Exxon global compilation (Haq et al., 1988). Original data from these previous works are shifted to a common geologic time scale (Gradstein et al., 2004) using stage boundaries, planktonic foraminiferal zones (Hardenbol et al., 1998), or both. With the exception of the northern Mexico studies, each of the seven supersequences from Valanginian through early Campanian time is present in all comparison profiles.

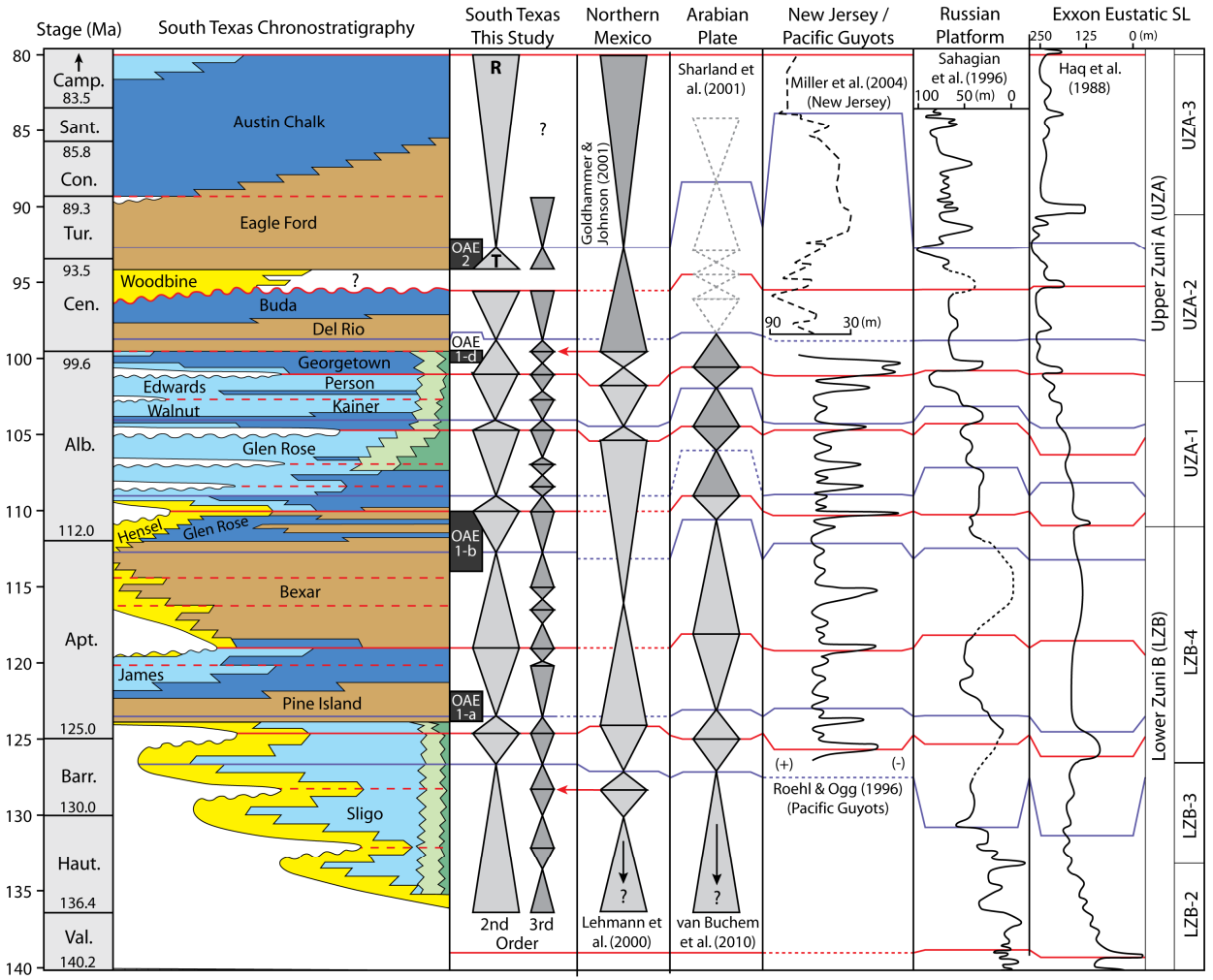

Figure 2.15: Chronostratigraphic chart and comparison of T-R sequences in this study to those of other platforms and eustatic sea-level curves. Accommodation triangles with white fill represent sequences controlled by local tectonics.

Possible errors in supersequence absolute ages and correlations include: (1) improperly shifted time scales, (2) incomplete paleontologic information, and (3) linear extrapolation of sediment accumulation rates between dates or within foraminiferal zones.

Northern Mexico

In the Mexican Cupido carbonate platform bordering the western Gulf of Mexico, at least two Hauterivian-Barremian "composite sequences" are present (Lehmann et al., 2000) and they may be equivalent to the Sligo-2 and Sligo-3 sequences (Figures 2.9 and 2.15). The Cu-2 sequence boundary in the upper Cupido platform (Lehmann et al., 2000; Goldhammer and Johnson, 2001) is likely equivalent to the top Sligo supersequence boundary. Similar to the south Texas section, carbonates in the upper portion of the Cupido platform ("Cupidito" facies) backstep and record a late Hauterivian transgressive trend prior to platform drowning by La Pena shales in the lower Aptian (Goldhammer et al., 1991). Neither the James nor the Bexar supersequence boundaries are recognized and flooding appears to have peaked in the late Aptian within the northern Mexico section (Lehmann et al., 1999). Their late Aptian MFS would be coincident with the Bexar supersequence maximum flood. The James and Bexar supersequence boundaries are recognized based on the presence of highstand shoreface depositional systems prograding from the back-stepped shoreline surrounding the Llano uplift. Without a land-attached shoreline, it would be difficult to distinguish these additional supersequences in deep-subtidal mudstones/wackestones that spread across the flat-topped Cupido platform during deposition of the upper Tamaulipas Fm.

Additional Albian sequence boundaries in the Aurora and Acatita formations outlined by Lehmann et al. (2000) appear to be equivalent to the top Glen Rose and

Fredericksburg supersequences, as well as the Georgetown-1 depositional sequence. Goldhammer and Johnson (2001) group the Cenomanian through Santonian sections of northern Mexico into a single supersequence that was tectonically modified during Laramide orogenesis.

Arabian Plate

A compelling comparison of stratigraphic patterns can be made with mixed carbonate-siliciclastic systems in Oman and the larger Arabian plate (Figure 2.15). Above the Valanginian unconformity, three Hauterivian-Barremian depositional sequences are recognized in the Lekhwair, Kharaib and equivalent formations of Oman, Saudi Arabia, Kuwait and Iraq (Sharland et al., 2001; Pittet et al., 2002; Hillgartner et al., 2003; Haq and Al-Qahtani, 2005). These are collectively grouped into a supersequence with the top boundary in the upper Kharaib Fm (Hillgartner et al., 2003; Van Buchem et al., 2010), which represents a significant drop in base level equivalent to the top-Sligo supersequence boundary. The early to middle Albian Hawar shale (Kharaib Fm) and the Shu'aiba Fm contain several depositional sequences and comprise a second-order sequence that is temporally equivalent to the James supersequence. Although it may be locally enhanced by regional tectonism, the top Shu'aiba supersequence unconformity is recognized across the Arabian Peninsula and likely represents a relative sea level drop of up to 50 meters (Sharland et al., 2001; Hillgartner et al., 2003; Haq and Al-Qahtani, 2005; Vahrenkamp, 2010; Van Buchem et al., 2010).

The late Aptian to early Albian K90 sequence of Sharland et al. (2001) contains the Bab Member of the Shu'aiba Fm and lower units of the Nahr Umr Fm in Oman. Van Buchem et al. (2010) assemble this succession and its four nested third-order sequences

into a second-order supersequence that is the temporal equivalent of the Bexar supersequence. The K100 sequence of the Nahr Umr Fm and the K110 sequence of the Mauddud Fm (Sharland et al., 2001; Haq and Al-Qahtani, 2005) approximate my respective Glen Rose and Fredericksburg supersequences within a 1 Myr margin of error.

Tilting of the Arabian plate may have occurred during the latest Aptian to Albian (van Buchem et al., 2002) and perhaps led to the increased deposition of siliciclastic sediment in the Nahr Umr Fm. Considering this possibility, I view the Albian sequence stratigraphic parallels to the Arabian Peninsula, particularly with respect to the Bexar and Glen Rose supersequences, as tentative correlations. Regional tectonism throughout the Upper Cretaceous obscured the eustatic signal; thus deposition of the Mishrif, Natih and younger formations is largely a result of local processes (van Buchem et al., 2002).

Eustatic Sea-Level Curves

Comparison of the south Texas sequence stratigraphy to eustatic Cretaceous sea level curves from diverse global settings (Figure 2.15) reveals encouraging results that corroborate the interpretations of this study and the previously published eustatic curves (Haq et al., 1988; Roehl and Ogg, 1996; Sahagian et al., 1996; Miller et al., 2004). Eustatic curves from the Russian Platform (Sahagian et al., 1996) and Exxon global compilation (Haq et al., 1988) both show a long-term eustatic rise above the Valanginian unconformity that peaked in the late Hauterivian and was followed by a significant early Albian drop in sea level. This trend is expressed by the Sligo supersequence; however the maximum flooding surface is placed in the Barremian rather than the Upper Hauterivian, which is possibly a result of relatively high thermal subsidence rates (Watts and Ryan, 1976) on the “young” south Texas passive margin. Higher-order drops in sea level shown

in the Russian platform curve may correspond to the top Sligo-1 and Sligo-2 depositional sequence boundaries.

The eustatic maximum flood in the lower Aptian Pine Island member and the fall capping the middle Aptian James supersequence are present in all three of the Pacific, Russian, and Exxon curves. A subtle inflection in the Russian platform curve may correspond to the third-order boundary between the James-1 and James-2 sequences. The top of the Bexar supersequence in the earliest-Albian is expressed strongly in the Pacific Guyots eustatic curve (Roehl and Ogg, 1996), yet it is more subtle in the Russian platform and Exxon versions. Records of maximum flooding in the Bexar supersequence are inconsistent but generally indicate a latest Aptian eustatic peak.

Sequence boundaries capping the middle Albian Glen Rose supersequence, as well as the LGR-1, UGR-1, and UGR-2 depositional sequences, are each expressed in the Pacific Guyots eustatic curve, whereas only the second-order trend is visible in the Russian platform record. The exact location of the Glen Rose supersequence boundary in the Exxon curve is relatively ambiguous. The drop in eustatic sea level which induced the top Fredericksburg supersequence boundary is clear in each of the three main eustatic curves. The contact between the Person-1 and Kainer-1 depositional sequences may be distinguishable in the Pacific Guyots record, but is unclear in the other records.

Drowning of the Pacific Guyots occurred in the latest Albian to early Cenomanian (Roehl and Ogg, 1996) and appears to coincide with drowning of the Comanche Shelf and Stuart City reef-margin in south Texas, suggesting that increased rates of eustatic rise in the upper Cretaceous quickly diminished shallow-marine carbonate productivity in tectonically stable settings. The unconformity forming the late-middle Cenomanian Washita supersequence boundary is present in the eustatic records from New Jersey (Miller et al., 2004), the Russian platform, and the Exxon global compilation. The first-

order eustatic trend peaked in the early Turonian as expressed in the EF-AC supersequence. This is consistent with the Exxon and Russian eustatic curves; however the New Jersey record does not show a eustatic maximum until Santonian time. An uppermost Turonian drop in base level is shown in the Russian and Exxon curves, which may be expressed in landward areas of south Texas by the third-order sequence boundary between the Eagle Ford and Austin Chalk Groups. Few common trends are observed in the remaining interval until an additional sea level fall in the lower Campanian, which corresponds to the top of the EF-AC supersequence. The remaining siliciclastic-dominated upper Cretaceous section in south Texas, which consists of the Taylor and Navarro groups, perhaps constitutes two additional supersequences observed on the New Jersey shelf and Exxon curves. This study lacks data to fully support this hypothesis and t interpretation is suggested based on published stratigraphic relationships (Sohl et al., 1991).

Taken as a whole, the eustatic sea level curve that most closely corresponds to my interpretations from south Texas is that constructed for the Pacific Guyots by Roehl and Ogg (1996). Given the sensitivity of carbonate depositional systems to paleobathymetry and their ability to quickly fill accommodation, it is not surprising that these two independent, but structurally quiescent, carbonate-dominated provinces display similar eustatic sea level records at second- and third-order scales. The eustatic record from the siliciclastic-dominated Russian platform by Sahagian et al. (1996) shows fewer third-order similarities, while the Exxon global compilation (Haq et al., 1988) only compares favorably for second-order supersequences.

CONCLUSIONS

Above the middle Valanginian unconformity and within the Hauterivian through lower Campanian section of the Sligo and Comanche shelves in south Texas, seven unconformity-bound, second-order, T-R supersequences are delineated, including the:

(1) Hosston-Sligo Supersequence (136-124 Ma)

(2) James Supersequence (124-119 Ma)

(3) Bexar Supersequence (119-110 Ma)

(4) Glen Rose Supersequence (110-104 Ma)

(5) Fredericksburg Supersequence (104-101 Ma)

(6) Washita Supersequence (101-96 Ma)

(7) Eagle Ford – Austin Chalk Supersequence (94-80 Ma).

Two additional supersequences may be present in siliciclastic-dominated strata of the Taylor and Navarro groups in the upper Campanian through Maastrichtian interval. Supersequence and depositional sequence boundaries do not necessarily correspond with boundaries of formal lithostratigraphic units.

Supersequence development was a function of eustatic sea level fluctuations induced by changes in volcanism along mid-ocean ridges and the emplacement of large igneous provinces. These eustatic changes, coupled with environmental perturbations from OAEs, induced the frequent transformation of supersequence morphologic profiles. These external factors thereby controlled the internal energy regimes, depositional processes, sediment accumulation rates, grain size patterns, lithofacies distributions, and faunal assemblages of the passive margin system.

Changes in platform morphology and shelf-margin trajectory only occurred at the scale of second-order supersequences. Lithofacies distributions within the

supersequences follow predictable patterns according to platform morphology. Shelf morphologies contain grain-dominated strata and intertidal lithofacies that frequently extended from the shoreline to the reefal shelf-margin and are present in both transgressive and highstand systems tracts. The shallowest and highest-energy lithofacies increase in abundance toward sequence boundaries of all scales. Mud-dominated lithofacies in the shelf systems are found at the base of high-frequency cycle sets and around maximum flooding surfaces. High-angle shelf morphologies generally transform to "empty-bucket" rimmed shelves during long-term (second-order) transgressive systems tracts. Grain-dominated strata are typically found at the reefal shelf-margin, whereas the drowned "empty-bucket" shelf-interior contains mud-dominated lithofacies. Maximum flooding surfaces of supersequences commonly correspond to condensed shales and transformed the rimmed-shelf profile to distally-steepened ramp morphologies. Because of their association with OAEs, undecompacted sediment accumulation rates of supersequences with distally-steepened ramp morphologies are approximately 65-95% less than those found in supersequences with shelf morphologies. Highstand systems tracts in ramp profiles exhibit grain-dominated strata that were anchored to shoreline depositional systems and mud content increases down-depositional dip. Gradual progradation of the distally-steepened ramp eventually established a low-angle shelf morphology, which later steepened to a high-angle rimmed shelf during subsequent transgressive systems tracts. Third-order depositional sequences are not easily discernable at the shelf-margin and their sequence boundaries are typically marked by subtle changes in faunal assemblages. Depositional sequences and higher-order cycle sets are primarily manifest in changing facies proportions and cycle stacking patterns of platform interior strata.

The supersequences identified in south Texas appear to be globally correlative with stratigraphic trends from isolated platforms in northern Mexico, mixed carbonate-siliciclastics of the Arabian plate, and eustatic sea level curves generated from diverse paleogeographic areas. Higher-order depositional sequences are not always recognized between basins. The best correspondence of stratigraphic patterns in the data occurs when compared to sedimentologic records generated from tectonically stable guyots in the Pacific Ocean. Comparison of my data to sea level curves derived from siliciclastic-dominated successions yields indistinct results. My findings suggest shallow-marine carbonate provinces that follow a predictable subsidence pattern offer the best opportunity to correlate eustatically controlled stratigraphic packages across basins and develop a global sea level curve. Passive margins with little structural overprint or tectonic influence, such as the Cretaceous Gulf of Mexico, and isolated carbonate platforms offer such opportunities. As demonstrated here, accomplishing this objective requires detailed sequence stratigraphic analysis using continuous rock data. Further work in the south Texas section to provide backstripped estimates of eustatic amplitudes will allow more direct comparison of the section to previously published eustatic sea level curves.

Chapter 3 – A Middle Hauterivian to Early Campanian Secular Carbon Isotope Profile from Shallow-Marine Carbonates Linked to Cretaceous Oceanic Anoxia, Northern Gulf of Mexico[2]

ABSTRACT

The ubiquity of carbonate platforms throughout the Cretaceous period is recognized as a product of high eustatic sea-levels and a distinct climatic optimum induced by rapid sea-floor spreading and elevated levels of atmospheric carbon-dioxide. Notably, a series of global oceanic anoxic events (OAEs) punctuate this time-interval and mark times of significantly reduced free oxygen in the world's oceans. The best records of these events are often from a series of one-dimensional shelf or basin strata where only abrupt shifts between oxygenated carbonates and anoxic shales are recorded. The Comanche Shelf of central Texas provides a unique opportunity to study these events within a well-constrained stratigraphic framework in which both the up-dip and down-dip limits of these events can be observed and the recovery of the platform to a background state can be timed and understood. Stable isotope data from middle Hatuerivian through early Campanian whole-core intervals of mixed carbonate-siliciclastic strata are used to construct a 53 Myr carbon isotope reference profile for the northern Gulf of Mexico. Correlation of this composite curve to numerous global reference profiles permits identification of several anoxic events and allows their impact on platform architecture and facies distributions to be documented. OAEs 1a, 1b, 1d, and 2 were equivalent to or followed by shale deposition in the Pine Island Member, Bexar Member, Del Rio

[2] Written for submission to *Paleoceanography*.

Formation, and Eagle Ford Group, respectively. OAE 3 corresponds to proximal Austin Chalk and distal Eagle Ford shale facies.

Using chemo- and sequence-stratigraphic observations, a four stage model is proposed to describe the changing facies patterns, faunas, sedimentation accumulation rates, platform architectures, and sea-level trends of transgressive-regressive supersequences that developed in response to global carbon-cycle perturbations. The four phases of platform evolution include the equilibrium, crisis, anoxic, and recovery stages. These are characterized by progradational shelf, retrogradational shelf, drowned shelf, and progradational ramp geometries, respectively. Heterotrophic fauna present during the anoxic and recovery stages are dominated by oysters or coccolithophorids and are markedly different from the coral-rudist-dominated phototrophic assemblages of the equilibrium and crisis stages. The crisis stage exhibits transgressive facies patterns, increased shale proportions, and contains well-documented biocalcification crises. Anoxic stages were coincident with eustatic peaks of moderate amplitude (~ 30 m) but relative sea-level rises and platform drowning were greatly enhanced by reduced sedimentation rates and back-ground deposition of organic-rich shale. In the recovery stage, the carbonate factory re-established at the shoreline and sediment accumulation rates slowly increased as dysoxia diminished. Full recovery to equilibrium conditions may or may not have followed. Geochemical and stratigraphic trends present in the four stages are consistent with increased volcanism along mid-ocean ridges and in large-igneous provinces as primary drivers of Cretaceous OAEs and the resulting transgressive-regressive supersequences.

INTRODUCTION

Oceanic anoxic events (OAEs) previously documented from numerous time intervals in the Cretaceous and latest Jurassic periods were concomitant with significant perturbations to the global carbon cycle. These perturbations are commonly manifest in the stratigraphic record by the anomolous occurrence of organic-rich shale units that were deposited under dysoxic to anoxic conditions and are sitting in sharp contact with shallow-water carbonate platform strata (Schlanger and Jenkyns, 1976; Jenkyns, 1980; Arthur and Sageman, 1994). While the exact causes of OAEs are still debated, they generally coincide with the maximum rates of eustatic rise during long-term transgressions (Schlanger and Jenkyns, 1976). Well-established background environmental conditions include high-rates of oceanic crust production (Larson, 1991) and elevated pCO_2 levels from volcanic degassing. Increased atmospheric pCO_2 caused diminished latitudinal thermal gradients (Barron et al., 1993), elevated sea-surface temperatures (Huber et al., 2002), and "sluggish" oceanographic circulation of warm, deep-ocean water-masses that were prone to vertical stratification (Schlanger and Jenkyns, 1976; Erbacher et al., 2001; Haupt and Seidov, 2001; Emeis and Weissert, 2009). Regardless of the mechanism invoked to trigger these events, it is clear that enhanced nutrient delivery to the marine realm dramatically increased surface-water primary productivity (Larson and Erba, 1999; Handoh and Lenton, 2003; Weissert and Erba, 2004; Mort et al., 2007; Elrick et al., 2009; Jimenez-Berrocoso et al., 2010). Preservation of the resulting organic material was enhanced by bottom-water anoxia that extended from ocean basins up onto continental shelves (Schlanger and Jenkyns, 1976; Weissert, 1989; Montoya-Pino et al., 2010). Associated with these oceanographic events are the coincidental drowning of several carbonate platforms (Arthur and Schlanger, 1979; Groetsch et al., 1993; Follmi et al., 1994; Weissert et al., 1998), decreases in

nannofossil abundance (Erba 1994; Mehay et al., 2009; Erba et al., 2010;), and extinction/radiation events of radiolaria and foraminifera (Erbacher et al., 1996; Erbacher and Thurow, 1997; Parente et al., 2008). Thus it is evident that the causes and consequences of the OAEs rippled throughout the marine ecosystem and were catastrophic for most biologic communities.

Global correlation of these inter-basinal events can be accomplished through development of vertical carbon isotope profiles derived from biostratigraphically constrained marine carbonate strata ($\delta^{13}C$) or the contained organic carbon ($\delta^{13}Corg$) (Bralower et al., 1999; Scholle and Arthur, 1980). Each interpreted period of global anoxia during the Valanginian (Weissert event), early Aptian (OAE 1a), early Albian (OAE 1b), late Albian (OAE 1d), Cenomanian/Turonian (OAE 2), and Coniacian/Santonian (OAE 3) is represented by a $\delta^{13}C$ excursion to heavier values, reflecting increased sequestration of isotopically light organic carbon during deposition of organic-rich sediments (Weissert, 1989; Gale et al., 1996; Jarvis et al., 2002; Leckie et al., 2002; Erba et al., 2004; Locklair et al., 2004; Weissert and Erba, 2004; Follmi et al., 2006; Jarvis et al., 2006). The diverse paleogeographic locations in which OAEs have been documented illustrate their global extent, and include sites from the paleo-Tethys Ocean, Atlantic Ocean, Pacific Ocean, the western Gulf of Mexico, and the Western Interior Seaway of North America (Pratt et al., 1984; Weissert, 1989; Vahrenkamp, 1996; Menegatti et al., 1998; Bralower et al., 1999; Stoll and Schrag, 2000; Wilson and Norris, 2001; Jarvis et al., 2002; Price, 2003; Herrle et al., 2004; Locklair et al., 2004; Tsikos et al., 2004; Wendler et al., 2009; Jimenez-Berrocoso et al., 2010). High-resolution composite $\delta^{13}C$ profiles for the Lower and Upper Cretaceous are developed from the Tethyan region and from English chalks, respectively (Weissert and Erba, 2004; Follmi et al., 2006; Jarvis et al., 2006). These records place the OAEs within a larger

chemostratigraphic context and offer valuable reference curves to which data from other regions can be correlated.

Using nine vertical $\delta^{13}C$ profiles from mixed carbonate-siliciclastic subsurface cores of the Comanche Shelf in south Texas, I have constructed a composite carbon isotope curve that is continuous for the middle Hauterivian through lower Campanian section of the northern Gulf of Mexico passive margin. The chemostratigraphic signatures of OAEs 1a, 1b, 2, and 3 are documented and detailed correlations to other global stratigraphic successions are provided. Regional anoxic events identified in other studies are commonly expressed in the chemostratigraphy shown here, but do not necessarily correspond to shale units in the south Texas section. By establishing a > 50 Myr reference curve for the northern Gulf of Mexico, this study fills a void in the distribution of temporally-extensive data sets documenting the paleogeographic coverage of Tethyan Cretaceous OAEs (see Figure 6 of Follmi et al, 2006). Furthermore, my high-resolution data significantly enhance the global $\delta^{13}C$ database for the middle to upper-Albian interval following OAE 1b.

Prior establishment of a detailed sequence-stratigraphic framework (Chapter 2) for the study interval allows regional sedimentologic analysis of each OAE and its effect on development of the shallow-marine carbonate platform. Integration of isotopic data with lithofacies cross-sections extending from the paleo-shoreline to shelf-margin enables two-dimensional analysis of both the demise and recovery of the carbonate system surrounding each anoxic event. By placing the globally recognized OAEs within a sequence stratigraphic context, I provide greater insight into their driving mechanisms and the long-term response of carbonate depositional systems.

GEOLOGIC SETTING

After late Triassic to early Jurassic rifting of the Pangean supercontinent and spreading of oceanic crust during the middle to late Jurassic (Salvador, 1991a; Sawyer et al., 1991), the northern Gulf of Mexico was transformed into a passive margin characterized by thermal subsidence (Winker and Buffler, 1988; Salvador, 1991b; Ewing, 2010). Following a regionally widespread Valanginian unconformity (Ewing, 2010), two mixed carbonate-siliciclastic rimmed-shelf systems, which are separated by Aptian siliciclastic-carbonate ramp clinoforms, developed in the Hauterivian-Barremian and Albian stages (Rose, 1972; Loucks, 1976; Bebout, 1977; Scott, 1993). The Albian Comanche shelf is overlain by predominately subtidal, mud-dominated carbonates and shales of the Cenomanian through lower Campanian (Scott et al., 1978; Dravis, 1980; Dawson, 1997; Scott et al., 2002; Lock and Peschier, 2006; Lock et al., 2007). Although not included within this study, deltaic siliciclastics and minor carbonates are present in the upper Campanian through Maastrichtian (Sohl et al., 1991). Data shown here are from continuous whole cores extracted from subsurface areas flanking the San Marcos Arch of the shelf interior and from the lower Cretaceous shelf margins (Figure 3.1). Terminal locations of the Sligo (Hauterivian-Barremian) and Stuart City (Albian) shelf margins are coincident in much of south Texas (Winker and Buffler, 1988), formed a prominent shelf-slope break observable on regional seismic lines (Tyrrell and Scott, 1989), and likely had shelf to basin relief on the order of 100's of meters.

STRATIGRAPHIC DATA

Chapter Two presented a regional sequence stratigraphic framework for the Hauterivian through lower Campanian section by combining data from subsurface reservoirs south of the Balcones Fault zone with outcrop measured sections. Decimeter-

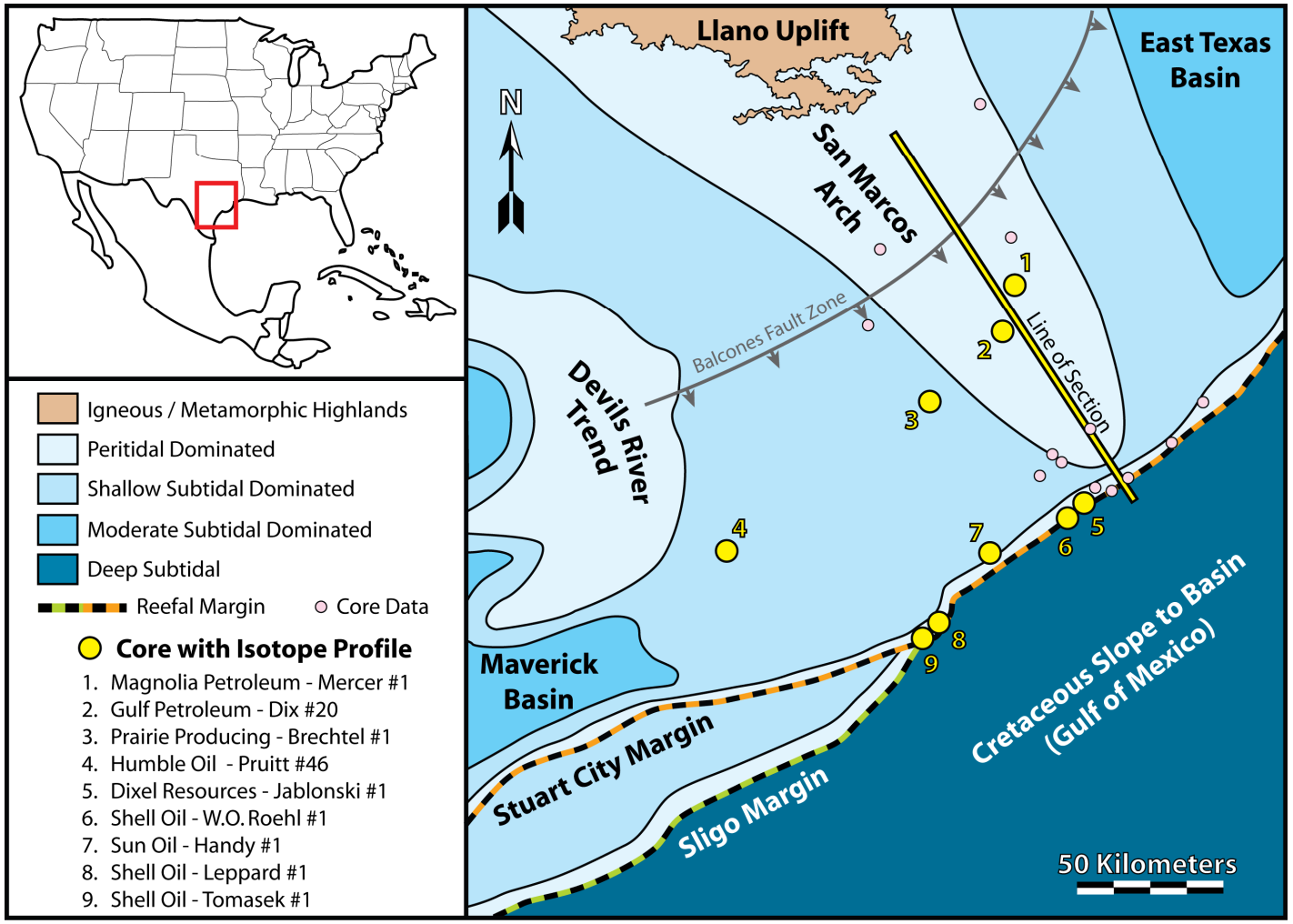

Figure 3.1: Paleogeographic map of the south Texas Comanche platform in the northern Gulf of Mexico and location of cores used for the study.

scale core descriptions were correlated with the aid of spontaneous potential, gamma ray, and resistivity borehole logs in order to construct a series of regional cross-sections documenting the evolution of the shelf systems. Published biostratigraphic data from the San Marcos Arch (Young, 1986), East Texas Basin (Jiang, 1989; Scott et al., 2002) and shelf margins (Coogan, 1977; Waite et al., 2007) further constrained regional correlations and ages of the sequence stratigraphic units. Sixteen depositional sequences of 1-3 Myr duration were delineated using high-frequency cycle stacking patterns, vertical lithofacies proportions, and exposure surfaces. Depositional sequences were grouped into seven supersequences of 3-14 Myr duration based on the presence of regional unconformities, shelf-interior facies tract offsets, and changes in shelf-margin trajectory (Figure 15 of Chapter 2). By comparison of independent biostratigraphic and chemostratigraphic data sets, this supersequence-scale tectono-eustatic signal in south Texas is recognizable in multiple basins and global sea-level curves.

ISOTOPE DATA AND METHODS

Nine cores incorporated into the regional stratigraphic model were selected for stable isotope analysis based on core length, continuity, age, and location within the platform (Figure 3.2). Cores were sampled at 0.15-2.5 meter spacing as a function of the expected relative sedimentation rate for the interval and known temporal variability in the global $\delta^{13}C$ signal. Powdered sample material was extracted from the cores using a 4.7 mm diameter drill-bit and a household drill. To obtain the original seawater $\delta^{13}C$ value at the time of deposition and prevent distortion of the long-term signal by any single component, mud-dominated rock matrix intervals consisting of terrigenous clay, carbonate micrite, fecal pellets, and finely-abraded skeletal fragments were targeted for

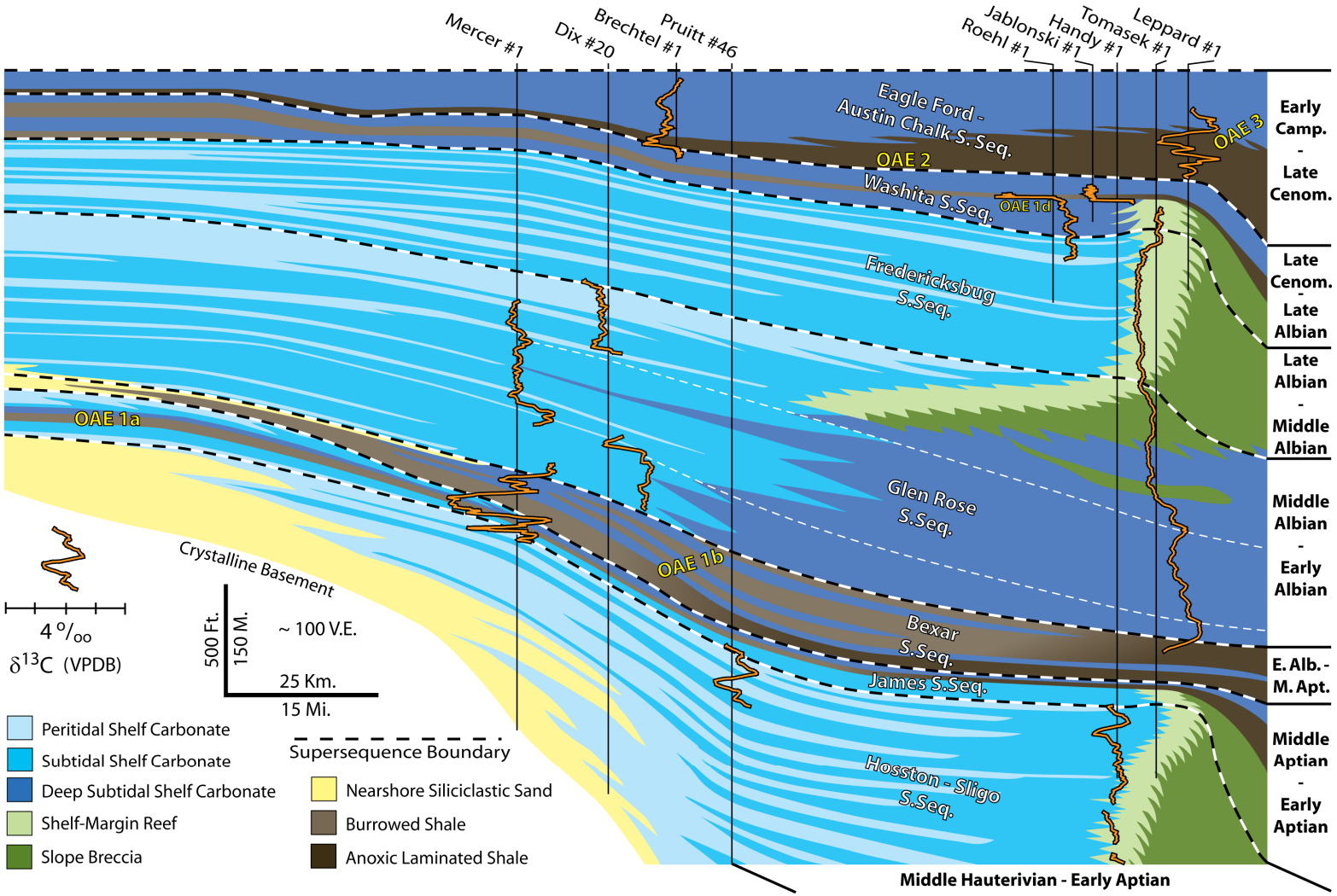

Figure 3.2: The nine $\delta^{13}C$ profiles in a simplified sequence stratigraphic cross-section of the Comanche shelf.

sampling. In some areas of the shelf, such as high-energy portions of the Stuart City margin, no matrix micrite was present for several tens of meters. In these intervals, samples represent the bulk composition of skeletal grains present (rudists, corals, foraminifera, red algae, among others). Individual skeletal grains, macroscopic cements, and strata beneath surfaces of subaerial exposure were not sampled. Completely dolomitized intervals were avoided, although minor dolomite fractions (< 5%) were probably incorporated into many samples from shelf-interior units.

Powdered samples from the Shell Leppard #1 and Shell Tomasek #1 cores were sent to the Analytical Laboratory for Paleoclimate Studies of the University of Texas at Austin for $\delta^{18}O$ and $\delta^{13}C$ analysis (Figures 1 and 2). These samples were prepared for analysis in a Kiel Device, which dissolves the carbonate material with phosphoric acid at 70˚C, and analyzed using a Thermo-Scientific MAT 253 mass-spectrometer. Results are reported relative to the Vienna Pee Dee Belemnite (VPBD) isotopic standard in per mil (‰) notation. Average external precision is 0.04‰ for $\delta^{18}O$ and 0.02‰ for $\delta^{13}C$ (1σ, n = 37, NBS-19). Long-term external precision based on NBS-19 is 0.05‰ for $\delta^{18}O$ and 0.03‰ for $\delta^{13}C$ (1σ). Powdered samples from the remaining seven cores were sent to the Stable Isotope Laboratory of the University of Miami for $\delta^{18}O$ and $\delta^{13}C$ analysis using dissolution in a common acid bath of phosphoric acid at 90˚C. Results are reported relative to the Vienna Pee Dee Belemnite (VPBD) isotopic standard. Analysis was performed using a Finnigan-MAT 251 mass-spectrometer and the precision of results based on long-term replicate analysis of standards is 0.08‰.

STABLE ISOTOPE RESULTS

Diagenesis of Primary $\delta^{13}C$ Values

The $\delta^{13}C$ values of well-preserved samples generally reflect the original composition of Cretaceous seawater at the moment of deposition and changing $\delta^{13}C$ ratios through time are a signal of variable global paleoceanographic conditions (Schlanger and Jenkyns, 1976; Scholle and Arthur, 1980). However, original stable isotope values of shallow-marine carbonate sediment are highly susceptible to open-system diagenesis because of common subaerial exposure with influx of meteoric fluids (Dickson and Coleman, 1980; Allan and Matthews, 1982; Immenhauser et al., 2001), burial pore waters (Moore, 2001), and cementation of primary porosity (Dickson and Coleman, 1980). In addition, carbon isotope values may vary by greater than 1‰ as a function of sediment mineralogic variability (Swart and Eberli, 2005), organic fractionation during skeleton secretion (Keith and Weber, 1965; Weber, 1965; Steuber, 1996; Swart et al., 2009), and potential spatial variability in $\delta^{13}C$ values of carbonate platform water (Patterson and Walter, 1994; Immenhauser et al., 2003). Despite these processes, $\delta^{13}C$ ratios of modern carbonate sediment show little facies-specific variability and no correlation to distance from the platform margin (Swart et al., 2009). Moreover, analysis of Valanginian-Huaterivian shallow-marine strata from the Alpine Tethys indicates that $\delta^{13}C$ values are commonly independent of depositional environment, and variations between matrix micrite, individual grains, and bulk samples is usually less than 0.5‰ (Amodio et al., 2008). Regardless of their propensity for early diagenesis and isotopic fractionation, shallow-marine carbonates are a potentially viable source of data for construction of globally correlative carbon isotope profiles (Jenkyns, 1995; Vahrenkamp, 1996; Groetsch et al., 1998; Wissler et al., 2003; Huck et al., 2010; Vahrenkamp, 2010).

A cross-plot of the $\delta^{18}O$ versus $\delta^{13}C$ values (n=889) from data collected for this investigation illustrates that approximately 95% of all samples cluster within a central field of values ranging from -6 – 0‰ $\delta^{18}O$ and 0 – 5‰ $\delta^{13}C$ (Figure 3.3). Linear regression of all data points indicates minimal covariance between $\delta^{18}O$ and $\delta^{13}C$ (R^2 = 0.19). With the exception of data from the Leppard #1 core, many sample points located outside of the central field are interpreted as diagenetically altered and have been discarded from moving averages for each core. Discarded data are from samples acquired in intervals with (1) diffuse burial dolomite in hemipelagic lime mud, (2) carbonate concretions, (3) reflux dolomite, or (4) abundant pyrite related to sulfate reduction of organic carbon. Each discarded sample is significantly deviant (usually >1 σ) in comparison to the surrounding data with respect to $\delta^{18}O$ or $\delta^{13}C$, or is considerably lighter (>1‰) than comparison reference curves.

Covariance in the bulk dataset is elevated by data from the Leppard #1 core, which exhibit significantly lighter $\delta^{18}O$ values and may have experienced a different diagenetic pathway relative to the remaining cores. When the Leppard #1 core data are excluded from the regression, the remaining data exhibit no covariance (R^2 = 0.05) and indicate that diagenesis affecting $\delta^{18}O$ ratios had little impact on the $\delta^{13}C$ seawater values recorded by the carbonate sediment. This conclusion was also reached by Prezbindowski (1981) in a more limited analysis of randomly selected samples from the Stuart City Fm.

Carbon isotope data are derived from diverse environments and lithofacies within the platform (intertidal, shallow subtidal, reef, slope, flooded shelf) that likely experienced widely different diagenetic pathways. Regardless, excursions of coeval $\delta^{13}C$ profiles in disparate settings are remarkably similar despite coming from different parts of the shelf (Figure 3.2). Moreover, absolute $\delta^{13}C$ values in late Albian data of the Comanche Shelf (1.9 – 3.7‰) closely correspond to those of glassy planktic foraminifera

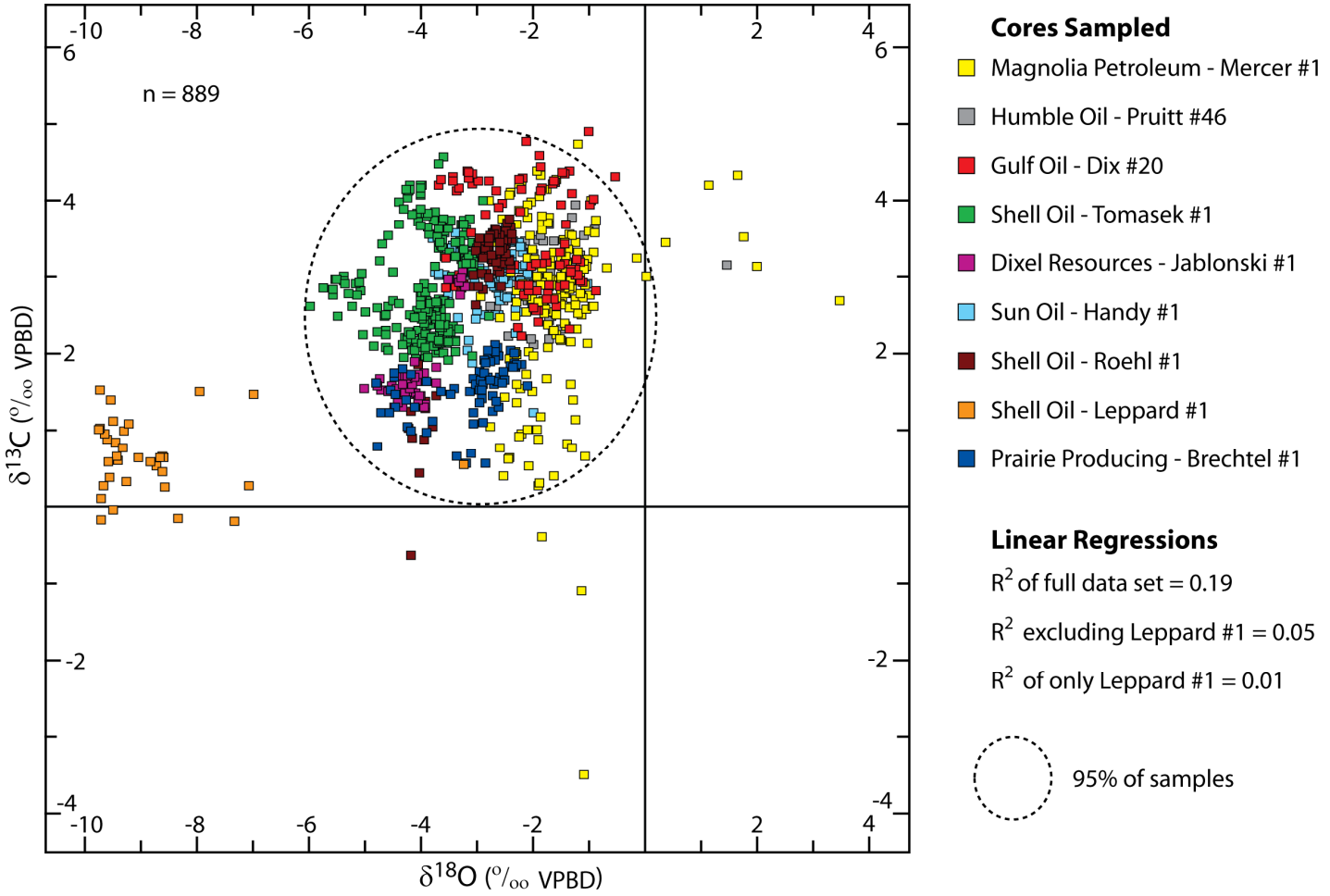

Figure 3.3: Plot of carbon- versus oxygen-isotope sample data. Points within the dashed oval represent 95% of all samples. With the exception of data from the Leppard #1 core, many points outside of the oval were discarded from moving averages because of suspected diagenetic overprints.

from the Lower Saxony Basin with ranges of 1.9 – 3.3‰ (Erbacher et al., 2011). Microsampled $\delta^{13}C$ values of fabric-retentive rudists, micrite, and early marine cements in multiple cores of the Sligo Fm vary from approximately 1.5 – 4.0‰, 1.5 – 3.75‰, and 2.5 – 3.5‰, respectively (Moldovanyi and Lohmann, 1984). These data are in excellent agreement with the 1.9 – 4.0‰ range of Sligo Fm matrix samples shown here. Statistical analysis of the south Texas data, regional similarities between vertical profiles, and overlap in absolute $\delta^{13}C$ values to those of diverse, internally- and externally-derived sample types indicate a broadly reliable record of global carbon isotope secular variability is present in the vertical profiles.

VERTICAL ISOTOPE PROFILES

Vertical oxygen and carbon isotope profiles are plotted against depth and shown with three- or five-point moving averages, simplified core descriptions, and the location of second-order supersequence boundaries. Moving averages of successive points are employed to limit the impact of any given sample and its potentially unique diagenetic pathway or sample composition. Data acquired in mud-dominated, moderate- or deep-subtidal (>20 m water depth) portions of the section exhibit less scatter in the vertical profiles and are presumed to have experienced closed-system diagenesis. These mud-dominated intervals are accompanied by a three-point moving average. Grain-dominated strata from intertidal, shallow-subtidal, and reefal settings exhibit greater scatter of both $\delta^{18}O$ and $\delta^{13}C$ vertical profiles. These intervals may have experienced more complex diagenetic pathways and are therefore accompanied by five-point moving averages. Open symbols denote data pairs with erratic $\delta^{18}O$ or $\delta^{13}C$ values that have been excluded from the moving averages. Each sampled well is discussed below.

Humble Oil - Pruitt #46 and Sun Oil - Handy #1

Cores from the Pruitt #46 and Handy #1 wellbores combine to span the upper Hauterivian through lowermost Aptian section (~235 meters) of the Sligo Formation (Fm) in the Hosston-Sligo supersequence (Figures 3.1, 3.2, 3.4). Oxygen and carbon isotope profiles for both cores are smoothed with 5-point moving averages. Lithofacies present in the Pruitt #46 core are generally representative of shallow-subtidal to intertidal middle-shelf environments. This core interval offers a thick stratigraphic column equivalent to the B7-B8 segments (Wissler et al., 2003) and C1-C2 segments (Menegatti et al., 1998) of the latest Barremian to earliest Aptian $\delta^{13}C$ record. The Handy #1 core contains a long-term progradational succession of subtidal outer-shelf depositional environments over reefal to back-reef platform-margin environments. The Hauterivian portion of the core contains multiple core gaps, but the Barremian and lower Aptian intervals are nearly continuous. Segments B1-B8 of Wissler et al. (2003) and C1-C2 of Menegatti et al. (1998) are tentatively identified. Multiple high-frequency cycles of relative sea level are present in each geochemical segment of both cores, yet cycle stacking patterns and vertical lithofacies proportions (i.e. subtidal versus intertidal) appear unrelated to segment boundaries.

Magnolia Petroleum - Mercer #1 and Gulf Oil - Dix #20

The combined stratigraphy of the Mercer #1 and Dix #20 cores together span the lower Aptian through the middle Albian interval (Figures 3.1, 3.2, 3.5, 3.6). Stratigraphic data and the secular $\delta^{13}C$ curve from the Mercer #1 core provide a detailed record of the middle-shelf response to OAEs 1a and 1b, as well as the intervening Fallot event. Data

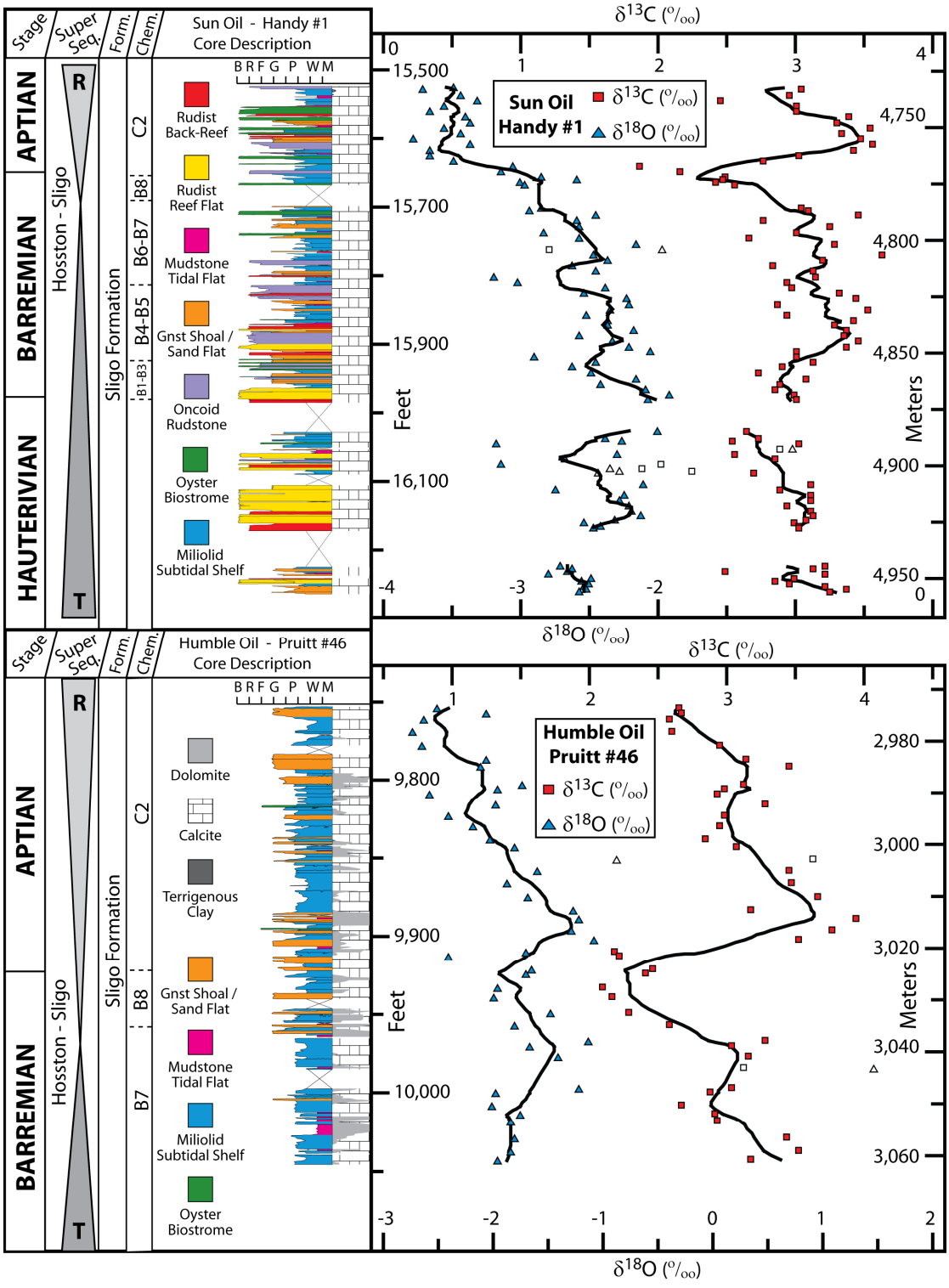

Figure 3.4: Core and stable isotope data for the Handy #1 and Pruitt #46 wells. Open

symbols for stable isotope pairs indicate data excluded from the moving average due to extreme values. Foraminiferal zonations (Foram) and stage boundaries are suggested based on correlations to global reference profiles. Second-order transgressive (T) / regressive (R) supersequences (Super Seq.), lithostratigraphic formation units (Form), and chemostratigraphic segments (Chem.) are also indicated.

are shown with a 3-point moving average in the lower segment of the Mercer #1 core and a 5-point moving average above the core gap. Data from the Dix #20 core contain a 5-point moving average. In the Mercer #1 profile through the Pearsall Fm (Figure 3.5), a negative excursion to 0.3‰ $\delta^{13}C$ in clay-rich oyster rudstones is followed by an immediate shift back to 3.3‰ $\delta^{13}C$ in the 5.6 meter Pine Island shale that corresponds to OAE1a. This shale member is overlain by molluscan grainstone and oncoid rudstone shoreface to offshore strata of the James Member in the Pearsall Fm. The uppermost portion of the James Member consists of echinoid-oyster wackestones and lime mudstones that contain minor terrigenous clay fractions and correspond to the Fallot Event. Immediately overlying the James Member are approximately 23 meters of brown, *Planolites*-burrowed shale of the Bexar Member, which also contains ammonites and plant fragments. The upper 10 meters of Bexar shale (~0.5 – 1.0‰ $\delta^{13}C$) and the first 28 meters of clay-rich, echinoid-oyster wackestone/packstone and oyster floatstone within the Glen Rose Fm (~2.1 – 3.2‰ $\delta^{13}C$) are temporally equivalent to the OAE 1b set of Foellmi et al. (2006).

Younger intervals of the Mercer #1 and Dix #20 cores consist of greater than 300 meters of cyclic subtidal to intertidal strata of the Glen Rose supersequence. This lower to middle Albian portion of the platform contains varied lithologies and fauna typical of the Comanche platform. Oysters and echinoids decrease in abundance up section while miliolid foraminifera, *Orbitolina* foraminifera, stromatoporoids, and rudist bivalves increase in abundance up section. Carbon isotope ratios in the Glen Rose supersequence

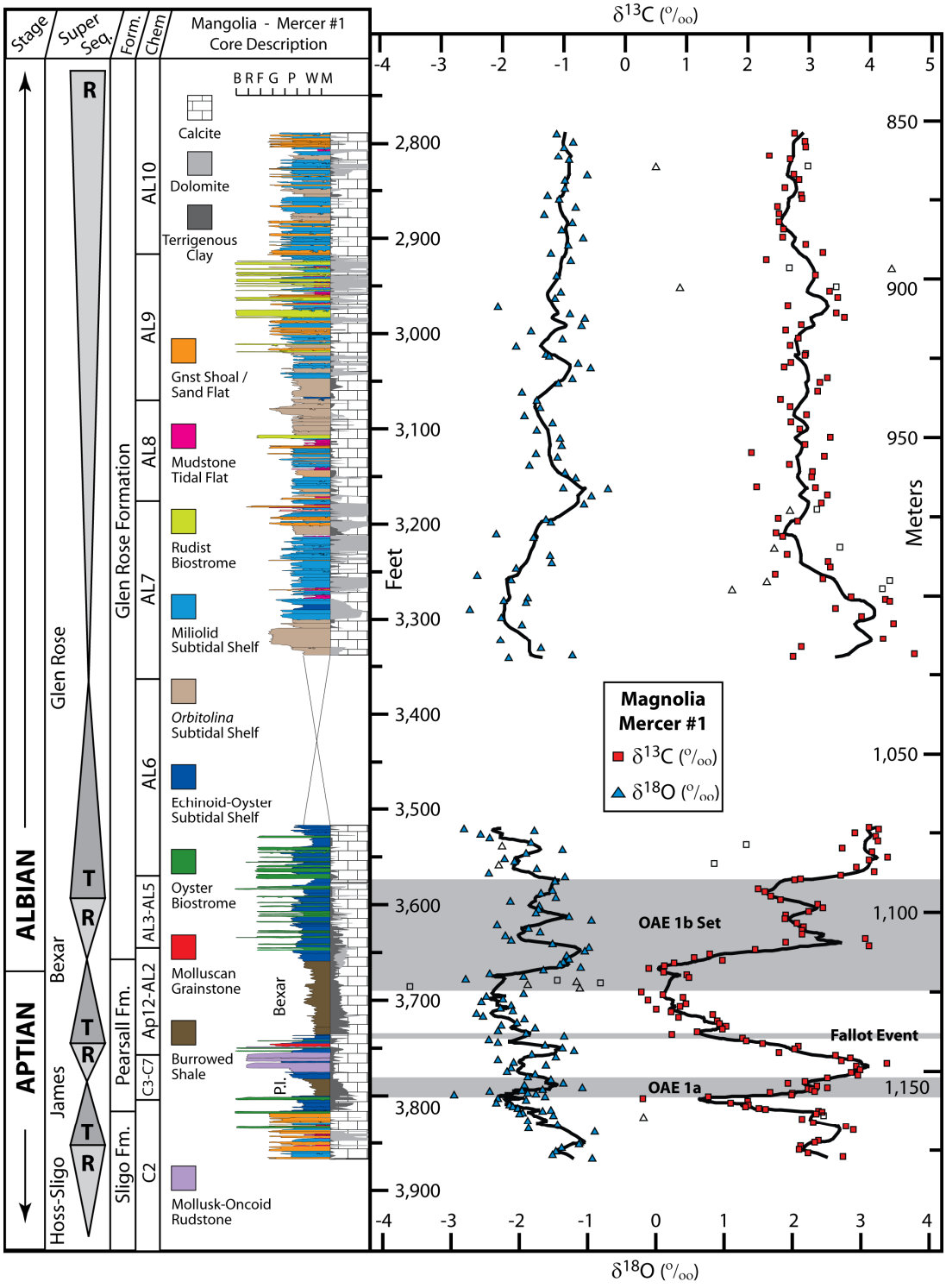

Figure 3.5: Core and stable isotope data for the Mercer #1 well.

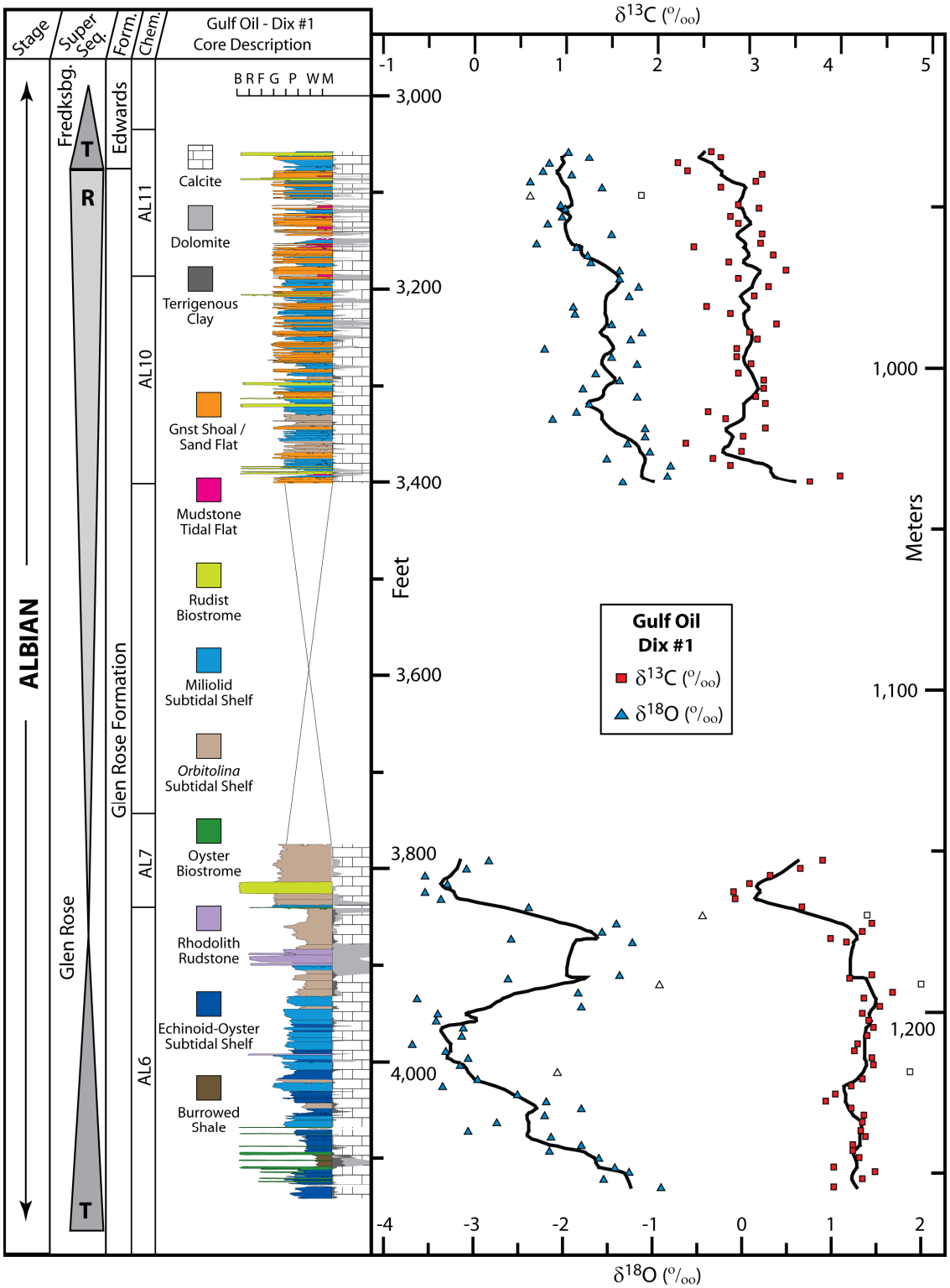

Figure 3.6: Core and stable isotope data for the Dix #20 well.

generally range from 2.0 – 4.5‰. Scatter in shelf-interior $\delta^{13}C$ profiles increases during the highstand of the supersequence and resulted from more frequent occurrences of dolomite, intertidal strata, and inferred short-term (~20-40 ka) subaerial exposure surfaces

Shell Oil - Tomasek #1

Core from the Tomasek #1 well includes upper-Albian strata from the Stuart City shelf margin and extends down into fore-reef and flooded shelf strata of the Glen Rose Fm (Figure 3.1, 3.2, 3.7). The core is nearly continuous for 612 meters and the resulting $\delta^{13}C$ profile exhibits a remarkably clean signature. The lower 10 meters contain argillaceous lime mudstones and oncolitic wackestones equivalent to the lower Glen Rose Fm and chemostratigraphically correspond to the end of OAE 1b. Above OAE 1b, approximately 200 meters of globigerinid-bearing, oncolitic wackestones and argillaceous lime mudstones in the lower half of the core reveal a $\delta^{13}C$ profile that decreases from 4‰ to 3‰ in a serrate manner. The remainder of the core contains rudist-rich lower slope breccias followed by prograding slope, reef, and back-reef lithofacies of the Stuart City Fm with $\delta^{13}C$ values ranging from 1.9 – 3.1‰. Data are smoothed with 5-point moving averages.

The character of the carbon isotope profile throughout the Tomasek #1 core allows refined correlation of shelf-interior strata from the Glen Rose, Fredericksburg, and Washita supersequences to deep-subtidal (>50 m depth), slope, and reef-margin facies (Figure 3.2). Such chemostratigraphic correlations demonstrate the timing of changes in platform depositional profile and permit conceptual links to be established between shelf-margin architecture and shelf-interior lithofacies distributions (Chapter 2).

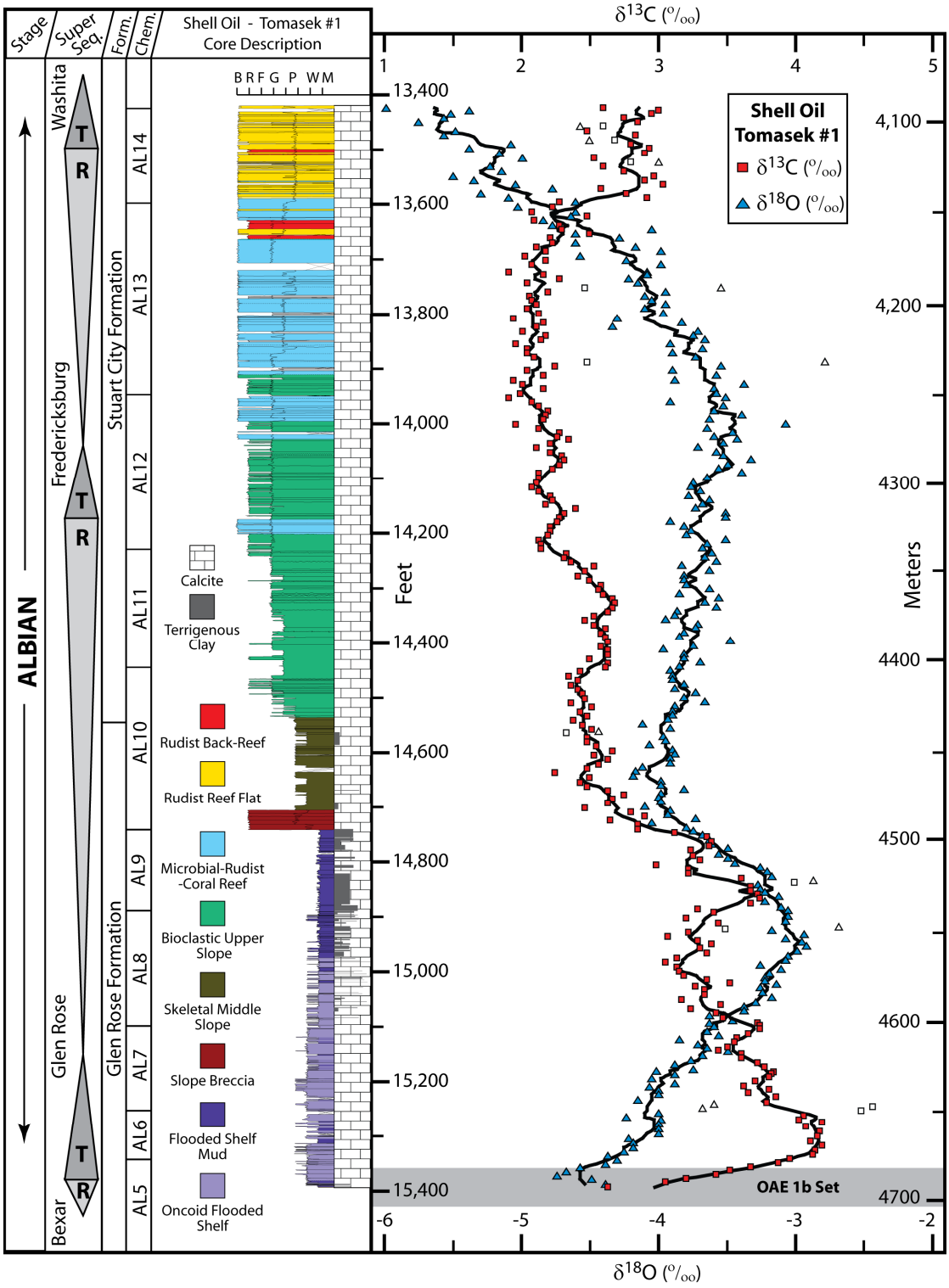

Figure 3.7: Core and stable isotope data for the Tomasek #1 well.

Shell Oil - W. Roehl #1

Core for the Roehl #1 well includes the uppermost portion of the Albian Stuart City margin above the Tomasek #1 core and it extends into *Planolites*-burrowed shale of the lower Cenomanian Del Rio Fm (Figures 3.1, 3.2, 3.8). Isotope data are smoothed with 3-point moving averages. Reefal and back-reef facies in the Fredericksburg and Washita supersequences generally contain $\delta^{13}C$ values from 3.0 – 3.7‰. Prior to drowning of the Stuart City margin at the base of the Cenomanian, the top 10 meters of Albian strata contain multiple beds of burrowed gastropod-peloid wackestone and rudist bafflestone in a black, lime-mud-dominated matrix. In these units, some rudists have thin valves and may have grown under stressed environmental conditions. Carbon isotope ratios of this interval decrease to 2.7‰ and approximate the chemostratigraphic position of OAE 1d.

Dixel Resources - Jablonski #1

Core from the Jablonski #1 wellbore is critical for completion of the carbon isotope profile for the early to middle Cenomanian. This short interval encapsulates 11.5 meters of globigerinid- and calcisphere-bearing shale in the Del Rio Fm and 10 meters of argillaceous, globigerinid-rich lime mudstone/wackestone in the lower third of the Buda Fm (Figures 3.1, 3.2, 3.9). Lithofacies of these two units vertically intercalate within the Jablonski #1 core. The Del Rio Fm, which is equivalent to the Grayson Fm in the East Texas Basin, is dated as early Cenomanian in age via biostratigraphy (Scott et al., 2002). Carbon isotope values in the Del Rio Fm and Buda Fm oscillate between 1.25 – 1.9‰ in both units. Isotope data are shown with 3-point moving averages and several points have been removed because of diagenetically related scatter in the oxygen isotope data set.

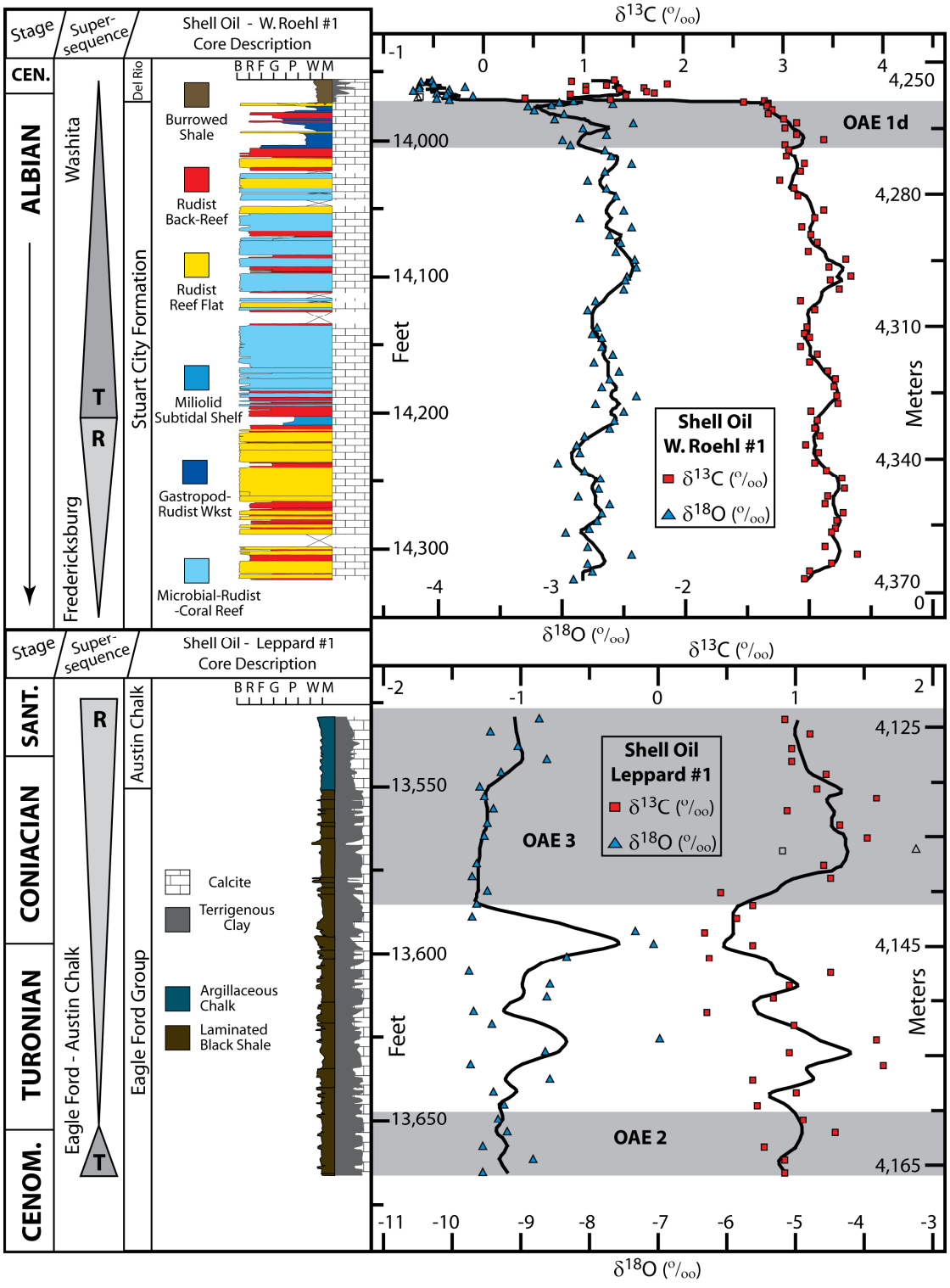

Figure 3.8: Core and stable isotope data for the Leppard #1 and Roehl #1 wells.

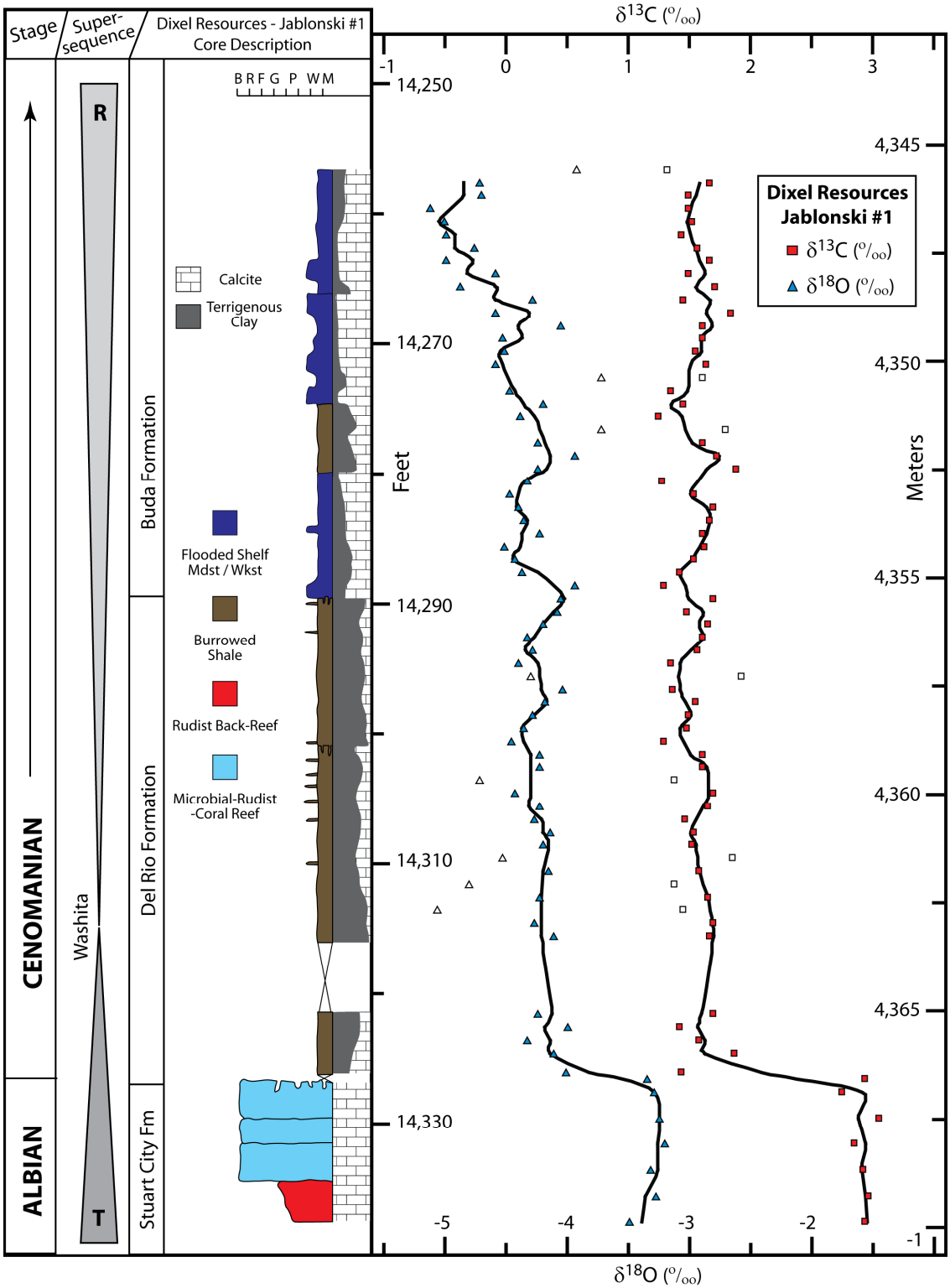

Figure 3.9: Core and stable isotope data for the Jablonski #1 well.

Prairie Producing - Brechtel #1 and Shell Oil - Leppard #1

The Brechtel #1 core includes a nearly continuous section of upper Cenomanian through lower Campanian strata from the middle-platform setting, including the upper Buda Fm, the Eagle Ford Group, and the Austin Chalk Group (Figure 3.1, 3.2, 3.10). Each unit includes planktic fauna characteristic of a flooded shelf setting, such as calcispheres and globigerinid foraminifera (Chapter 2). Isotope data are smoothed with 5-point moving averages. Within *Thallasinoides*- and *Planolites*-burrowed peloidal wackestones of the Buda Fm, $\delta^{13}C$ values range from 1.5 – 2.1‰ before trending to progressively lighter values approaching 0.5‰ in the upper 3 meters beneath the contact with the overlying Eagle Ford Group. This contact is equivalent to the Mid-Cretaceous Unconformity in many areas of the Gulf of Mexico (Buffler et al., 1980; Faust, 1990) and forms the top of the Washita supersequence. One and one-half meters of planar-laminated black shale in the lower Eagle Ford Group are late Cenomanian to early Turonian in age (Jiang, 1989), locally contain greater than 9 wt. % TOC (Dawson, 1997), and were deposited under anoxic to dysoxic conditions (Arthur and Sageman, 1994). Within the black shale, the carbon isotope profile for the Brechtel #1 core displays a small positive excursion to 1.7‰ and a later negative shift back to 1.0‰. The age, environmental interpretation, and $\delta^{13}C$ excursion suggest the lower Eagle Ford black shale is the stratigraphic expression of OAE 2 in south Texas. The overlying 7.5 meters of the Eagle Ford Group consist of intercalated, planar-laminated shale and silt-sized calcareous grainstone with bentonite horizons. This lithofacies assemblage was also likely deposited under anoxic to dysoxic conditions at the sediment-water interface and is vertically gradational into *Planolites*-burrowed, argillaceous to glauconitic chalks of the Austin Chalk Group. In the outcrop belt of central and north Texas, the top of the Eagle Ford Group is biostratigraphically

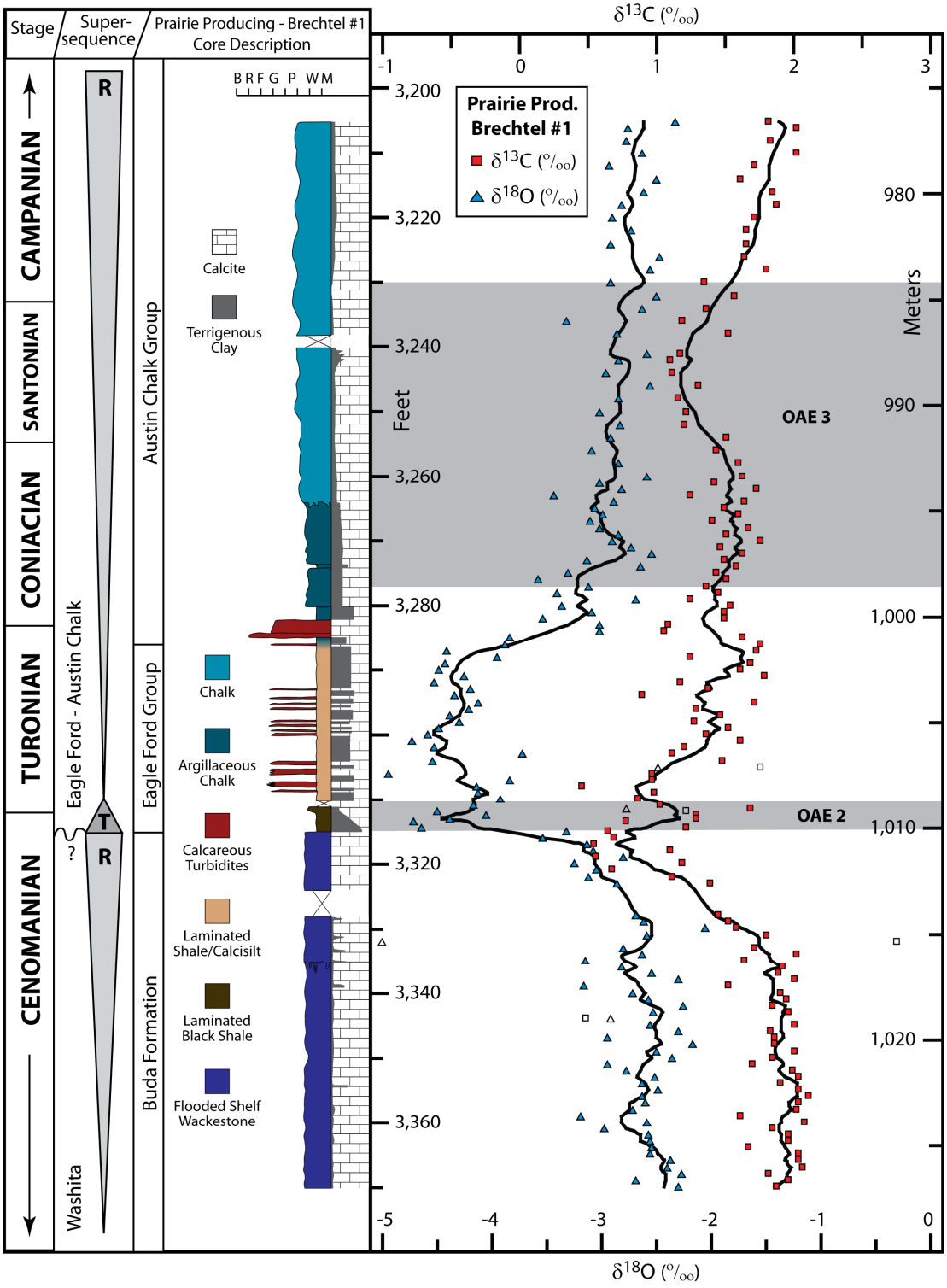

Figure 3.10: Core and stable isotope data for the Brechtel #1 well.

dated as latest-Turonian in age and Austin Chalk strata are dated as young as the early Campanian (Jiang, 1989). Although they are burrowed and were thus deposited under relatively more oxygenated conditions (Arthur and Sageman, 1994), Austin Chalk lithofacies contain up to 3.7% TOC (Grabowski Jr., 1995). Carbon isotopes values from laminated shale/calcisilt of the Eagle Ford Group and strata from the Austin Chalk Group are bound in the range of approximately 0.5 – 2‰.

Core from the Leppard #1 well contains 36.5 meters of planar laminated black shale in the Eagle Ford Group that unconformably overlays Albian strata of the Stuart City margin (Figures 3.1, 3.2, 3.8). Bentonite horizons are scattered and the anoxic black-shale lithofacies is directly overlain by 6.9 meters of *Zoophycos*- and *Planolites*-burrowed, argillaceous chalk in the Austin Chalk Group. The uppermost 3 meters of Austin Chalk lithofacies were not recovered in the cored interval. Oxygen isotope data from the Leppard #1 core are extremely negative relative to other cores in the study (Figure 3.2) and are widely variable from -9.8 – -3.2‰. For this reason, $\delta^{18}O$ values are very likely to be diagenetically controlled and thus sampling is sparse through the interval. Nonetheless, linear regression of $\delta^{18}O$ versus $\delta^{13}C$ values internal to the Leppard #1 indicates that the stable isotope sets lack covariance ($R^2 = 0.01$). Hence the relatively extreme diagenesis in the Leppard #1 core, which displaced original $\delta^{18}O$ ratios of distal lithofacies in the Eagle Ford and Austin Chalk Groups, did little to affect the short-term excursions of the original $\delta^{13}C$ profile. Data are smoothed with a 3-point moving average.

CORRELATION TO REFERENCE PROFILES

Reference $\delta^{13}C$ profiles recording secular changes in the global carbon cycle are available for most stages of the Cretaceous, some of which are calibrated to numerical

time scales (Scholle and Arthur, 1980; Jenkyns, 1995; Menegatti et al., 1998; Gale et al., 1996; Bralower et al., 1999; Erba et al., 1999; Stoll and Schrag, 2000; Wissler et al., 2003; Herrle et al., 2004; Weissert and Erba, 2004; Follmi et al., 2006; Godet et al., 2006; Jarvis et al., 2006; Vahrenkamp, 2010). I use the time-calibrated reference profiles as a basis for correlation of $\delta^{13}C$ curves that were originally plotted against their respective stratigraphic sections. For each thickness-based profile, I used stage boundaries and paleontologic zonations of planktonic foraminifera, ammonites, and nannofossils as pinning-points for comparison and for scaling of the original $\delta^{13}C$ curves from thickness to time representations. Biostratigraphic zonations of some south Texas intervals are poorly constrained in the subsurface, including the Hauterivian to Barremian and Coniacian to Campanian. Therefore many temporal correlations of Comanche Platform data are considered working hypotheses. Excursions in $\delta^{13}C_{org}$ profiles are assumed to mimic those of $\delta^{13}C$ profiles derived from carbonate material; however their absolute values and magnitudes significantly differ (Kump and Arthur, 1999).

Hauterivian – Barremian Isotope Profiles

The compilation profile of Follmi et al. (2006) from the Vocontian Trough of the northern Tethys is used as a time-calibrated reference curve for the Hauterivian-Barremian interval (Figure 3.11). Secondary reference profiles include those from the Cismon Apticore of the central Tethys (Erba et al., 1999) and from Resolution Guyot of the mid-Pacific (Jenkyns, 1995). Barremian chemostratigraphic segments B1-B8 (Wissler et al., 2003) and early Aptian segments C1-C2 (Menegatti et al., 1998) are used for correlation of time-horizons. Hauterivian and Barremian strata from the Comanche shelf include greater than 200 meters of shallow-marine carbonates from the Hosston-Sligo

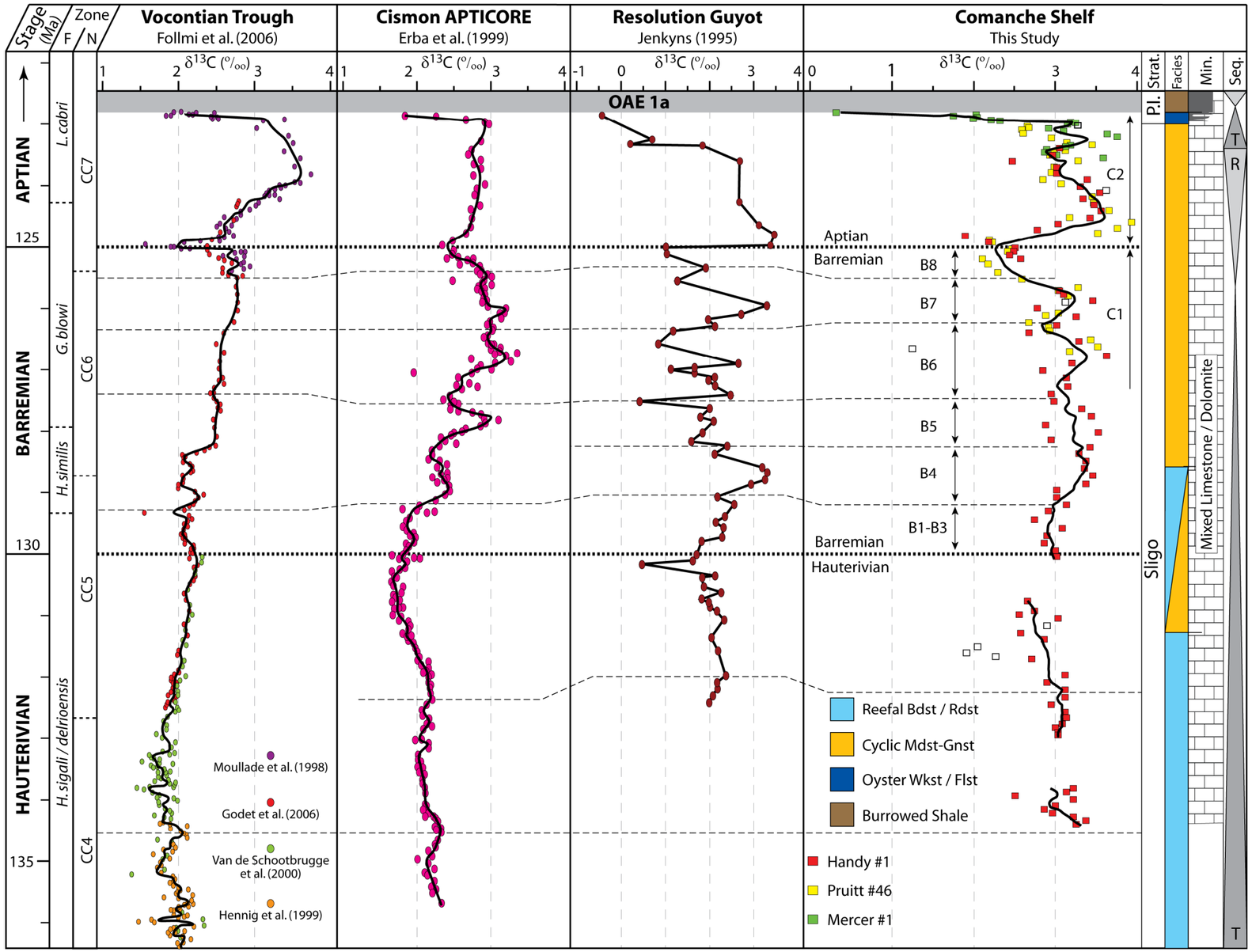

Figure 3.11: Correlation of Comanche Shelf $\delta^{13}C$ data to Hauterivian and Barremian reference profiles. Segments B1-B8 and C1-C2 are from Wissler et al. (2003) and Menegatti et al. (1998), respectively.

supersequence. Core gaps prevent precise correlation of the south Texas data to reference curves in the Hauterivian stage.

A concave-right $\delta^{13}C$ trend straddles the Hauterivian-Barremian boundary and is present in all data excluding the Vocontian Trough (Figure 3.11). This chemostratigraphic signature spans roughly 3 Myr and may be characteristic of the stage boundary in areas outside of the northern Tethys. Outside of the Vocontian trough data, the Barremian profile from south Texas is consistent with the reference profiles in segments B1-B3 and B6-B8. Correlation in segments B4-B5 is tenuous and chemostratigraphic trends are generally inconsistent, indicating that further work may be needed in the middle Barremian stage. A prominent negative excursion with amplitude ranging from 0.8 – 2.5‰ is associated with the Barremian-Aptian stage boundary (C1-C2 transition) and is well defined in all records.

The broad character and excursions of the Vocontian Trough composite profile are generally dissimilar to those of the Cismon, Resolution Guyot, and Comanche Shelf data sets during the Hauterivian and Barremian stages. As discussed at length by Follmi et al. (2006), this dissimilarity may be the result of changing nutrient levels, modes of carbonate sediment production (heterozoan versus photozoan), and dominant mineralogy (Godet et al., 2006) in the north Tethyan margin. South Texas data somewhat conform to the high-resolution record from the Cismon Apticore in the central Tethys but best match the profile from Resolution Guyot in the mid-Pacific. Greater similarity between Comanche Shelf and Resolution Guyot $\delta^{13}C$ profiles was promoted by consistent photozoan carbonate sedimentation and relatively constant aragonite:calcite mineralogic ratios in sediment produced at those sites.

Aptian Isotope Profiles

Secular $\delta^{13}C$ changes in the Aptian (Figure 3.12) are well-constrained in the Vocontian Trough composite profile of Follmi et al. (2006) by data with centimeter-scale sample spacing and high-resolution biostratigraphy (Moullade et al., 1998; Herrle et al., 2004;). Excellent reference profiles are also available from the Shu'aiba Fm of the southern Tethys (Vahrenkamp, 2010) and from hemipelagic sediments of the western Gulf of Mexico (Bralower et al., 1999). Chemostratigraphic segments C2-C8 (Menegatti et al., 1998) and Ap6-AL6 (Herrle et al., 2004) are used for correlation in the Aptian through lower Albian interval containing OAE's 1a and 1b (Figure 3.12). Additional periods of anoxia during the Niveau Noir and Niveau Fallot events are also correlated amongst the records. In comparison to the reference curves, data from the Comanche Shelf are widely spaced through much of the Aptian, yet many chemostratigraphic segments are generally identifiable.

Lowermost Aptian strata on the Comanche shelf include cyclic, subtidal to intertidal carbonates in the regressive portion of the Hosston-Sligo supersequence and the transgressive portion of the James supersequence (upper Sligo Fm). Terrigenous clay proportions on the carbonate shelf increase vertically within segment C2 and preceded the onset of OAE 1a by approximately 2.5 meters or 500 ka. This occurred during a negative excursion from 3.2‰ to 0.3‰ as burrowed, skeletal-oyster wackestone/packstone and oyster biostromes spread across the shelf. The trough of the excursion at segment C3 is developed within a reworked oyster biostrome with a shale matrix. Deposition of *Planolites*-burrowed shale in the Pine Island Member ensued during segments C4-C6 and coincided with the Niveau Goguel (Herrle et al., 2004) and Livello Selli events (Wezel, 1985; Arthur et al., 1990; Erbacher and Thurow, 1997) of

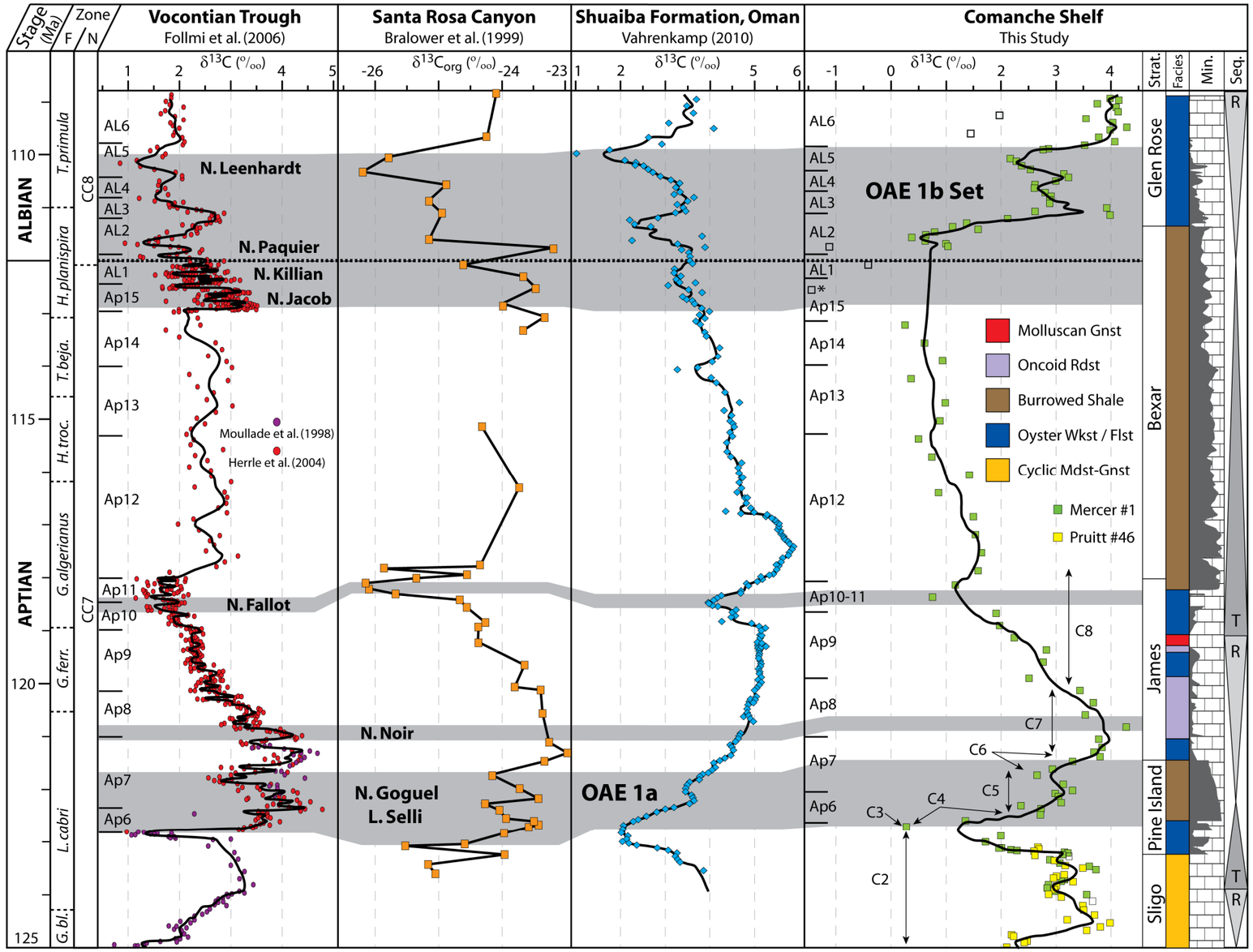

Figure 3.12: Correlation of Comanche Shelf $\delta^{13}C$ data to reference profiles of the Aptian stage. Chemostratigraphic segments C2-C8 and AP6-AL6 are from Menegatti et al. (1998) and Herrle et al. (2004), respectively. The open symbol denoted by an asterisk in segment AP15 has a value of -3.51‰ $\delta^{13}C$.

OAE 1a. Maximum flooding of the James supersequence coincides with OAE 1a. Shale deposition and drowning of the Comanche Shelf during OAE 1a is congruent with the response of northern Tethyan platforms (Follmi et al., 1994; Weissert et al., 1998; Wissler et al., 2003). Termination of carbonate sedimentation in the Gulf of Mexico suggests that time-equivalent *Lithocodium-Bacinella* blooms in the Shu'aiba and Adriatic platforms (Vahrenkamp, 1996; Groetsch et al., 1998; Immenhauser et al., 2005; Huck et al., 2010) were a sedimentary response confined to the central and southern Tethys.

Following Pine Island shale deposition during OAE 1a, carbonate shelf sedimentation resumed with deposition of oyster wackestones, oncoid rudstones, and molluscan grainstones in the highstand of the James supersequence. The Fallot event (Friedrich et al., 2003) in segments Ap10-Ap11 is present in all four comparison profiles and occurred at the onset of the second drowning episode on the Comanche Shelf. The connection between platform drowning and the Fallot event indicates the environmental perturbation during the Ap10-Ap11 negative excursion not only caused elevated rates of organic carbon burial in the Gulf of Mexico, Vocontian Basin, and eastern Pacific (Bralower et al., 1999; Friedrich et al., 2003), but also substantially disrupted shallow-marine ecosystems. Deposition of shale in the Bexar Member of the Pearsall Fm transpired following the Fallot event during segments Ap12-AL2. The Jacob, Killian, and Paquier events of the Aptian-Albian OAE 1b set are equivalent to the upper Bexar shale interval, although carbonate sedimentation resumed prior to the Leenhardt event (Figures 3.2, 3.5, 3.12). Maximum flooding of the Bexar supersequence was coincident with shale deposition and anoxic events in OAE 1b.

Despite marked dissimilarity of the Vocontian Trough profile in the Hauterivian-Barremian stages, Aptian excursions in the north Tethyan data (Follmi et al., 2006) are replicated closely by the additional reference profiles (Bralower et al., 1999;

Vahrenkamp, 2010) and the Comanche Shelf curve. In the interval encompassing OAE 1a and OAE 1b from segment Ap6 to AL6, global environmental transformations and synchronous changes in the oceanic carbon reservoir clearly outweighed any local environmental factors that may have led to differences in the reference profiles.

Albian Isotope Profiles

Reference profiles for the Albian include those from Resolution Guyot (Jenkyns, 1995), northern Mexico (Scholle and Arthur, 1980; Bralower et al., 1999), the Nahr Umr Fm of Oman (Immenhauser et al., 2001), and Blake Nose in the western Atlantic (Wilson and Norris, 2001). Correlations in the Albian are hampered by the lack of a time-calibrated $\delta^{13}C$ reference curve (Figure 3.13). Nonetheless, ages published for the Blake Nose profile and for sequences identified in the Nahr Umr Fm (Immenhauser et al., 2001; Immenhauser and Scott, 2002) provide some time constraints. Although the data from Oman have been extensively overprinted by subaerial exposure surfaces, disconformities, and frequent negative excursions, the broader trends created by successive samples appear consistent with those of the reference profiles and south Texas data. Albian $\delta^{13}C$ excursions are divided by chemostratigraphic segments C11-C15 (Bralower et al., 1999) and AL2-AL6 (Herrle et al., 2004). These excursions have been further documented here using segments AL7-AL19 defined with data from the Tomasek #1 and Roehl #1 cores (Figures 3.7, 3.8). Following the methodology of Wissler et al. (2003), new segment boundaries are marked by $\delta^{13}C$ profile turning points, changes in gradient, or excursion shape. Moreover, each segment is recognizable in multiple reference profiles.

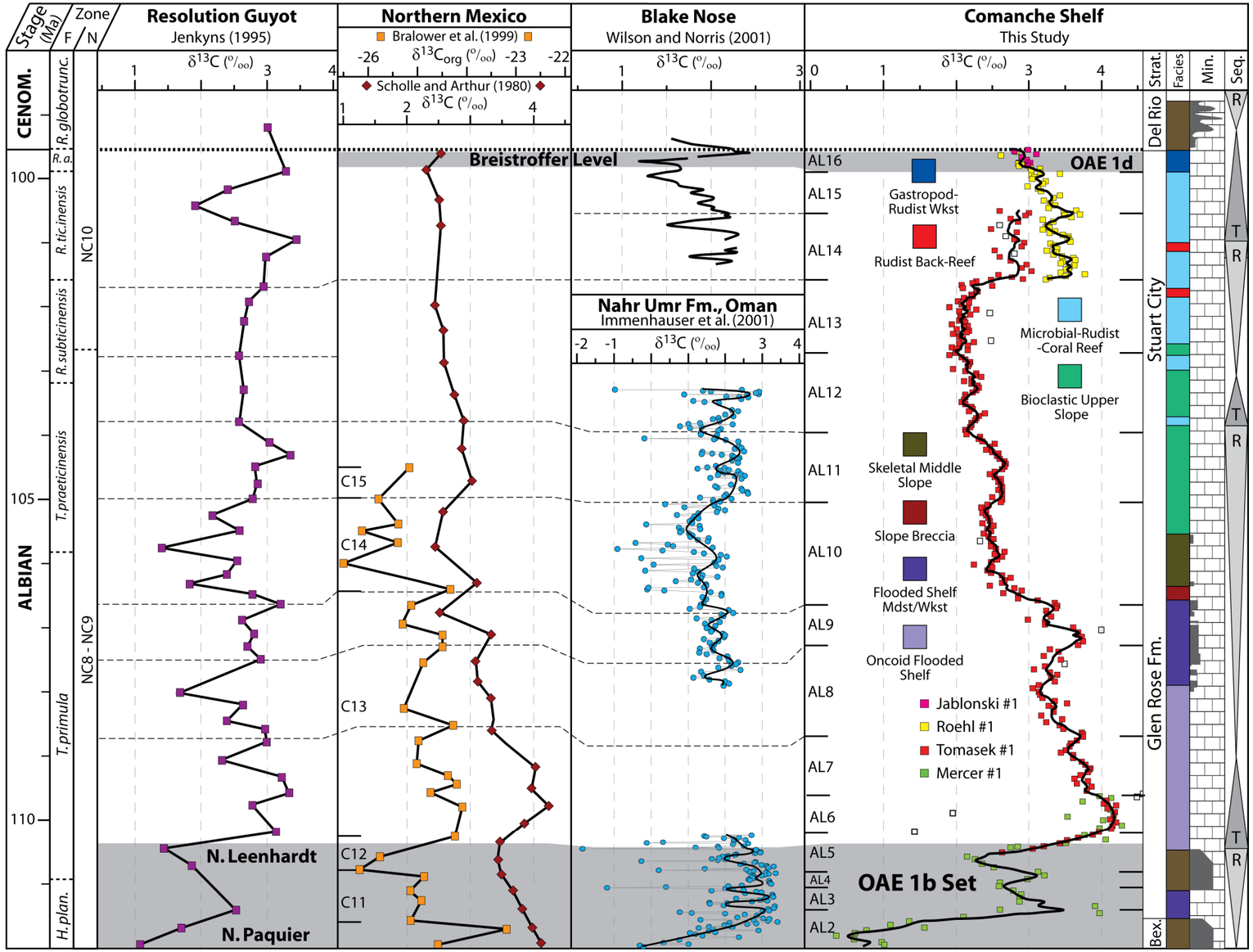

Figure 3.13: Correlation of Comanche Shelf $\delta^{13}C$ data to reference profiles of the Albian stage. Chemostratigraphic segments AL2-AL6 and C11-C15 are from Herrle et al. (2004) and Bralower et al. (1999), respectively. Segments AL7-AL19 are defined using Comanche Shelf data.

After OAE 1b and the positive shift to values of 4.1‰ $\delta^{13}C$ in AL6 of the early Albian, an oscillatory decrease to values of 3.5 – 3.6‰ in AL7 was followed by a concave-right decrease to 3.1 ‰ and increase to 3.4‰ in AL8. A pronounced peak, trough, and peak in segment AL9 corresponds to in influx of terrigenous clay in distal flooded shelf mudstones of the Glen Rose supersequence. The subsequent negative trend to 2.4‰ in AL10 is followed by a concave-left trend to increasing to values of 2.6‰ and then decreasing to values of 2.1‰ in segment AL11. AL12 shows an oscillatory decrease to a minimum of 2.0‰, followed by a slow increase to 2.2‰ in AL13. A rapid increase to a range of 2.5 – 3.0‰ occurs at the base of AL14. Carbon isotope data from the Roehl #1 core in AL14 are heavier than the Tomasek #1 data by approximately 0.5‰, but follow a similar pattern. The reason for this offset is unknown. In AL15, the Roehl #1 data decrease from 3.6‰ to 3.0‰ in a manner that closely follows the high-resolution data from the western Atlantic at ODP site 1052 (Wilson and Norris, 2001). AL16 is defined by a further decrease to 2.8‰ and may be equivalent to the OAE 1-d interval. In south Texas, the signature of OAE 1d is poorly developed compared to the high-resolution record documented by Wilson and Norris (2001) from the western Atlantic (Figure 3.13). This may be the result of truncation by a submarine hiatus at the contact between the Stuart City and Del Rio Formations, or the signature of the event may simply be below the resolution of the data.

Cenomanian Isoptope Profiles

High-resolution $\delta^{13}C$ data from chalks of the Speeton section in England (Jarvis et al., 2006) provide a time-calibrated record of secular variability in the Cenomanian stage (Figure 3.14). Organic carbon data from the eastern Atlantic coast of Morocco (Gertsch

et al., 2010) provide an additional record for the upper Cenomanian. Correlation of events recognized in the English chalk data is complicated by the low-amplitudes of the excursions (<0.5 pm) and scatter in the Moroccan and south Texas profiles. In addition, the middle to upper Cenomanian interval is demonstrably absent in many areas of the Comanche platform where it is truncated by the Mid-Cretaceous unconformity (Young, 1986; Scott et al., 2002). Petrographic evidence for this unconformity is lacking in the Brechtel #1 core but biostratigraphic analysis suggests an early to middle Cenomanian age of the Buda Fm (R.W. Scott, personal communication). Because data from the Jablonski #1 profile exhibit much less scatter compared to the Roehl #1 profile, the moving average of the Jablonski #1 data is used for correlation where available.

The positive excursion related to the Albian-Cenomanian Boundary event is not recorded but is replaced by a submarine hiatus atop the Stuart City margin. The return excursion to lighter values and three positive excursions identified by Jarvis et al. (2006) as lower Cenomanian events 1-3 are present in *Planolites*-burrowed shale of the Del Rio Fm. Seemingly erratic trends in the transition to globigerinid-bearing mudstones of the lower Buda formation are inconsistent with data from the Engish Chalk, yet the middle Buda Fm data provide a better fit surrounding the mid-Dixoni event. Near the level of the mid-Cenomanian event, a prominent negative trend from 2.0‰ to 0.5‰ is present in the upper Buda Fm. This trend most likely reflects a diagenetic overprint from flux of isotopically light pore fluids through the upper 4 m of the Buda Fm, perhaps during subaerial exposure at the mid-Cretaceous unconformity or during sulfate reduction of organic matter in the overlying Eagle Ford shale. Subsequently, the onset of OAE 2 in the latest Cenomanian is marked by a positive excursion at the Bonarelli level that is globally recognized (Schlanger and Jenkyns, 1976; Scholle and Arthur, 1980).

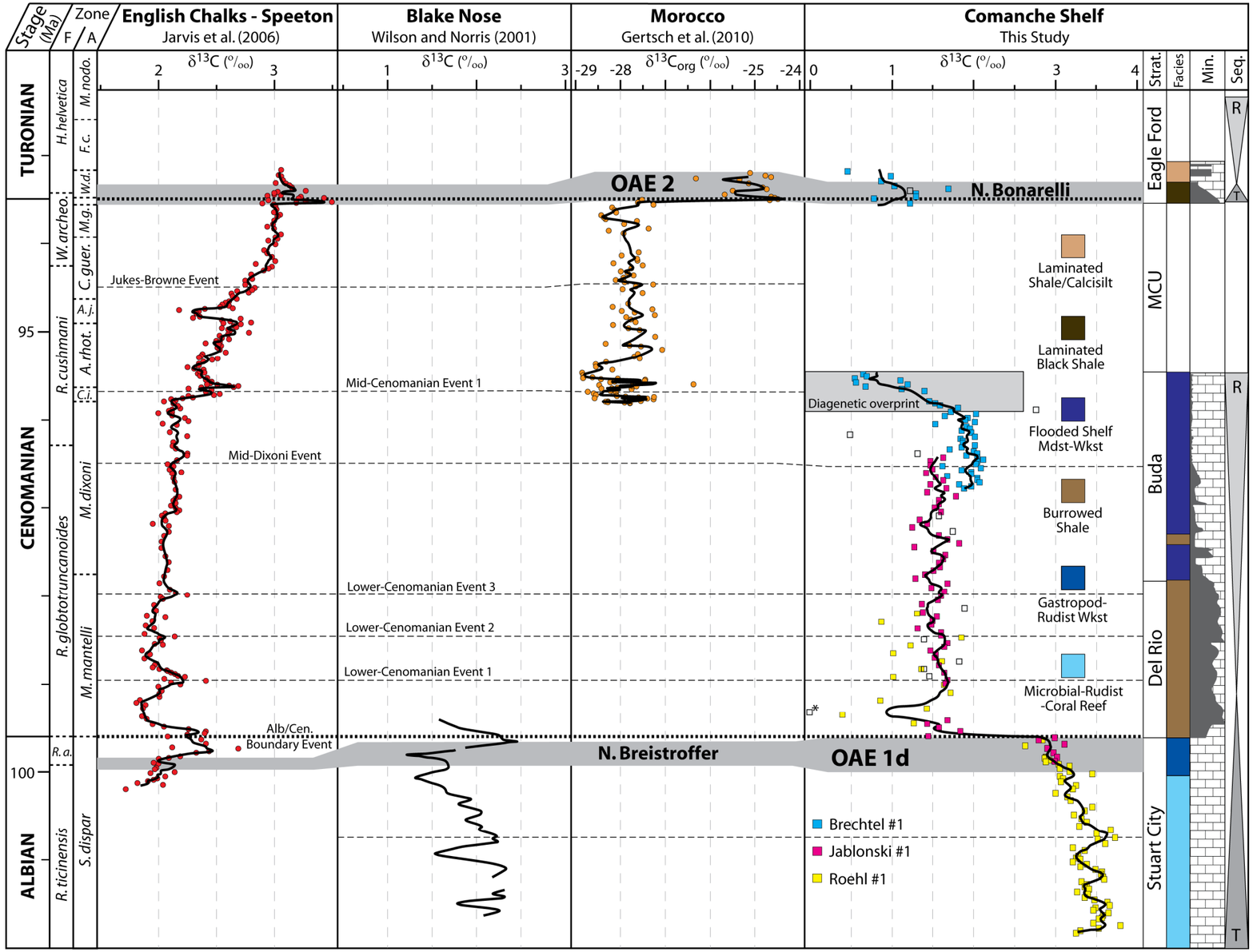

Figure 3.14: Correlation of Comanche Shelf $\delta^{13}C$ data to reference profiles of the Cenomanian stage. The symbol denoted by an asterisk has a value of -0.64‰ $\delta^{13}C$. MCU refers to the Mid-Cretaceous Unconformity.

Turonian – Campanian Isotope Profiles

The composite secular $\delta^{13}C$ profile for Turonian- through Campanian-age English Chalk (Jarvis et al., 2006) provides an excellent time-calibrated reference profile and is well-matched by high-resolution profiles from the southern neo-Tethys of Tibet (Wendler et al., 2009) and central Tethys of Italy (Stoll and Schrag, 2000). The 1.5‰ excursion of individual data points to heavier $\delta^{13}C$ values across the Cenomanian-Turonian boundary is possibly the geochemical signature of OAE 2 and corresponds to lower Eagle Ford Group planar-laminated black shale on the Comanche Shelf (Figure 3.15). These black shales represent transgression and maximum flooding during the Eagle Ford-Austin Chalk supersequence. The absolute $\delta^{13}C$ values in south Texas are in the range of 0.0 – 1.5‰, which is significantly lower than the 2.5 – 4.5‰ range observed in the reference profiles.

After OAE 2, anoxic conditions on the middle platform of the Comanche Shelf continued throughout deposition of planar-laminated shale/calcisilt in Turonian-age strata of the upper Eagle Ford Group. The temporal extent of this facies indicates that anoxia lasted through much of the Turonian on the middle-platform. The Round Down and Hitch Wood events in the middle and late Turonian appear to be present in a moving average of the Brechtel #1 data, although a persistent positive $\delta^{13}C$ trend in the Turonian is opposite to the negative trend observed in the Tibetan and English chalk profiles (Figure 3.15). This positive $\delta^{13}C$ drift may be a diagenetic overprint related to sulphate reduction of isotopically depleted organic matter (Irwin et al., 1977) and its decreasing impact upward through the Eagle Ford Group (Ryan Harbor, personal communication). In the Brechtel #1 profile, a concave-left trend toward more positive values during the Coniacian is

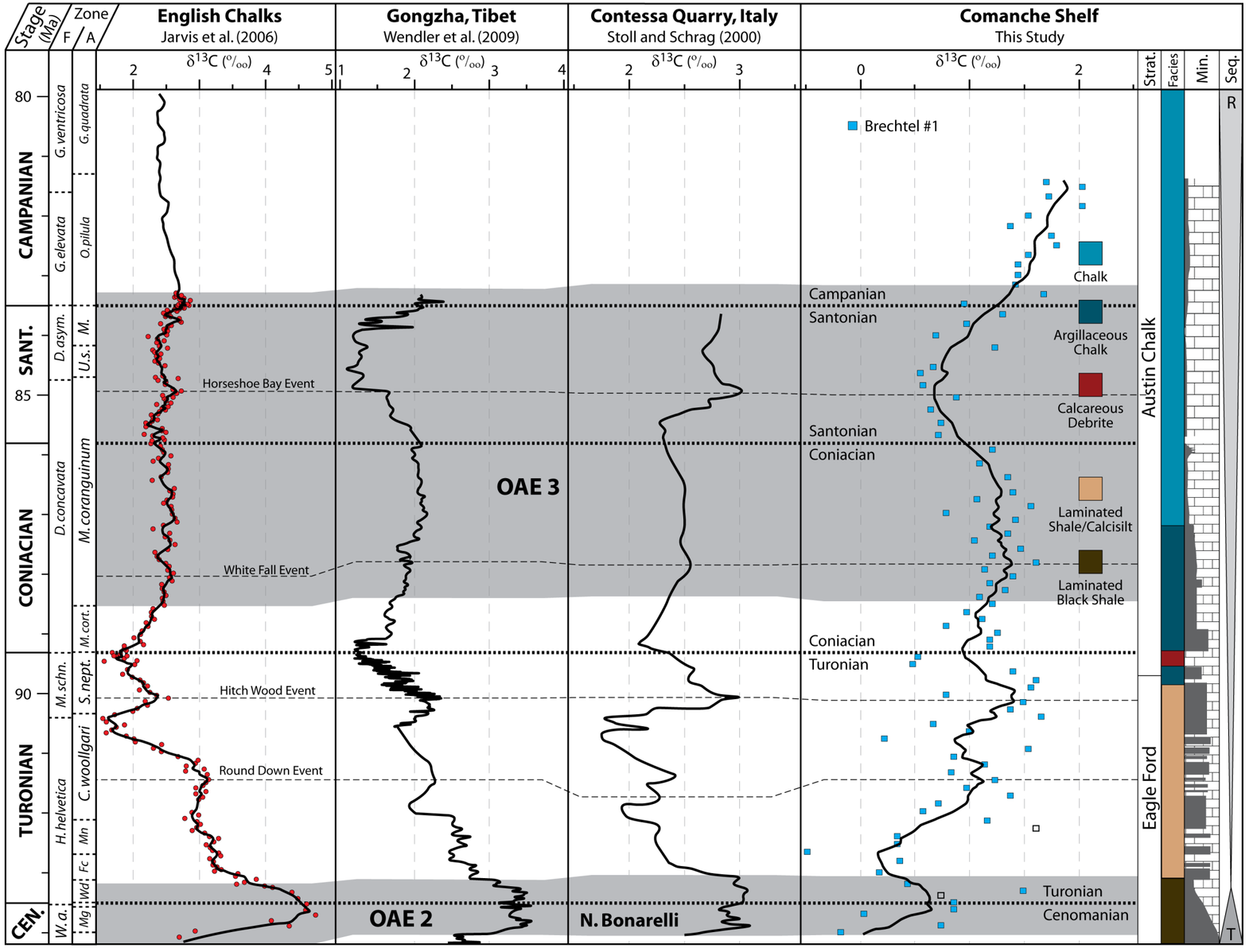

Figure 3.15: Correlation of Comanche Shelf δ^{13}Cdata to reference profiles of the Turonian through early Campanian stages.

contemporaneous with a vertical facies change from more- to less-argillaceous chalk. A $\delta^{13}C$ minimum in the Santonian is consistent across the reference profiles and is interrupted by a positive excursion of variable amplitude during the Horseshoe Bay event. In the Comanche Shelf data, a positive $\delta^{13}C$ trend continued from the late Santonian into the early Campanian.

OAE CONTROL OF COMANCHE SHELF DROWNING EVENTS

On four separate occasions eustatic sea-level rise and environmental stress related to oceanic anoxic events caused termination of carbonate deposition in south Texas. Two such events contributed to the demise of well-developed phototrophic carbonate systems with high-angle, rimmed shelf depositional profiles. Furthermore, each of the four platform drowning episodes related to OAEs 1a, 1b, 1d, and 2 were concurrent with or were immediately followed by shale deposition across the shelf. The four carbonate platform drowning events on the Comanche shelf are here examined in the context of recent hypotheses for the causal mechanisms of OAEs, which are generally focused on the impact of increased submarine volcanism in large igneous provinces (Sinton and Duncan, 1997; Larson and Erba, 1999; Weissert and Erba, 2004; Kuroda et al., 2007).

Notably, large igneous province volcanism caused displacement of ocean-water by submarine volcanic material, which was expressed by eustatic sea level rises. Volcanism also increased atmospheric pCO_2 concentrations and caused greater ocean water acidity; processes that led to global warming, intensification of the hydrologic cycle, increased continental run-off and weathering, and biocalcification crises of calcareous organisms. Leaching of volcanic metals by submarine hydrothermal water was combined with greater transport of phosphorous from land to the marine realm. This

nutrient delivery stimulated primary productivity in the world's oceans and ultimately led to oceanic anoxia (Erbacher et al., 1996; Bralower et al., 1999; Larson and Erba, 1999; Kump and Arthur, 1999; Weissert and Erba, 2004; Mort et al., 2007; Emeis and Weissert, 2009; Mehay et al., 2009; Tejada et al., 2009; Erba et al., 2010).

Early Aptian Drowning Event

Transgression during the early Aptian James supersequence combined with the effects of OAE 1a to drown shelf and reef-margin carbonates of the Sligo Formation (Figures 3.2, 3.16). Emplacement of submarine volcanics in the Ontong-Java Plateau (Larson, 1991; Larson and Erba, 1999; Tejada et al., 2002) was coincident with an early Aptian eustatic rise during the James supersequence that is observed in global stratigraphic records (Chapter 2; Haq et al., 1988; Roehl and Ogg, 1996; Sahagian et al., 1996; Lehmann et al., 2000; Van Buchem et al., 2010). Prior to OAE 1a, increasing shale content in transgressive Sligo shelf carbonates of segment C2 is indicative of greater terrestrial weathering and/or decreased carbonate sedimentation rates (Figures 3.5, 3.12). Undecompacted sediment accumulation rates at this time decreased by more than 60%, from 2.6 cm/ky to 1.0 cm/ky. A globally documented nannoconid crisis suggestive of decreasing ocean-water pH (Erba, 1994; Bralower et al., 1999; Larson and Erba, 1999; Erba et al., 2010) was concurrent with retrogradation of echinoid-oyster wackestones and oyster biostromes across the shelf interior (Figure 3.16). Increased terrigenous clay proportions, the rise in eustatic sea level, and the surge in ocean-water acidity increasingly stressed the carbonate factory, as evidenced by: (1) establishment of an oyster-dominated fauna, (2) decreasing Sligo shelf sediment accumulationrates, and (3) eventual drowning of the platform. These conditions arose prior to the Livello Selli event

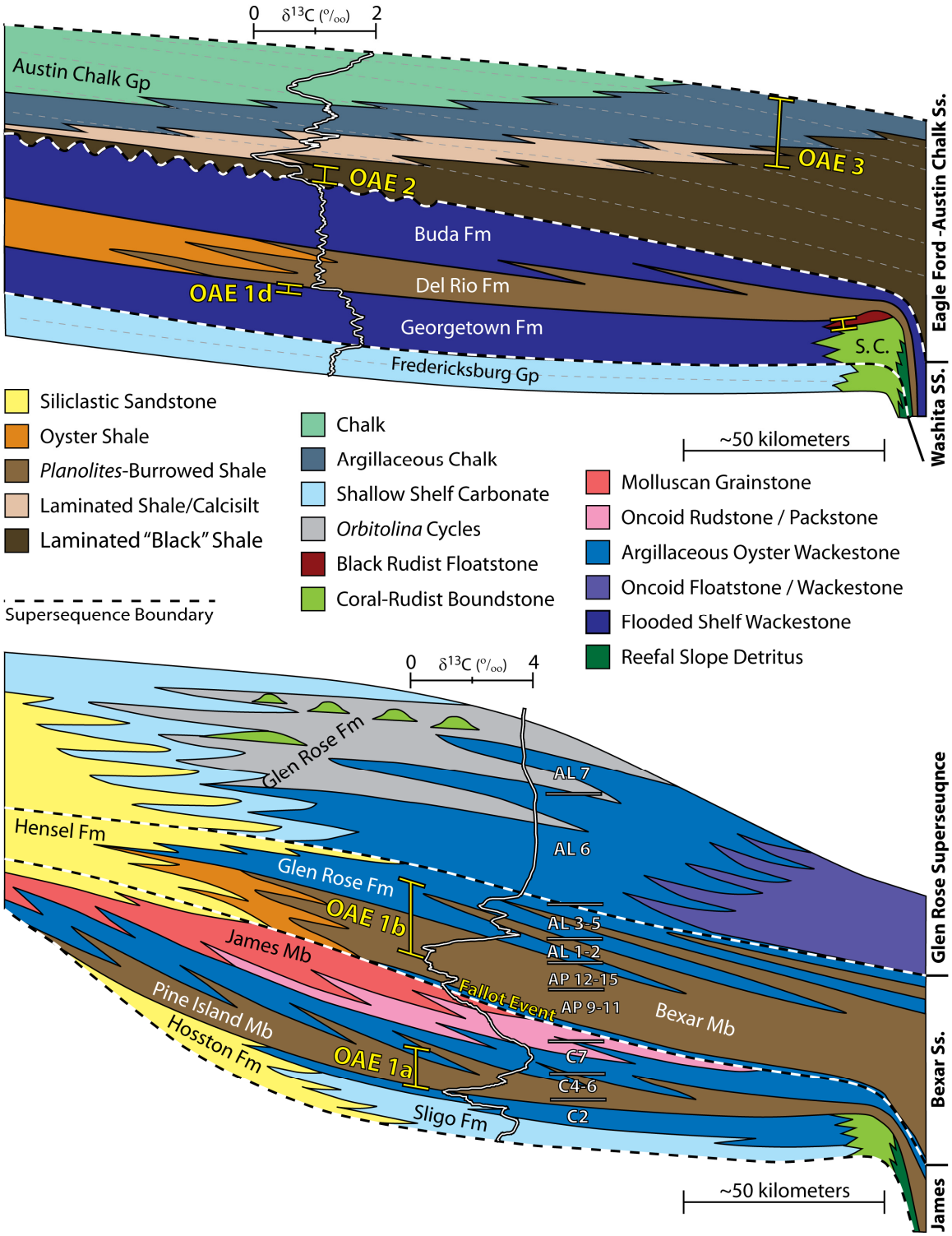

Figure 3.16: Response of the platform to OAEs, showing schematic depositional profiles

and simplified lithofacies distributions on the Comanche Shelf prior to, during, and following each OAE. Not drawn to vertical scale. $\delta^{13}C$ profiles are from the composite curve shown in Figure 3.19.

in OAE 1a and are paired with a trend of decreasing $\delta^{13}C$ values consistent with increased output of depleted volcanogenic CO2. Sequence stratigraphic interpretations from the Comanche shelf indicate that development of OAE 1a during segments C4-C6 occurred in the Pine Island shale at the peak of a second-order eustatic rise (Chapter 2). This brown shale unit contains ammonites and numerous plant fragments in the most landward core of the study area (Canyon Lake core set; Figure 2.4) located nearly 130 km from the Barremian shelf-edge (Figure 3.1). Over the former shelf margin, Pine Island lithofacies transition to ammonite-rich, planar-laminated black shale indicative of strongly dysoxic to anoxic conditions (R.G. Loucks, personal communication). Sediment accumulation rates in the middle-platform dropped to 0.55 cm/ky, indicating that the dramatic increase in relative sea-level resulted from a moderate eustatic rise (20-30 m) that was greatly enhanced by diminished sedimentation rates and subsidence of the passive margin.

During and immediately following OAE 1a, carbonate sedimentation was largely confined to molluscan grainstones in highstand shoreface systems of the James supersequence (Figure 3.16). Grainstone ramp clinoforms prograded from the Llano uplift and passed down depositional dip into oncoid rudstones to echinoid-oyster wackestones that distally interfingered with dysoxic, burrowed shale of the upper Pine Island member (Loucks, 1976; Chapter 2). Because sediment accumulation rates remained low at 0.6 cm/ky, progradation of carbonate clinoforms was not the result of increasing carbonate factory productivity, but rather a product of falling eustatic sea-level and diminished siliciclastic clay infux. Low sedimentation rates and a heterotrophic fauna

dominated by oysters imply that the recovering carbonate factory continued to languish in stressed environmental conditions following OAE 1a. As such, additional environmental perturbations associated with the Fallot event readily caused termination of the feeble carbonate factory and introduced a shift to dysoxic shale deposition in the Bexar Member (Figures 3.12, 3.16).

Late Aptian Drowning Event

The second drowning episode of the platform and the onset of burrowed-shale deposition began with the Fallot Event and continued through the Paquier event of the OAE 1b set. The Fallot Event and the OAE 1b set were preceded by long-term negative $\delta^{13}C$ trends in segments Ap8-Ap9 and Ap12-Ap15, respectively (Figure 3.12). Similar to OAE 1a, second-order eustatic rise in the Bexar supersequence (Chapter 2) and the negative $\delta^{13}C$ excursions were coincident with large igneous province volcanism in the Nauru-Mariana Basin and the Kerguelen Plateau (Duncan, 2002; Tejada et al., 2002; Weissert and Erba, 2004).

Following the analogy to OAE 1a, platform drowning likely resulted from a combination of increasing ocean acidification (Weissert and Erba, 2004), continued terrigenous clay influx, and eustatic sea level-rise (~10-20 m). Shale accumulation and deepening of relative sea-level were augmented by minimal sediment accumulation rates of 0.35 cm/ky and continued shelf subsidence. *Planolites*-burrowed Bexar shale of the middle-platform transitioned distally to planar-laminated black shale above the former shelf-margin (R.G. Loucks, personal communication). While shale facies were deposited across most of the shelf during OAE 1b, the shoreline consisted of glauconitic siliciclastic sandstone with carbonate caliche profiles in the Hensel Fm (Chapter 2; Amsbury, 1996).

Oyster biostromes were transitional between shoreline siliciclastic sandstones and offshore shale.

After the Paquier Event in AL 2, carbonate sedimentation resumed as echinoid-oyster wackestones and oyster biostromes of the lower Glen Rose Fm interfingered with Bexar shales during the temporal equivalent of the Leenhardt event and the remainder of OAE 1b (Figures 3.2, 3.16). Crinoids were locally abundant beneath the top Bexar supersequence boundary (Amsbury, 1996). Following OAE 1b in transgression of the Glen Rose supersequence, shallow-marine carbonate packstone to grainstone cycles of the lower Glen Rose were confined to the inner-ramp, while the middle-ramp was dominated by environmentally stressed echinoid-oyster and Oribitolina facies (Chapter 2). In deeper areas of the platform, outer-ramp sedimentation was condensed into oncoid wackestones and lime mudstones in segments AL5-AL6. The later widespread occurrence of coral-rudist biostromes and patch reefs (Perkins, 1974; Loucks and Kerans, 2003; Scott et al., 2007) represented the return of normal marine conditions on the platform during segment AL 7.

Late Albian Drowning Event

Continued phototrophic sedimentation in the middle to late Albian transformed the ramp profile of the lower Glen Rose Fm into a rimmed-shelf with high-angle morphologies in the Stuart City margin (Figure 3.2). The stratigraphic position of the OAE 1d in the latest Albian is within the transgressive systems tract of the Washita supersequence and immediately preceded the demise of the Stuart City margin. The sedimentologic change to black rudist floatstones and peloid-gastropod wackestones in the uppermost Albian portion of the Stuart City margin (Figures 3.8 and 3.13) suggests

environmental stress linked to OAE 1d played a role in shelf-margin drowning. Although no late Albian volcanism in large igneous provinces is currently documented, several other carbonate platforms drowned at the same time, possibly as a result of OAE 1d (Groetsch et al., 1993). Final shelf-margin drowning occurred during maximum flooding of the Washita supersequence and deposition of Del Rio shale. Similar to sediments deposited during OAEs 1a and 1b, fauna in the Del Rio Fm were dominated by oysters (Figure 3.16) (Lock et al., 2007). Partial recovery of the carbonate system occurred with deposition of peloidal packstone/wackestone in the Buda Fm that distally interfingered with Del Rio shale (Figures 3.9, 3.16).

Cenomanian-Turonian Drowning Event

Eustatic rise and oceanic anoxia during OAE 2 led to the fourth drowning episode of the Comanche shelf and deposition of Eagle Ford black shale during maximum flooding of the Eagle Ford-Austin Chalk supersequence. Similar to OAEs 1a and 1b, OAE 2 is temporally linked to volcanism in large igneous provinces from the Caribbean, Madagascar and the Ontong-Java oceanic plateaus (Sinton and Duncan, 1997; Kuroda et al., 2007; Turgeon and Creaser, 2008; Elrick et al., 2009). Correlation of $\delta^{13}C$ profiles indicates that upper Eagle Ford laminated shale/calcisilt lithofacies and Austin Chalk lithofacies in the Brechtel #1 core of the middle-ramp may have changed facies along isochronous time horizons to laminated black shale lithofacies in the Leppard #1 core above the former shelf margin (Figures 3.1, 3.16, 3.17). Progradational ramp clinoforms consisted of shallower chalk foresets with deeper shale toesets. These gradational facies changes occurred along depositional timelines as the increased depth below storm-wave base prevented mixing of the water-column. Data from both cores illustrate that anoxic

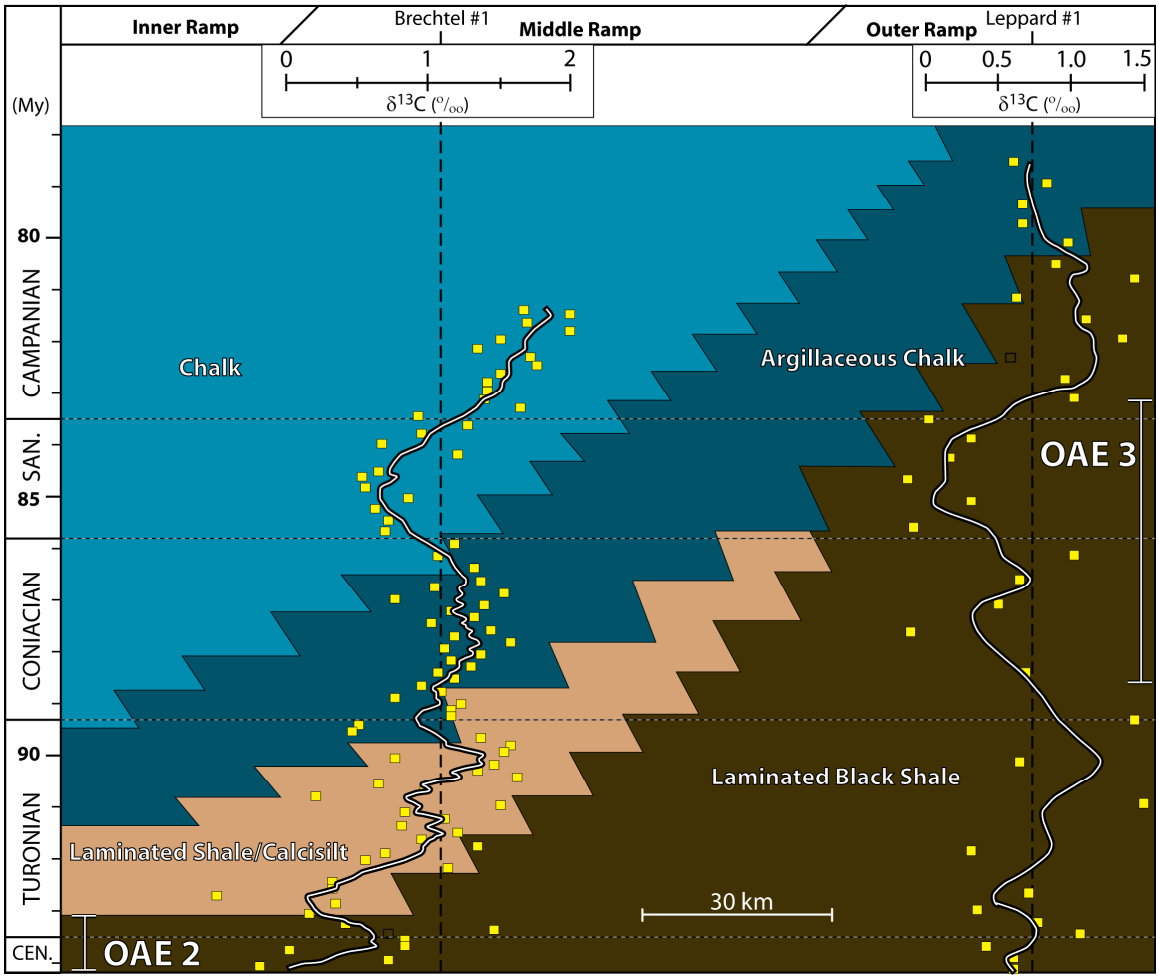

Figure 3.17: $\delta^{13}C$ data and lithofacies from the Brechtel #1 and Leppard #1 cores in the middle- and outer-ramp illustrate the possible time-equivalence of proximal Austin Chalk and distal Eagle Ford shale strata.

conditions at the sediment-water interface lasted from the Cenomanian/Turonian boundary event through much of the Turonian in the middle shelf but persisted through the early Campanian in deeper, more distal settings. As a result, periods of elevated organic-carbon deposition during OAE 2 (Schlanger and Jenkyns, 1976) and OAE 3 in the Coniacian-Santonian (Jenkyns, 1980; Locklair et al., 2011) were merged into a single episode of anoxia in distal areas of the Comanche Shelf (Figures 3.15, 3.16, 3.17). The shallow-marine carbonate factory never fully recovered from the environmental stress that accompanied OAE 2. Temporally extended anoxia in south Texas may represent upwelling of nutrient-enriched waters over the drowned Stuart City shelf margin. This hypothesis is a similar scenario to the upwelling zones offshore Venezuela that were responsible for continuous deposition of late Cenomanian through Coniacian organic-rich sediments in the La Luna Fm (Schlanger et al., 1987; De Romero et al., 2003). Published biostratigraphic data from the subsurface of south Texas are unavailable to confirm or reject the hypothesized stable isotope correlation and interpretation presented here.

ENVIRONMENTAL CONTROL OF CRETACEOUS TRANSGRESSIVE-REGRESSIVE SUPERSEQUENCES

Synthesis of carbon isotope profiles, facies trends, and sequence stratigraphic interpretations from the Comanche Shelf reveal an environmental control on many globally correlative transgressive-regressive supersequences of the Cretaceous. A four-phase model describes the response of land-attached carbonate platforms to changing environmental conditions surrounding OAEs (Figure 3.18). Results are specific to the Comanche shelf, but are generally applicable to additional land-attached platforms such as the northern Tethyan margin (Follmi et al., 1994; Follmi et al., 2006). Not all transgressive-regressive supersequence phases are present surrounding each OAE, but the

idealized model is intended to capture a full cycle of platform drowning and stabilization. The model is not applicable in areas such as the southern Tethys where platform drowning and shale deposition did not occur (Huck et al., 2010).

The initial equilibrium phase (Figure 3.18) assumes normal marine conditions and the presence of a high-angle, rimmed shelf with a coral- and rudist-dominated macrofauna. Additional phototrophic organisms, such as miliolid foraminifera and green algae, were present across the shelf. Examples include the Hauterivian-Barremian Sligo shelf and the middle to late Albian Stuart City margin. Values of $\delta^{13}C$ profiles were confined in a narrow range and terrigenous clay accumulation was minimal to absent. Eustacy was slowly increasing to stationary, yet high sediment acccumulation rates (2.6-5.5 cm/ky; Chapter 2) led to decreasing accommodation with aggradational to progradational shelf-margin trajectories and regressive shelf-interior facies patterns.

In the crisis phase, increasing volcanism in large igneous provinces led to greater atmospheric concentration of isotopically depleted CO2 (Kump and Arthur, 1999) that is reflected in decreasing $\delta^{13}C$ values (Figure 3.18). Ocean-water acidity increased in response to elevated pCO_2 levels, and decreased saturation of ocean-water with respect to CaCO3 likely reduced the calcification ability of numerous marine organisms such as coral and green algae (Gattuso et al., 1998; Kleypas et al., 1999; Riebesell et al., 2000; Wissler et al., 2003). The link between increased volcanic pCO_2 concentration and marine biocalcification rates is confirmed by documented crises of nannoconids prior to the onset of oceanic anoxia and deposition of organic-rich shale (Erba, 1994; Bralower et al., 1999; Erba et al., 2010). During this phase, the Comanche Shelf exhibited transgressive facies patterns in the uppermost Sligo Fm shelf, James Member ramp, and Stuart City shelf margin. Relative sea-level rise at the time was in part a result of rising eustacy and in part due to decreased carbonate sedimentation rates in response to

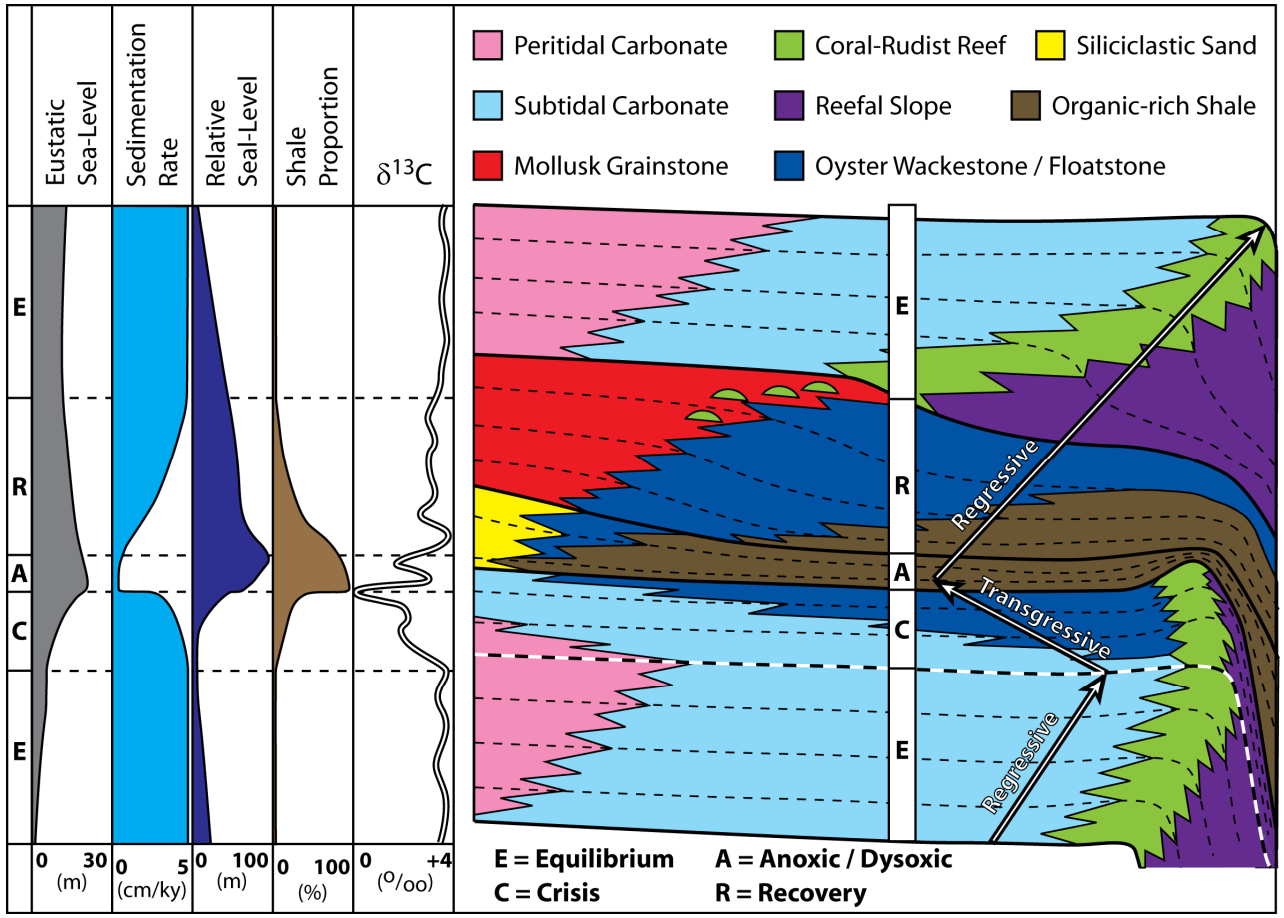

Figure 3.18: Schematic diagram illustrating phases of environmentally controlled, globally correlative transgressive-regressive supersequences. Characteristics of the equilibrium, crisis, anoxic/dysoxic, and recovery phases are discussed in the text. Graphs at left are a summary of multiple supersequences with estimated values for eustatic sea level, relative sea level, and shale proportion. The $\delta^{13}C$ curve is schematic.

increasing ocean-water acidity. Coral-rudist assemblages decreased in abundance, oyster biostromes transgressed across the shelf, and terrigenous shale began accumulating with increasing proportions. Clearly the Comanche shelf was repeatedly in crisis. The end of this phase is marked by a $\delta^{13}C$ trough that was induced by a triggering mechanism for oceanic anoxia.

Oceanic anoxic events, organic-rich shale deposition, and positive $\delta^{13}C$ excursions characterize the anoxic phase (Figure 3.18). Whether the immediate cause was related to methane hydrate release (Jahren et al., 2001) or volcanic release of trace metals into the water column (Larson and Erba, 1999), surface-water productivity peaked, marine oxygen levels plummeted and carbonate platform drowning occurred. Eustatic sea level may have reached 10-30 meters above equilibrium phase levels, but relative sea-level rise of 50-100 meters and maximum flooding of the platform was enhanced by low sediment accumulation rates (0.3-0.5 cm/ky) and platform subsidence. Shale deposition was as much a function of background sedimentation with high rates of organic-carbon burial as it was a result of increased clay input from continental weathering. Radiolaria and benthic foraminifera assemblages underwent rapid extinction and radiation episodes in response to fluctuating nutrient levels (Erbacher et al., 1996; Parente et al., 2008). Shoreline sedimentation in low-angle ramp clinoforms consisted of reworked mollusk-oyster debris or glauconitic siliciclastic sandstones. This is clearly documented during OAEs 1a and 1b of the James and Bexar supersequences. Similar facies trends are observed in northern Tethyan margins (Follmi et al., 1994; Follmi et al., 2006).

Following oceanic anoxia, the recovery phase of the platform is characterized by diminished volcanogenic processes and stabilizing $\delta^{13}C$ profiles with minor excursions (Figure 3.18). The carbonate factory was re-established in bathymetrically shallow areas near the shoreline as ocean-water acidity decreased and sedimentation rates slowly

increased. Carbonate factories on isolated platforms, such as those in the Pacific Ocean (Groetsch et al., 1993; Jenkyns, 1995), may not have begun the recovery process, precisely because they lacked shallow shorelines from which to establish active sedimentation. Recovery fauna deposited in dysoxic conditions amidst decreasing shale accumulation consisted of oyster-dominated assemblages with lesser echinoderms following OAEs 1a, 1b, and 1d. Following OAE 2, recovery assemblages contained abundant coccolithophorids, common inoceramid bivalves, and lesser oysters in the upper Eagle Ford Group and Austin Chalk. Eustatic sea levels were slowly falling to stationary in the supersequence highstand and caused progradation of ramp clinoforms with regressive platform geometries. Coral-rudist assemblages were generally absent, but were slowly introduced in bioherms and isolated platform-margin reefs as normal marine conditions returned. Equilibrium conditions commonly followed and regressive shelf-margin reefs were established. Many carbonate shelves never fully recovered, as was the case of the Comanche Shelf following OAEs 2 and 3.

CONCLUSIONS

Compilation of the nine $\delta^{13}C$ profiles from the Comanche Shelf allows construction of a continuous secular carbon isotope curve spanning approximately 53 Myr that is derived from lower Hauterivian through lower Campanian strata exceeding 1,000 meters in thickness (Figure 3.19). Prior to global oceanic anoxic events, second-order transgressions and negative trends in $\delta^{13}C$ profiles are consistent with increased rates of submarine volcanism in large-igneous provinces as the primary driver of OAEs 1a, 1b, 1d and 2. If isolated as the only external forcing mechanism, eustatic sea-level rises of 10-60 m/Myr (Hancock and Kauffman, 1979; Haq et al., 1988; Sahagian et al.,

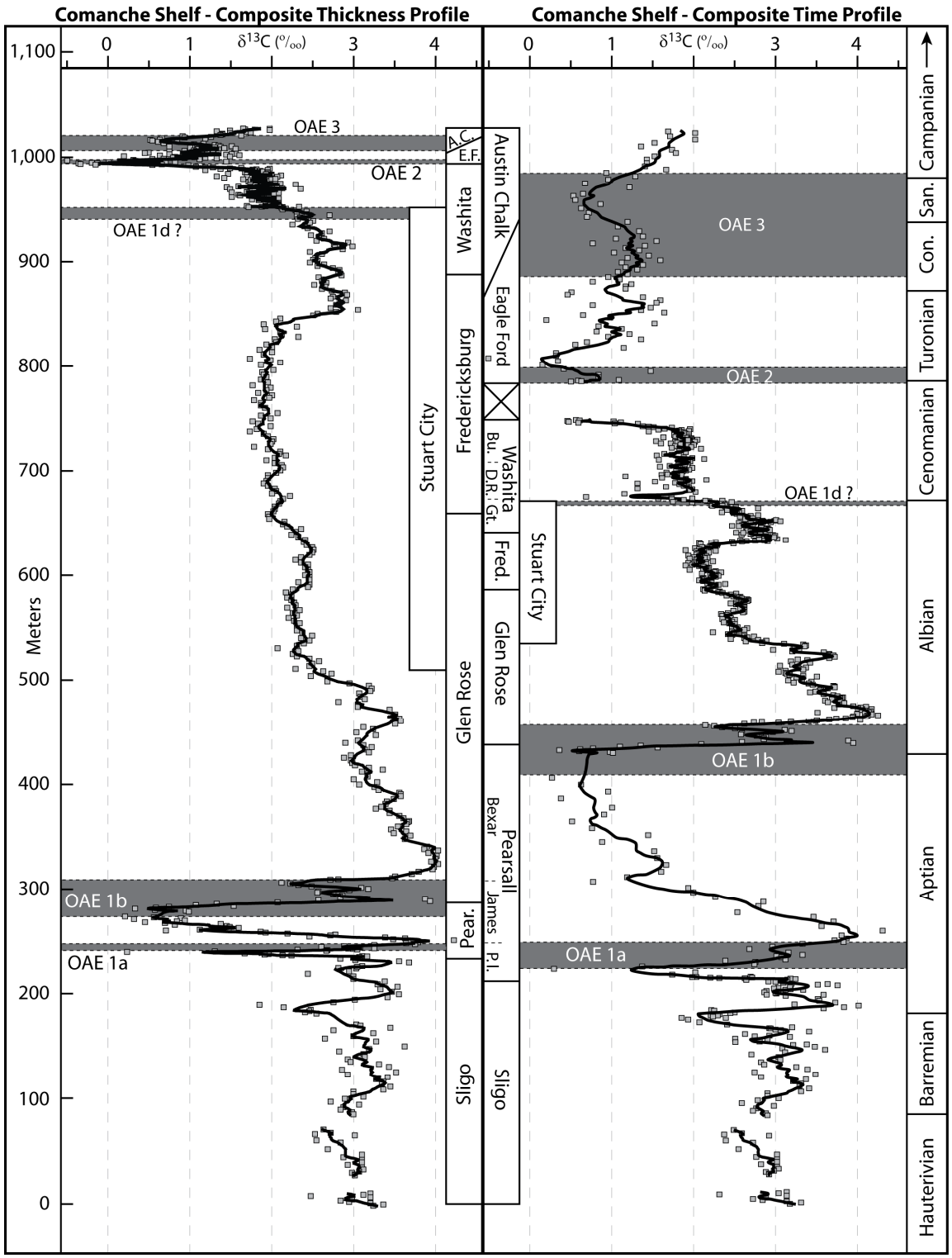

Figure 3.19: Composite $\delta^{13}C$ curves for the Comanche Shelf. At left the curve is shown

plotted against cumulative thickness of the stratigraphic section. At right the curve is plotted against time. Oceanic anoxic events represent condensed sections on the platform and less than 8% of the total section thickness, but comprise nearly 39% of the time recorded by the middle Hauterivian through lower Campanian interval.

1996; Miller et al., 2004) were probably insufficient to cause platform drowning on the Comanche Shelf when compared to reef-margin sediment accumulation rates of 71 m/Myr in the Stuart City reef-margin. Additional forcing mechanisms must have been involved to cause repeated drowning of otherwise healthy carbonate factories in the Sligo and Stuart City depositional systems. Environmental perturbations during the OAEs, especially increased surface water acidity and influx of siliciclastics from intensified continental weathering (Weissert and Erba, 2004; Emeis and Weissert, 2009; Erba et al., 2010), caused carbonate sediment production to essentially cease during the anoxic events. Thus volcanism in large-igneous provinces led to a combination of eustatic sea level rise and environmental stress that repeatedly caused carbonate sedimentation to terminate on the Comanche Shelf.

Using the south Texas composite $\delta^{13}C$ profile, I document the impact of OAEs 1a, 1b, 1d, 2 and 3 on the morphologic development of the Comanche shelf. Four carbonate platform drowning events caused development of transgressive-regressive supersequences characterized by equilibrium, crisis, anoxic, and recovery phases. Stratigraphic packages of the greatest thickness and the highest sediment accumulation rates averaging 4 cm/ky occur in the equilibrium phases and are found in carbonate-dominated shelves of the Hauterivian-Barremian and Albian intervals (Figures 3.2, 3.19). Crisis phases are associated with transgressive facies trends, diminishing sedimentation rates, and increasing shale accumulation. The thinnest stratigraphic packages with the lowest sediment accumulation rates averaging 0.3-0.5 cm/ky occur during oceanic anoxic

phases. The associated shale intervals deposited during or immediately after the OAEs represent maximum flooding zones of the James, Bexar, Washita, and Eagle Ford–Austin Chalk second-order supersequences. Pine Island Member, Bexar Member, Del Rio Fm, and Eagle Ford Group shale units in south Texas are associated with OAEs and represent only 8% of the total section thickness but encompass approximately 39% of the time through which platform sediments were deposited. Following each OAE, recovery phases of the carbonate factory were re-established at the shoreline via regressive ramp depositional systems containing oyster- or coccolithophorid-dominated recovery faunas.

Detailed correlation of Hauterivian and Barremian data from the Comanche Shelf to global reference profiles indicates that additional isotope investigations outside of the northern Tethys may provide additional insight into global carbon cycling prior to OAE 1a. Aptian data are consistent across the various reference profiles and provide supplemental information regarding the global impact of Aptian environmental perturbations across the spectrum of marine environments. Comanche Shelf data presented for the Albian stage show minimal scatter and are valuable as a high-resolution data set that allows refined definition of globally correlative chemostratigraphic segments. Carbon isotope correlations for the Cenomanian are somewhat equivocal because excursions during the stage are of low amplitude. Correlation of Comanche Shelf data from the Turonian through lower Campanian interval to global reference sections is readily accomplished despite the broad overprint of regional diagenesis in the Eagle Ford Group. Multiple profiles from these stages illustrate the time-transgressive nature of dysoxic/anoxic lithofacies boundaries as a function of location along the Comanche Shelf depositional profile.

Chapter 4 – Temporal and Spatial Variability of a Cretaceous (Albian) Shelf-margin Reef Complex, Stuart City Formation, Northern Gulf of Mexico

ABSTRACT

Sedimentologic and sequence stratigraphic analysis of seismic and core data from the middle to late Albian Stuart City margin in the northern Gulf of Mexico illustrates the diverse shelf-to-basin morphologies, clinoform architectures, and facies trends developed in response to varied external forcing mechanisms. Low-angle shelf margin clinoforms with strongly progradational trajectories developed during a period of slow eustatic rise in the middle Albian Glen Rose supersequence. High-angle, rimmed-shelf clinoforms with aggradational trajectories aggraded a steep (40-80˚ dip) reef-wall in the early to late Albian Fredericksburg supersequence because of moderate rates of eustatic rise. Establishment of an empty-bucket shelf-margin profile with aggradational to retrogradational trajectories was related to rapid rates of eustatic rise during the late Albian transgressive systems tract of the Washita supersequence. Evolving shelf-margin morphologies associated with each supersequence necessitate distinct depositional models to represent temporal changes in Stuart City margin facies proportions and faunal distributions. Steepening of the reef-wall and stabilization of the reef-flat was facilitated by pervasive early-marine cementation and binding by the *Lithocodium-Bacinella* microbial association. Numerous syndepositional fractures with multiple stages of opening attest to the high-angle profile of the shelf-margin.

During each supersequence, laterally variable shelf-margin architectures and facies distributions were induced by antecedent structural/depositional topography and

differential subsidence rates related to the San Marcos Arch and surrounding salt embayments/basins. Isolated syndepositional faulting in the late Albian further modified vertical facies trends and cycle stacking patterns of the shelf-margin. Drowning of the Stuart City margin and Comanche Shelf at the Albian-Cenomanian boundary occurred in response to environmental stress in the latest-Albian OAE 1d and maximum flooding of the Washita supersequence. Complete evolution of the Stuart City margin, from initiation to maturation to termination, was a function of eustatic sea level, structural/tectonic, and environmental changes, although margin variability over shorter-time scales (1-3 Myr) and more specific areas was increasingly dominated by one of the above regime variables.

INTRODUCTION

Cretaceous shelf-margins are well-known for their abundance of morphologically diverse rudist bivalves. Early Cretaceous margins contained reefal assemblages with a mix of coral, algae, stromatoporoids, and primitive rudists such as caprinids, caprotinids, and requienids. In contrast, coral-algal and stromatoporoid components were often volumetrically insignificant in Late Cretaceous shelf-margins, which were increasingly dominated by gregarious banks of advanced rudists such as radiolitids and hippuritids (Kauffman and Johnson, 1988; Scott, 1988; Scott et al., 1990; Gili et al., 1995; Steuber, 2002). Albian reefs represent a transitional period during this fundamental shift from early Cretaceous coral-algal-rudist assemblages to Late Cretaceous rudist-dominated assemblages (Scott, 1984; Kauffman and Johnson, 1988). Studies of Albian reefal shelf-margins are few, with most localities found in the tectonically complex Basque-Cantabrian Basin (Fernandez-Mendiola and Garcia-Mondejar, 1989), reefal upper slope

deposits in Oman (Immenhauser et al., 2001), and the northern Gulf of Mexico region (Bebout, 1974; Bay, 1977; Scott, 1990; Lehmann et al., 1999). Despite these examples, paradigms for changing facies patterns and stratal architectures of Albian reef-margins in response to complex external forcing mechanisms are not well established. The subsurface Stuart City Formation of the Albian Comanche Shelf (Figure 4.1) in the northern Gulf of Mexico contains a biologically and lithologically diverse shelf-margin reef system (Bebout, 1974; Bebout and Loucks, 1974; Scott, 1990). It represents a unique opportunity to document the internal facies and architectural evolution of an Albian shelf-margin system in response to fundamental variables such as eustacy, structural/tectonic setting, and environmental stress related to oceanic anoxic events.

Extensive analyses of Stuart City margin facies, sedimentology, diagenesis, biostratigraphy, seismic-stratigraphy, geochemistry, and reservoir trends are available in previous studies (Winter, 1961; McNamee, 1969; Bebout and Loucks, 1974; Bebout et al., 1977; Coogan, 1977; Wooten and Dunaway, 1977; Prezbindowski, 1981; Tartamella, 1982; Scott, 1984; Tyrrell and Scott, 1989; Scott, 1990; Yurewicz et al., 1993; Fritz et al., 2000; Waite et al., 2007). This paper augments the existing knowledge-base by analyzing numerous whole cores from the Stuart City margin and developing sequential depositional models to illustrate the mosaic of facies distributions at the intersection of shelf-interior, reefal, and slope environments. Geologic significance of the facies variations is heightened by placing them within a well-defined sequence stratigraphic context (Chapter 2) and integrating them with shelf-interior stratigraphic patterns. Stages of reef initiation, maturation, and termination during the Glen Rose, Fredericksburg, and Washita supersequences are examined and demonstrated to contain disparate facies assemblages that reflect evolving shelf-margin morphology. Such morphologic transformations are linked to shelf-margin trajectory and second-order eustatic sea-level

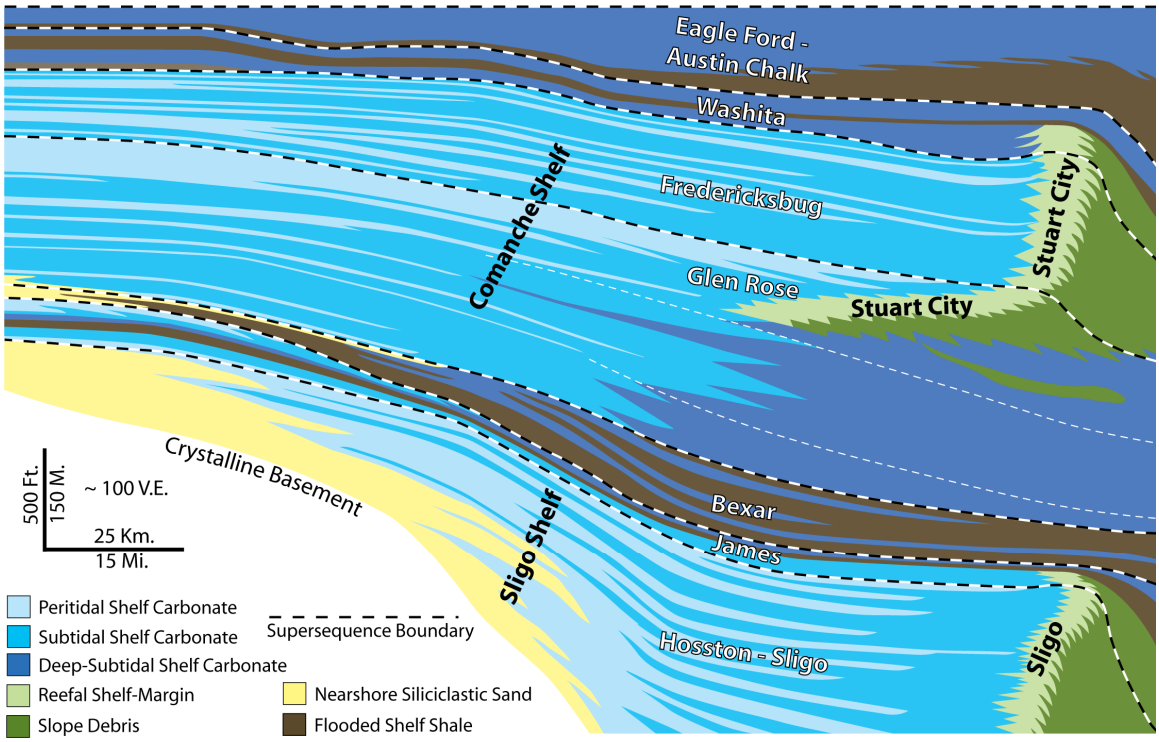

Figure 4.1: A simplified regional cross-section of Lower- and Upper-Cretaceous supersequences in the Sligo and Comanche Shelves of south Texas. Note the changing Stuart City margin trajectories and large-scale shelf-to-basin morphologies in the Glen Rose, Fredericksburg and Washita supersequences.

cycles, but are modified by environmental stress, antecedent structural topography, and regional syndepositional faulting. When placed within this context, faunal distributions are shown to be well-ordered, with reef construction greatly enhanced by pervasive binding of the *Lithocodium-Bacinella* micro-organism association.

To substantiate these claims, Stuart City margin facies associations are presented, example vertical facies successions are illustrated, and core-based shelf-margin profiles are discussed. Depositional models and cross-sections depicting spatial and temporal reef-margin variability are integrated with regional sequence stratigraphic, structural/tectonic, and paleoceanographic information to document external factors governing this mid-Cretaceous reef system. Regime variables affecting reef-margin evolution are then outlined and extrapolated to encompass other reefal systems of the Cretaceous and broader Phanerozoic.

GEOLOGIC BACKGROUND AND DATA DISTRIBUTION

The Coahuilan (Hauterivian – early Aptian) and Comanchean (Albian) shelves span the width of the northern Gulf of Mexico from Texas to Florida (Winker and Buffler, 1988) and comprise more than 1,300 meters (4,265 ft) of mixed carbonate-siliciclastic strata in south Texas. The first-order control on the location of both shelf-margins is the crustal structure of the Gulf of Mexico and differential subsidence rates between more slowly subsiding, moderately-attenuated and more rapidly subsiding, highly-attenuated continental crust (Buffler et al., 1980; Buffler and Sawyer, 1985; Winker and Buffler, 1988). Regional variations in crustal structure related to salt-withdrawal basins and basement uplifts profoundly influenced depositional patterns of shelf-interior and shelf-margin systems in areas such as the East Texas Basin, Maverick

Basin, Llano Uplift, and San Marcos Arch (Figure 4.2) (Winter, 1961; Rose, 1972; Young, 1986; Waite, 2009).

Sequence stratigraphic analysis of slabbed-cores and wireline logs from the Cretaceous section in south Texas indicates that seven second-order supersequences of 3-14 Myr duration are recognizable in the Sligo (Coahuilan) and Comanche shelves (Figure 4.1) (Chapter 1). Eustatic sea-level changes, combined with environmental perturbations during oceanic anoxic events (OAEs), were the forcing mechanisms dictating the character of regional facies patterns, sediment accumulation rates, and platform morphologies in these globally-correlative packages. The supersequences consist of 16 higher-order, 1-3 Myr depositional sequences, which are defined based on vertical facies proportions and cycle stacking patterns of the shelf-interior (Chapter 2). Carbon isotope profiles of shelf-interior and shelf-margin cores (Chapter 3), in conjunction with paleontologic information (Coogan, 1977; Young, 1986; Jiang, 1989; Scott et al., 2002; Waite et al., 2007), provide means for establishing temporal links between shelf-interior and shelf-margin lithologic units.

The Sligo shelf-margin in south Texas (Bebout, 1977) is penetrated by comparatively few wellbores and little core data is available, thus it is largely omitted from facies analysis in this study. The Sligo Fm is overlain by thin transgressive shale and regressive carbonate units of distally-steepened ramp clinoforms in the Pearsall Formation (Loucks, 1976) (Chapter 1). Carbonates of the Glen Rose Fm, Fredericksburg Group, and Stuart City Fm (Winter, 1961; Rose, 1972; Bay, 1977;) later prograded over Sligo Fm and Pearsall Fm carbonates to establish the Comanche shelf (Figure 4.1). In the present study area (Figure 4.2), the terminal location of the Stuart City margin is approximately stacked above the terminal Sligo reef-margin, but frequently diverges

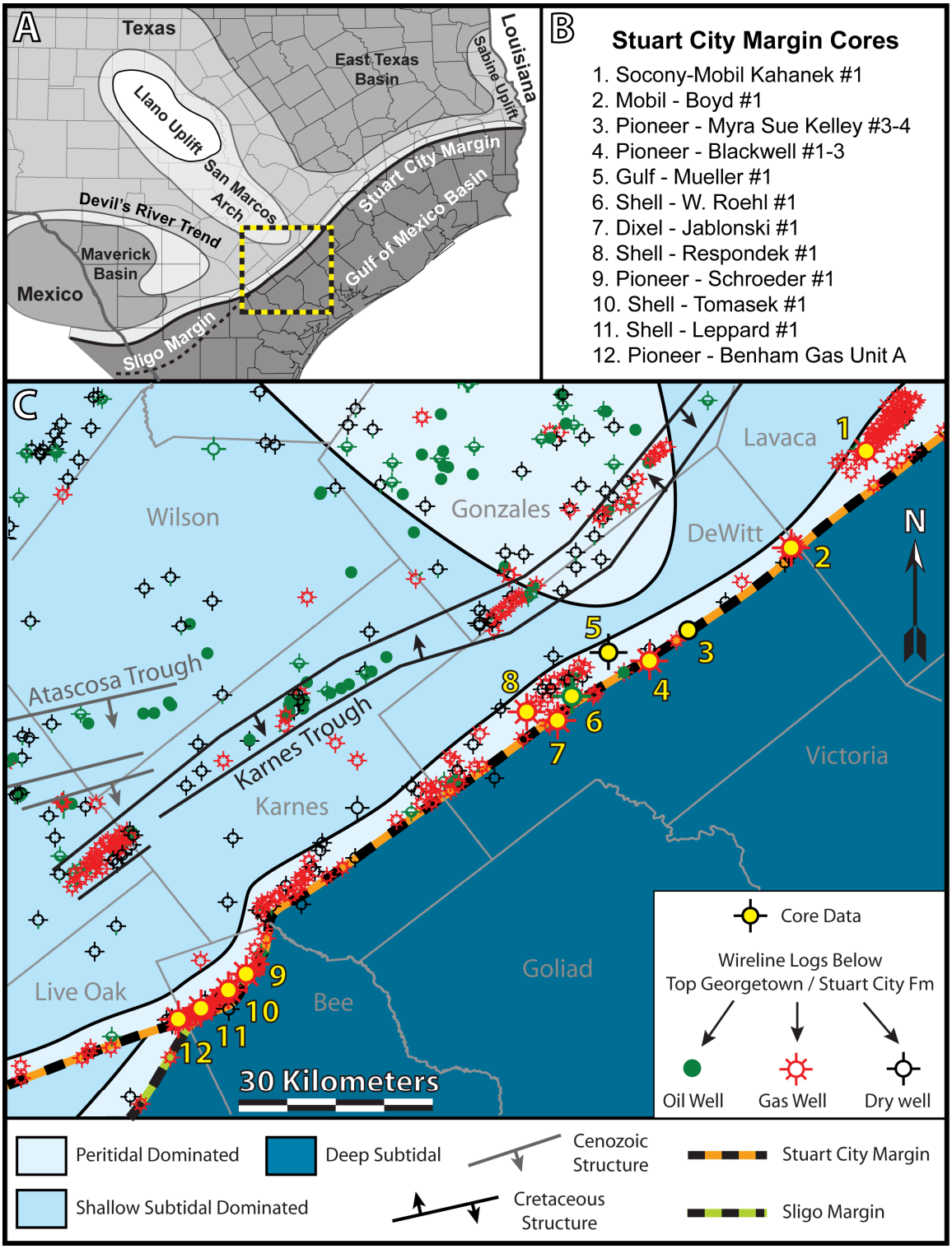

Figure 4.2: Shelf margin study area with (A) paleogeographic map of south Texas during

the Cretaceous showing terminal Stuart City and Sligo shelf-margin locations, as well as major tectonic/structural elements affecting patterns of deposition. (B) List of cores used for this study. (C) Inset showing terminal Cretaceous shelf-margins, core locations, wireline log locations, structural features, and county boundaries in the study area. Cores 9-12 are located in Pawnee Field. Cores 1-8 are located in numerous Stuart City fields.

landward or seaward by less than 10 km (Wooten and Dunaway, 1977; Winker and Buffler, 1988; Waite, 2009;).

Wireline log data from the Stuart City margin are abundant but of poor quality and character, thus they are employed only as a means of establishing stratigraphic datums using near isochronous formation contacts in the Upper Cretaceous. Twelve Stuart City margin cores totaling 1,925 m (6,320 ft) of section were selected from Bee, DeWitt, and Lavaca Counties (Figure 4.2) because of their preservation quality and continuity, usually in excess of 90 m (300 ft). Core-slab samples were described at the centimeter-scale and descriptions were augmented with petrographic thin-section observations. By comparison with data from Bebout and Loucks (1974) and Scott (1990), the flooded-shelf, shelf-interior, shelf-margin, and slope environments encountered in the cores are presumed to represent the full spectrum of facies present in the Stuart City trend. Industry 3-D seismic volumes were frequently referenced to assess local shelf-margin architecture and determine core positions with respect to terminal margin locations.

FACIES ASSEMBLAGE DESCRIPTION AND INTERPRETATION

Because of vast changes in paleobathymetry (supratidal to >100 m; >330 ft) along the dip-oriented profile from outer-shelf to slope environments, numerous lithofacies are encountered (Figures 4.3-4.9). Rather than providing a detailed analysis of each facies,

this section presents unifying characteristics of facies assemblages, brief facies descriptions, and interpretations of depositional environments. Bedding-dip inclinations are estimated using modern analogues of similar high-angle reef-margins, as well as outcropping Albian reef systems (James and Ginsburg, 1979; Fernandez-Mendiola and Garcia-Mondejar, 1989; Ginsburg et al., 1991; Neuweiler, 1993; Gomez-Perez et al., 1999; Adams and Schlager, 2000; Immenhauser et al., 2001). Facies water-depths during deposition are estimated using data from time-equivalent outcrops (Neuweiler, 1993; Gomez-Perez et al., 1999), modern analogues (McMaster and Conover, 1966; Mortyn and Charles, 2003), and vertical distance below intertidal sedimentary structures. The terms low-, moderate, and high-energy are used in a relative sense. Low-energy settings resulted in mud-dominated sediments with high proportions of *in situ* fauna and minimal fragmentation of skeletal structures. Moderate-energy settings exhibit packstone rock fabrics with a mix of *in situ* fauna and storm-reworked skeletal fragments. High-energy settings led to deposition of grainstone or rudstone rock fabrics within or near fair-weather wave-base that display hydrodynamic sedimentary structures and lack *in situ* or whole fauna.

Flooded Shelf Facies Assemblage

Facies in this assemblage each contain common to abundant globigerinid foraminifera and rare to abundant calcispheres. Globigerinid-calcisphere mudstones/wackestones with subordinate terrigenous clay are present in the distal lower Glen Rose Fm and the Georgetown Fm, below and landward of the Stuart City Fm, respectively. Globigerinid-oncoid wackestones/floatstones (Figure 4.3-B) with millimeter- to centimeter-scale cyanobacterial oncoids are present only in the distal lower

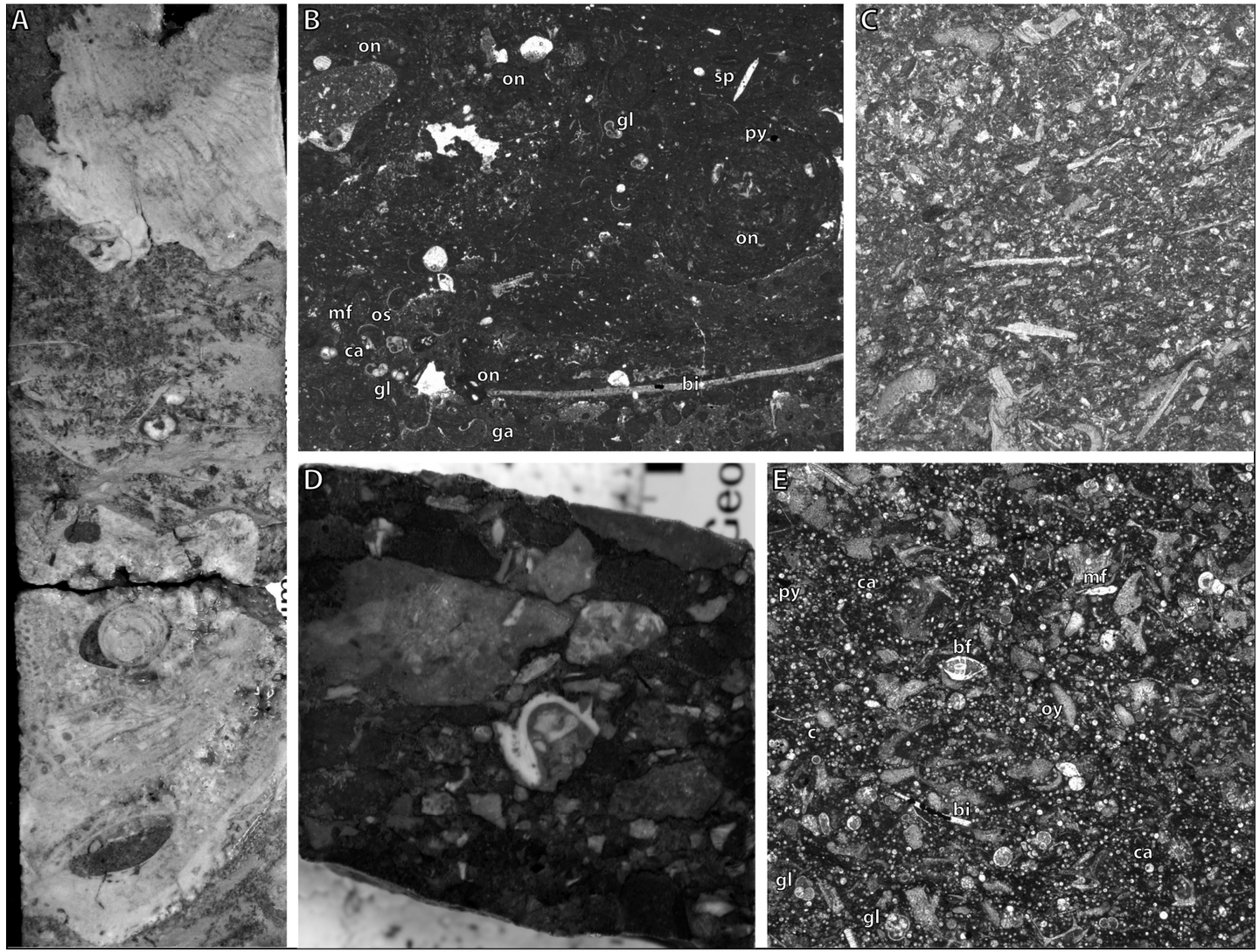

Figure 4.3: Flooded-shelf and fore-reef/slope facies plates. (A) Bioclastic rudstone core slab with an overturned coral (top) and caprinid rudist (bottom). Width of view = 5 cm. (B) Globigerinid-oncoid wackestone/floatstone with cyanobacterial oncoids (on), globigerinid foraminifera (gl), ostracodes (os), calcispheres (ca), monoserial foraminifera (mf), siliceous sponge spicules (sp), bivalve fragments (bi), and pyrite (py). Width of view = 9 mm. (C) Peloidal-skeletal packstone with rudist bivalve and un-identified skeletal fragments. Width of view = 12 mm (D) Polymictic breccia with fragments of skeletal packstone derived from the Stuart City reef-margin. White caprinid fragment is in the clast at center. Width of view = 5 cm. (E) Globigerinid-shale with numerous calcispheres, globigerinid foraminifera, monoserial foraminifera, oyster fragments (oy), bivalve fragments, pyrite, and a benthic foraminifera (bf). Width of view = 5 mm.

Glen Rose Fm. Both facies contain rare to common ostracodes, bivalve fragments, siliceous sponge spicules, and monoserial foraminifera. Globigerinid-shale (Figure 4.3-E) in the Del Rio Fm overlying the Stuart City margin contains significant terrigenous clay volumes with abraded oyster fragments, rare echinoderms, abundant pyrite, and monoserial foraminifera. All of the above facies are *Planolites*-burrowed and may contain mineralized, bored hardgrounds.

These facies are interpreted to represent low-energy, deep-subtidal depositional environments above the flooded (drowned) Sligo and Stuart City shelf-margins. Using modern *Globigerina* foraminifera as an analogue (Mortyn and Charles, 2003), estimated water depths during deposition of globigerinid-calcisphere mudstone/wackestone and globigerinid-shale may have been as shallow as 50 m (165 ft) but were likely on the order of 100 – 200 meters (330 – 660 ft). Similarly globigerinid-oncoid wackestone/floatstone facies must have been deposited above storm wave-base in as little as 50 m (165 ft) of water, but may have been up to 100 m (330 ft) deep if compared to modern oncoids found in rippled carbonate sands of the Canary Islands shelf (McMaster and Conover, 1966; Scott, 1990).

Fore-reef / Slope Facies Assemblage

Each facies in this assemblage contains allochems that appear to have been sourced from within or directly in front of the reef-margin, including rudist, coral and stromatoporoid fragments. They are vertically intermediate between flooded shelf facies of the lower Glen Rose Fm and reefal facies of the Stuart City Fm. Peloid-skeletal wackestones/packstones (Figures 4.3-C) contain finely abraded rudist, bivalve, coral, and undifferentiated skeletal fragments, as well fecal pellets. *Planolites* burrows are common

and terrigenous clay fractions are minimal. Bedding contacts rarely show subtle inclination in core samples. This facies is interpreted as lower fore-reef sediment deposited below storm wave-base in approximately 50-100 meters of water on a gently inclined (< 10˚ dip), low- to moderate-energy portion of the slope.

Bioclastic grainstones/rudstones (Figure 4.3-A) are dominated by fine-grained to very coarse-grained fragments of caprinid and radiolitid rudists, and common branching stick-coral fragments (*Pleurocora coalescens*). Pebble- to cobble-size grains consist of robust caprinids, domal coral, red algae, and stromatoporoids that are commonly overturned, corroded, and severely abraded. Grainstone matrix sediment is typically cross-stratified. This facies is envisioned as debris from storm-reworked portions of the reef front and biostromes in the upper fore-reef. Laterally migrating sand waves may have been present in lower-angle intervals of the high-energy slope. Water depths were possibly in the range of 20-50 meters.

Polymictic breccias (Figure 4.3-D) up to 10 meters in thickness contain carbonate mud-dominated matrix sediment and 0.5-10 cm-scale lithoclasts of skeletal packstone and rudist grainstone. Many lithoclasts have whole and fragmented caprinids. This facies is interpreted to consist of debris flows sourced from progradational and over-steepened reef environments. As shown in the Basque-Cantabria Basin (Fernandez-Mendiola and Garcia-Mondejar, 1989; Gale et al., 1996; Gomez Perez et al., 1999), slope angles of breccia talus mixed with bioclastic rudstone debris may have reached up to 35˚.

Reef-wall Facies Assemblage

Facies outlined here are unified by ubiquitous binding from association of the problematic micro-organism *Lithocodium aggregatum* Elliot (1956) and the

cyanobacterium *Bacinella irregularis* Radoicic (1959). A review of possible origins for *Lithocodium aggregatum* is presented by Rameil et al. (2010). Owing to their frequent comingling (Figure 4.4) and following previous authors, these enigmatic microbialites are referred to as *Lithocodium-Bacinella* from this point forward (Dupraz and Strasser, 2002; Rameil et al., 2010). Cavities lined with early-marine cement are abundant, as are geopetal structures and pholad clam borings. Matrix sediment is grain-dominated and consists of locally sourced bioclastic fragments. Gastropods and the foraminifera *Dictyoconus walnutensis* increase in abundance in shallower facies. Vertical microbial growth fabrics are frequently encountered and suggest early cementation of sediment.

Microbial-sponge bindstones (Figure 4.4-D) encountered only in the Schroeder #1 core are characterized by the presence of numerous calcitic and siliceous sponges. Also present are a variety of unidentified microbial organisms, among which *Lithocodium-Bacinella* are prevalent. Laminar stromatoporoids similar to the Devonian genus *Syringostroma* are common and specimens of the platy coral *Microsolena* are present. These fauna are interpreted to represent relatively low-light conditions at the base of a steeply inclined (40-70˚ dip), deep reef-wall (70-100 m; 230-330 ft). Albian microbial-sponge bindstones of the Basque-Cantabrian Basin were deposited in a similar setting at the bottom of rigid reefal successions (Neuweiler, 1993).

Lithocodium-Bacinella-stromatoporoid bindstones (Figure 4.4-F) vertically supercede sponge-rich facies of the Schroeder #1 core and form basal reef facies in many of the remaining cores. Laminar stromatoporoids are common to abundant and platy to branching *Microsolena*, *Actinostroma*, and delicate *Pleurocora* coral are rare to common. Sponges are rare to common and encrusting red algae are present. Digitate microbial protrusions and grain-dominated *Lithocodium-Bacinella* stromatolites with 10-15 cm of vertical relief are common. Allochems are ordinarily encrusted by *Lithocodium-*

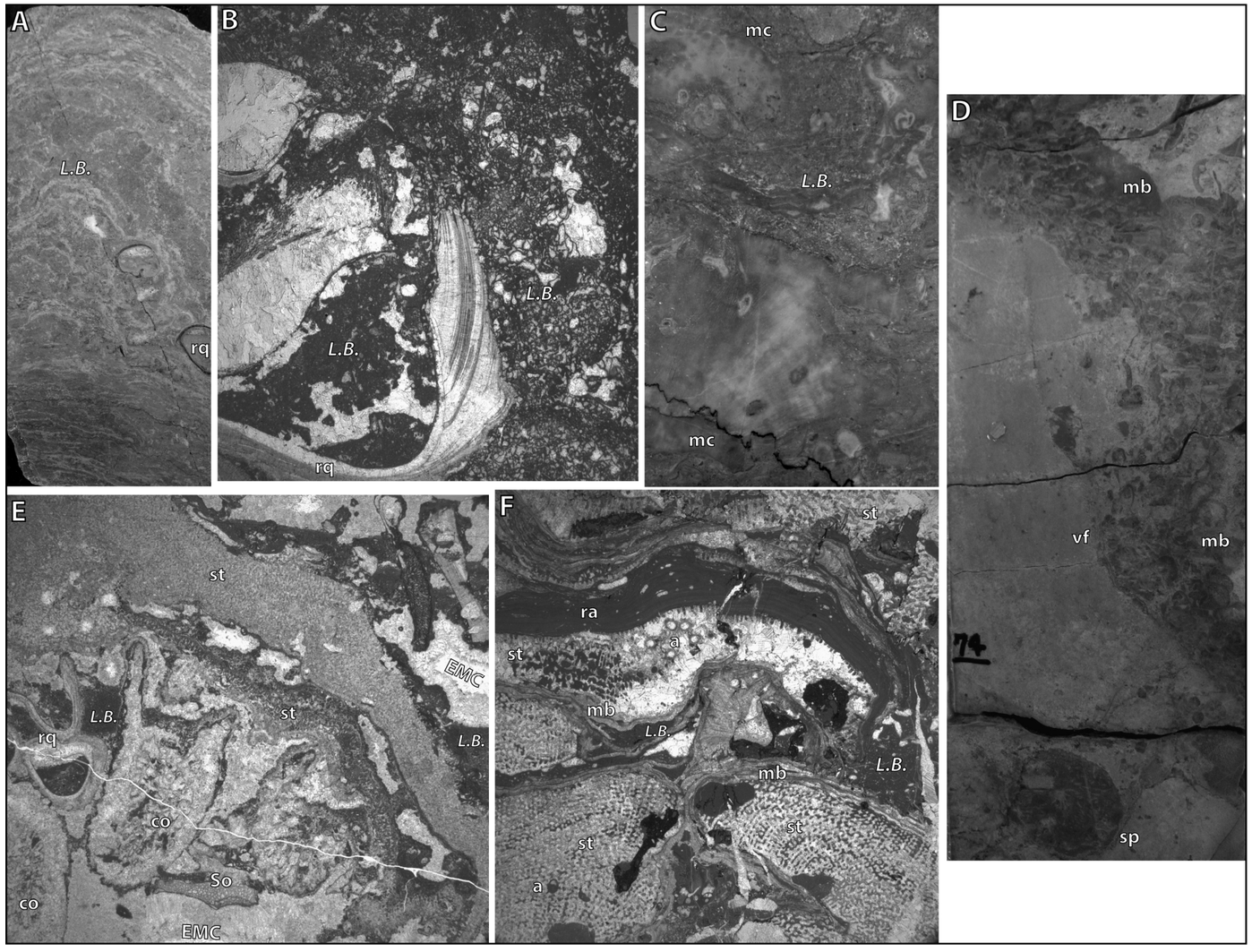

Figure 4.4: Reef-wall facies plates. (A) Domal *Lithocodium-Bacinella* grainstone stromatolites (*L.B.*) with encrusting requienid rudists (rq). Width of view = 12.7 cm (B) Photomicrograph of the same facies illustrating the microbial fabrics of *Lithocodium-Bacinella*. Width of view = 18 mm. (C) *Lithocodium-Bacinella*-coral framestone with massive coral (mc) and microbial fabrics. Width of view = 10 cm (D) Microbial-sponge bindstone with vertical fabrics (vf), microbial binding (mb), and sponges (sp). Width of view = 10 cm. (E) Mixed-fauna boundstones with branching coral (co) encrusted by requienids (rq), laminar stromatoporoids (st), and *Lithocodium-Bacinella*. Note voids created by *Lithocodium-Bacinella* that are filled with early-marine cement (EMC). Also present are *Solenopora* red algae (So). Width of view = 18 mm. (F) *Lithocodium-Bacinella*-stromatoporoid bindstone with laminar stromatoporoids exhibiting astrorhiza (a) and encrusted by red algae (ra), *Lithocodium-Bacinella*, and uknown microbial binders (mb). Width of view = 18 mm.

Bacinella. The depositional environment is interpreted as a lower- to middle-reef-wall, possibly in 50-80 meters of water.

Lithocodium-Bacinella-coral framestones (Figure 4.4-C) contain a variety of common to abundant domal, massive, and branching corals. Caprinids are common and requienids are rare. The branching to massive red algae *Solenopora* is commonly encountered. Grainstone stromatolites are present, as are rare laminar and bulbous stromatoporoids. Matrix sediment is grain-dominated. This facies was deposited in the shelf-slope break to upper reef-wall (5-60˚ dip) and interpreted water depths ranged from approximately 5-30 meters.

Lithocodium-Bacinella grainstone stromatolites (Figure 4.4-A,B) consist of very fine-grained peloids, skeletal fragments, and miliolid foraminifera bound by abundant laminae of *Lithocodium-Bacinella*. Small requienid rudists are attached to the stromatolites. Grainstone stromatolite cycles are comprised of domed forms at the base but commonly transition upwards to flat forms at cycle tops. They are interpreted to occupy a subtidal (< 10 m; <33 ft) to intertidal shelf-crest position at the high-energy shelf edge.

Mixed-fauna boundstones (Figure 4.4-E) exhibit a varied assemblage of organisms including *Solenopora* red algae, massive to branching corals, bulbous stromatoporoids, and *Lithocodium-Bacinella*, as well as caprinid, requienid, and radiolitid rudists. Vertical growth fabrics are infrequently encountered, however *Lithocodium-Bacinella* are often diffusively grown within matrix sediment and are found encrusting all grain types. Caprinid and requienid rudists are common to abundant and remaining fauna are rare to common. Mixed-fauna boundstones spanned reef-flat to reef-margin environments and lacked organically-constructed vertical structures. The increased

abundance of delicate branching corals and the predominance of packstone versus grainstone matrix fabrics suggest this facies was in a low- to moderate-energy setting.

Syndepositional fractures (Figure 4.5-F) mentioned in Waite et al. (2007) are present throughout the reef-wall and the reef-flat. They are recognized by steeply inclined (> 45˚), sharp contacts between reefal host-rock and allocthonous fracture fill. Early-stage syndepositional fractures are up to 4.5 meters in vertical thickness and are filled with reef derived carbonate sediment. Late-stage syndepositional fractures are filled with dark, pyritic sediment rich in terrigenous clay and containing planktic foraminifera identified by Waite et al. (2007) as early Cenomanian in age. Several early-stage syndepositional fractures were reopened by late-stage events and contain calcite spar related to faulting or regional tectonic stress. The syndepositional fractures provide additional evidence for over-steepening of an early-cemented, high-angle reef-margin. Potential failure and collapse of reef facies along syndepositional fracture planes may have served to locally modify the depositional profile with creation of near-vertical erosional escarpments.

Reef-flat Facies Assemblage

Reef-flat facies are distinguished by the abundance of rudist bivalves, which may or may not be mixed with stromatoporoids, coral, and red algae. *Dictyoconus walnutensis* is common to abundant. Bedding planes are near-horizontal in core samples.

Requienid bindstones (Figure 4.5-A,D) contain robust, abundant requienid rudists that are encrusted by adjacent requienids, *Lithocodium-Bacinella*, and bulbous stromatoporoids. Caprinids may be present to common. Numerous hardgrounds bored by pholad clams provide evidence that mud-dominated packstone to grain-dominated

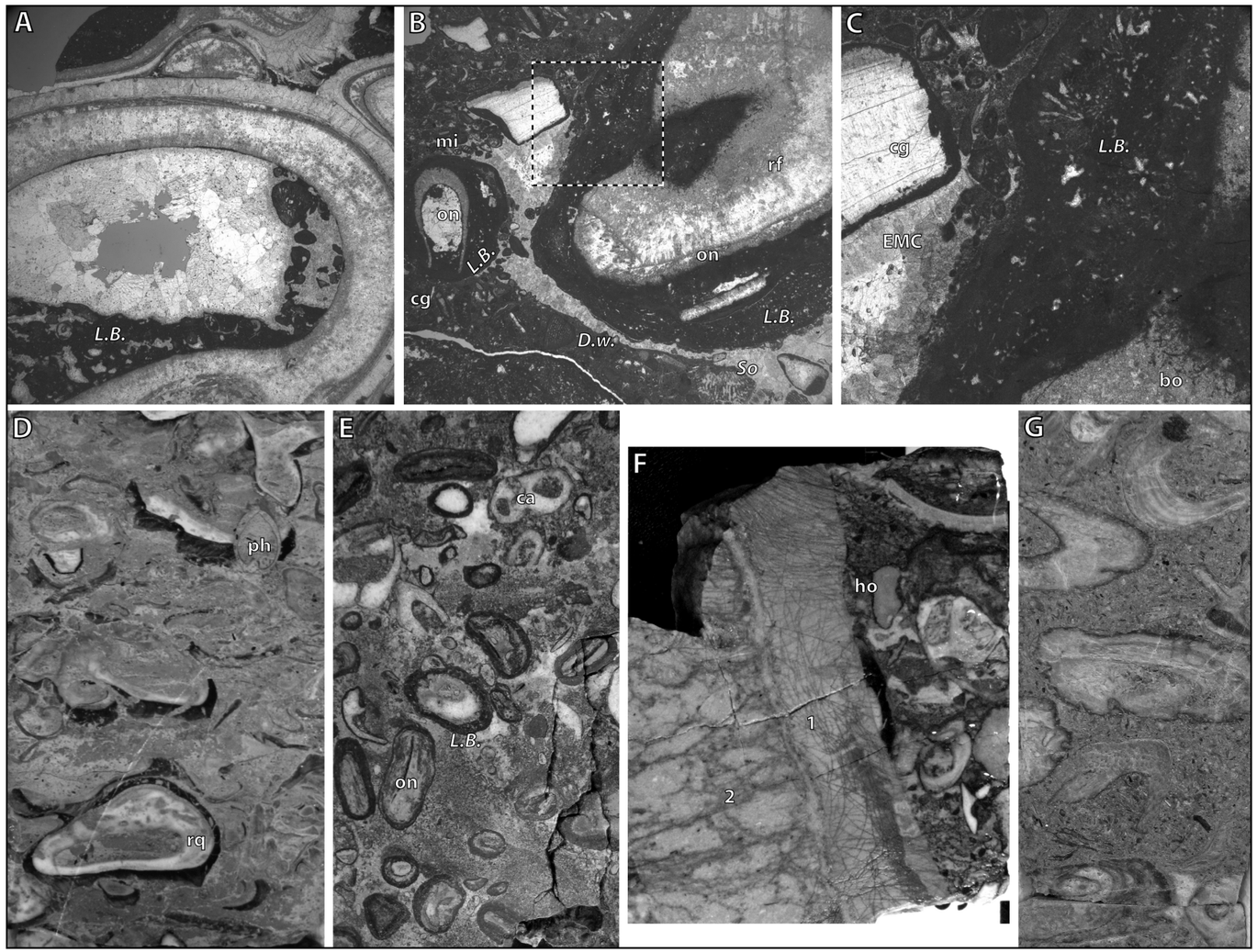

Figure 4.5: Reef-flat and back-reef facies plates. (A) Requienid bindstone exhibiting requienid rudists which have encrusted each other. *Lithocodium-Bacinella* (*L.B.*) are present between and within rudist cavities. Width of view = 25 mm. (B) *Lithocodium-Bacinella*-oncoid rudstone with rudist fragments (rf) forming oncoid (on) nuclei. *Lithocodium-Bacinella* also form coated grains (cg). Also present are the miliolid (mi) and *Dictyoconus walnutensis* foraminifera, as well as *Solenopora* red algae. Width of view = 18 mm. (C) Inset area from (B), exhibiting coated grains, thick oncoid cortices of *Lithocodium-Bacinella*, and microbial borings (bo) into oncoid nucleus. Microbial binding of sediment and grains created open pore-spaces later filled with early-marine cement (EMC). Width of view = 6 mm. (D) Requienid bindstone with numerous requienids (rq) binding adjacent rudists. Pholad clams (ph) bored into sediment that was bound and cemented during deposition. Width of view = 10 cm. (E) Core sample of *Lithocodium-Bacinella*-oncoid rudstone detailed in photomicrographs of (B) and (C). Width of view = 12 cm). (F) Early-stage syndepositional fracture, showing sharp boundary with host rock (ho) and two stages of opening, each followed by sediment in-fill (first 1 then 2). Width of view = 5 cm. (G) Core sample of caprinid bafflestone in a skeletal grainstone matrix.

packstone matrix sediment was bound or cemented shortly after deposition. Compared to overlying exposure surfaces, water depths were likely less than 10 m (33 ft).

Caprinid bafflestones (Figure 4.5-G) possess whole, recumbent caprinid rudists in a grain-dominated packstone to grainstone matrix. Requienids are rare to common, radiolitid and monpleurid rudists are rare to common, and corals are rare. Caprinids are not typically bound by *Lithocodium-Bacinella*. This facies represents moderate- to high-energy portions of the reef-flat and water depths during deposition appear to have been less than 5 meters.

Back-Reef Facies Assemblage

Back-reef facies are unified by the volumetric abundance of detrital grains that are commonly coated by *Lithocodium-Bacinella*. Miliolid and dictyoconid foraminifera are common.

Dictyoconus-skeletal grainstones and rudist rudstones (Figure 4.6-A,B) are hydrodynamic accumulations of sand- and pebble-size requienid, caprinid, and coral fragments. Beds are commonly stratified, show inverse or normal grading, and are 10 cm to 2 m (0.3 to 6.5 ft) thick. Many grainstone/rudstone intervals display pendant cements (Figure 4.6-G) indicative of brief vadose subaerial exposure (Bebout, 1974) that was probably less than 100 ky. Debris accumulations in these high-energy facies are interpreted as storm berms, shoals, and reworked rudist biostromes.

Lithocodium-Bacinella-oncoid rudstones (Figure 4.5-B,C,E) display pebble- to cobble-sized oncoids with *Lithocodium-Bacinella* cortices commonly nucleated around rudist fragments. This facies typically stretched across both the reef-flat and back-reef settings. Bulbous stromatoporoids and whole requienids are also present. Matrix

allochems largely consist of coated-grains. These rudstones were probably deposited in 5-15 meters of water and frequently shoal upward into *Lithocodium-Bacinella*-coated grain packstone/grainstone (Figure 4.6-C) with organically-coated bioclasts and miliolids. These grainstones may be stratified or contain keystone vugs suggestive of intertidal deposition in intertidal shoals or beaches.

Pleurocora bafflestones (Figure 4.6-D) consist of whole and broken specimens of the thin, branching coral *Pleurocora coalescens*. Additional corals, caprinids, stromatoporoids and *Solenopora* are present. Thickets of *Pleurocora* bafflestone are found in lower-energy settings of middle-reef-wall, reef-flat, and back-reef environments.

Toucasid-chondrodont bafflestones/floatstones with *Pleurocora* coral and mud-dominated matrix sediment are representative of low-energy conditions and are transitional into shelf-interior facies.

Gastropod-rudist floatstones with sparse requienids, caprinids and bivalves are present in the uppermost Stuart City Fm. Their black matrix may represent elevated organic contents and/or poorly oxygenated conditions during deposition.

Shelf-Interior Facies Assemblage

Meter-scale cycles of burrowed, gastropod-miliolid wackestone/packstone and burrowed, peloid-miliolid packstone/grainstone (Figure 4.6-E) characterize the shelf-interior. Cycles are commonly capped by fenestral-algal laminites (Figure 4.6-F) deposited in tidal flats and contain polychaete worm tubes or root horizons. Oncoid floatstones and toucasid fragments may also be present in subtidal portions of the cycles.

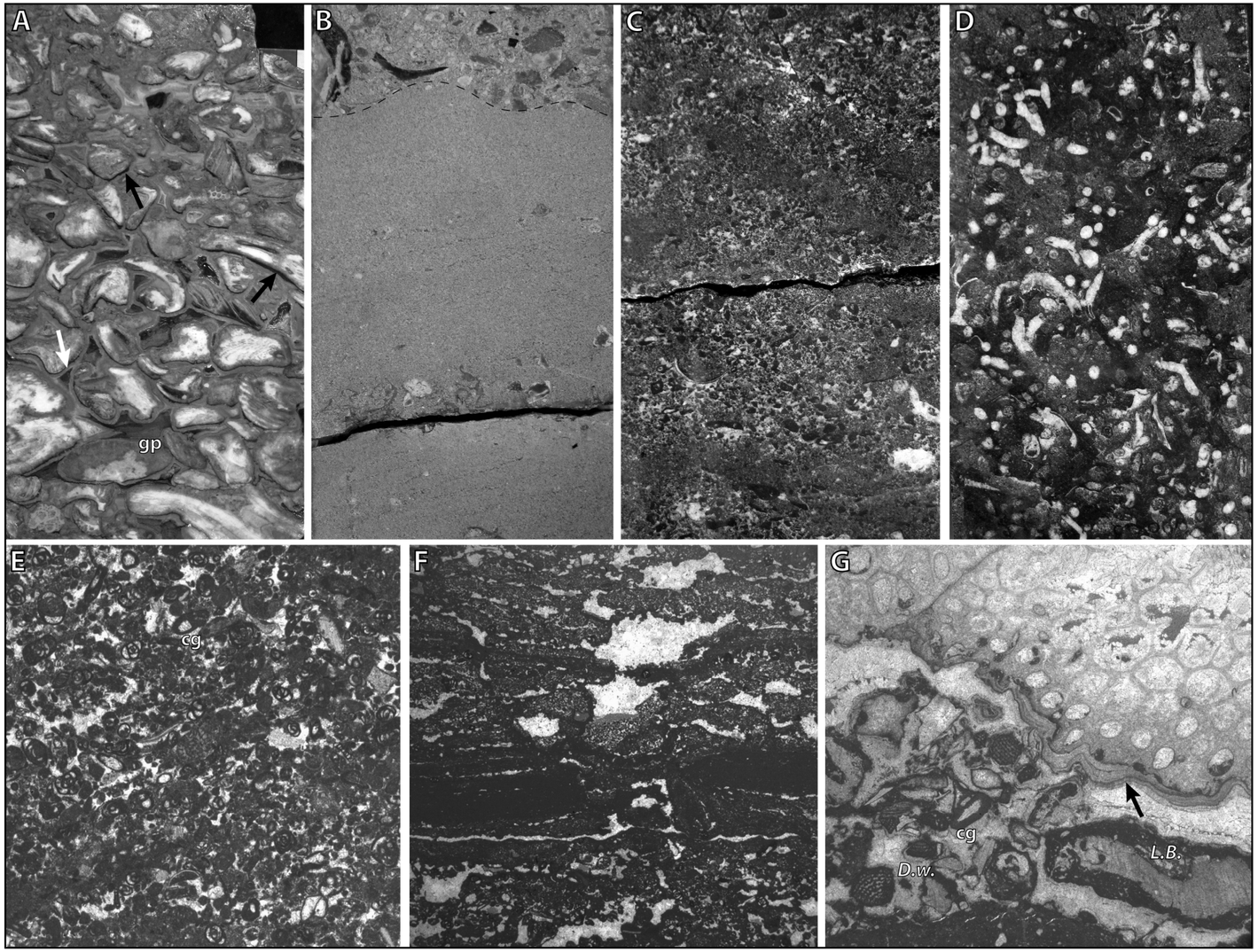

Figure 4.6: Back-reef and shelf-interior facies plates. (A) Rudist rudstone exhibiting pendant cements formed during subaerial exposure (black arrows), early-marine cement (white arrow), and geopetal fabrics (gp). Width of view = 12 cm. (B) Stratified and rippled *Dictyoconus*-skeletal grainstone overlain by rudist rudstone. Width of view = 10 cm. (C) *Lithocodium-Bacinella* coated-grain grainstone. Width of view = 12 cm (D*) Pleurocora* bafflestone. Width of view = 12 cm. (E) Photomicrography of a peloid-miliolid grain-dominated packstone with coated grains (cg) and abundant miliolid foraminifera. Width of view = 9 mm. (F) Fenestral algal laminate with silt- to very fine-grained matrix sediment and geopetal structures. Width of view = 25 mm. (G) Rudist rudstone with a large caprinid fragment at top, as well as coated-grains (cg) lined with *Lithocodium-Bacinella* and *Dictyoconus* foraminifera (*D.w.*). Black arrow points to pendant cement. Width of view = 25 mm.

CORE-BASED FACIES PROFILES

Stuart City Vertical Profile

Following description of several cores along the Stuart City margin, an idealized vertical profile broadly representative of major depositional environments in the reef trend was compiled using data from Bee and Lavaca Counties (Figures 4.7, 4.8). Individual cores may show different facies successions and more or less discrete faunal zonations; particularly in DeWitt County. Beginning above the Pearsall Fm, the full succession is indicative of long-term shelf-margin progradation during the middle to late Albian. Ascending through the profile, approximately 195 m (640 ft) of flooded-shelf carbonate facies in the lower Glen Rose Fm are sharply overlain by stacked polymictic breccia debrites, which are the first indication of up-dip reefal development. These are followed by coarsening-upward packages of lower and upper fore-reef facies interpreted to reflect shallowing-upward relative sea-level cycles and cycle sets (Figure 4.7).

Stuart City Fm fore-reef strata are then interrupted by upper reef-margin and reef-flat facies. Ensuing intervals show a relative deepening to bioclastic grainstone/rudstone and a subsequent aggradational trend in sponge-, stromatoporoid-, and coral-dominated reef-wall facies with abundant *Lithocodium-Bacinella*. Additional examples of high-angle Albian reefs are associated with binding by *Lithocodium-Bacinella* (Neuweiler, 1993; Immenhauser et al., 2001), and their presence in the Stuart City margin likely contributed to the vertical morphology of the reef-wall. Grainstone stromatolites formed by this microbial association cap the reef crest. High-frequency cycles of relative sea-level are difficult to recognize in the reef-wall because of its gradational facies contacts and massive character (Figure 4.7). Rather than using more common analyses of rock-fabric, grain-size trends, and sedimentary structures (Kerans and Tinker, 1997), intermediate-scale reef-wall cycles are only divisible by interpreting faunal proportions.

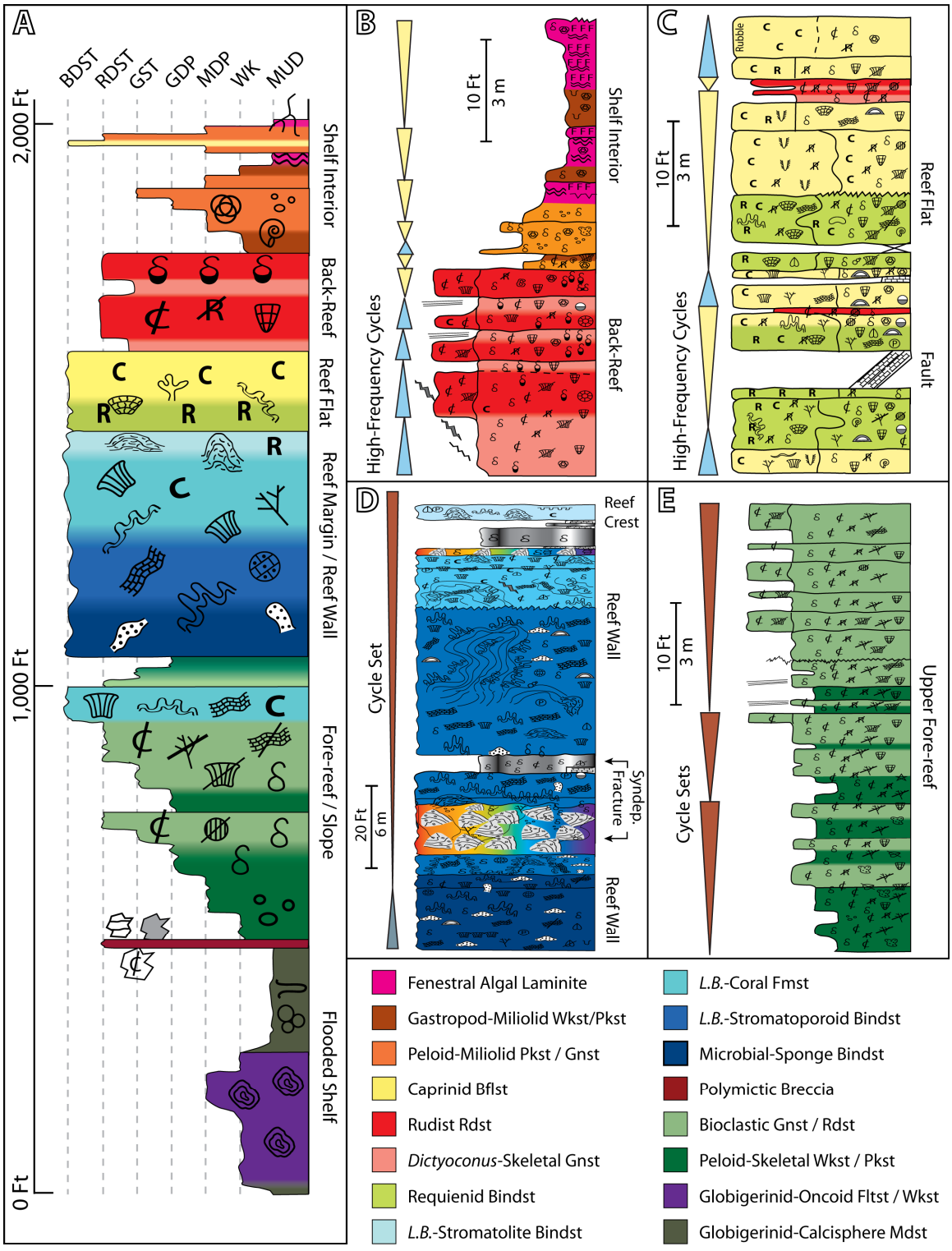

Figure 4.7: Vertical profile of the Stuart City margin. (A) An idealized vertical profile for

the Stuart City margin in Bee County. Also shown are insets with example core descriptions and high-frequency cycles or cycle sets from (B) back-reef to shelf-interior intervals, (C) the reef-flat, (D) the reef-wall to reef crest, and (E) the upper fore-reef. A symbol key is available in Figure 4.8.

In contrast, symmetric high-frequency cycles in the overlying reef-flat oscillate between relatively deeper requienid bindstones and shallower caprinid bafflestones. These cycles are commonly capped by thin-bedded rudist rudstones (Figure 4.7). Rarely, *Pleurocora* bafflestones and mixed-fauna boundstones may have spread across the reef-flat. During these periods of deposition, abundant and increasingly diverse fauna typically found in lower energy, deeper reef environments suggests intense competition for resources (Dupraz and Strasser, 2002) during intermediate-scale transgressions.

Thick, repetitive accumulations (20-70 m; 65-230 ft) of back-reef rudist grainstone/rudstone facies may be internally autocyclic because the sediment is interpreted to be externally sourced from the reef-flat during storms; a process not likely related to relative sea-level cycles. Long-term transitions between back-reef units and overlying shelf-interior packages may reflect intermediate-scale cycle sets.

Stuart City Depositional Profile Variability

To illustrate the lateral and temporal facies variability in the Stuart City margin, a series of depositional profiles were created from one-dimensional core data (Figure 4.9). These examples exhibit end-member facies transitions resulting from second-order eustatic sea-level changes and disparate influences of structural/tectonic elements.

Cores from the Tomasek #1 and Schroeder #1 wellbores, both of which are located in Pawnee Field of Bee County, display sharply different facies transitions (Figures 4.2, 4.9). In the highstand of the Glen Rose supersequence, the Tomasek #1 core

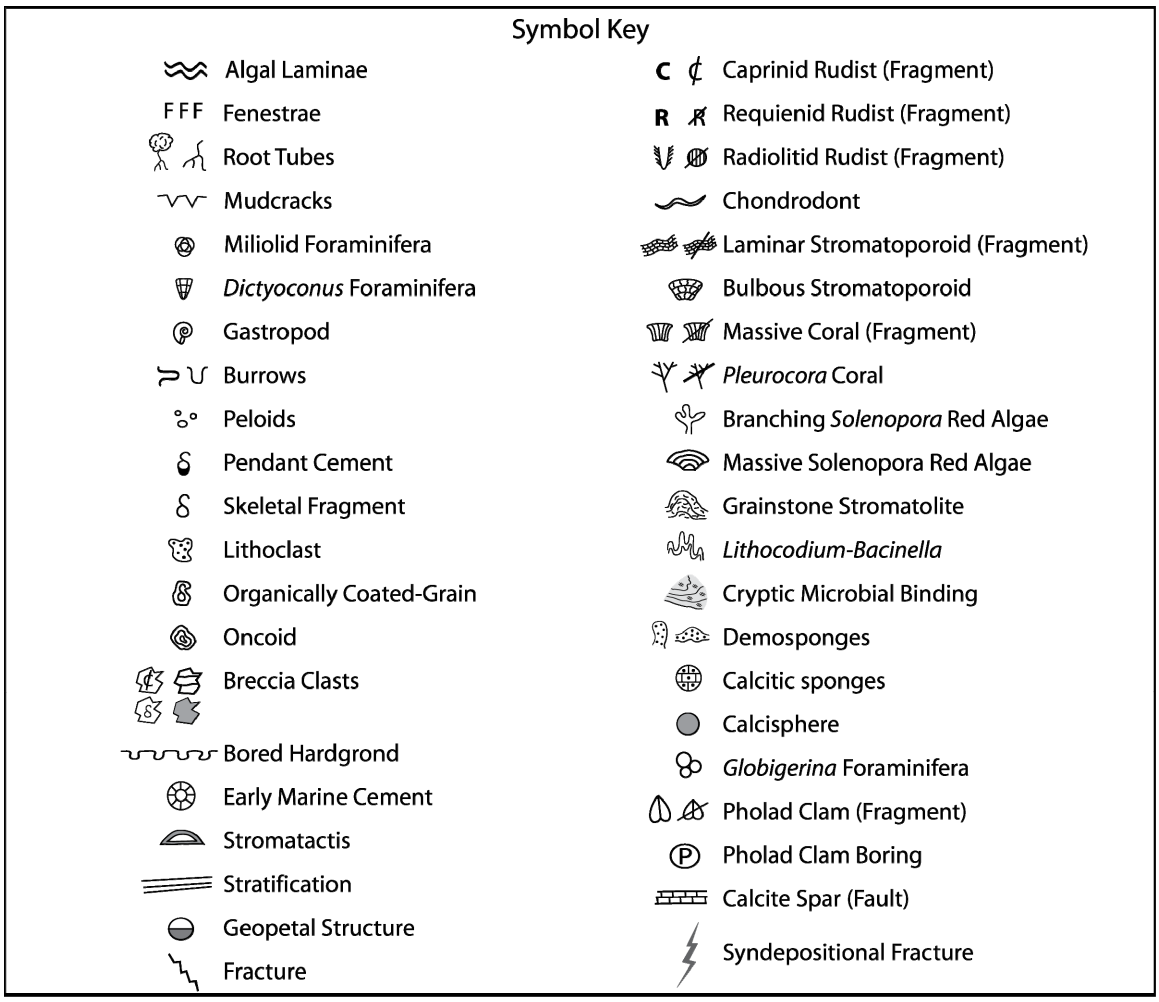

Figure 4.8: Symbol key for core descriptions, depositional profiles, and depositional models.

developed a high-energy, upper fore-reef, whereas the Schroeder #1 core had a greater proportion of sponges, stromatoporoids, and branching corals in a more tranquil reef-margin. Both cores show a deepening trend in the basal Fredericksburg supersequenece. The Schroeder #1 margin developed microbial-sponge bindstones in the aggradational lower reef-wall and vertical microbial growth fabrics are common. Early- and late-stage syndepositional fractures dissect the reef and display large apertures greater than 50 cm in vertical dimension. In contrast, the Tomasek #1 core contains fewer vertical growth fabrics but exhibits *Pleurocora* bafflestone thickets in the middle reef-wall. Small-aperture syndepositional fractures with early-stage fill are less pervasive than those of the Schroeder #1 profile.

From the above observations, the depositional profile of the Schroeder #1 core is interpreted to have been much steeper than that of the Tomasek #1 core, despite being located just 5 km along strike. Tracings of dip-oriented seismic lines through both core locations display clinoform geometries that appear to confirm these interpretations (Figure 4.10). As postulated by Waite (2009), regional antecedent structural/depositional elements may have acted as controls on Stuart City development and influenced the

facies variations observed in core. One such controlling factor concerns the relative location of the Stuart City margin with respect to the terminal Sligo margin. In examples such as the Schroeder #1 core where the Stuart City margin was perched above or prograded beyond the underlying Sligo shelf-margin, compaction of mud-dominated slope/basin facies possibly led to increased subsidence and Stuart City aggradation. Furthermore, progradation of the Stuart City margin into bathymetrically deeper areas beyond the Sligo margin may have caused steepening of the margin profile. As documented in outcrop examples from Devonian and Permian reef-margins (Ward, 1996; Hunt and Fitchen, 1999; Frost and Kerans, 2009), both factors can lead to increased

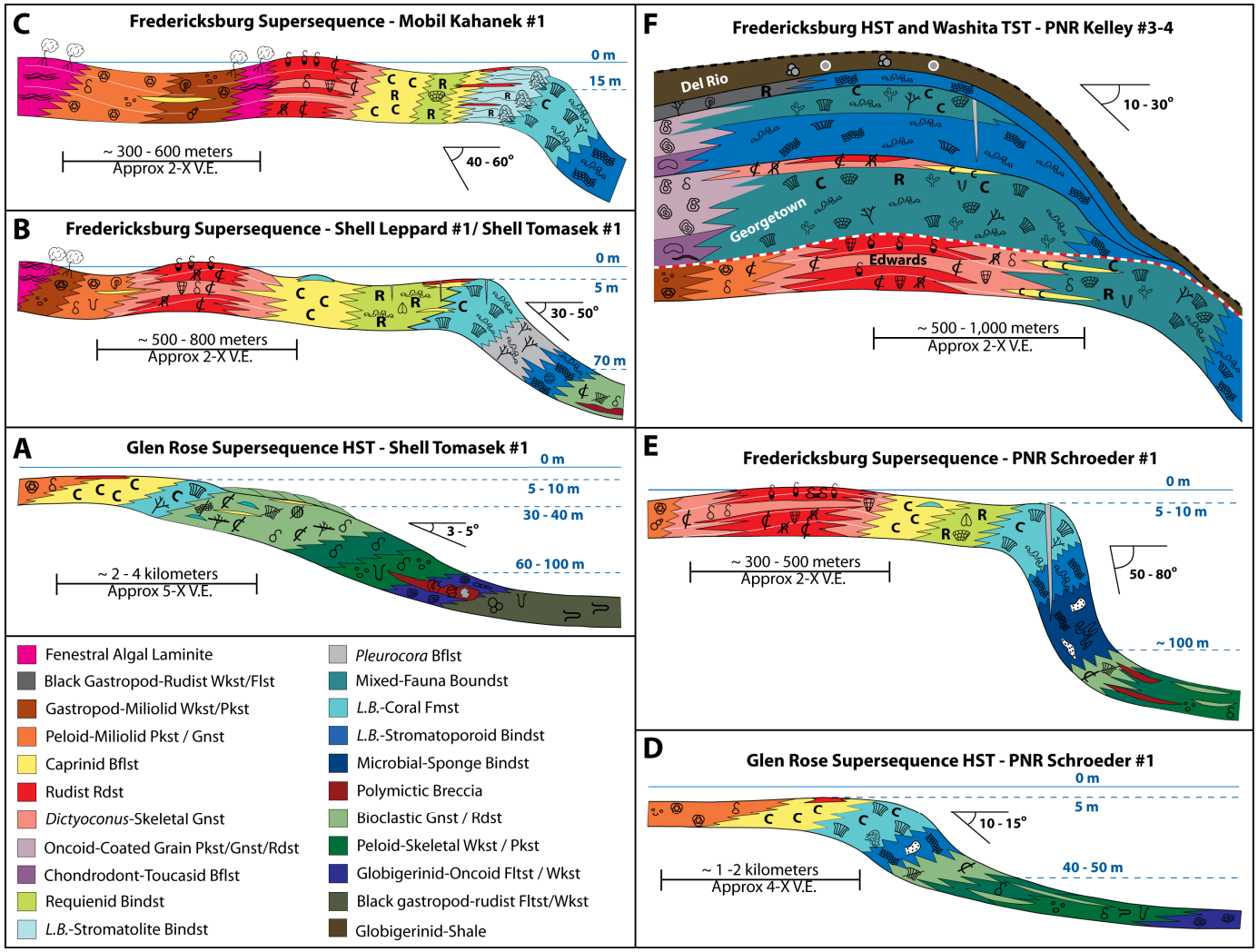

Figure 4.9: Idealized depositional profiles based on several cores described for this study.

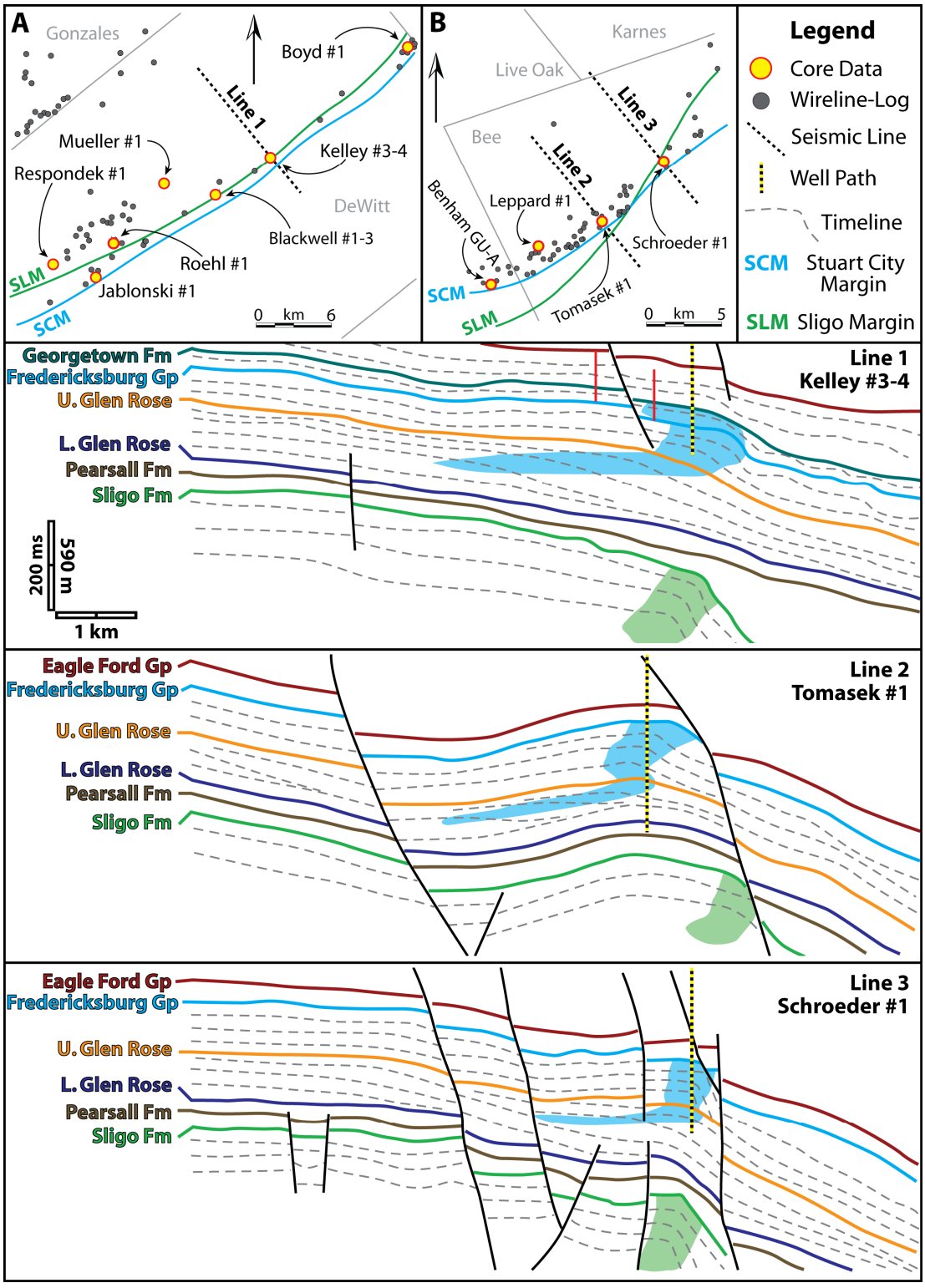

Figure 4.10: Seismic line-tracings across the Stuart City margin. Maps for DeWitt County

(A) and Bee County (B) showing locations of seismic profiles used for line-tracings. Cores used for shelf-margin cross-sections are shown in yellow. Note the steepening of stratal geometries within the Stuart City margin (light blue) from line1 to line 3. The underlying Sligo shelf margin is highlighted in green. The red bar shown in seismic line 1 illustrates thickening of Upper Cretaceous and uppermost Stuart City reflections across a syndepositional fault.

frequency of extensive syndepositional fracture systems. In areas landward of the terminal Sligo shelf-margin, for instance the Tomasek #1 core, the Stuart City system may have been supported by more rigid carbonates of the underlying Sligo Fm, had less accommodation to fill in order to prograde, and hence developed a lower-angle profile.

An interpreted depositional profile of the Kelley #3-4 core and accompanying seismic tracing suggest similar control of underlying tectonic elements (Figures 4.2, 4.9, 4.10). In the Fredericksburg supersequence, reef-margin facies display poorly ordered lateral zonation and mixed-fauna boundstones predominate. Faunal zones without distinct boundaries are surmised to reflect deposition of relatively low-angle (20-30˚ dip) shelf-margin clinoforms with less releif (40-60 m; 130-200 ft) relative to the Schroeder #1 and Tomasek #1 cores (80-100 m; 260-330 ft) (Figure 4.9). This interpretation is consistent with computer simulations of modern coral-reef systems in which changes to vertical reef morphologic components most drastically affect zonation patterns (Graus and Macintyre, 1989). Low-releif, lower-angle clinoform dimensions may be the result of deposition in a zone of lesser subsidence on the San Marcos Arch. In a manner reminiscent of the seismic tracings through the Tomasek #1 and Schroeder #1 well bores, minor steepening of Fredericksburg-age shelf-margin clinoforms is observed beyond the terminal Sligo shelf-edge. Syndepostional faulting in DeWitt County also appears to have been active as an additional structural control during Stuart City margin deposition. A syndepositional normal fault through Upper Cretaceous reflections shows thickening of 25 milliseconds,

or approximately 74 meters (243 ft), in the hanging-wall block containing the Kelley #3-4 core (Figure 4.10). Thickening of reefal reflections cannot be unequivocally demonstrated in seismic; however syndepositional faulting of late Albian strata (Georgetown Fm) is documented in the nearby Karnes Trough (Rose, 1972) and thus minor offset of this fault in the late Albian is probable.

In Lavaca County, the depositional profile based on the Kahanek #1 core deomonstrates that simple spatial variation inherent to reefal sedimentary processes may have also led to dissimilar Stuart City margin profiles (Figures 4.2, 4.9). This example displays the best developed cycles of *Lithocodium-Bacinella* grainstone stromatolites. Cyclic, domal to planar morphologies of the stromatolites are suggestive of a raised reef crest and are reminiscent of modern red-algal ridges in Bermuda and Pacific atolls (see examples in Ginsburg and Schroeder, 1973; Bosence, 1983). The core also shows root zones in fenestral algal-laminate facies of tidal flat islands (Baker and Scott, 1985), some of which are present on the leeward side of the back-reef grainstone/rudstone complexes.

SUPERSEQUENCE SHELF-MARGIN MODELS

Despite modification of facies and architectural trends between structural settings, analysis of seismic-scale clinoforms and numerous vertical facies profiles suggests that consistent changes in shelf-margin trajectory were induced by second-order eustatic sea-level changes identified in shelf-interior supersequences (Figure 4.1) (Chapter 2). Basic elements of this concept have been introduced by previous authors and long-term changes in trajectory are thought to reflect eustatic cycles driven by variable mid-ocean ridge spreading rates (Coogan, 1977; Tartamella, 1982; Chapter 2). Because of the shelf-margin response to these long-term changes in accommodation, distinct depositional

models depicting shelf-margin architecture and facies distributions are required for the Glen Rose, Fredericksburg, and Washita supersequences.

Glen Rose Supersequence Equivalent Reef

The Stuart City margin initiated during the highstand systems tract of the Glen Rose supersequence (Figure 4.1), although evidence for this is indirect and based on the presence of reef-derived slope debris in the Tomasek #1 and Schroeder #1 cores. Seismic tracings indicate shelf-margin clinoforms were strongly progradational (Figure 4.10); an observation consistent with the limited-accommodation setting interpreted from stacked intertidal cycles of the shelf-interior. The shelf-to-basin profile in the Glen Rose supersequence model is characterized by low-angle fore-reef slopes that range from approximately 3˚–15˚ in dip as a function of location with respect to the terminal Sligo Fm margin (Figure 4.11). Lower-angle variants of this system contain greater proportions of reef debris and higher-energy fore-reef facies, possibly including mobile sand waves on the upper slope. Higher-angle areas of the Glen Rose margin exhibit moderate-energy lower-reef environments. In both cases, much of the energy from open-ocean waves was likely attenuated by clinoforms with oncolitic toe-sets and packstone to rudstone fore-reef facies. As a result, back-reef rudist grainstone/rudstone facies may not have been generated or are minimal in volume. Notably, requienid rudist debris is largely absent, thus reef-flat facies during this period of margin progradation may have been dominated by caprinid bafflestones.

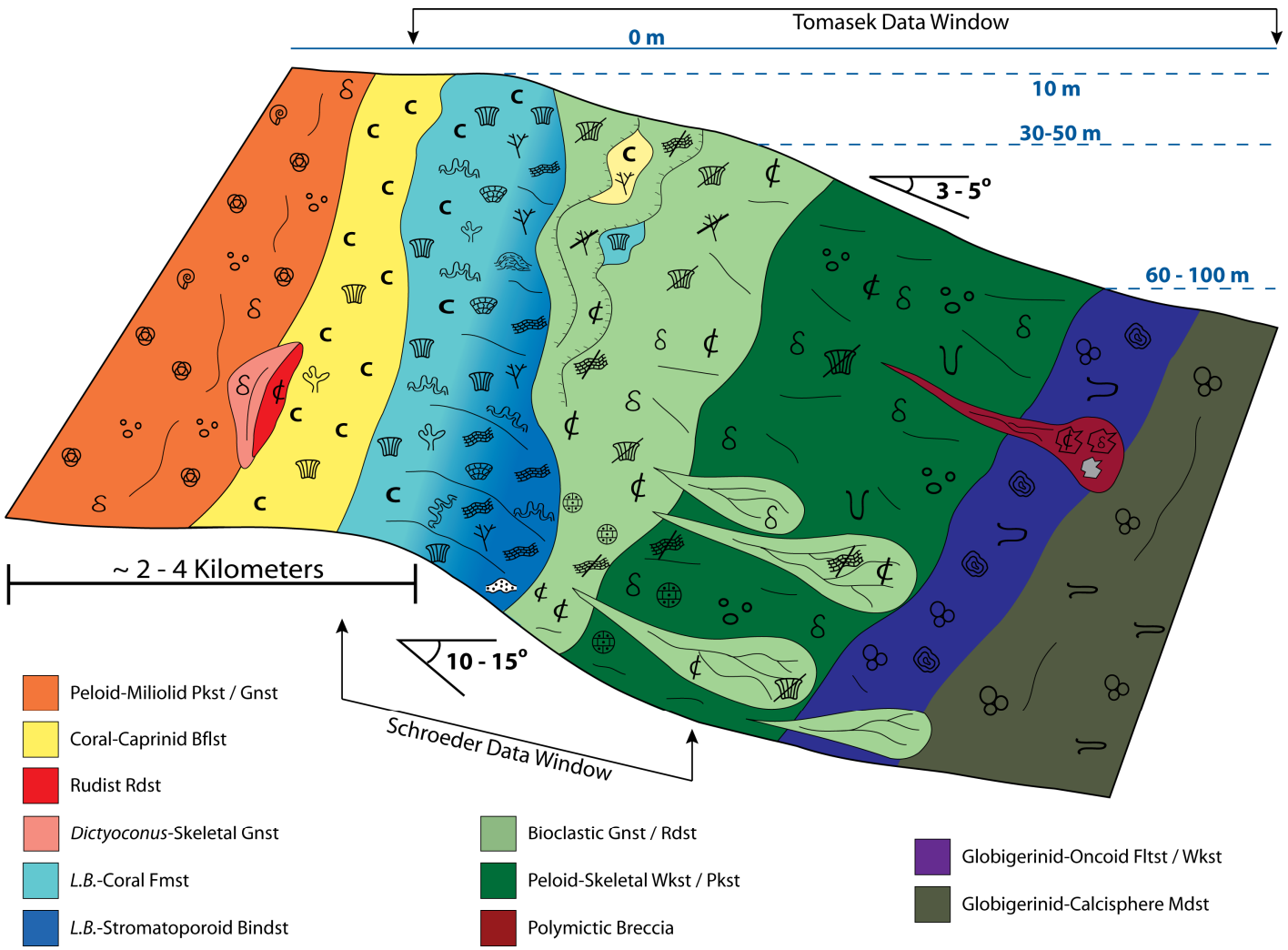

Figure 4.11: Glen Rose supersequence HST depositional model for the Stuart City margin.

Fredericksburg Supersequence Equivalent Reef

As noted by previous authors (Coogan, 1977; Tartamella, 1982; Waite, 2009) and confirmed by seismic tracings, Fredericksburg-equivalent portions of the Stuart City display a distinctly aggradational shelf-margin trajectory (Figures 4.1, 4.10). Multiple cores represent this time-interval of Stuart City deposition and provide a wealth of information regarding variability along this high-angle rimmed-shelf (Figure 4.12). Transgression at the base of the Fredericksburg supersequence led to deposition of subtidal wackestone-packstone cycles in the shelf-interior (Chapter 2), deepening of shelf-margin facies, and steepening clinoform foresets. Along the low-subsidence San Marcos Arch, reef-margin geometries steepened only slightly (20˚–30˚ dip), aggraded lower-releif reef-walls, and margin facies contain a mix of fauna that lack discrete faunal zones. A sharply-zoned, extensively aggraded reef-wall developed its steepest (50˚–80˚ dip) and highest-releif (80-100 m; 260-330 ft) clinoforms off the axis of the San Marcos Arch where the Stuart City margin prograded beyond the underlying Sligo shelf edge. Abundance of syndepositional fractures and fracture aperture both increase with steepness and height of the margin. Atop the reef-wall, shelf-crest stromatolites are variably present. Requienid bindstones and caprinid bafflestones are a distinctive feature of the reef-flat and were the source of debris for semi-continuous rudist grainstone/rudstone storm berms. These storm berms were commonly exposed and created an efficient energy barrier which sheltered shelf-interior facies from open-ocean waves. A result of this configuration is a rapid lateral facies transition (<100 m; <330 ft) between grain-dominated, back-reef facies and mud-dominated facies of the shelf-interior.

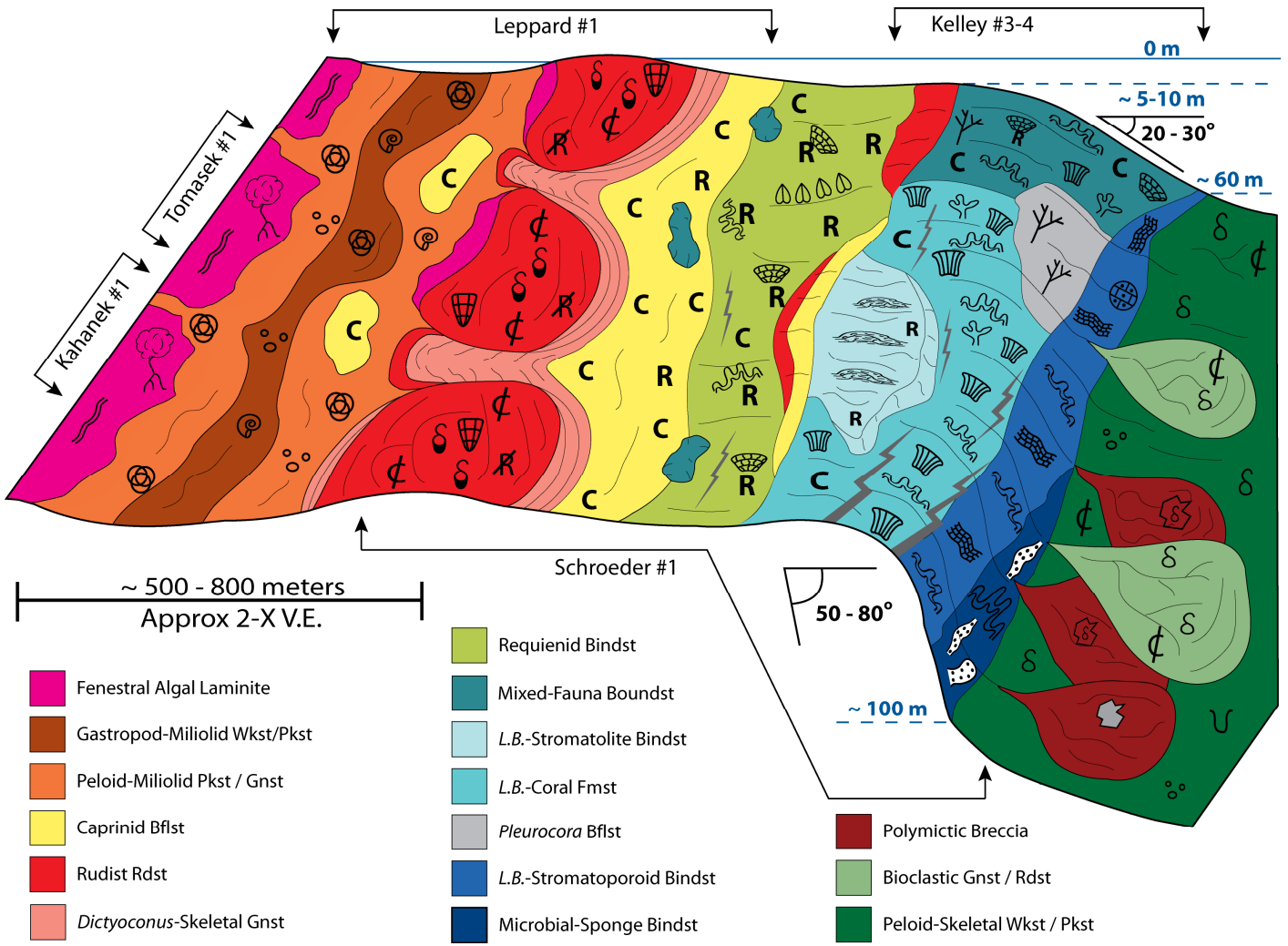

Figure 4.12: Fredericksburg supersequence depositional model for the portion of the Stuart City margin.

Washita Supersequence Equivalent Reef

In the Stuart City margin, the sedimentologic record of transgression at the base of the Washita supersequence is inconsistent. The shelf-to-basin profile at the time was that of an 'empty-bucket' and exhibited a fully aggraded to back-stepping shelf-margin with a shelf-interior that was drowned a mere 20 kilometers farther landward (Figure 4.1) (Chapter 2). In DeWitt County, Washita-age rudists are present in multiple cores below flooded-shelf shale in the Del Rio Fm (Coogan, 1977; R.W. Scott, personal communication). This fact requires that a portion of the reef-margin must be equivalent to the Georgetown depositional sequence, which forms most of the transgressive systems tract in the Washita supersequence. A depositional model of the Georgetown-age shelf-margin in DeWitt County (Figure 4.13) shows the abundance of *Lithocodium-Bacinella* increased significantly in most shelf-margin environments. This micro-organism association was a dominant component of reef-wall boundstones, reef-flat requienid bindstones, back-reef oncoids/coated grains, and subtidal stromatolites. Rudist grainstone/rudstone storm berms and algal-laminated tidal flats became less common and more isolated in comparison to the Fredericksburg depositional model (Figures 4.12, 4.13). Additional back-reef facies included *Pleurocora* bafflestone and toucasid-chondrodont bafflestone deposited in a muddy, low-energy setting.

D eWitt County Cross-Section

Depositional models for the Fredericksburg and Washita supersequences (Figures 4.12, 4.13) are paired with two facies cross-sections through multiple cored wells. The cross-sections illustrate the impact of transgression and syndepositional faulting on reef-margin facies proportions. In the cross-section from DeWitt County, differences in Del

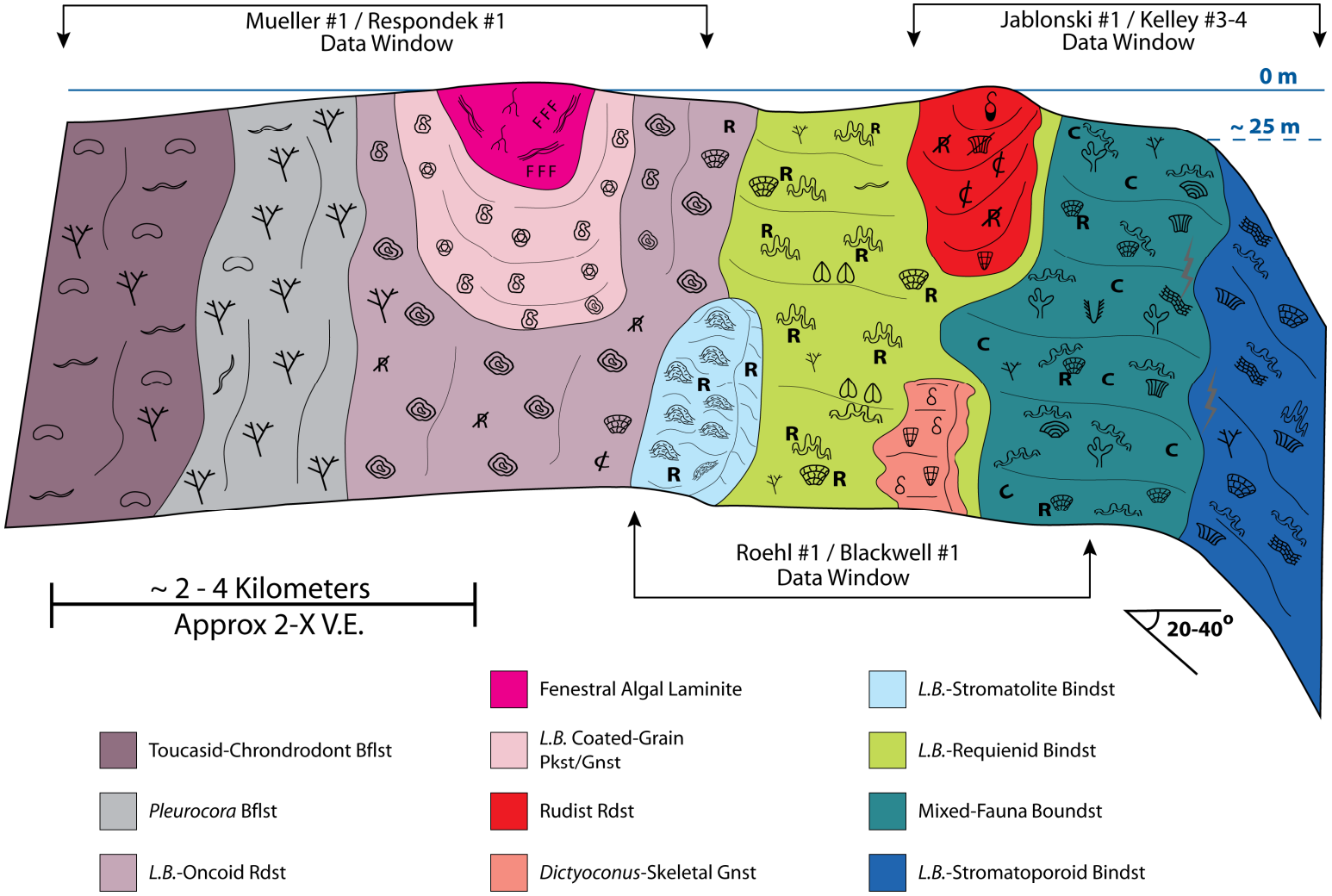

Figure 4.13: Washita supersequence TST depositional model for the Stuart City margin in DeWitt County.

Rio shale thickness above the Stuart City margin, as determined from wireline logs, are likely associated with Upper Cretaceous syndepositional faults observed in seismic (Figures 4.2, 4.10, 4.14). Divergence in facies proportions between cores indicates that the faults were also active in the late Albian portion of the Stuart City. A deepening trend across the Fredericksburg/Washita supersequence boundary was in part a result of eustatic transgression (Scott et al., 2002; Chapter 2), but was likely enhanced by regional syndepositional faults and downward displacement of the margin. The first known occurrence of Washita-age rudists (*Mexicaprina* sp.) is approximately 20 meters above the interpreted supersequence boundary. This belated first occurrence could be a result of preservation bias or may indicate that early fault offset led to increased margin subsidence and locally modified the location of the supersequence boundary relative to its shelf-interior position.

Regardless of fault timing relative to eustatic sea-level rise, the increase in accommodation caused complete reorganization of reef-flat and back-reef facies (Figures 4.12, 4.13, 4.14). Approaching the supersequence boundary, progressively thinning high-frequency cycle sets of miliolid-dominated shelf-interior strata are inter-fingered with well-organized, discrete back-reef and reef-flat geobodies. Above the supersequence boundary, transgressive cycle sets thickened and the width of the Georgetown-equivalent Stuart City profile widened relative to the Fredericksburg-equivalent profile. Fredericksburg-age shelf-interior strata were superseded by *Lithocodium-Bacinella* oncoid/coated-grain packstones to rudstones and toucasid-chondrodont-*Pleurocora* bafflestones of the back-reef environment. Subtidal *Lithocodium-Bacinella* grainstone stromatolites formed a transgressive reef crest above the former reef-flat. During maximum flooding of the Georgetown depositional sequence, mixed-fauna boundstones spread across the reef-flat and back-reef setting. Later establishment of a requienid

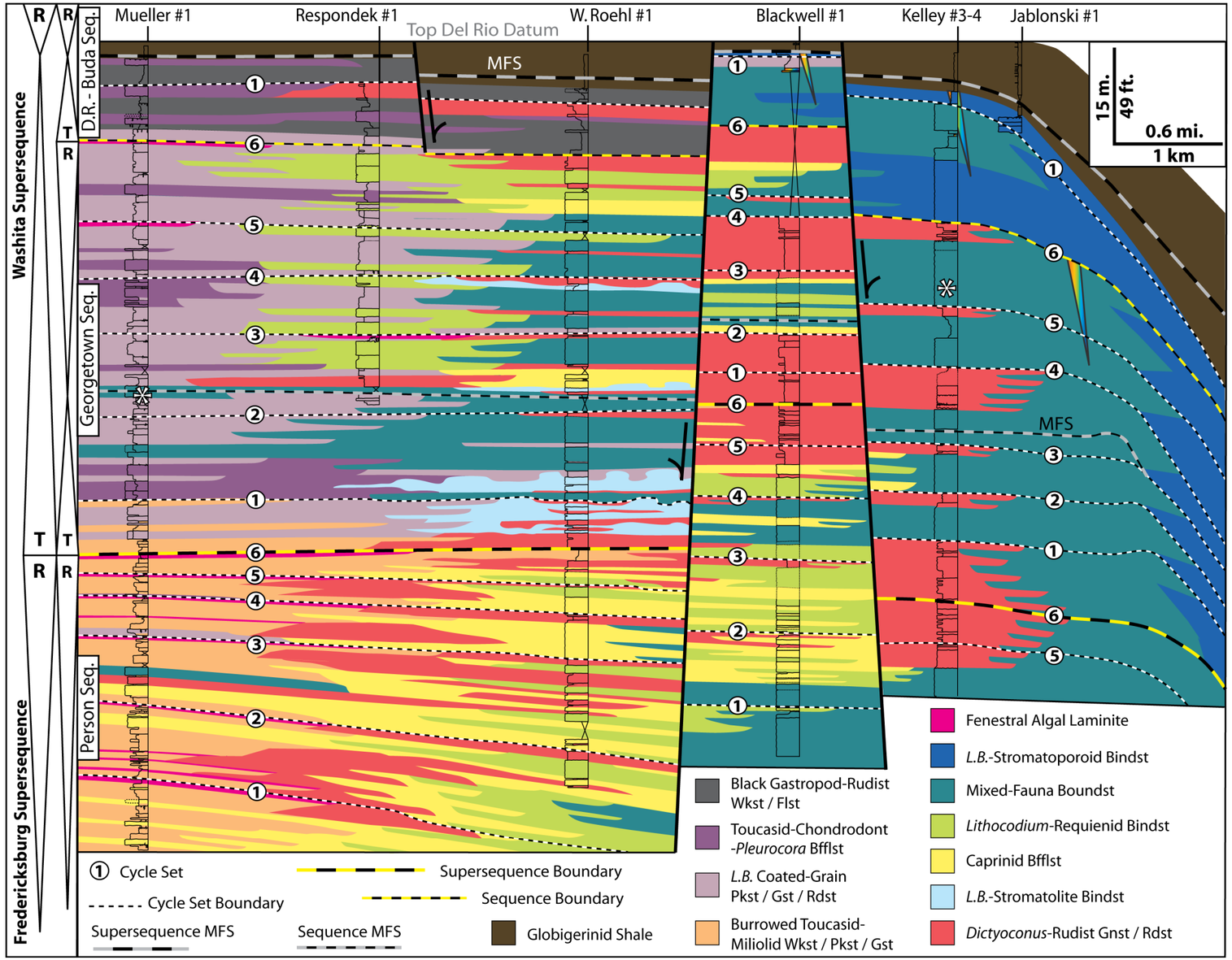

Figure 4.14: Sequence-stratigraphic cross-section based on shelf-margin cores in DeWitt County. Core locations are shown in figures 4.2 and 4.10. Asterisks denote the locations of Washita-age rudists. Large, rainbow-filled spikes denote early-stage syndepositional fractures and are not drawn to scale.

bindstone reef-flat in the highstand of the depositional sequence was limited and the caprinid bafflestone facies belt was nearly eliminated. Rudist grainstone/rudstone facies shifted toward the shelf-edge and do not show pendant cements from subaerial exposure, except within the high-standing fault block containing the Blackwell #1 well-bore. The shelf-margin is interpreted to have gained a more aggradational to slightly retrogradational trajectory with a steeper reef-wall in comparison to underlying sequences.

Bee County Cross-Section

Deepening facies trends and reef-margin backstepping in DeWitt County are in stark contrast to observations from Pawnee Field in Bee County, where syndepositional faulting did not affect stratigraphic patterns (Figures 4.2, 4.15). Delineation of the Georgetown depositional sequence (Washita TST) in Bee County is largely conceptual and based on regional stratigraphic relationships defined in Chapter 2. Here there is no paleontologic evidence for the presence of Georgetown-equivalent strata; however, Washita-age rudists are present elsewhere in the Stuart City margin (Figure 4.14). Moreover, equivalence of Georgetown Fm flooded-shelf facies to the high-energy Devils River margin bordering the Maverick Basin provides a contemporaneous example of a second fully-aggraded shelf margin on the Comanche Shelf (Rose, 1972; Kerans, 2002; Scott and Kerans, 2002).

The facies succession across the margin in Pawnee Field shows essentially continuous aggradation/progradation and shallowing of the shelf-margin through the Washita supersequence transgression (Figure 4.15). Because both intervals contain similar facies proportions, the depositional model presented for the Fredericksburg

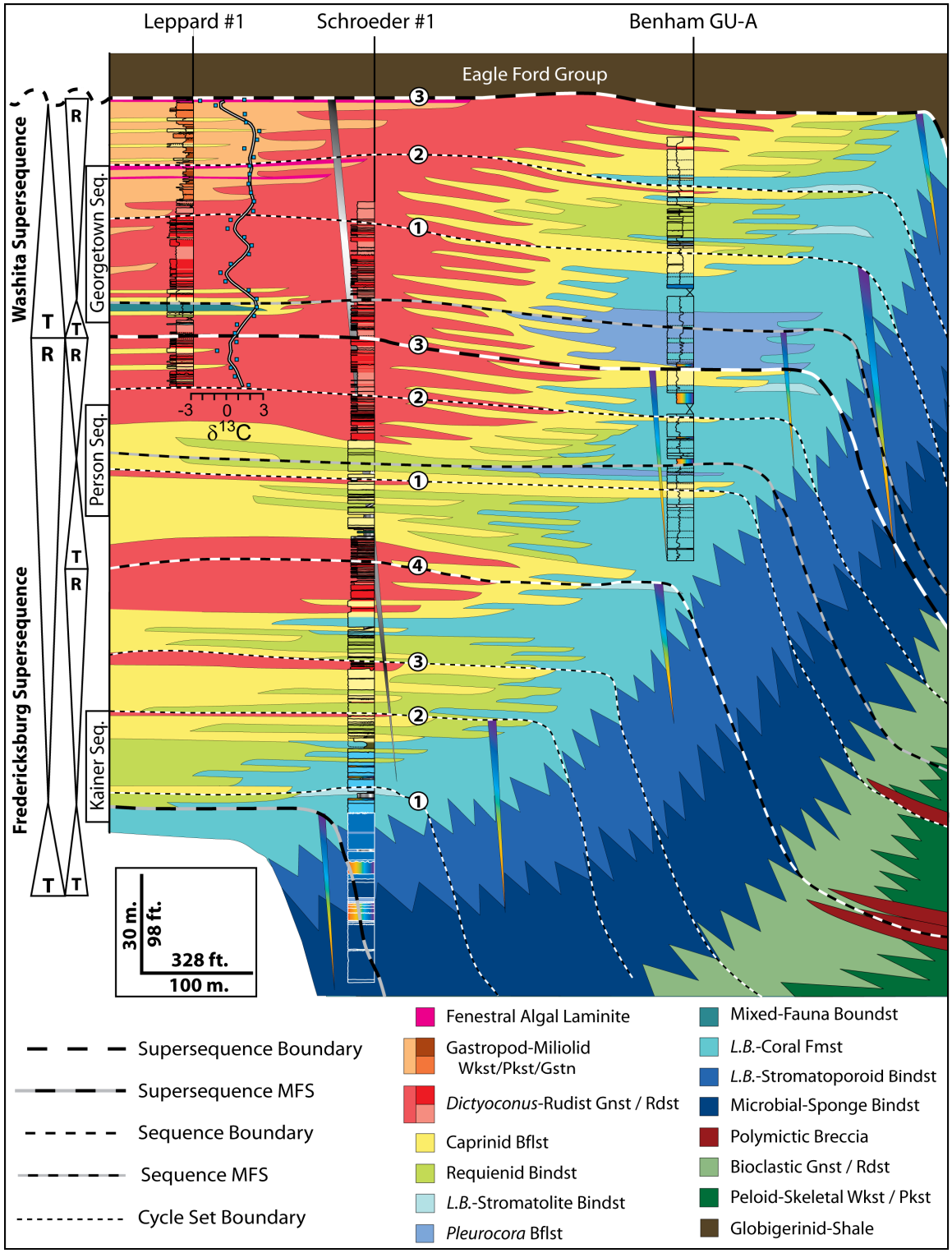

Figure 4.15: Sequence-stratigraphic cross-section based on shelf-margin cores in Bee

County. Core locations are shown in figures 4.2 and 4.10. Rainbow-filled spikes represent early-stage syndepositional fractures. Grey- and white-filled spikes represent late-stage syndepositional fractures with Washita-age foraminifera and contain elevated terrigenous clay contents. Syndepositional fractures are not drawn to scale. Carbon isotope data are relative to the Vienna-Pee Dee Belemnite standard and are shown with a three-point moving average. Negative excursions of the carbon isotope data within rudist rudstones are associated with pendant cement zones indicative of subaerial exposure. These excursions are interpreted as the product of meteoric diagenesis.

supersequence (Figure 4.12) is equally applicable for Georgetown-equivalent strata. Fewer cycle sets are recognizable in the Bee County cross-section compared to the number found in DeWitt County. This may be the result of consistently limited accommodation that was more easily filled by reefal sediments and consequently some cycle sets are amalgamated. Seaward excursions of caprinid bafflestone mark the top of high-frequency cycle-sets near the shelf-edge. Landward shifts in requienid bindstone and thick, subtidal intervals of back-reef rudist grainstone indicate cycle-set maximum flooding intervals. Sequence boundaries are associated with vadose pendant cement zones indicative of back-reef subaerial exposure. The most vertically extensive of these zones is used for placement of the Fredericksburg/Washita supersequence boundary. Above this contact, caprinid bafflestones near the shelf-margin retreated landward toward the back-reef. Maximum flooding of the Georgetown sequence established low-energy *Pleurocora* bafflestones on the reef-flat and allowed mixed-fauna patch reefs to develop behind diminished back-reef grainstone/rudstone complexes. margin progradation resumed in the highstand of the Georgetown sequence and brought tidal flat-capped cycles from the shelf-interior across back-reef environments. Beneath each depositional sequence boundary, progradation distances of shelf-interior, back-reef, and reef-flat facies belts were significantly greater than distances of reef-wall and slope progradation

(Figure 4.15). This relationship caused the width of reef-margin clinoform topsets to diminish significantly.

Stuart City margin Drowning

Although stratal relationships preceding reef drowning vary between DeWitt and Bee Counties, termination of the Stuart City margin in both localities is interpreted to have occurred during maximum flooding of the Washita supersequence and deposition of Del Rio Fm shale. This is clearly the case in DeWitt County, where six high-frequency cycle sets in the Georgetown depositional sequence form a transgressive-regressive package nested within the Washita supersequence (Figure 4.14). The overlying Del Rio – Buda depositional sequence contains two transgressive cycle sets in the Stuart City Fm. In this interval, *Lithocodium-Bacinella*-stromatoporoid bindstones retrograded on top of the shelf-margin and were equivalent to black, gastropod-rudist wackestone/floatstone of the reef-flat to back-reef. Enhanced vertical aggradation of the reef-wall at this time was accompanied by the appearance of syndepositional fractures not observed in underlying sequences. These cycle sets represent an intermediate phase of reef drowning in DeWitt County and are followed by pyritic, burrowed globigerinid-shale in the Del Rio Fm.

The drowning sequence in DeWitt County contrasts with that of Bee County, where both the Del Rio Fm and Buda Fm are missing at a major unconformity between the Stuart City Fm overlying Eagle Ford Group shale (Figure 4.15). Because the shelf-margin at Pawnee Field was fully aggraded, sea level rise and Del Rio Fm deposition may have been preceded by Milankovitch-scale (< 400 ky) exposure at the top of the Georgetown depositional sequence. Carbon isotope data from the Leppard #1 core exhibit a negative shift of approximately 5‰ $\delta^{13}C$ beneath the top Stuart City Fm. This

geochemical signature is consistent with subaerial exposure (Allan and Matthews, 1982) above the upper Washita supersequence boundary during a 1-2 Myr time-span at the mid-Cretaceous unconformity. These data are evidence to support the interpretation that globigerinid-bearing, flooded-shelf facies of the Del Rio and Buda Formations were eroded in Bee County, whereas they were preserved in DeWitt County because of syndepositional faulting.

In both Bee and DeWitt Counties, Stuart City margin facies successions suggest they were generally healthy carbonate margins prior to drowning in the Washita maximum flood. Because of their elevated sedimentation rates, there is no prior reason to expect drowning of these reef systems simply due to eustatic sea level rise or syndepositional faulting (Schlager, 1981; Schlager, 1991; Rosales, 1999). For example, despite active faulting and downward displacement of the shelf-margin during the transgressive Georgetown depositional sequence, portions of the Stuart City margin in DeWitt County remained fully aggraded to sea-level (Figure 4.14). An external forcing mechanism other than eustatic sea level rise must have contributed to drowning. The synchronous demise of carbonate platforms in the Tethyan, Pacific, Atlantic, Carribbean, and Gulf of Mexico regions during the latest-Albian imply that the dominant mechanism was global in extent. Platform demise in these regions was also paired with a pattern of high-frequency eustatic sea-level fall to rise similar to that documented in south Texas (Groetsch et al., 1993; Rosales, 1999). One possible drowning mechanism is environmental stress related to the latest-Albian OAE 1d (Gale et al., 1996; Groetsch et al., 1993; Wilson and Norris, 2001; Bornemann et al., 2005), the onset and duration of which was temporally coincident with final stages of Stuart City margin deposition (Chapter 2). The occurrence of black, gastropod-rudist wackestone/floatstone in back-reef strata immediately beneath Del Rio shale from DeWitt County is interpreted here to

represent increased environmental stress during the anoxic event (Figure 4.14). Such stresses stem from periods of increased volcanism and elevated levels of atmospheric pCO_2. These conditions led to increased surface-water acidity, greater input of siliciclastic clay from enhanced activity in the hydrologic cycle, and reduced oxygenation of the water column due to biologic consumption of volcanic trace metals and phosphorous (Sinton and Duncan, 1997; Larson and Erba, 1999; Mort et al., 2007; Elrick et al., 2009; Emeis and Weissert, 2009). From these local and global relationships, it is evident that maximum flooding in the Washita supersequence and environmental stresses from OAE 1d combined to cause drowning of the Stuart City margin.

EXTERNAL CONTROLS ON STUART CITY MARGIN DEPOSITION

Core, geophysical, and paleontologic data from numerous locations along the Stuart City margin show that facies distributions and margin architecture at a given location were the result of interaction between eustacy and structural/tectonic elements. Pairing of these processes with environmental stress during OAE 1d led to varying facies successions prior to margin drowning at the Albian-Cenomanian boundary. From these observations, it is clear that changes in the structural/tectonic, eustatic, and environmental setting of a reef-margin are the fundamental regime variables dictating shelf-margin faunal distributions, facies proportions, stratigraphic architecture, and large-scale shelf to basin morphology. This concept is modified from previous authors (Schlager, 1991; Handford and Loucks, 1993; Hunt and Tucker, 1993) and is similar to models for siliciclastic sequences, in which eustasy, tectonics, and sediment supply are the primary regime variables (Van Wagoner et al., 1988). In the case of a carbonate-dominated shelf-margin, sediment supply is generated by autochthonous reef-building organisms sensitive

to ambient environmental conditions such as light intensity, temperature, currents, and ocean-water chemistry. A change in any one of these parameters will lead to changes in dominant fauna and/or their productivity, thereby affecting reef-margin sediment production rates (Tucker and Wright, 1990; Schlager, 2005).

Carbonate margin regime variables (eustasy, structure, and environment) are easily plotted in a ternary diagram to illustrate their relative influence on margin character (Figure 4.16). The qualitative ternary diagram is applied to Cretaceous shelf-margins of south Texas and extended to included additional Phanerozoic examples. In the Comanche Shelf, changes in the broad shelf-to-basin morphology were a consequence of slow, moderate, and rapid rates of eustatic rise. The margin response was a strongly progradational, low-angle shelf in the Glen Rose supersequence, an aggradational, high-angle rimmed-shelf in the Fredericksburg supersequence, and an aggradational/retrogradational 'empty-bucket' shelf in the Washita supersequence (Figures 4.1, 4.16). These morphologies, though somewhat varied along strike, were consistent across the Stuart City trend. As outlined in earlier sections, changing facies proportions and shelf-margin architectures in the Stuart City margin were unique as a result of these eustatically-driven changes in shelf morphology. A fourth eustatic condition not observed in the Stuart City margin, falling sea-level, would produce subaerial exposure or a terraced to forced-regressive morphology (Figure 4.16). Examples include Pleistocene lowstand coral-reef terraces in Hawaii and the northern Red Sea (Szabo and Moore, 1986; Gvirtzman, 1994), Hauterivian forced regressive wedges of the Urgonian platform (Hunt and Tucker, 1993), and down-stepping shelf margin cycles in the late-highstand of the Permian Upper San Andres Fm (Sonnenfeld and Cross, 1993).

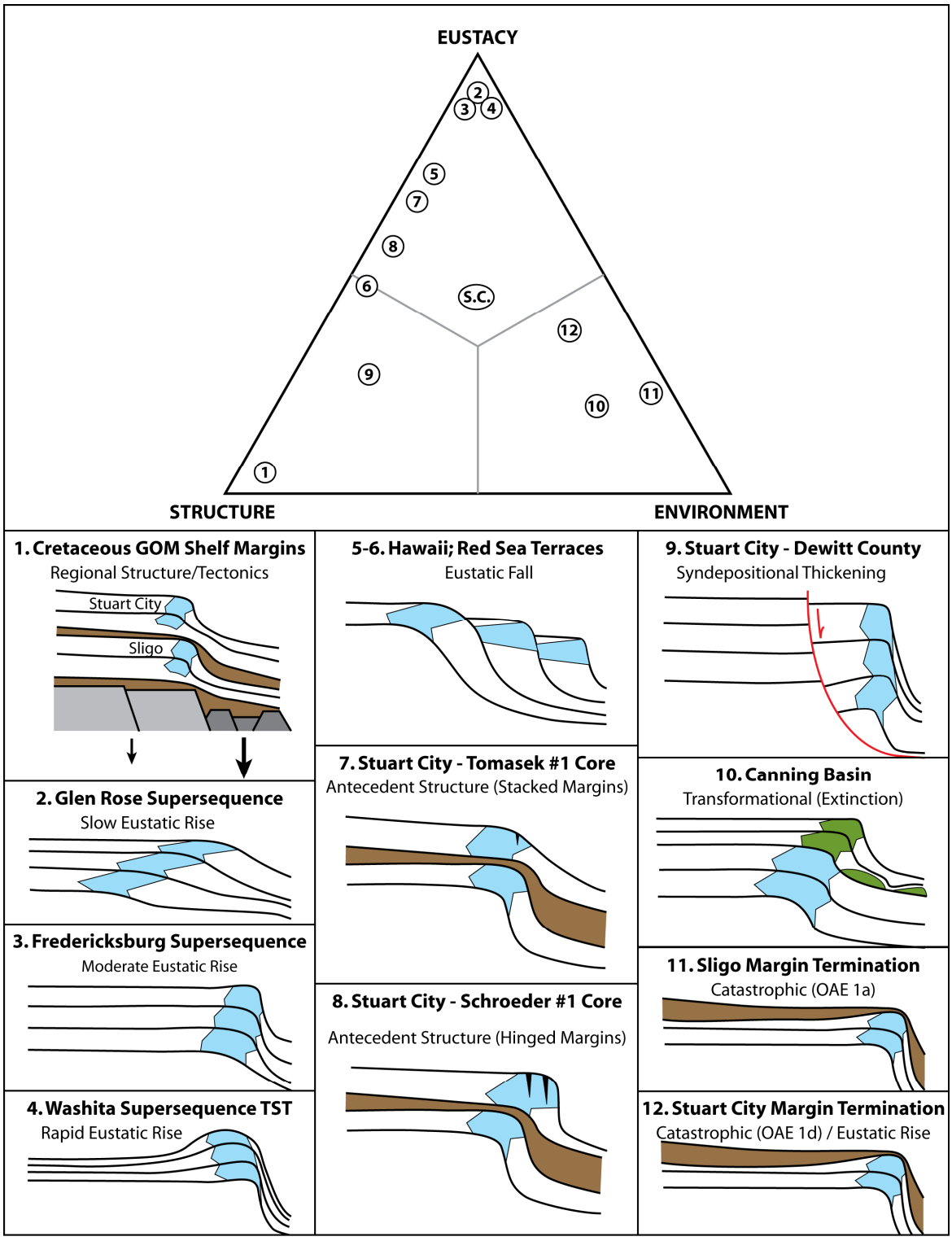

Figure 4.16: A ternary diagram illustrating the relative impact of the three main regime

variables (eustacy, structure/tectonics, environment) controlling Stuart City margin trajectory, stratigraphic architecture, and facies distributions. Examples are discussed in the text.

From a structural perspective, the terminal locations of both the Sligo and Stuart City margins were controlled by differential subsidence as a function of boundaries between moderately- and highly-attenuated continental crust (Figures 4.2, 4.16). This first-order structural/tectonic regime variable appears to have been prevalent through much of the northern Gulf of Mexico (Winker and Buffler, 1988). At a finer scale, lateral variability in shelf-margin architecture at any one point in time was the result of antecedent structural topographic elements. For example, Stuart City depositional profiles were steepest and syndepositional fractures were most pervasive in "hinged margins" where the reef had prograded beyond the antecedent Sligo shelf-edge (Schroeder #1 core) (Figures 4.9, 4.12, 4.16). In "stacked margins" where the Stuart City was on top of the Sligo shelf and subsidence rates were lower, the depositional profile was less steep (Tomasek #1). Reef-margin deposition on the low-subsidence San Marcos Arch created the lowest-angle depositional profile for the Fredericksburg supersequence (Kelley #3-4). In contrast, salt withdrawal and increased subsidence in the Maverick Basin (Winter, 1961) caused the Stuart City margin to develop approximately 50 kilometers farther landward relative to the terminal Sligo margin (Figure 4.2) (Waite, 2009). Lastly, syndepositional faulting served as another mode of structural control in the carbonate margin (Figure 4.16). In Dewitt County, syndepositional faults acted in conjunction with eustatic sea-level rise to force reef-margin retrogradation and deepening facies trends. Global case studies illustrating the impact of structural/tectonic elements on carbonate margin development are abundant, including those from the lower Paleozoic of the northern Canada Appalachians, the lower Cretaceous Cupido Platform, the Cretaceous to

early Cenozoic Bimini and Andros Banks, Miocene platforms in the Gulf of Suez, and Oligocene platforms in Papua New Guinea (Eberli and Ginsburg, 1987; J Burchette, 1988; James et al., 1989; Pigram et al., 1989; Lehmann et al., 1999).

Chief environmental parameters controlling shelf-margin development in Cretaceous systems are related to oceanic anoxic events. These events commonly caused platform margin drowning or changes in platform faunal abundances (Scott, 1988; Follmi et al., 1994; Scott, 1995; Huck et al., 2010). In south Texas, drowning profiles of the Sligo and Stuart City shelf-margins are linked to the combined effects of eustatic sea-level rise and environmental stress during OAEs 1a and 1d (Figure 4.16). These anoxic events were not a factor in the internal character of the margins, but they did abruptly terminate carbonate deposition (Chapter 3). Such environmental changes that cause termination of a carbonate margin are here considered 'catastrophic,' and other examples consist of climate-induced mass extinctions, platform transport into un-inhabitable paleolatitudinal zones, rapid ocean-water temperature changes, or increased nutrient supply from changing oceanographic circulation (Hallock and Schlager, 1986; Johnson et al., 1996; Wilson et al., 1998; Fluegel and Kiessling, 2002; Mutti et al., 2005) Other environmental changes that simply modify the internal facies patterns, faunal composition, or architecture of a platform are here considered 'transformational.' Examples include the Canning basin shelf-margin surrounding the late Devonian mass-extinction (Figure 4.16), and changing trophic structures due to varied siliciclastic input in Jurassic coral-microbialite reefs (Playford, 1980; Dupraz and Strasser, 2002).

CONCLUSIONS

Sedimentologic and sequence stratigraphic analysis of numerous whole cores from the Stuart City Fm provides an enhanced understanding of the internal facies and architectural evolution of middle to late Albian reefal shelf-margins. Dominant reef-builders consisted of sponges, stromatoporoids, coral, rudists and the ubiquitous microbial association of *Lithocodium-Bacinella*. Early cementation and binding by *Lithocodium-Bacinella* allowed the shelf-margin to steepen through time and may be common factors required for development of high-angle Albian shelves.

Temporal variability in the margin was largely driven by increasing rates of long-term accommodation creation during three second-order supersequences. Changing shelf-margin trajectories resulting from these eustatic cycles necessitate the use of separate depositional models to accurately depict differences in facies distribution and shelf-margin architecture for each supersequence. Higher-order depositional sequences did not affect shelf-margin trajectory but detailed facies cross-sections illustrate that they affected shelf-margin facies proportions within each sequence.

Initiation of the Stuart City margin occurred in the Glen Rose supersequence, during which low rates of eustatic rise caused limited accommodation and strongly-progradational trajectories of low-angle shelf-margin clinoforms (3-15˚ dip). The reefal margin at this time contained a high-energy fore-reef, while stromatoporoid- and coral-dominated reef-margin facies were volumetrically limited and commonly reworked. Caprinid rudists dominated the reef-flat and requienid rudists were rare to absent. Back-reef grainstone/rudstone complexes were generally absent or minimal in extent.

Maturation of the Stuart City margin occurred in the Fredericksburg supersequence, during which moderate rates of eustatic sea-level rise caused aggradational shelf-margin trajectories and development of a high-angle, rimmed shelf.

Faunal zonation and facies distributions during this supersequence were best-defined in areas of greater tectonic/structural subsidence with steeper slopes. A rigid, vertical reef-wall (~100 m; 330 ft high) with steep slopes (up to 80˚ dip) and common syndepositional fractures was constructed by sponges, laminar stromatoporoids, coral, and *Lithocodium-Bacinella*. The reef-flat consisted of cyclic requienid bindstones and caprinid bafflestones that were the source of laterally extensive rudist grainstone/rudstone storm berms and shoals. These grainstone/rudstone complexes sheltered a low-energy shelf-interior with cyclic, subtidal miliolid and fenestral tidal flat facies.

During transgression of the Washita supersequence, the shoreline-to-basin morphology was that of an empty-bucket and margin facies trends varied. In Bee County, the margin remained fully aggraded to sea-level and the Fredericksburg depositional model remains applicable. In DeWitt County, the margin shows retrogradational trajectories and deepening of facies. Transitions between the reef-wall, reef-flat and back-reef were widened along depositional dip. Requienid bindstones dominated the reef-flat and the submerged back-reef consisted of *Lithocodium-Bacinella* oncoids and coated-grains. Margin drowning occurred during maximum flooding of the Washita supersequence and Del Rio shale deposition. Reef drowning immediately followed the temporal extent of OAE 1d, suggesting that combined effects of environmental stress and eustatic sea-level rise terminated the platform margin.

Strike-oriented facies and architectural variability at a given point in time was influenced by regional antecedent structural/tectonic heterogeneity and syndepositional faulting. On the San Marcos Arch, decreased subsidence rates resulted in relatively lower-angle clinoforms with shallower (shorter) foresets in comparison to the surrounding salt-basins. Where the Stuart City margin prograded beyond the underlying Sligo shelf edge, the ‘hinged’ reef-margin is steeper, shows deeper reef-wall faunal

assemblages, and exhibits the most extensive syndepositional fractures. Lastly, syndepositional faulting led to disparate facies patterns along strike, with deepening trends observed where the shelf-margin was actively down-faulted during deposition.

Factors affecting the temporal and spatial variability in the Stuart City margin are classified as eustatic, structural, or environmental in origin. Through its full lateral and temporal extent, evolution of the Stuart City margin was a function of all three regime variables. However, within shorter time-frames or in geographic areas of limited extent, the observed facies patterns and shelf-margin architectures were more heavily influenced by a single regime variable.

General Conclusions

This study advances the current understanding of Cretaceous carbonate depositional systems by integrating detailed sequence stratigraphic data from shelf-interior and shelf-margin environments of a broad carbonate platform with geochemical stable-isotope analyses. The results demonstrate the response of carbonate depositional systems to sea level fluctuations of varying amplitude and frequency (see Immenhauser and Scott, 2002) as well as to environmental perturbations. Disruptions to the global carbon cycle that were manifest in oceanic anoxic events clearly transformed the dynamics of Cretaceous carbonate sedimentary processes.

Results of this dissertation acknowledge that Cretaceous shelf-interior environments were sensitive to slowly-changing accommodation regimes during typical periods of healthy carbonate sedimentation in phototrophic systems. However, the results challenge the common practice of interpreting carbonate sequences solely as a function of relative seal level. Instead, it is clear that long-term Cretaceous transgressive-regressive cycles were as much a result of changing oceanographic and environmental conditions as they were a result of simple eustatic fluctuations. Nonetheless, both processes appear to have been induced by volcanism in large-igneous provinces and along mid-ocean ridges. Submarine volcanic processes can easily be invoked to explain eustatic sea-level cycles spanning several million years at the scale of first-order sequences and second-order supersequences. Often, second-order sea level rises were coincident with intense submarine volcanism, increased frequency of oceanic anoxic events, and widespread episodes of carbonate platform drowning. However, additional work is required to explain the driving mechanisms behind third-order depositional sequences and higher-order cycles. After extensive analysis, it is the opinion of the author that this level of

stratigraphic cyclicity is not commonly correlative between ocean basins, except in rare circumstances of uniform platform subsidence that are free from the influence of varying structural/tectonic processes.

Environmental and eustatic parameters discussed above combined to create transgressive-regressive supersequences recognizable in global Cretaceous carbonate platforms. Due to the severe nature of the oceanographic disturbances inherent to oceanic anoxic events, many carbonate platforms were unable to recover from drowning and renew shallow-marine sedimentation. This study clearly documents the two-dimensional response of land-attached carbonate systems to environmental stress. The default consequence was for the carbonate factory to reassemble at the shoreline or on structural bathymetric highs. This required that the carbonate platform prograde ramp clinoforms across the former shelf in order to establish a new shelf-margin.

Shelf-margin sedimentation was most active in periods of environmental equilibrium. Diverse fauna and high-rates of platform margin sedimentation were only able to aggrade healthy reefal systems when unaffected by environmental stress. During these periods of shelf-margin sedimentation, facies patterns and faunal distributions were inherently controlled by second-order accommodation trends. The structural setting commonly modified the dimensions of shelf-margin clinoforms, but the broad morphology of the shelf was consistent during each supersequence. Comparison of sedimentation rates in Cretaceous reef-margins with rates of eustatic sea level rise suggest that drowning of healthy microbial-coral-rudist reef-margins, as occurred in the early Aptian and late Albian of south Texas, would not have taken place were it not for the catastrophic effects of oceanic anoxic events. The end.

Supplemental Data

Data used for these studies, such as core descriptions, measured sections, and stable isotope values are available as supporting material and can be downloaded online or obtained from the author.

References

Abbott, P.L. 1966. The Glen Rose section in the Canyon Reservoir area, Comal County, Texas., M.A. Thesis, The University of Texas at Austin, 146 pp.

Achauer, C.W. and Johnson, J.H. 1969. Algal stromatolites in the James Reef Complex (Lower Cretaceous), Fairway Field, Texas. Journal of Sedimentary Petrology, 39: 1466-1472.

Aconcha, E.S., Kerans, C. and Zeng, H. 2008. Seismic Geomorphology Applied to Lower Glen Rose Patch Reefs in the Maverick Basin, Southwest Texas. Transactions - Gulf Coast Association of Geological Societies, 58: 3-23.

Adams, E.W. and Schlager, W. 2000. Basic Types of Submarine Slope Curvature. Journal of Sedimentary Research, 70: 814-828.

Allan, J.R. and Matthews, R.K. 1982. Isotope signatures associated with early meteoric diagenesis. Sedimentology, 29: 797-817.

Alsharhan, A.S. and Nairn, A.E.M. 1993. Carbonate platform models of Arabian Cretaceous reservoirs. In: Cretaceous carbonate platforms (Eds J.A.T. Simo, R.W. Scott, and J.-P. Masse): AAPG Memoir, 56: 173-184.

Ambrose, W.A., Hentz, T.F., Bonnaffe, F., Loucks, R.G., Brown, L.F., Jr., Wang, F.P. and Potter, E.C. 2009. Sequence-stratigraphic controls on complex reservoir architecture of highstand fluvial-dominated deltaic and lowstand valley-fill deposits in the Upper Cretaceous (Cenomanian) Woodbine Group, East Texas field: Regional and local perspectives. AAPG Bulletin, 93: 231-269.

Amodio, S., Ferreri, V., D'Argenio, B., Weissert, H. and Sprovieri, M. 2008. Carbon-isotope stratigraphy and cyclostratigraphy of shallow-marine carbonates; the case of San Lorenzello, Lower Cretaceous of southern Italy. Cretaceous Research, 29: 803-813.

Amsbury, D.L. 1965. Porosity Distribution in the Outcropping Edwards Formation of North-Central Texas, EPR Report 863. Exploration and Production Research Division; Shell Development Company, Houston, TX, 24 pp.

Amsbury, D.L. 1974. Stratigraphic petrology of lower and middle Trinity rocks on the San Marcos platform, south-central Texas. Geoscience and Man, 8: 1-35.

Amsbury, D.L. 1996. Pearsall (Aptian Cretaceous) subsurface to outcrop sequence stratigraphy, central Texas. Transactions - Gulf Coast Association of Geological Societies, 46: 1-7.

Arnaud-Vanneau, A. and Arnaud, H. 1990. Hauterivian to lower Aptian carbonate shelf sedimentation and sequence stratigraphy in the Jura and northern Subalpine chains (southeastern France and Swiss Jura). In: Carbonate Platforms: Facies,

Sequences, and Evolution (Eds M.E. Tucker, J.L. Wilson, P.D. Crevello, J.R. Sarg, and J.F. Read): Special Publication of the International Association of Sedimentologists, 9: 203-233.

Arthur, M.A., Jenkyns, H.C., Brumsack, H.J. and Schlanger, S.O. 1990. Stratigraphy, geochemistry, and paleoceanography of organic carbon-rich Cretaceous sequences. In: Cretaceous Resources, Events and Rhythms (Eds. R.N. Ginsburg and B. Beaudoin,) Kluwer Academic Publishers, Dordrecht, pp. 75-119.

Arthur, M.A. and Sageman, B.B. 1994. Marine black shales; depositional mechanisms and environments of ancient deposits. Annual Review of Earth and Planetary Sciences, 22: 499-551.

Arthur, M.A. and Schlanger, S.O. 1979. Cretaceous 'oceanic anoxic events' as causal factors in development of reef-reservoired giant oil fields. AAPG Bulletin, 63: 870-885.

Arthur, M.A., Schlanger, S.O. and Jenkyns, H.C. 1987. The Cenomanian-Turonian oceanic anoxic event; II, Palaeoceanographic controls on organic-matter production and preservation. In: Marine Petroleum Source Rocks (Eds J. Brooks and A.J. Fleet), Geological Society Special Publications, 26, pp. 401-420.

Bachmann, M., Bassiouni, M.A.A. and Kuss, J. 2003. Timing of Mid-Cretaceous carbonate platform depositional cycles, northern Sinai, Egypt. Palaeogeography, Palaeoclimatology, Palaeoecology, 200: 131-162.

Bachmann, M. and Hirsch, F. 2006. Lower Cretaceous carbonate platform of the eastern Levant (Galilee and the Golan Heights): stratigraphy and second-order sea-level change. Cretaceous Research, 27: 487-512.

Bachmann, M. and Kuss, J. 1998. The Middle Cretaceous carbonate ramp of the northern Sinai; sequence stratigraphy and facies distribution. In: Carbonate Ramps (Eds V.P. Wright and T.P. Burchette), Geological Society Special Publications, 149: 253-280.

Baker, H.W. and Scott, E. 1985. Intermittent subaerial exposure responsible for porosity development in Edwards limestone, Lavaca County, Texas. In: Lower Cretaceous depositional environment from shoreline to slope - a core workshop (Eds D.G. Bebout and D. Ratcliff), Gulf Coast Association Geological Societies Annual Meeting, pp. 55-63, Austin.

Banner, F.T., Finch, E.M. and Simmons, M.D. 1990. On Lithocodium Elliott (calcareous algae); its palaeobiological and stratigraphical significance. Journal of Micropalaeontology, 9: 21-35.

Barron, E.J., Fawcett, P.J., Pollard, D. and Thompson, S.L. 1993. Model simulations of Cretaceous climates; the role of geography and carbon dioxide. Philosophical Transactions - Royal Society London, 341: 307-316.

Barron, E.J. and Peterson, W.H. 1990. Mid-Cretaceous ocean circulation; results from model sensitivity studies. Paleoceanography, 5: 319-337.

Barron, E.J. and Washington, W.M. 1983. Numerical climate modeling: An exploration frontier in petroleum source rock prediction. AAPG Bulletin, 69: 448-459.

Bauer, J., Kuss, J. and Steuber, T. 2003. Sequence architecture and carbonate platform configuration (late Cenomanian-Santonian), Sinai, Egypt. Sedimentology, 50: 387-414.

Bay, A.R. 1982. Evolution and porosity of carbonate shoaling cycles, Lower Cretaceous-lower Glen Rose, South Texas. Transactions - Gulf Coast Association of Geological Societies, 32: 101-119.

Bay, T.A., Jr. 1977. Lower Cretaceous Stratigraphic Models from Texas and Mexico. In: Cretaceous Carbonates of Texas and Mexico: Applications to Subsurface Exploration (Eds D.G. Bebout and R.G. Loucks), Texas Bureau of Economic Geology Report of Investigations No 89, pp. 12-30.

Bebout, D.G. 1974. Lower Cretaceous Stuart City shelf margin of south Texas; its depositional and diagenetic environments and their relationship to porosity. Transactions - Gulf Coast Association of Geological Societies, 24: 138-159.

Bebout, D.G. 1977. Sligo and Hosston depositional patterns, subsurface of South Texas. In: Cretaceous Carbonates of Texas and Mexico: Applications to Subsurface Exploration (Eds D.G. Bebout and R.G. Loucks), Texas Bureau of Economic Geology Report of Investigations No 89, pp. 79-96.

Bebout, D.G., Budd, D.A. and Schatzinger, R.A. 1981. Depositional and diagenetic history of the Sligo and Hosston formations (Lower Cretaceous) in South Texas. Texas Bureau of Economic Geology Report of Investigations No 109, Austin, TX, 70 pp.

Bebout, D.G. and Loucks, R.G. 1974. Stuart City Trend Lower Cretaceous, South Texas: A Carbonate Shelf-Margin Model for Hydrocarbon Exploration. Texas Bureau of Economic Geology Report of Investigations No 78, Austin, TX, 80 pp.

Bebout, D.G. and Loucks, R.G. (Eds) 1977. Cretaceous Carbonates of Texas & Mexico - Applications to Subsurface Exploration. Texas Bureau of Economic Geology Report of Investigations No. 89, Austin, TX, 332 pp.

Bebout, D.G. and Schatzinger, R.A. 1978. Distribution and geometry of an oolite-shoal complex; Lower Cretaceous Sligo Formation, South Texas. Transactions - Gulf Coast Association of Geological Societies, 28: 33-45.

Bebout, D.G., Schatzinger, R.A. and Loucks, R.G. 1977. Porosity distribution in the Stuart City Trend, Lower Cretaceous, South Texas, In: Cretaceous Carbonates of Texas and Mexico: Applications to Subsurface Exploration (Eds D.G. Bebout and

R.G. Loucks), Texas Bureau of Economic Geology Report of Investigations No 89, pp. 234-256.

Berner, R.A. 1970. Sedimentary Pyrite Formation. American Journal of Science, 268: 1-23.

Bertani, R.T. and Carozzi, A.V. 1985. Lagoa Feia Formation (Lower Cretaceous), Campos Basin, offshore Brazil; rift valley stage lacustrine carbonate reservoirs; I. Journal of Petroleum Geology, 8: 37-58.

Bornemann, A., Pross, J., Reichelt, K., Herrle, J.O., Hemleben, C. and Mutterlose, J. 2005. Reconstruction of short-term palaeoceanographic changes during the formation of the Late Albian 'Niveau Breistroffer' black shales (Oceanic Anoxic Event 1d, SE France). Journal of the Geological Society, 162: 623-639.

Bosence, D.W.J. 1983. Coralline algal reef frameworks. Journal of the Geological Society, 140: 365-376.

Bralower, T.J., CoBabe, E., Clement, B., Sliter, W.V., Osburn, C.L. and Longoria, J. 1999. The record of global change in Mid-Cretaceous (Barremian-Albian) sections from the Sierra Madre, northeastern Mexico. Journal of Foraminiferal Research, 29: 418-437.

Bralower, T.J., Fullagar, P.D., Paull, C.K., Dwyer, G.S. and Leckie, R.M. 1997. Mid-Cretaceous strontium-isotope stratigraphy of deep-sea sections. Geological Society of America Bulletin, 109: 1421-1442.

Buffler, R., Watkins, J.S., Schaub, F.J. and Worzel, J.L. 1980. Structure and early geologic history of the deep central Gulf of Mexico Basin. Proceedings, Symposium on the Origin of the Gulf of Mexico and the Early Opening of the Central Atlantic, Louisiana State University, Baton Rouge, 3-16 pp.

Buffler, R.T. and Sawyer, D.S. 1985. Distribution of crust and early history, Gulf of Mexico basin. Transactions - Gulf Coast Association of Geological Societies, 35: 333-344.

Burchette, T.P. 1988. Tectonic control on carbonate platform facies distribution and sequence development: Miocene, Gulf of Suez. Sedimentary Geology, 59: 179-204.

Burkholder, J.F. and Lumsden, D.N. 1973. Petrographic analysis of a subsurface portion of the Glen Rose Formation (lower Cretaceous), south Texas. Transactions - Gulf Coast Association of Geological Societies, 23: 278-287.

Cherchi, A. and Schroeder, R. 2006. Remarks on the systematic position of Lithocodium Elliott, a problematic microorganism from the Mesozoic carbonate platforms of the Tethyan Realm. Facies, 52: 435-440.

Clarke, L.J. and Jenkyns, H.C. 1999. New oxygen isotope evidence for long-term Cretaceous climatic change in the Southern Hemisphere. Geology, 27: 699-702.

Coogan, A.H. 1977. Early and Middle Cretaceous Hippuritacea (rudists) of the Gulf Coast. In: Cretaceous Carbonates of Texas and Mexico: Applications to Subsurface Exploration (Eds D.G. Bebout and R.G. Loucks), Texas Bureau of Economic Geology Report of Investigations No 89, pp. 32-70.

Cook, T.D. 1979. Exploration history of South Texas Lower Cretaceous carbonate platform. AAPG Bulletin, 63: 32-49.

Dawson, W.C. 1997. Limestone microfacies and sequence stratigraphy: Eagle Ford Group (Cenomanian-Turonian) north-central Texas outcrops. Transactions - Gulf Coast Association of Geological Societies, 47: 99-106.

Dawson, W.C. 2000. Shale microfacies; Eagle Ford Group (Cenomanian-Turonian) north-central Texas outcrops and subsurface equivalents. Transactions - Gulf Coast Association of Geological Societies, 50: 607-621.

de Gea, G.A., Castro, J.M., Aguado, R., Ruiz-Ortiz, P.A. and Company, M. 2003. Lower Aptian carbon isotope stratigraphy from a distal carbonate shelf setting; the Cau section, Prebetic Zone, SE Spain. Palaeogeography, Palaeoclimatology, Palaeoecology, 200: 207-219.

De Romero, L.M., Truskowski, I.M., Bralower, T.J., Bergen, J.A., Odreman, O., Zachos, J.C. and Galea-Alvarez, F.A. 2003. An Integrated Calcareous Microfossil Biostratigraphic and Carbon-Isotope Stratigraphic Framework for the La Luna Formation, Western Venezuela. Palaios, 18: 349-366.

Denison, R.E., Miller, N.R., Scott, R.W. and Reaser, D.F. 2003. Strontium isotope stratigraphy of the Comanchean Series in North Texas and southern Oklahoma. Geological Society of America Bulletin, 115: 669-682.

Dickson, J.A.D. and Coleman, M.L. 1980. Changes in carbon and oxygen isotope composition during limestone diagenesis. Sedimentology, 27: 107-118.

Dravis, J.J. 1980. Sedimentology and diagenesis of the Upper Cretaceous Austin Chalk Formation, South Texas and northern Mexico. PhD Dissertation, Rice University, Houston, TX. 513 p.

Duncan, R.A. 2002. A time frame for construction of the Kerguelen Plateau and Broken Ridge. Journal of Petrology, 43: 1109-1119.

Dupraz, C. and Strasser, A. 2002. Nutritional Modes in Coral-Microbialite Reefs (Jurassic, Oxfordian, Switzerland): Evolution of Trophic Structure as a Response to Environmental Change. Palaios, 17: 449-471.

Eberli, G.P., Bernoulli, D., Sanders, D. and Vecsei, A. 1993. From aggradation to progradation; the Maiella Platform, Abruzzi, Italy. In: Cretaceous carbonate platforms (Eds J.A.T. Simo, R.W. Scott, and J.-P. Masse): AAPG Memoir, 56: 213-232.

Eberli, G.P. and Ginsburg, R.N. 1987. Segmentation and coalescence of Cenozoic carbonate platforms, northwestern Great Bahama Bank. Geology, 15: 75-79.

Elliot, G.F. 1956. Further records of fossil calcareous algae from the Middle East. Micropaleontology, 2: 327-334.

Ellis, P.G. and McClay, K.R. 1988. Listric extensional fault systems - results of analogue model experiments. Basin Research, 1: 55-70.

Elrick, M. 1995. Cyclostratigraphy of Middle Devonian carbonates of the Eastern Great Basin. Journal of Sedimentary Research, 65: 61-79.

Elrick, M., Molina-Garza, R., Duncan, R. and Snow, L. 2009. C-Isotope stratigraphy and paleoenvironmental changes across OAE2 (mid-Cretaceous) from shallow-water platform carbonates of southern Mexico. Earth and Planetary Science Letters, 277: 295-306.

Embry, A.F. and Johannessen, E.P. 1993. T-R sequence stratigraphy, facies analysis and reservoir distribution in the uppermost Triassic-Lower Jurassic succession, western Sverdrup Basin, Arctic Canada. In: Arctic Geology and Petroleum Potential, Special Publication (Eds T.O. Vorren, E. Bergsager, O.A. Dahl-Stamnes, E. Holter, B. Johansen, E. Lie and T.B. Lund) Special Publication - Norwegian Petroleum Society, NPF, 2: 121-146.

Emeis, K.-C. and Weissert, H. 2009. Tethyan-Mediterranean organic carbon-rich sediments from Mesozoic black shales to sapropels. Sedimentology, 56: 247-266.

Enos, P. 1988. Evolution of pore space in the Poza Rica trend (Mid-Cretaceous), Mexico. Sedimentology, 35: 287-325.

Enos, P. and Stephens, B.P. 1993. Mid-Cretaceous basin margin carbonates, east-central Mexico. Sedimentology, 40: 539-556.

Erba, E. 1994. Nonnofossils and superplumes: The Early Aptian "nannoconid crisis". Paleoceanography, 9: 483-501.

Erba, E., Bartolini, A. and Larson, R.L. 2004. Valanginian Weissert oceanic anoxic event. Geology, 32: 149-152.

Erba, E., Bottini, C., Weissert, H.J. and Keller, C.E. 2010. Calcareous nannoplankton response to surface-water acidification around Oceanic Anoxic Event 1a. Science, 329: 428-432.

Erba, E., Channell, J.E.T., Claps, M., Jones, C., Larson, R., Opdyke, B., Premoli Silva, I., Riva, A., Salvini, G. and Torricelli, S. 1999. Integrated stratigraphy of the Cismon Apticore (southern Alps, Italy); a "reference section" for the Barremian-Aptian interval at low latitudes. Journal of Foraminiferal Research, 29: 371-391.

Erbacher, J., Friedrich, O., Wilson, P.A., Birch, H. and Mutterlose, J. 2005. Stable organic carbon isotope stratigraphy across Oceanic Anoxic Event 2 of Demerara

Rise, western tropical Atlantic. Geochemistry, Geophysics, Geosystems – G3, 6: Q06010, doi:10.1029/2004GC000850.

Erbacher, J., Friedrich, O., Wilson, P.A., Lehmann, J. and Weiss, W. 2011. Short-term warming events during the boreal Albian (mid?Cretaceous). Geology, 39: 223-226.

Erbacher, J., Gerth, W., Schmiedl, G. and Hemleben, C. 1998. Benthic foraminiferal assemblages of late Aptian-early Albian black shale intervals in the Vocontian Basin, SE France. Cretaceous Research, 19: 805-826.

Erbacher, J., Huber, B.T., Norris, R.D. and Markey, M. 2001. Increased thermohaline stratification as a possible cause for an ocean anoxic event in the Cretaceous Period. Nature, 409: 325-327.

Erbacher, J. and Thurow, J. 1997. Influence of oceanic anoxic events on the evolution of Mid-Cretaceous Radiolaria in the North Atlantic and western Tethys. Marine Micropaleontology, 30: 139-158.

Erbacher, J., Thurow, J. and Littke, R. 1996. Evolution patterns of radiolaria and organic matter variations: A new approach to identify sea-level changes in mid-Cretaceous pelagic environments. Geology, 24: 499-502.

Everts, A.J.W. and Reijmer, J.J.G. 1995. Clinoform composition and margin geometries of a Lower Cretaceous carbonate platform (Vercors, SE France). Palaeogeography, Palaeoclimatology, Palaeoecology, 119: 19-33.

Everts, A.J.W., Stafleu, J., Schlager, W., Fouke, B.W. and Zwart, E.W. 1995. Stratal patterns, sediment composition, and sequence stratigraphy at the margin of the Vercors carbonate platform (Lower Cretaceous, SE France). Journal of Sedimentary Research, 65: 119-131.

Ewing, T.E. 1991. Structural framework. In: The geology of North America (Ed A. Salvador), J, pp. 31-52. Geological Society of America: Boulder, CO, United States.

Ewing, T.E. 2010. Pre-Pearsall Geology and Exploration Plays in South Texas. Transactions - Gulf Coast Association of Geological Societies, 60: 241-260.

Faust, M.J. 1990. Seismic stratigraphy of the mid-Cretaceous unconformity (MCU) in the central Gulf of Mexico basin. Geophysics, 55: 868-884.

Fernandez-Mendiola, P.A. and Garcia-Mondejar, J. 1989. Evolution of a Mid-Cretaceous carbonate platform, Gorbea (northern Spain). Sedimentary Geology, 64: 111-126.

Ferreri, V., Weissert, H., D'Argenio, B. and Buonocunto, F.P. 1997. Carbon isotope stratigraphy; a tool for basin to carbonate platform correlation. Terra Nova, 9: 57-61.

Fisher, W.L. and Rodda, P.U. 1969. Edwards Formation (Lower Cretaceous), Texas; dolomitization in a carbonate platform system. AAPG Bulletin, 53: 55-72.

Fitchen, W.M., Bebout, D.G. and Prezbindowski, D.R. 1997. Production from Cretaceous high-permeability carbonate grainstones; Alabama Ferry, North Unit, Leon County, Texas. In: R.P. Major, Oil and Gas on Texas state lands: An assessment of the resource and characterization of type reservoirs: Texas Bureau of Economic Geology Report of Investigations No 241, 117-126 pp.

Flawn, P.T., Goldstein, A., King, P.B. and Weaver, C.E. 1961. The Ouachita Sytem, The University of Texas at Austin - Bureau of Economic Geology Publication 6120, 401 pp.

Fluegel, E. and Kiessling, W. 2002. Patterns of Phanerozoic reef crises. Special Publication - Society for Sedimentary Geology, 72: 691-733.

Foellmi, K.B., Godet, A., Bodin, S. and Linder, P. 2006. Interactions between environmental change and shallow water carbonate buildup along the northern Tethyan margin and their impact on the Early Cretaceous carbon isotope record. Paleoceanography, 21: 1-16.

Folk, R.L. 1973. Evidence for Peritidal Deposition of Devonian Caballos Novaculite, Marathon Basin, Texas. AAPG Bulletin, 57: 702-725.

Follmi, K.B., Godet, A., Bodin, S. and Linder, P. 2006. Interactions between environmental change and shallow water carbonate buildup along the northern Tethyan margin and their impact on the Early Cretaceous carbon isotope record. Paleoceanography, 21: 1-16.

Follmi, K.B., Weissert, H., Bisping, M. and Funk, H. 1994. Phosphogenesis, carbon-isotope stratigraphy, and carbonate-platform evolution along the Lower Cretaceous northern Tethyan margin. Geological Society of America Bulletin, 106: 729-746.

Forgotson, J.M., Jr. 1957. Stratigraphy of Comanchean Cretaceous Trinity group [Gulf Coastal Plain]. AAPG Bulletin, 41: 2328-2363.

Forster, A., Schouten, S., Baas, M. and Sinninghe Damste, J.S. 2007. Mid-Cretaceous (Albian-Santonian) sea surface temperature record of the tropical Atlantic Ocean. Geology, 35: 919-922.

Fouke, B.W., Everts, A.-J.W., Zwart, E.W., Schlager, W., Smalley, P.C. and Weissert, H. 1996. Subaerial exposure unconformities on the Vercors carbonate platform, SE France, and their sequence stratigraphic significance. Geological Society Special Publications, 104: 295-320.

Frey, F.A., Coffin, M.F., Wallace, P.J., Weis, D., Zhao, X., Wise, S.W., Waehnert, V., Teagle, D.A.H., Saccocia, P.J., Reusch, D.N., Pringle, M.S., Nicolaysen, K.E., Neal, C.R., Mueller, R.D., Moore, C.L., Mahoney, J.J., Keszthelyi, L., Inokuchi,

H., Duncan, R.A., Delius, H., Damuth, J.E., Damasceno, D., Coxall, H.K., Borre, M.K., Boehm, F., Barling, J., Arndt, N.T. and Antretter, M. 2000. Origin and evolution of a submarine large igneous province; the Kerguelen Plateau and Broken Ridge, southern Indian Ocean. Earth and Planetary Science Letters, 176: 73-89.

Friedrich, O. 2006. Paleoenvironmental changes across the Cenomanian/Turonian boundary event (oceanic anoxic event 2) as indicated by benthic Foraminifera from the Demerara Rise (ODP Leg 207). In: Revue de Micropaleontologie (Eds J. Erbacher and J. Mutterlose), 49, pp. 139-121.

Friedrich, O., Reichelt, K., Herrle, J.O., Lehmann, J., Pross, J. and Hemleben, C. 2003. Formation of the late Aptian Niveau Fallot black shales in the Vocontian Basin (SE France); evidence from Foraminifera, palynomorphs, and stable isotopes. Marine Micropaleontology, 49: 65-85.

Fritz, D.A., Belsher, T.W., Medlin, J.M., Stubbs, J.L., Wright, R.P. and Harris, P.M. 2000. New exploration concepts for the Edwards and Sligo margins, Cretaceous of onshore Texas. AAPG Bulletin, 84: 905-922.

Frost, E.L.I. and Kerans, C. 2009. Platform-margin trajectory as a control on syndepositional fracture patterns, Canning Basin, western Australia. Journal of Sedimentary Research, 79: 44-55.

Fullmer, S. and Lucia, F.J. 2005. Burial history of central Texas Cretaceous carbonates. Transactions - Gulf Coast Association of Geological Societies, 55: 225-232.

Gale, A.S., Kennedy, W.J., Burnett, J.A., Caron, M. and Kidd, B.E. 1996. The Late Albian to Early Cenomanian succession at Mont Risou near Rosans (Drome , SE France): an integrated study (ammonites, inoceramids, planktonic foraminifera, nannofossils, oxygen and carbon isotopes). Cretaceous Research, 17: 515-606.

Gale, A.S., Kennedy, W.J., Voigt, S. and Walaszczyk, I. 2005. Stratigraphy of the upper Cenomanian-lower Turonian Chalk succession at Eastbourne, Sussex, UK; ammonites, inoceramid bivalves and stable carbon isotopes. Cretaceous Research, 26: 460-487.

Galloway, W.E., Henry, C.D. and Smith, G.E. 1982. Depositional framework, hydrostratigraphy, and uranium mineralization of the Oakville sandstone (Miocene), Texas coastal plain, Texas Bureau of Economic Geology Report of Investigations No 113. The University of Texas at Austin, Bureau of Economic Geology, 51 pp.

Gattuso, J.P. and Buddemeier, R.W. 2000. Ocean biogeochemistry; calcification and CO2. Nature (London), 407: 311-313.

Gattuso, J.P., Frankignoulle, M., Bourge, I., Romaine, S. and Buddemeier, R.W. 1998. Effect of calcium carbonate saturation of seawater on coral calcification. Global and Planetary Change, 18: 37-46.

Gertsch, B., Adatte, T., Keller, G., Tantawy, A.A.A.M., Berner, Z., Mort, H.P. and Fleitmann, D. 2010. Middle and late Cenomanian oceanic anoxic events in shallow and deeper shelf environments of western Morocco. Sedimentology, 57: 1430-1462.

Gil, J., Garcia-Hidalgo, J.F., Segura, M., Garcia, A. and Carenas, B. 2006. Stratigraphic architecture, palaeogeography and sea-level changes of a third order depositional sequence; the late Turonian-early Coniacian in the northern Iberian Ranges and Central System (Spain). Sedimentary Geology, 191: 191-225.

Gili, E., Masse, J.-P. and Skelton, P.W. 1995. Rudists as gregarious sediment-dwellers, not reef-builders, on Cretaceous carbonate platforms. Palaeogeography, Palaeoclimatology, Palaeoecology, 118: 245-267.

Ginsburg, R.N., Hardie, L.A., Bricker, O.P., Garrett, P. and Wanless, H.R. 1977. Exposure index; a quantitative approach to defining position within the tidal zone. In: Sedimentation on the Modern Carbonate Tidal Flats of Northwest Andros Island, Bahamas (Ed L.A. Hardie) Johns Hopkins University Press, p 7-11.

Ginsburg, R.N., Harris, P.M., Eberli, G.P. and Swart, P.K. 1991. The growth potential of a bypass margin, Great Bahama Bank. Journal of Sedimentary Petrology, 61: 976-987.

Ginsburg, R.N. and Schroeder, J.H. 1973. Growth and submarine fossilization of algal cup reefs, Bermuda. Sedimentology, 20: 575-614.

Godet, A., Bodin, S., Foellmi, K.B., Vermeulen, J., Gardin, S., Fiet, N., Adatte, T., Berner, Z., Stueben, D. and van de Schootbrugge, B. 2006. Evolution of the marine stable carbon-isotope record during the Early Cretaceous; a focus on the late Hauterivian and Barremian in the Tethyan realm. Earth and Planetary Science Letters, 242: 254-271.

Godet, A., Foellmi, K.B., Bodin, S., de Kaenel, E., Matera, V. and Adatte, T. 2010. Stratigraphic, sedimentological and palaeoenvironmental constraints on the rise of the Urgonian Platform in the western Swiss Jura. Sedimentology, 57: 1088-1125.

Goldhammer, R.K., Dunn, P.A. and Hardie, L.A. 1987. High frequency glacio-eustatic sealevel oscillations with Milankovitch characteristics recorded in Middle Triassic platform carbonates in northern Italy. American Journal of Science, 287: 853-892.

Goldhammer, R.K., Dunn, P.A. and Hardie, L.A. 1990. Depositional cycles, composite sea-level changes, cycle stacking patterns, and the hierarchy of stratigraphic forcing: Examples from Alpine Triassic platform carbonates. Geological Society of America Bulletin, 102: 535-562.

Goldhammer, R.K. and Johnson, C.A. 2001. Middle Jurassic-Upper Cretaceous paleogeographic evolution and sequence-stratigraphic framework of the Northwest Gulf of Mexico rim. In: The western Gulf of Mexico basin; tectonics,

sedimentary basins, and petroleum systems (Eds C. Bartolini, R.T. Buffler and A. Cantu-Chapa), AAPG Memoir 75, pp. 45-81.

Goldhammer, R.K., Lehmann, P.J., Todd, R.G., Wilson, J.L., Ward, W.C. and Johnson, C.R. 1991. Sequence Stratigraphy and cyclostratigraphy of the Mesozoic of the Sierra Madre Oriental, northeast Mexico, a field guidebook. Gulf Coast Section, Society for Sedimentary Geology, 85 pp.

Gomez-Perez, I., Fernandez Mendiola, P.A. and Garcia Mondejar, J. 1999. Depositional architecture of a rimmed carbonate platform (Albian, Gorbea, western Pyrenees). Sedimentology, 46: 337-356.

Grabowski Jr., G.J. 1995. Organic-rich chalks and calcareous mudstones of the Upper Cretaceous Austin Chalk and Eagle Ford formation, south-central Texas, USA. In: Petroleum source rocks (Ed B. Katz), pp. 209-234. Springer-Verlag, New York.

Gradstein, F.M., Ogg, J.G. and Smith, A.G. 2004. A geologic time scale. Cambridge University Press, Cambridge, 589 pp.

Graus, R.R. and Macintyre, I.G. 1989. The zonation patterns of Caribbean coral reefs as controlled by wave and light energy input, bathymetric setting and reef morphology: computer simulation experiments. Coral Reefs, 8: 9-18.

Groetsch, J., Billing, I. and Vahrenkamp, V. 1998. Carbon-isotope stratigraphy in shallow-water carbonates; implications for Cretaceous black-shale deposition. Sedimentology, 45: 623-634.

Groetsch, J., Schroeder, R., Noe, S. and Fluegel, E. 1993. Carbonate platforms as recorders of high-amplitude eustatic sea-level fluctuations; the late Albian appenninica-event. Basin Research, 5: 197-212.

Grotzinger, J.P. 1986. Cyclicity and paleoenvironmental dynamics, Rocknest platform, northwest Canada. Geological Society of America Bulletin, 97: 1208-1231.

Gvirtzman, G. 1994. Fluctuations of sea level during the past 400 000 years; the record of Sinai, Egypt (northern Red Sea). Coral Reefs, 13: 203-214.

Hallam, A. 1971. Re-evaluation of the palaeogeographic arguement for an expanding earth. Nature, 232: 180-182.

Hallock, P. and Schlager, W. 1986. Nutrient excess and the demise of coral reefs and carbonate platforms. Palaios, 1: 389-398.

Hancock, J.M. 1989. Sea-level changes in the British region during the Late Cretaceous. Proceedings of the Geologists' Association, 100: 565-594.

Hancock, J.M. and Kauffman, E.G. 1979. The great transgressions of the Late Cretaceous. Journal of the Geological Society, 136: 175-186.

Hancock, J.M. and Walaszczyk, I. 2004. Mid-Turonian to Coniacian changes of sea level around Dallas, Texas. Cretaceous Research, 25: 459-471.

Handford, C.R. and Loucks, R.G. 1993. Carbonate depositional sequences and systems tracts; responses of carbonate platforms to relative sea-level changes. AAPG Memoir, 57: 3-41.

Handoh, I.C. and Lenton, T.M. 2003. Periodic mid-Cretaceous oceanic anoxic events linked by oscillations of the phosphorous and oxygen biogeochemical cycles. Global Biogeochemical Cycles, 17: 1-11.

Haq, B.U. and Al-Qahtani, A.M. 2005. Phanerozoic cycles of sea-level change on the Arabian Platform. GeoArabia (Manama), 10: 127-160.

Haq, B.U., Hardenbol, J. and Vail, P.R. 1987. Chronology of fluctuating sea levels since the Triassic. Science, 235: 1156-1167.

Haq, B.U., Hardenbol, J. and Vail, P.R. 1988. Mesozoic and Cenozoic chronostratigraphy and cycles of sea-level change. In: Sea-Level Changes: an Integrated Approach, (Eds C.K. Wilgus, B.S. Hastings, C.G.S.C. Kendall, H.W. Posamentier, C.A. Ross, and J.C. Van Wagoner) Special Publication - Society of Economic Paleontologists and Mineralogists, 42: 72-108.

Hardenbol, J. and Robaszynski, F. 1998. Introduction to the Upper Cretaceous. In: Mesozoic and Cenozoic Sequence Stratigraphy of European Basins (Eds P.-C. de Graciansky, J. Hardenbol, T. Jacquin and P.R. Vail), Special Publication - Society for Sedimentary Geology 60, pp. 329-332.

Hardenbol, J., Thierry, J., Farley, M.B., Jacquin, T., de Graciansky, P.-C. and Vail, P.R. 1998. Mesozoic and Cenozoic Sequence Stratigraphy of European Basins, SEPM Special Publication 60. Society for Sedimentary Geology, Tulsa.

Hardie, L.A. 1996. Secular variation in seawater chemistry: An explanation for the coupled secular variation in the mineralogies of marine limestones and potash evaporites over the past 600 m.y. Geology, 24: 279-283.

Haupt, B.J. and Seidov, D. 2001. Warm deep-water ocean conveyor during Cretaceous time. Geology, 29: 295-a-298.

Hays, J.D. and Pitman, W.C. 1973. Lithospheric Plate Motion, Sea Level Changes and Climatic and Ecological Consequences. Nature, 246: 18-22.

Heimhofer, U., Hochuli, P.A., Herrle, J.O., Andersen, N. and Weissert, H. 2004. Absence of major vegetation and palaeoatmospheric pCO ₂ changes associated with oceanic anoxic event 1a (early Aptian, SE France). Earth and Planetary Science Letters, 223: 303-318.

Hennig, S., Weissert, H. and Bulot, L. 1999. C-isotope stratigraphy, a calibration tool between ammonite- and magnetostratigraphy; the Valanginian-Hauterivian transition. Geologica Carpathica (Bratislava), 50: 91-96.

Hentz, T.F. and Ruppel, S.C. 2010. Regional Lithostratigraphy of the Eagle Ford Shale: Maverick Basin to East Texas Basin. Transactions - Gulf Coast Association of Geological Societies, 60: 325-337.

Herrle, J.O., Koessler, P., Friedrich, O., Erlenkeuser, H. and Hemleben, C. 2004. High-resolution carbon isotope records of the Aptian to lower Albian from SE France and the Mazagan Plateau (DSDP Site 545); a stratigraphic tool for paleoceanographic and paleobiologic reconstruction. Earth and Planetary Science Letters, 218: 149-161.

Hill, R.T. 1887a. The Texas section of the American Cretaceous. American Journal of Science, 34: 287-309.

Hill, R.T. 1887b. The topography and geology of the Cross Timbers and surrounding regions in northern Texas. American Journal of Science, 33: 291-303.

Hill, R.T. 1891. The Comanche Series of the Texas-Arkansas region. Geological Society of America Bulletin, 2: 503-528.

Hillgartner, H., van Buchem, F.S.P., Gaumet, F., Razin, P., Pittet, B., Grotsch, J. and Droste, H. 2003. The Barremian-Aptian Evolution of the Eastern Arabian Carbonate Platform Margin (Northern Oman). Journal of Sedimentary Research, 73: 756-773.

Hofmann, P., Stusser, I., Wagner, T., Schouten, S. and Damste, J.S.S. 2008. Climate-ocean coupling off north-west Africa during the lower Albian; the Oceanic Anoxic Event 1b. Palaeogeography, Palaeoclimatology, Palaeoecology, 262: 157-165.

Hovorka, S.D. 1996. High-frequency cyclicity during eustatic sea-level rise; Edwards Group of the Balcones fault zone. Transactions - Gulf Coast Association of Geological Societies, 46: 179-184.

Hovorka, S.D. and Nance, H.S. 1994. Dynamic depositional and early diagenetic processes in a deep-water shelf setting, Upper Cretaceous Austin Chalk, north Texas. Transactions - Gulf Coast Association of Geological Societies, 44: 269-276.

Huber, B.T., Norris, R.D. and MacLeod, K.G. 2002. Deep-sea paleotemperature record of extreme warmth during the Cretaceous. Geology, 30: 123-126.

Huck, S., Rameil, N., Korbar, T., Heimhofer, U., Wieczorek, T.D. and Immenhauser, A. 2010. Latitudinally different responses of Tethyan shoal-water carbonate systems to the Early Aptian oceanic anoxic event (OAE 1a). Sedimentology, 57: 1585-1614.

Hunt, D. and Tucker, M.E. 1993. Sequence stratigraphy of carbonate shelves with an example from the mid-Cretaceous (Urgonian) of Southeast France. Special Publication of the International Association of Sedimentologists, 18: 307-341.

Hunt, D.W. and Fitchen, W.M. 1999. Compaction and the dynamics of carbonate platform development; insights from the Permian Delaware and Midland basins; southeastern New Mexico and West Texas, USA. In: Advances in Carbonate Sequence Stratigraphy; Application to Reservoirs, Outcrops and Models (Eds P.M. Harris, A.H. Saller and J.A. Simo), pp. 75-106. Society of Economic Paleontologists and Mineralogists, Special Publication 63.

Imlay, R.W. 1945. Subsurface Lower Cretaceous formations of south Texas. AAPG Bulletin, 29: 1416-1469.

Immenhauser, A., Della Porta, G., Kenter, J.A.M. and Bahamonde, J.R. 2003. An alternative model for positive shifts in shallow-marine carbonate $\delta^{13}C$ and $\delta^{18}O$. Sedimentology, 50: 953-959.

Immenhauser, A., Hillgaertner, H. and van Bentum, E. 2005. Microbial-foraminiferal episodes in the early Aptian of the southern Tethyan margin; ecological significance and possible relation to oceanic anoxic event 1a. Sedimentology, 52: 77-99.

Immenhauser, A., Schlager, W., Burns, S.J., Scott, R.W., Geel, T., Lehmann, J., van der Gaast, S. and Bolder-Schrijver, L.J.A. 1999. Late Aptian to late Albian sea-level fluctuations constrained by geochemical and biological evidence (Nahr Umr Formation, Oman). Journal of Sedimentary Research, 69: 434-446.

Immenhauser, A. and Scott, R.W. 1999. Global correlation of middle Cretaceous sea-level events. Geology, 27: 551-554.

Immenhauser, A. and Scott, R.W. 2002. An estimate of Albian sea-level amplitudes and its implication for the duration of stratigraphic hiatuses. Sedimentary Geology, 152: 19-28.

Immenhauser, A., van der Kooij, B., van Vliet, A., Schlager, W. and Scott, R.W. 2001. An ocean-facing Aptian-Albian carbonate margin, Oman. Sedimentology, 48: 1187-1207.

Inden, R.F. and Moore, C.H. 1983. Beach environment. AAPG Memoir, 33: 211-265.

Irwin, H., Curtis, C. and Coleman, M. 1977. Isotopic evidence for source of diagenetic carbonates formed during burial of organic-rich sediments. Nature (London), 269: 209-213.

Jahren, A.H., Arens, N.C., Sarmiento, G., Guerrero, J. and Amundston, R. 2001. Terrestrial record of methan hydrate dissociation in the Early Cretaceous. Geology, 29: 159-162.

James, N.P. and Ginsburg, R.N. 1979. The morphology, sediments and organisms of the deep barrier reef and fore-reef. In: The seaward margin of Belize barrier and atoll reefs (Eds N.P. James and R.N. Ginsburg), International Association of Sedimentologists Special Publication 3, pp. 25-64.

James, N.P., Stevens, R.K., Barnes, C.R. and Knight, I. 1989. Evolution of a lower Paleozoic continental-margin carbonate platform, northern Canadian Appalachians. In: Controls on carbonate platform and basin development, (Eds P.D. Crevello, J.L. Wilson, J.F. Sarg, and J.F. Read) Society of Economic Paleontologists and Mineralogists Special Publication 44: 123-146.

Janson, X., Kerans, C., Loucks, R., Marhx, M.A., Reyes, C. and Murguia, F. 2011. Seismic architecture of a Lower Cretaceous platform-to-slope system, Santa Agueda and Poza Rica fields, Mexico. AAPG Bulletin, 95: 105-146.

Jarvis, I., Mabrouk, A., Moody, R.T.J. and de Cabrera, S. 2002. Late Cretaceous (Campanian) carbon isotope events, sea-level change and correlation of the Tethyan and Boreal realms. Palaeogeography, Palaeoclimatology, Palaeoecology, 188: 215-248.

Jarvis, I.A.N., Gale, A.S., Jenkyns, H.C. and Pearce, M.A. 2006. Secular variation in Late Cretaceous carbon isotopes: a new □13C carbonate reference curve for the Cenomanian-Campanian (99.6-70.6 Ma). Geological Magazine, 143: 561-608.

Jenkyns, H.C. 1980. Cretaceous anoxic events; from continents to oceans. Journal of the Geological Society of London, 137, 171-188.

Jenkyns, H.C. 1995. Carbon-isotope stratigraphy and paleoceanographic significance of the Lower Cretaceous shallow-water carbonates of Resolution Guyot, Mid-Pacific Mountains. Proceedings of the Ocean Drilling Program, Scientific Results, 143: 99-104.

Jenkyns, H.C. 2003. Evidence for rapid climate change in the Mesozoic-Palaeogene greenhouse world. Philosophical Transactions - Royal Society London, 361: 1885-1916.

Jiang, M.J. 1989. Biostratigraphy and geochronology of the Eagle Ford Shale, Austin Chalk, and lower Taylor marl in Texas based on calcareous nannofossils. PhD Dissertation, Texas A&M University, College Station, TX, 496 pp.

Jimenez Berrocoso, A., MacLeod, K.G., Martin, E.E., Bourbon, E., Londono, C.I. and Basak, C. 2010. Nutrient trap for Late Cretaceous organic-rich black shales in the tropical North Atlantic. Geology, 38: 1111-1114.

Johnson, C.C., Barron, E.J., Kauffman, E.G., Arthur, M.A., Fawcett, P.J. and Yasuda, M.K. 1996. Middle Cetaceous reef collapse linked to ocean heat transport. Geology, 24: 376-380.

Jones, C.E. and Jenkyns, H.C. 2001. Seawater strontium isotopes, oceanic anoxic events, and seafloor hydrothermal activity in the Jurassic and Cretaceous. American Journal of Science, 301: 112-149.

Kauffman, E.G. and Johnson, C.C. 1988. The morphological and ecological evolution of Middle and Upper Cretaceous reef-building rudistids. Palaios, 3: 194-216.

Keith, M.L. and Weber, J.N. 1965. Systematic relationships between carbon and oxygen isotopes in carbonates deposited by modern corals and algae. Science, 150: 498-501.

Keller, G., Berner, Z., Adatte, T. and Stueben, D. 2004. Cenomanian-Turonian and $\delta^{13}C$, and $\delta^{18}O$, sea level and salinity variations at Pueblo, Colorado. Palaeogeography, Palaeoclimatology, Palaeoecology, 211: 19-43.

Kerans, C. 2002. Styles of rudist buildup development along the northern margin of the Maverick Basin, Pecos River canyon, Southwest Texas. Transactions - Gulf Coast Association of Geological Societies, 52: 501-516.

Kerans, C. and Loucks, R.G. 2002. Stratigraphic setting and controls on occurrence of high-energy carbonate beach deposits; Lower Cretaceous of the Gulf of Mexico. Transactions - Gulf Coast Association of Geological Societies, 52: 517-526.

Kerans, C. and Tinker, S.W. 1997. Sequence Stratigraphy and Characterization of Carbonate Reservoirs, SEPM Short Course No. 40. Society for Sedimentary Geology, Tulsa, OK, 130 pp.

Kleypas, J.A., Buddemeier, R.W., Archer, D., Gattuso, J.P., Langdon, C. and Opdyke, B.N. 1999. Geochemical consequences of increased atmospheric carbon dioxide on coral reefs. Science, 284: 181-198.

Kominz, M.A. 1984. Oceanic ridge volumes and sea-level change; an error analysis. AAPG Memoir, 36: 109-127.

Koutsoukos, E.A.M., Destro, N., de Azambuja Filho, N.C. and Spadini, A.R. 1993. Upper Aptian-lower Coniacian carbonate sequences in the Sergipe Basin, northeastern Brazil. In: Cretaceous carbonate platforms (Eds J.A.T. Simo, R.W. Scott, and J.-P. Masse): AAPG Memoir, 56: 127-144.

Koutsoukos, E.A.M., Mello, M.R. and de Azambuja Filho, N.C. 1991. Micropalaeontological and geochemical evidence of Mid-Cretaceous dysoxic-anoxic palaeoenvironments in the Sergipe Basin, northeastern Brazil. In: Modern and Ancient Continental Shelf Anoxia, (Eds R.V. Tyson and T.H. Pearson) Geological Society Special Publications, 58: 427-447.

Kump, L.R. and Arthur, M.A. 1999. Interpreting carbon-isotope excursions: carbonates and organic matter. Chemical Geology, 161: 181-198.

Kuroda, J., Ogawa, N.O., Tanimizu, M., Coffin, M.F., Tokuyama, H., Kitazato, H. and Ohkouchi, N. 2007. Contemporaneous massive subaerial volcanism and Late Cretaceous Oceanic Anoxic Event 2. Earth and Planetary Science Letters, 256: 211-223.

Larson, R.L. 1991. Latest pulse of Earth: Evidence for a mid-Cretaceous superplume. Geology, 19: 547-550.

Larson, R.L. and Erba, E. 1999. Onset of the mid-Cretaceous greenhouse in the Barremian-Aptian: Igneous events and the biological, sedimentary, and geochemical responses. Paleoceanography, 14: 663-678.

Leckie, R.M., Bralower, T.J. and Cashman, R. 2002. Oceanic anoxic events and plankton evolution; biotic response to tectonic forcing during the Mid-Cretaceous. Paleoceanography, 17.

Lehmann, C., Osleger, D.A. and Montanez, I. 2000. Sequence stratigraphy of Lower Cretaceous (Barremian-Albian) carbonate platforms of northeastern Mexico; regional and global correlations. Journal of Sedimentary Research, 70: 373-391.

Lehmann, C., Osleger, D.A., Montanez, I.P., Sliter, W.V., Arnaud-Vanneau, A. and Banner, J.L. 1999. Evolution of Cupido and Coahuila carbonate platforms, Early Cretaceous, northeastern Mexico. Geological Society of America Bulletin, 111: 1010-1029.

Lehrmann, D.J. and Goldhammer, R.K. 1999. Secular variation in parasequence and facies stacking patterns of platform carbonates; a guide to application of stacking-patterns analysis in strata of diverse ages and settings. In: Recent Advances in Carbonate Sequence Stratigraphy; Applications to Reservoirs, Outcrops and Models, (Eds P.M. Harris, A.H. Saller, J.A. Simo) Society for Sedimentary Geology Special Publication , 63: 187-225.

Li, X., Jenkyns, H.C., Wang, C., Hu, X., Chen, X., Wei, Y., Huang, Y. and Cui, J. 2006. Upper Cretaceous carbon- and oxygen-isotope stratigraphy of hemipelagic carbonate facies from southern Tibet, China. Journal of the Geological Society of London, 163: 375-382.

Li, Y.-X., Bralower, T.J., Montanez, I.P., Osleger, D.A., Arthur, M.A., Bice, D.M., Herbert, T.D., Erba, E. and Premoli Silva, I. 2008. Toward an orbital chronology for the early Aptian oceanic anoxic event (OAE1a, approximately 120 Ma). Earth and Planetary Science Letters, 271: 88-100.

Liro, L.M., Dawson, W.C., Katz, B. and Robison, V.D. 1994. Sequence Stratigraphic Elements and Geochemical Variability within a "Condensed Section": Eagle Ford Group, East-Central Texas. Transactions - Gulf Coast Association of Geological Societies, 44: 303-402.

Lock, B.E., Bases, F.S. and Glaser, R.A. 2007. The Cenomanian sequence stratigraphy of central to West Texas. Transactions - Gulf Coast Association of Geological Societies, 57: 465-479.

Lock, B.E. and Peschier, L. 2006. Boquillas (Eagle Ford) upper slope sediments, West Texas; outcrop analogs for potential shale reservoirs. Transactions - Gulf Coast Association of Geological Societies, 56: 491-508.

Locklair, R., Sageman, B. and Lerman, A. 2011. Marine carbon burial flux and the carbon isotope record of Late Cretaceous (Coniacian–Santonian) Oceanic Anoxic Event III. Sedimentary Geology, 235: 38-49.

Locklair, R.E., Sageman, B. and Anonymous 2004. Development of a Coniacian-Santonian orbital time scale and comparative estimates of primary production vs. dilution for Late Cretaceous chalk facies. Abstracts with Programs - Geological Society of America, 36: 304.

Loucks, R.G. 1976. Pearsall formation, Lower Cretaceous, south Texas: depositional facies and carbonate diagenesis and their relationship to porosity. PhD Dissertation, The University of Texas at Austin, Austin, 362 pp.

Loucks, R.G. 1977. Porosity development and distribution in shoal-water carbonate complexes; subsurface Pearsall Formation (Lower Cretaceous), South Texas. In: Cretaceous Carbonates of Texas and Mexico: Applications to Subsurface Exploration (Eds D.G. Bebout and R.G. Loucks), Texas Bureau of Economic Geology Report of Investigations No. 89, pp. 97-126.

Loucks, R.G. 2002. Controls on reservoir quality in platform-interior limestones around the Gulf of Mexico; example from the Lower Cretaceous Pearsall Formation in South Texas. Transactions - Gulf Coast Association of Geological Societies, 52: 659-672.

Loucks, R.G. and Kerans, C. 2003. Lower Cretaceous Glen Rose 'patch reef' reservoir in the Chittim Field, Maverick County, south Texas. Transactions - Gulf Coast Association of Geological Societies, 53: 490-503.

Lozo, F.E., Nelson, H.F., Young, K.P., Shelburne, O.B. and Sandidge, J.R. 1959. Symposium on Edwards limestone in central Texas, University of Texas Publication 5905, Austin, TX, 235 pp.

Lozo, F.E. and Smith, C.I. 1964. Revision of Comanche Cretaceous stratigraphic nomenclature, southern Edwards Plateau, southwest Texas. Transactions - Gulf Coast Association of Geological Societies, 14: 285-306.

Lozo, F.E. and Stricklin, F.L., Jr. 1956. Stratigraphic notes on the outcrop basal Cretaceous, central Texas. Transactions - Gulf Coast Association of Geological Societies, 6: 67-78.

Lozo, F.E., Stricklin, F.L., Smith, C.I., Amsbury, D.L. and Perkins, B.F. 1958. Field Conference Guidebook: Features of Shelf-Carbonate Deposits, Lower Cretaceous of Central Texas. In: Third Carbonate Seminar: Depositional Environments - Porosity Relations, Shell Development Company, EPR Division Publication 10, pp. 60.

Mancini, E.A., Obid, J., Badali, M., Liu, K. and Parcell, W.C. 2008. Sequence-stratigraphic analysis of Jurassic and Cretaceous strata and petroleum exploration

in the central and eastern Gulf coastal plain, United States. AAPG Bulletin, 92: 1655-1686.

Mancini, E.A. and Puckett, T.M. 2002. Transgressive-regressive cycles in Lower Cretaceous strata, Mississippi Interior Salt Basin area of the northeastern Gulf of Mexico. Cretaceous Research, 23: 409-438.

Mancini, E.A. and Scott, R.W. 2006. Sequence stratigraphy of Comanchean Cretaceous outcrop strata of Northeast and South-Central Texas; implications for enhanced petroleum exploration. Transactions - Gulf Coast Association of Geological Societies, 56: 539-550.

McFarlan, E., Jr. 1977. Lower Cretaceous sedimentary facies and sea level changes, U.S. Gulf Coast. In: Cretaceous Carbonates of Texas and Mexico: Applications to Subsurface Exploration (Eds D.G. Bebout and R.G. Loucks), Texas Bureau of Economic Geology Report of Investigations No. 89, pp. 5-11.

McFarlan, E., Jr. and Menes, L.S. 1991. Lower Cretaceous. In: The geology of North America (Ed A. Salvador), J, pp. 181-204. Geological Society of America: Boulder, CO, United States.

McMaster, R.L. and Conover, J.T. 1966. Recent algal stromatolites from the Canary Islands. Journal of Geology, 74: 647-652.

McNamee, D.F. 1969. The Glen Rose reef complex of east Texas and central Louisiana. Transactions - Gulf Coast Association of Geological Societies, 19: 11-21.

Mehay, S., Keller, C.E., Bernasconi, S.M., Weissert, H., Erba, E., Bottini, C. and Hochuli, P.A. 2009. A Volcanic CO2 pulse triggered the Cretaceous Oceanic Anoxix Event 1a and a biocalcification crisis. Geology, 37: 819-822.

Menegatti, A.P., Weissert, H., Brown, R.S., Tyson, R.V., Farrimond, P., Strasser, A. and Caron, M. 1998. High-resolution delta (super 13) C stratigraphy through the early Aptian 'Livello Selli' of the Alpine Tethys. Paleoceanography, 13: 530-545.

Moldovanyi, E.P., and Lohmann, K.C. 1984. Isotopic and petrographic record of phreatic diagenesis: lower Cretaceous Sligo and Cupido formations. Journal of Sedimentary Petrology, 54: 972-985.

Miller, K.G., Sugarman, P.J., Browning, J.V., Kominz, M.A., Olsson, R.K., Feigenson, M.D. and Hernandez, J.C. 2004. Upper Cretaceous sequences and sea-level history, New Jersey Coastal Plain. Geological Society of America Bulletin, 116: 368-393.

Miller, K.G., Wright, J.D. and Browning, J.V. 2005. Visions of ice sheets in a greenhouse world. Marine Geology, 217: 215-231.

Mitchum, R.M. and Van Wagoner, J.C. 1991. High-frequency sequences and their stacking patterns; sequence-stratigraphic evidence of high-frequency eustatic cycles. Sedimentary Geology, 70: 131-160.

Montanez, I.P. and Read, J.F. 1992. Eustatic control on early dolomitization of cyclic peritidal carbonates: Evidence from the Early Ordovician Upper Knox Group, Appalachians. Geological Society of America Bulletin, 104: 872-886.

Montgomery, S. 1990. A quarterly investigation into the nation's most promising petroleum horizons and provinces, Horizontal drilling in the Austin Chalk: Part 1: Geology, Drilling History and Field rules. Petroleum Frontiers, 7.

Montgomery, S.L., Petty, A.J. and Post, P.J. 2002. James Limestone, northeastern Gulf of Mexico: Refound opportunity in a Lower Cretaceous trend. AAPG Bulletin, 86: 381-397.

Montoya-Pino, C., Weyer, S., Anbar, A.D., Pross, J., Oschmann, W., van de Schootbrugge, B. and Arz, H.W. 2010. Global enhancement of ocean anoxia during Oceanic Anoxic Event 2: A quantitative approach using U isotopes. Geology, 38: 315-318.

Moore, C.H. 1996. Anatomy of a sequence boundary-Lower Cretaceous Glen Rose/Fredericksburg, Central Texas Platform. Transactions - Gulf Coast Association of Geological Societies, 46: 313-320.

Moore, C.H. 2001. Carbonate Reservoirs, Porosity Evolution and Diagenesis in a Sequence Stratigraphic Framework. Elsevier, New York, 444. pp.

Moore, C.H., Jr. 1964. Stratigraphy of the Fredericksburg division, south-central Texas. Texas Bureau of Economic Geology Report of Investigations No. 52: Austin, TX, United States, United States, 48 pp.

Moore, C.H., Jr. and Martin, K.G. 1966. Comparison of quartz and carbonate shallow marine sandstones, Fredericksburg Cretaceous, central Texas. Bulletin of the American Association of Petroleum Geologists, 50: 981-1000.

Moriya, K., Wilson, P.A., Friedrich, O., Erbacher, J. and Kawahata, H. 2007. Testing for ice sheets during the mid-Cretaceous greenhouse using glassy foraminiferal calcite from the mid-Cenomanian tropics on Demerara Rise. Geology, 35: 615-618.

Mort, H.P., Adatte, T., Follmi, K.B., Keller, G., Steinmann, P., Matera, V., Berner, Z. and Stuben, D. 2007. Phosphorus and the roles of productivity and nutrient recycling during oceanic anoxic event 2. Geology, 35: 483-486.

Mortyn, P.G. and Charles, C.D. 2003. Planktonic foraminiferal depth habitat and delta d18O calibrations; plankton tow results from the Atlantic sector of the Southern Ocean. Paleoceanography, 18, NO. 2, 1037, doi:10.1029/2001PA000637.

Moullade, M., Kuhnt, W., Bergen, J.A., Massed, J.P. and Tronchetti, G. 1998. Correlation of biostratigraphic and stable isotope events in the Aptian historical stratotype of La Bedoule (Southeast France). Comptes Rendus de l'Academie des Sciences, Serie II. Sciences de la Terre et des Planetes, 327: 693-698.

Mutti, M., Droxler, A.W. and Cunningham, A.D. 2005. Evolution of the northern Nicaragua Rise during the Oligocene-Miocene; drowning by environmental factors. Sedimentary Geology, 175: 237-258.

Nelson, H.F. 1959. Deposition and Alteration of the Edwards Limestone, Central Texas. In: Symposium on Edwards Limestone in Central Texas (Eds F.E. Lozo, H.F. Nelson, K.P. Young, O.B. Shelburne and J.R. Sandidge), University of Texas Publication 5905, pp. 21-104.

Neuweiler, F. 1993. Development of Albian microbialites and microbialite reefs at marginal platform areas of the Vasco-Cantabrian Basin (Soba reef area, Cantabria, N. Spain). Facies, 29: 231-250.

Osleger, D.A., Barnaby, R. and Kerans, C. 2004. A Laterally Accreting Grainstone Margin from the Albian of Northern Mexico: Outcrop Model for Cretaceous Carbonate Reservoirs. In: Integration of outcrop and modern analogs in reservoir modeling (Eds M.G. Grammer, P.M. Harris and G.P. Eberli), AAPG Memoir 80, pp. 93-107.

Parente, M., Frijia, G. and Di Lucia, M. 2007. Carbon-isotope stratigraphy of Cenomanian-Turonian platform carbonates from the southern Apennines (Italy): a chemostratigraphic approach to the problem of correlation between shallow-water and deep-water successions. Journal of the Geological Society, 164: 609-620.

Parente, M., Frijia, G., Di Lucia, M., Jenkyns, H.C., Woodfine, R.G. and Baroncini, F. 2008. Stepwise extinction of larger foraminifers at the Cenomanian-Turonian boundary: A shallow-water perspective on nutrient fluctuations during Oceanic Anoxic Event 2 (Bonarelli Event). Geology, 36: 715-718.

Patterson, W.P. and Walter, L.M. 1994. Depletion of 13C in seawater {Sigma}C02 on modern carbonate platforms: Significance for the carbon isotopic record of carbonates. Geology, 22: 885-888.

Perkins, B.F. 1974. Paleoecology of a rudist reef complex in the Comanche Cretaceous Glen Rose Limestone of central Texas. Geoscience and Man, 8: 131-173.

Pessagno, E.A. 1969. Upper Cretaceous stratigraphy of the western Gulf Coast area of Mexico, Texas, and Arkansas. Geological Society of America Memoir, 111, 139 pp.

Pigram, C.J., Davies, P.J., Feary, D.A. and Symonds, P.A. 1989. Tectonic controls on carbonate platform evolution in southern Papua New Guinea: Passive margin to foreland basin. Geology, 17: 199-202.

Pittet, B., van Buchem, F.S.P., Hillgaertner, H., Razin, P., Groetsch, J. and Droste, H. 2002. Ecological succession, palaeoenvironmental change, and depositional sequences of Barremian-Aptian shallow-water carbonates in northern Oman. Sedimentology, 49: 555-581.

Pittman, J.G. 1989. Stratigraphy of Glen Rose Formation, western Gulf Coastal Plain. Transactions - Gulf Coast Association of Geological Societies, 73: 247-264.

Playford, P.E. 1980. Devonian "great barrier reef" of Canning Basin, Western Australia. AAPG Bulletin, 64: 814-840.

Poulsen, C.J., Barron, E.J., Arthur, M.A. and Peterson, W.H. 2001. Response of the Mid-Cretaceous global oceanic circulation to tectonic and CO_2 forcings. Paleoceanography, 16: 576-592.

Poulsen, C.J., Gendaszek, A.S. and Jacob, R.L. 2003. Did the rifting of the Atlantic Ocean cause the Cretaceous thermal maximum? Geology Boulder, 31: 115-118.

Pratt, L.M., Arthur, M.A., Dean, W.E. and Scholle, P.A. 1984. Paleoceanographic cycles and events during the Late Cretaceous in the Western Interior Seaway. In: Cretaceous Evolution of the Western Interior Basin of North America (Eds W.G.E. Caldwell and E.G. Kaufman), Special Paper 39: 333-353.

Prezbindowski, D.R. 1981. Carbonate rock-water diagenesis Lower Cretaceous, Stuart City trend, south Texas. PhD Dissertation, University of Texas at Austin, Austin, 236 pp.

Price, G.D. 2003. New constraints upon isotope variation during the early Cretaceous (Barremian-Cenomanian) from the Pacific Ocean. Geological Magazine, 140: 513-522.

Puceat, E., Lecuyer, C., Sheppard, S.M.F., Dromart, G., Reboulet, S. and Grandjean, P. 2003. Thermal evolution of Cretaceous Tethyan marine waters inferred from oxygen isotope composition of fish tooth enamels. Paleoceanography, 18, NO. 2, 1029, doi:10.1029/2002PA000823

Radoicic, R. 1959. Nekoliko problematic nih mikrofosila iz dinarske krede. Bull. Serv. Geol. Geophys. R. P. Serbie, 17: 87-92.

Rameil, N., Immenhauser, A., Warrlich, G., Hillgaertner, H. and Droste, H.J. 2010. Morphological patterns of Aptian Lithocodium-Bacinella geobodies; relation to environment and scale. Sedimentology, 57: 883-911.

Read, J.F. 1998. Phanerozoic carbonate ramps from greenhouse, transitional and ice-house worlds; clues from field and modelling studies. Geological Society Special Publications, 149: 107-135.

Reboulet, S., Giraud, F. and Proux, O. 2005. Ammonoid Abundance Variations Related to Changes in Trophic Conditions Across the Oceanic Anoxic Event 1d (Latest Albian, SE France). Palaios, 20: 121-141.

Riebesell, U., Zondervan, I., Rost, B., Tortell, P.D., Zeebe, R.E. and Morel, F.M. 2000. Reduced calcification of marine plankton in response to increased atmospheric pCO_2. Nature (London), 407: 364-367.

Roehl, U. and Ogg, J.G. 1996. Aptian-Albian sea level history from guyots in the western Pacific. Paleoceanography, 11: 595-624.

Rosales, I. 1999. Controls on carbonate-platform evolution on active fault blocks; The Lower Cretaceous Castro Urdiales platform (Aptian-Albian, Northern Spain). Journal of Sedimentary Research, 69: 447-465.

Rose, P.R. 1972. Edwards Group, Surface and Subsurface, Central Texas. Texas Bureau of Economic Geology Report of Investigations 74, The University of Texas at Austin, Austin, TX, 198 pp.

Sahagian, D., Pinous, O., Olferiev, A. and Zakharov, V. 1996. Eustatic Curve for the Middle Jurassic-Cretaceous Based on Russian Platform and Siberian Stratigraphy: Zonal Resolution. AAPG Bulletin, 80: 1433-1458.

Salvador, A. 1991a. Origin and development of the Gulf of Mexico Basin. In: The geology of North America (Ed A. Salvador), pp. 389-444. Geological Society of America : Boulder, CO, United States.

Salvador, A. 1991b. Triassic-Jurassic. In: The geology of North America (Ed A. Salvador), pp. 131-180. Geological Society of America: Boulder, CO, United States.

Sawyer, D.S., Buffler, R.T. and Pilger, R.H., Jr. 1991. The crust under the Gulf of Mexico Basin. In: The geology of North America (Ed A. Salvador), J, pp. 53-72. Geological Society of America: Boulder, CO, United States.

Schlager, W. 1981. The paradox of drowned reefs and carbonate platforms. Geological Society of America Bulletin, 92: 197-211.

Schlager, W. 1991. Depositional bias and environmental change - important factors in sequence stratigraphy. Sedimentary Geology, 70: 109-130.

Schlager, W. 2005. Carbonate Sedimentology and Sequence Stratigraphy. Concepts in Sedimentology and Paleontology 8. Society of Economic Paleontologists and Mineralogists, Tulsa, OK, 200 pp.

Schlanger, S.O., Arthur, M.A., Jenkyns, H.C. and Scholle, P.A. 1987. The Cenomanian-Turonian oceanic anoxic event; I, Stratigraphy and distribution of organic carbon-rich beds and the marine $\delta^{13}C$ excursion. In: Marine Petroleum Source Rocks (Eds J. Brooks and A.J. Fleet), Geological Society Special Publications, 26, pp. 371-399.

Schlanger, S.O. and Jenkyns, H.C. 1976. Cretaceous oceanic anoxic events; causes and consequences. Netherlands Journal of Geosciences, 55: 179-184.

Scholle, P.A. and Arthur, M.A. 1980. Carbon isotope fluctuations in Cretaceous pelagic limestones; potential stratigraphic and petroleum exploration tool. AAPG Bulletin, 64: 67-87.

Scotese, C.R., Gahagan, L.M. and Larson, R.L. 1988. Plate tectonic reconstructions of the Cretaceous and Cenozoic ocean basins. Tectonophysics, 155: 27-48.

Scott, R.J. 2003. The Maverick Basin: New technology -- New Success. In: Structure and Stratigraphy of south Texas and Northeast Mexico: Applications to Exploration, CD ROM, pp. 18. GCSSEPM Foundation, South Texas Geological Society.

Scott, R.W. 1979. Depositional model of Early Cretaceous coral-algal-rudist reefs, Arizona. AAPG Bulletin, 63: 1108-1127.

Scott, R.W. 1981. Biotic relations in Early Cretaceous coral-algal-rudist reefs, Arizona. Journal of Paleontology, 55: 463-478.

Scott, R.W. 1984. Evolution of Early Cretaceous reefs in the Gulf of Mexico. Palaeontographica Americana, 54: 406-412.

Scott, R.W. 1988. Evolution of Late Jurassic and Early Cretaceous reef biotas. Palaios, 3: 184-193.

Scott, R.W. 1990a. Chronostratigraphy of the Cretaceous carbonate shelf, southeastern Arabia. Geological Society Special Publications, 49: 89-108.

Scott, R.W. 1990b. Models and stratigraphy of Mid Cretaceous reef communities, Gulf of Mexico. SEPM Concepts in Sedimentology and Paleontology, 2, 102 pp.

Scott, R.W. 1993. Cretaceous carbonate platform, U.S. Gulf Coast. In: Cretaceous Carbonate Platforms (Eds T.J.A. Simo, R.W. Scott and J.-P. Masse), AAPG Memoir 56, pp. 97-109.

Scott, R.W. 1995. Global environmental controls on Cretaceous reefal ecosystems. Palaeogeography, Palaeoclimatology, Palaeoecology, 119: 187-199.

Scott, R.W., Benson, D.G., Morin, R.W., Shaffer, B.L. and Oboh-Ikuenobe, F.E. 2002. Integrated Albian-lower Cenomanian chronostratigraphy standard, Trinity River section, Texas. In: R.W. Scott, GCSSEPM Foundation Special Publications in Geology, 1: 277-334.

Scott, R.W., Fee, D., Magee, R. and Laali, H. 1978. Epeiric depositional models for the Lower Cretaceous Washita Group; North-central Texas. Texas Bureau of Economic Geology Report of Investigations, 94, University of Texas at Austin, Austin, TX, 23 pp.

Scott, R.W., Fernandez-Mendiola, P.A., Gili, E. and Simo, A. 1990. Persistence of coral-rudist reefs into the Late Cretaceous. Palaios, 5: 98-110.

Scott, R.W., Franks, P.C., Stein, J.A., Bergen, J.A. and Evetts, M.J. 1994. Graphic correlation tests the synchronous Mid-Cretaceous depositional cycles: Western Interior and Gulf Coast. In: Unconformity-related hydrocarbons in sedimentary sequences (Eds J.C. Dolson, M.L. Hendricks and W.A. Westcott), pp. 89-98. Rocky Mountain Association of Geologists, Denver, Colorado.

Scott, R.W. and Kerans, C. 2002. Late Albian carbonate platform chronostratigraphy, Devils River Formation cycles, West Texas, In: Proceedings of Annual Rudist Biostratigraphy Congress (Ed P.W. Skelton), pp. 26.

Scott, R.W., Laali, H. and Fee, D. 1975. Density-current strata in Lower Cretaceous Washita Group, north-central Texas. Journal of Sedimentary Petrology, 45: 562-575.

Scott, R.W., Molineux, A.M., Loeser, H. and Mancini, E.A. 2007. Lower Albian sequence stratigraphy and coral buildups; Glen Rose Formation, Texas, U.S.A. In: Cretaceous Rudists and Carbonate Platforms: Environmental Feedback (Ed R.W. Scott) Society for Sedimentary Geology Special Publication, 87: 181-191.

Scott, R.W., Schlager, W., Fouke, B. and Nederbragt, S.A. 2000. Are Mid-Cretaceous Eustatic Events Recorded in Middle East Carbonate Platforms. In: Middle East Models of Jurassic/Cretaceous Carbonate Systems (Eds A.S. Alsharan and R.W. Scott), SEPM Special Publication 69, p 77-88.

Sharland, P.R., Archer, R., Casey, D.M., Davies, R.B., Hall, S.H., Heward, A.P., Horbury, A.D. and Simmons, M.D. 2001. Arabian Plate Sequence Stratigraphy, GeoArabian Special Publication 2. Gulf PetroLink, Manama, Bahrain, 371 pp.

Shiraishi, F. and Kano, A. 2004. Composition and spatial distribution of microencrusters and microbial crusts in Upper Jurassic-Lowermost Cretaceous reef limestone (Torinosu Limestone, southwest Japan). Facies, 50: 217-227.

Shumard, B.F. 1860. Observations upon the Cretaceous strata of Texas. St. Louis Academy of Science Transactions, 1: 582-590.

Simo, J.A.T. 1993. Cretaceous carbonate platforms and stratigraphic sequences, south-central Pyrenees, Spain. In: Cretaceous carbonate platforms (Eds J.A.T. Simo, R.W. Scott, and J.-P. Masse): AAPG Memoir, 56: 325-342.

Sinton, C.W. and Duncan, R.A. 1997. Potential links between ocean plateau volcanism and global ocean anoxia at the Cenomanian-Turonian boundary. Economic Geology, 92: 836-842.

Sloss, L.L. 1963. Sequences in the Cratonic Interior of North America. Geological Society of America Bulletin, 74: 93-114.

Sohl, N.F., Martinez R, E., Salmeron-Urena, P. and Soto-Jaramillo, F. 1991. Upper Cretaceous In: The Geology of North America (Ed A. Salvador), J, pp. 205-244. Geological Society of America: Boulder, CO, United States.

Sonnenfeld, M.D. and Cross, T.A. 1993. Volumetric partitioning and facies differentiation within the Permian upper San Andres Formation of Last Chance Canyon, Guadalupe Mountains, New Mexico. In: Carbonate Sequence Stratigraphy: Recent Developments and Applications (Ed B. Loucks and R.J. Sarg) AAPG Memoir, 57, pp. 435-474.

Stanley, S.M. and Hardie, L.A. 1998. Secular oscillations in the carbonate mineralogy of reef-building and sediment-producing organisms driven by tectonically forced shifts in seawater chemistry. Palaeogeography, Palaeoclimatology, Palaeoecology, 144: 3-19.

Stapp, W.L. 1977. The geology of the fractured Austin and Buda formations in the subsurface of South Texas. Transactions - Gulf Coast Association of Geological Societies, 27: 208-229.

Steuber, T. 2002. Plate tectonic control on the evolution of Cretaceous platform-carbonate production. Geology, 30: 259-262.

Stoll, H.M. and Schrag, D.P. 2000. High-resolution stable isotope records from the Upper Cretaceous rocks of Italy and Spain: Glacial episodes in a greenhouse planet? Geological Society of America Bulletin, 112: 308-319.

Steuber, T. 1996. Stable isotope sclerochronology of rudist bivalves: Growth rates and late Cretaceous seasonality. Geology, 24: 315-318.

Strasser, A. 1988. Shallowing-upward sequences in Purbeckian peritidal carbonates (lowermost Cretaceous, Swiss and French Jura Mountains). Sedimentology, 35: 369-383.

Stricklin, F.L., Jr., Smith, C.I. and Lozo, F.E. 1971. Stratigraphy of lower Cretaceous Trinity deposits of central Texas. Texas Bureau of Economic Geology Report of Investigations, 71. University of Texas at Austin, Austin, TX, 63 pp.

Surles, M.A. 1987. Stratigraphy of the Eagle Ford Group (Upper Cretaceous) and its source-rock potential in the East Texas Basin. Baylor Geological Studies, Bulletin, 45.

Swart, P.K. and Eberli, G.P. 2005. The nature of the $\delta^{13}C$ of periplatform sediments; implications for stratigraphy and the global carbon cycle. Sedimentary Geology, 175: 115-129.

Swart, P.K., Reijmer, J.J.G. and Otto, R. 2009. A re-evaluation of facies on Great Bahama Bank; II, Variations in the $\delta^{13}C$, $\delta^{18}O$ and mineralogy of surface sediments. Special Publication of the International Association of Sedimentologists, 41: 47-59.

Szabo, B.J. and Moore, J.G. 1986. Age of -360-m reef terrace, Hawaii, and the rate of late Pleistocene subsidence of the island. Geology, 14: 967-968.

Talbert, S.J. and Atchley, S.C. 2000. Sequence stratigraphy of the Lower Cretaceous (Albian) Fredericksburg Group, central and North Texas. Transactions - Gulf Coast Association of Geological Societies, 50: 369-377.

Tartamella, N.J. 1982. An ecostratigraphic model for shelf platform development of middle Cretaceous (Stuart City) limestones of south Texas. Transactions - Gulf Coast Association of Geological Societies, 32: 483-495.

Tejada, M.L.G., Mahoney, J.J., Neal, C.R., Duncan, R.A. and Petterson, M.G. 2002. Basement geochemistry and geochronology of central Malaita, Solomon Islands, with implications for the origin and evolution of the Ontong Java Plateau. Journal of Petrology, 43: 449-484.

Tejada, M.L.G., Suzuki, K., Kuroda, J., Coccioni, R., Mahoney, J.J., Naohiko, O., Sakamoto, T. and Tatsumi, Y. 2009. Ontong Java Plateau eruption as a trigger for the early Aptian oceanic anoxic event. Geology, 37: 855-858.

Tsikos, H., Karakitsios, V., Van Breugel, Y., Walsworth-Bell, B.E.N., Bombardiere, L., Petrizzo, M.R., Damste, J.S.S., Schouten, S., Erba, E., Silva, I.P., Farrimond, P., Tyson, R.V. and Jenkyns, H.C. 2004. Organic-carbon deposition in the Cretaceous of the Ionian Basin, NW Greece: the Paquier Event (OAE 1b) revisited. Geological Magazine, 141: 401-416.

Tucker, M.E. and Wright, V.P. 1990. Carbonate Sedimentology. Blackwell Scientific Publications, Oxford, 482 pp.

Turgeon, S.C. and Creaser, R.A. 2008. Cretaceous oceanic anoxic event 2 triggered by a massive magmatic episode. Nature (London), 454: 323-326.

Tyrrell, W.W., Jr. and Scott, R.W. 1989. Early Cretaceous shelf margins, Vernon Parish, Louisiana. In: Atlas of Seismic Stratigraphy (Ed A.W. Bally), AAPG Studies in Geology 27, pp. 11-17.

Vahrenkamp, V.C. 1996. Carbon isotope stratigraphy of the upper Kharaib and Shuaiba Formations; implications for the Early Cretaceous evolution of the Arabian Gulf region. AAPG Bulletin, 80: 647-662.

Vahrenkamp, V.C. 2010. Chemostratigraphy of the Lower Cretaceous Shu'aiba Formation: A $\delta^{13}C$ reference profile for the Aptian Stage from the southern Neo-Tethys Ocean. In: Barremian – Aptian stratigraphy and hydrocarbon habitat of the eastern Arabian Plate (Eds F.S.P. van Buchem, M.I. Al-Husseini, F. Maurer and H.J. Droste), GeoArabia Special Publication 4, pp. 107-138.

Vahrenkamp, V.C., Franssen, R.C.M.W., Grotsch, J. and Munoz, P.J. 1993. Maracaibo Platform (Aptian-Albian), northwestern Venezuela. AAPG Memoir, 56: 25-33.

van Buchem, F.S.P., Al-Husseini, M.I., Maurer, F., Droste, H.J. and Yose, L.A. 2010. Sequence-stratigraphic synthesis of the Barremian - Aptian of the eastern Arabian Plate and implications for the petroleum habitat. In: Barremian - Aptian stratigraphy and hydrocarbon habitat of the eastern Arabian Plate (Eds F.S.P. Van Buchem, M.I. Al-Husseini, F. Maurer and H.J. Droste), GeoArabia Special Publication 4, pp. 9-48.

van Buchem, F.S.P., Razin, P., Homewood, P.W., Oterdoom, W.H. and Philip, J. 2002. Stratigraphic Organization of Carbonate Ramps and Organic-Rich Intrashelf Basins: Natih Formation (Middle Cretaceous) of Northern Oman. AAPG Bulletin, 86: 21-53.

van de Schootbrugge, B., Foellmi, K.B., Bulot, L.G. and Burns, S.J. 2000. Paleoceanographic changes during the Early Cretaceous (Valanginian-Hauterivian): evidence from oxygen and carbon stable isotopes. Earth and Planetary Science Letters, 181: 15-31.

Van Wagoner, J.C., Posamentier, H.W., Mitchum, R.M., Vail, P.R., Sarg, J.F., Loutit, T.S. and Hardenbol, J. 1988. An overview of the fundamentals of sequence stratigraphy and key definitions. In: Sea-Level Changs – an Integrated Approach (Eds C.K. Wilgus, H. Posamentier, C.A. Ross and C.G.St.C. Kendall) SEPM Special Publication, 42: 39-45.

Wagner, T., Herrle, J.O., Sinninghe Damste, J.S., Schouten, S., Stuesser, I. and Hofmann, P. 2008. Rapid warming and salinity changes of Cretaceous surface waters in the subtropical North Atlantic. Geology, 36: 203-206.

Wagner, T., Wallmann, K., Herrle, J.O., Hofmann, P. and Stuesser, I. 2007. Consequences of moderate approximately 25,000 yr lasting emission of light CO (sub 2) into the mid-Cretaceous ocean. Earth and Planetary Science Letters, 259: 200-211.

Waite, L.E. 2009. Stuart City trend of the Edwards Formation, south Texas, revisted: new data, new concepts. Bulletin of the South Texas Geologic Society, 50: 15-36.

Waite, L.E., Scott, R.W. and Kerans, C. 2007. Middle Albian age of the regional dense marker bed of the Edwards Group, Pawnee Field, south-central Texas. Transactions - Gulf Coast Association of Geological Societies, 57: 759-774.

Ward, W.B. 1996. Platform evolution and diagenesis of Frasnian carbonate platforms, Devonian reef complexes, Napier Range, Canning Basin, Western Australia, PhD Dissertation, State University of New York at Stony Brook, 566 pp.

Ward, W.C. and Ward, W.B. 2007. Stratigraphy of middle part of Glen Rose Formation (Lower Albian), Canyon Lake Gorge, Central Texas, U.S.A. In: Cretaceous Rudists and Carbonate Platforms: Environmental Feedback (Ed R.W. Scott), SEPM Special Publication, 87: 193-210.

Watts, A.B. and Ryan, W.B.F. 1976. Flexure of the lithosphere and continental margin basins. Tectonophysics, 36: 25-44.

Weber, J.N. 1965. Fractionation of stable isotopes of O and C in marine calcareous organisms. Geochemica et Cosmochimica Acta, 30: 681-703.

Weber, J.N. 1968. Fractionation of the stable isotopes of carbon and oxygen in calcareous marine invertebrates; the Asteroidea, Ophiuroidea and Crinoidea. Geochimica et Cosmochimica Acta, 32: 33-70.

Weber, J.N. and Woodhead, P.M.J. 1970. Carbon and oxygen isotope fractionation in the skeletal carbonate of reef-building corals. Chemical Geology, 6: 93-117.

Weissert, H. 1989. C-isotope stratigraphy, a monitor of paleoenvironmental change; a case study from the Early Cretaceous. Surveys in Geophysics, 10: 1-61.

Weissert, H. and Erba, E. 2004. Volcanism, CO2 and palaeoclimate: a Late Jurassic-Early Cretaceous carbon and oxygen isotope record. Journal of the Geological Society, 161: 695-702.

Weissert, H., Lini, A., Foellmi, K.B. and Kuhn, O. 1998. Correlation of Early Cretaceous carbon isotope stratigraphy and platform drowning events; a possible link? Palaeogeography, Palaeoclimatology, Palaeoecology, 137: 189-203.

Wendler, I., Wendler, J., Graefe, K.U., Lehmann, J. and Willems, H. 2009. Turonian to Santonian carbon isotope data from the Tethys Himalaya, southern Tibet. Cretaceous Research, 30: 961-979.

Wilson, P.A., Jenkyns, H.C., Elderfield, H. and Larson, R.L. 1998. The paradox of drowned carbonate platforms and the origin of Cretaceous Pacific guyots. Nature, 392: 889-894.

Wilson, P.A. and Norris, R.D. 2001. Warm tropical ocean surface and global anoxia during the Mid-Cretaceous period. Nature, 412: 425-428.

Wilson, P.A., Norris, R.D. and Cooper, M.J. 2002. Testing the Cretaceous greenhouse hypothesis using glassy foraminiferal calcite from the core of the Turonian tropics on Demerara Rise. Geology, 30: 607-610.

Winker, C.D. and Buffler, R.T. 1988. Paleogeographic evolution of early deep-water Gulf of Mexico and margins, Jurassic to Middle Cretaceous (Comanchean). AAPG Bulletin, 72: 318-346.

Winter, J.A. 1961. Stratigraphy of the lower Cretaceous (subsurface) of South Texas. Transactions - Gulf Coast Association of Geological Societies, 11: 15-24.

Wissler, L., Funk, H. and Weissert, H. 2003. Response of Early Cretaceous carbonate platforms to changes in atmospheric carbon dioxide levels. Palaeogeography, Palaeoclimatology, Palaeoecology, 200: 187-205.

Wooten, J.W. and Dunaway, W.E. 1977. Lower Cretaceous carbonates of central South Texas; a shelf-margin study. In: Cretaceous Carbonates of Texas and Mexico: Applications to Subsurface Exploration (Eds D.G. Bebout and R.G. Loucks), Texas Bureau of Economic Geology Report of Investigations No 89, pp. 71-78.

Young, K. 1986. Cretaceous, marine inundations of the San Marcos Platform, Texas. Cretaceous Research, 7: 117-140.

Yurewicz, D.A., Marler, T.B., Meyerholtz, K.A. and Siroky, F.X. 1993. Early Cretaceous carbonate platform, north rim of the Gulf of Mexico, Mississippi and Louisiana. In: Cretaceous carbonate platforms (Eds J.A.T. Simo, R.W. Scott, and J.-P. Masse): AAPG Memoir, 56: 81-96.

Zahm, L.C., Kerans, C. and Wilson, J.L. 1995. Cyclostratigraphic and ichnofacies analysis of the upper Albian Salmon Peak Formation, Maverick Basin, Texas. Transactions - Gulf Coast Association of Geological Societies, 45: 595-604.